The role of Annexin-A1 in the pathophysiology of diabetes.

A thesis presented by

Gareth S. D. Purvis

Registered at

Bart's and the London School of Medicine and Dentistry

Queen Mary University of London

For the degree of

Doctor of Philosophy

Translational Medicine and Therapeutics

The William Harvey Research Institute

John Vane Science Centre

Charterhouse Square

London

EC1M 6BQ

Declaration

I, Gareth Samuel Desmond Purvis, confirm that the research included within this thesis is my own work or carried out in collaboration with, or support by others, that this is duly acknowledged below and is duly acknowledged below and my contribution indicated.

I attest that I have exercised reasonable care to ensure that the work is original, and does not to the best of my knowledge break and UK laws, infringe any third party copyright or other Intellectual Property Right, or contain confidential material.

I accept that the College has the right to use plagiarism detection software to check the electronics version of the thesis.

I confirm that this thesis has not been previously submitted for the award of a degree by this, or any other university.

The copyright of the thesis rests with the author and no quotation from it or information derived from it may be published without prior written consent of the author.

Signature:

Date: 17/08/2017

Details of Collaboration: Collaboration with Prof Massimo Collino and Dr Fausto Chiazza for kindly assisting me in performing the western blots. George Elia and Emily Austin for Wax blocking and section cutting of my samples.

Abstract

Diabetes is a complex disease characterised by hyperglycaemia, which often leads to microvascular complications including diabetic nephropathy and cardiomyopathy. In this thesis, I have investigated the role of Annexin-A1 (ANXA1), an endogenous anti-inflammatory peptide, in two experimental murine models of diabetes caused by streptozotocin (STZ) or high-fat high-sugar diet (HFD), which mimic type-1 (T1DM) and type-2 diabetes (T2DM) respectively. I have also investigated the levels of ANXA1 in patients with either T1DM or T2DM.

Patients with T1DM have increased plasma ANXA1 levels. In a murine models of type 1 diabetes loss of endogenous ANXA1 aggravates both cardiac and renal dysfunction in mice. Specifically, I have shown that key mediators of the MAPK pathway (p38, JNK and ERK1/2) are constitutively activated in ANXA1$^{-/-}$ mice, and activation of these pathways is exacerbated in diabetic ANXA1$^{-/-}$ mice. Administration of human recombinant (hr) ANXA1 did not alter the diabetic phenotype in diabetic WT mice, but attenuated the cardiac and renal dysfunction caused by STZ. Interestingly, late administration of ANXA1 (after significant cardiac and renal dysfunction had already developed) halted the progression of both cardiac and renal dysfunction.

Patients with T2DM have increased plasma ANXA1 levels. HFD-fed ANXA1$^{-/-}$ mice have a more severe diabetic phenotype compared to HFD-fed WT mice. Therapeutic administration of hrANXA1 prevented the development of a diabetic phenotype. Specifically, I have shown that the insulin signalling pathway is further perturbed in diabetic mice resulting in severe insulin resistance, and that these signalling abnormalities were prevented by therapeutic administration of hrANXA1. In addition, loss of endogenous ANXA1 aggravates both cardiac and renal dysfunction in mice with experimental T2DM. The GTPase RhoA is constituently activated in ANXA1$^{-/-}$ mice leading downstream activation of MYPT1. Feeding a HFD also activated the small GTPase RhoA, leading to

increased MYPT1 activity, which could be attenuated with treatment with hrANXA1.

Mice subjected to HFD for 12 weeks had a more 'leaky' blood brain barrier (BBB), which is further exacerbated in ANXA1$^{-/-}$ mice fed a HFD. Compared to mice fed a chow diet, mice fed a HFD had an augmented CD4^{+} T-cell profile; with a clear decline in CD4^{+}FoxP3^{+} (anti-inflammatory) and increase in CD4^{+}RORgt^{+} (pro-inflammatory) cells. Administration of hrANXA1 to mice fed on HFD restored BBB integrity and CD4+ T-cells profile similar to mice fed on normal chow diet. Mice fed a HFD also had more activated CD4^{+} T-cells, which adhered more readily and transmigrated through a brain endothelial mono-layer *ex vivo*. In contrast, administration of hrANXA1 to mice fed on HFD reduced re-activity of CD4+ T-cells, reducing the number of adherent CD4^{+} T-cells to the brain endothelial mono-layer.

Acknowledgements

Firstly, I would like to thank the British Heart Foundation for funding my MRes/PhD through their 4-year studentship programme. Next I would like to thank Professor Christoph Thiemermann for his support and guidance throughout my time in his lab. He has given me numerous opportunities to present my work at meeting both nationally and international meetings, making memories I will have forever. I next have to thank Dr Egle Solito for all her support during my PhD and in the lab, your knowledge and lab skill has been a huge help to me. I know I have two great mentors here at The William Harvey Research Institute, not to mention all the other staff that I have had many a talk with over a glass (or 3) of wine. To our Italian collaborators Prof Massimo Collino and Dr Fausto Chiazza, for your help with westerns, and the many meeting we had about the directions of our many on-going collaborations. These talks help get an outside point of view on our data. I am also indebted to Dr Danilo Norata (Milan) and Prof Lugi Gnudi (King's College London) for providing the patient samples for my studies. To George Alia and Emily Austin in the BCI pathology for imparting all your knowledge of histology and staining to me. A special message to Flow and Mel both of whom I have spent the highs and lows with. Flow for always being so positive and encouraging to me, and Mel for our committee meetings in the robot room. To the many members of Team TMT over my time here, Florence, Jianmin, Rachel, Amy, Vicky, G, Regina, Lukas, Thaiana, Noriaki, Kitty and Dauda you have made this experience bearable, with support, guidance and nights to the pub.

List of Published Papers

1. **Purvis GSD**, Chiazza F, Azevedo Loiola R, Kusters DHM, Reutelingsperger C, Collino M, Baragetti A, Norata D, Solito E and Thiemermann C. (2017): AnnexinA1 regulates RhoA activation in a murine model of insulin resistance and diabetic nephropathy. Submitted to JCI.

2. **Purvis GSD**, Chiazza F, Chen J, Azevedo Loiola R, Martin L, Kusters DHM, Reutelingsperger C, Gnudi L, Yaqoob MM, Collino M, Thiemermann C and Solito E. (2017): Treatment with Annexin A1 attenuates the development of diabetic nephropathy and cardiomyopathy, in murine type 1 diabetes, through restoration of AKT signalling. under revision – Diabetoligia

3. Johnson FL, Patel NS, **Purvis GSD**, Chiazza F, Chen J, Sordi D, Hache G, Merezhko VV, Collino M, Yaqoob MM and Thiemermann C. (2017) Inhibition of IκB kinase at 24 h after acute kidney injury improves recovery of renal function and attenuates fibrosis. J Am Heart Assoc.

4. Yamada N, Martin LB, Zechendorf E, **Purvis GSD**, Chiazza F, Varrone B, Collino M, Shephard J, Heinbockel L, Gutsmann T, Correa W, Brsndenburg K, Marx G, Schuerholz T, Brohi K and Thiemermann C. (2017) Novel Synthetic, Host-defense Peptide Protects Against Organ Injury/Dysfunction in a Rat Model of Severe Hemorrhagic Shock. Ann Surg.

5. Chen J, Kieswich JE, Chiazza F, Moyes Aj, Gobbetti T, **Purvis GSD**, Salvatori DC, Patel NS, Perretti M, Hobbs AJ, Collno M, Yaqoob MM and Thiemermann C. (2016) IκB Kinase Inhibitor Attenuates Sepsis-Induced Cardiac Dysfunction in CKD. J Am Soc Nephrol 28:94–105.

6. **Purvis GSD**, Chiazza F, Collino M, and Bunyard P and Thiemermann C. BTK inhibition reduces the development of diabetic nephropathy by reducing NF-κB and NLRP3 inflammasome activation. *In preparation*.

7. **Purvis GSD,** Azevedo Loiola R, Thiemermann C and Solito E. Linking peripheral inflammation and the blood brain barrier in type-2 diabetes. *In preparation*.

List of published abstracts

1. Al Zoubi SYY, Chen J. Martin L, Murphy C, **Purvis GSD**, Chiazza F, Collotta D, Yaqoob MM, Collino M, and Thiemermann C. Inhibition of IκB kinase (IKK) attenuates the multiple organ dysfunction associated with polymicrobial sepsis in mice with pre-existing type 2 diabetes mellitus (T2DM). Oral presentation at The Congress of European Shock Society 2017.

2. **Purvis GSD**, Bunyard P and Thiemermann C. BTK inhibition reduced the development of diabetic nephropathy by reducing NF-κB and NLRP3 inflammasome activation. Oral presentation at the World Congress on Inflammation 2017, London. OP-54.

3. Zoubi SYY, Chen J, **Purvis GSD**, Chiazza F, Collotta D, Tacoub MM, Collino M and Thiemermann C. Inhibition of IκB kinase caused by sepsis in mice with pre-existing type 2 diebetes mellitus. Oral presentation at the World Congress on Inflammation 2017, London. OP-76

4. **Purvis GSD**, Chiazza F, Maggioli, Collino M, Solito E and Thiemermann C. Endogenous Annexin-A1 is a Protective Determinant in HFD-induced Insulin Resistance and Diabetic Nephropathy. Poster presentation at Experimental Biology 2017, Chicago. 2519. (***Research recognition award***)

5. **Purvis GSD**, Azevedo-Loiola R, Keswich J, Theimermann C and Solito E. Role of Annexin-A1 on blood-brain barrier functionality. (2017) Diabetic medicine. vol. 34, 64-64. Poster presentation at Diabetes UK.

6. **Purvis GSD**, Chiazza F, Maggioli, Collino M, Solito E and Thiemermann C. Endogenous Annexin-A1 is a Protective Determinant in HFD-induced Insulin Resistance and Diabetic Nephropathy. (2017) Diabetic medicine. vol. 34, 26-26. Oral and poster presentation at Diabetes UK.

7. **Purvis GSD**, Chiazza F, Maggioli, Collino M, Solito E and Thiemermann C. Endogenous Annexin-A1 is a Protective Determinant in HFD-induced Insulin Resistance and Diabetic Nephropathy. Oral and poster presentation at The British Pharmacological Society, Pharmacology 16. OB050. (***Oral communication prize*****)**

8. Chen J, Kieswich JE, Chiazza F, Moyes AJ, Gobbetti T, **Purvis GSD**, Salvatori DC, Patel NS, Perretti M, Hobbs AJ, Collno M, Yaqoob MM and Thiemermann C. IκB Kinase Inhibitor Attenuates Sepsis-Induced Cardiac Dysfunction in CKD. SHOCK. vol. 46, 29-30. Oral presentation at European Shock Society 2016, Coln.

9. **Purvis GSD**, Chen J, Reutelingsperger C, Kuster D, Solito E and Thiemermann C. Role Of Annexin-A1 In The Cardiac And Renal Dysfunction Associated With Experimental Type-1 Diabetes Mellitus. Poster presentation at American Diabetes Association 2016. New Orleans. 11-LB.

10. **Purvis GSD**, Chen J, Reutelingsperger C, Kuster D, Solito E and Thiemermann C. Role Of Annexin-A1 In The Cardiac And Renal Dysfunction Associated With Experimental Type-1 Diabetes Mellitus. Presented at BHF 4-year PhD cardiovascular science annual meeting. Glasgow. OP7.

11. **Purvis GSD**, Chen J, Reutelingsperger C, Kuster D, Solito E and Thiemermann C. Role Of Annexin-A1 In The Cardiac And Renal Dysfunction Associated With Experimental Type-1 Diabetes Mellitus. Poster presentation at The British Pharmacological Society, Pharmacology 15. London. PB184.

12. **Purvis GSD**, Chen J, Reutelingsperger C, Kuster D, Solito E and Thiemermann C. Annexin-A1 plays a critical protective role in the development of cardiac and renal dysfunction associated with diabetes. Oral presentation at The 8th conference on Annexins. Maastricht. 16:30.

Contents

Chapter I: General Introduction

2.4.3. Protein levels of ANXA1 in a murine model of STZ-induced type-1 diabetes mellitus.

2.4.4. The effect of endogenous ANXA1 on OGTT in a murine model of STZ-induced type-1 diabetes mellitus.

2.4.5. The effect of endogenous ANXA1 on renal dysfunction in a murine model of STZ-induced type-1 diabetes mellitus.

2.4.6. The effect of endogenous ANXA1 on tubular function in a murine model of STZ-induced type-1 diabetes mellitus.

2.4.7. The effect of endogenous ANXA1 on glomerular hypertrophy in a murine model of STZ-induced type-1 diabetes mellitus.

2.4.8. The effect of endogenous ANXA1 on renal fibrosis in a model of STZ-induced type-1 diabetes mellitus.

2.4.9. The effect of endogenous ANXA1 on cardiac dysfunction in a murine model of STZ-induced type-1 diabetes mellitus.

2.4.10. Effect of endogenous ANXA1 on cardiac hypertrophy in a murine model of STZ-induced type-1 diabetes mellitus.

2.4.11. Effect of endogenous ANXA1 on phosphorylation of p-38, JNK and ERK1/2 in kidneys from mice subjected to STZ-induced type-1 diabetes mellitus

2.4.12. Effect of endogenous ANXA1 on phosphorylation of Akt in kidneys from mice subjected to STZ-induced type-1 diabetes mellitus

2.4.13. The effect of endogenous ANXA1 on phosphorylation of p-38, JNK and ERK1/2 in kidneys from mice subjected to STZ-induced type-1 diabetes mellitus.

2.4.14. The effect of endogenous ANXA1 on phosphorylation of Akt in hearts from mice subjected to STZ-induced type-1 diabetes mellitus.

2.4.15. The effect of administration of hrANXA1 on non-fasted blood glucose, serum insulin and OGTT in mice subjected to STZ-induced type-1 diabetes mellitus.

2.4.16. The effect of administration of hrANXA1 on renal dysfunction in mice subjected to STZ-induced type-1 diabetes mellitus.

2.4.17. The effect of administration of hrANXA1 on the cardiac dysfunction in WT-mice subjected to STZ-induced type-1 diabetes mellitus.

Abbreviations

ACR	Albumin to creatinine ratio
AGE	Advanced glycated end products
Akt	Protein kinase B
ANXA1	AnnexinA1
ATP	Adenosine triphosphate
AWERB	Animal Welfare Ethics Review Board
BBB	Blood brain barrier
BCA	Bicinchoninic acid
BMEC	Brain microvascular endothelial cells
BMI	Body mass Index
Ca^{2+}	Calcium ion
CAD	Coronary artery disease
CNS	Central nervous system
COX2	Cyclooxygenase-2
CRP	C-reactive protein
CSF	Cerebrospinal fluid
DAG	Diacylglycerol
DCM	Diabetic cardiomyopathy
DN	Diabetic nephropathy
DNA	Deoxyribonucleic acid
ECM	Extracellular matrix
EF	Ejection fraction
ESRD	End-stage renal disease
FAC	Fractional area change
FS	Fractional shortening
GFR	Glomerular filtration rate
GLUT1	Glucose transporter 1
GLUT2	Glucose transporter 2
GLUT4	Glucose transporter 4
Hr	Human recombinant
IL	Interleukin

IP_3	Inositol trisphosphate
IRS-1	Insulin receptor substrate
IRS-1	Insulin receptor substrates-1
K^+	Potassium ions
NADPH	Nicotinamide adenine dinucleotide phosphate
NF-κB	Nuclear transcription factor-kappa b
ns	non-significant
OGTT	Oral glucose tolerance test
PCT	Proximal convoluted tubules
PI3K	Phosphoinositide-3 kinase
PIP_2	Phosphatidylinositol 4,5-bisphosphate
PKC	Protein kinase C
PLC	Phospholipase C
PVDF	polyvinyldenedifluoride
ROC	Receiver operator curve
ROS	Reactive oxygen species
SEM	Standard error of the mean
Ser	Serine
STZ	Streptozotocin
TGF-β	Transforming growth factor-Beta
WT	Wild type

Units

C	Degree Celsius
g	Gram
h	Hour
kg	Kilogram
mg	Milligram
min	Minute
ml	Millilitre
mM	Milli molar
mmHg	Millimetre of mercury
mmol	Milli moles
mmol/L	Millimoles per litre
nm	Nanometre
RPM	Revolutions per minute
ug	Microgram
v/v	Volume per volume
w/v	Weight per volume
µl	Microlitre
µm	Micrometre
µmol/L	Micromoles per litre
M	Molar

Chapter I:

General Introduction

1.1 Regulation of blood glucose

The principal hormone involved in blood glucose regulation is insulin, which is produced within beta cells in the islets of Langerhans of the pancreas. When blood glucose levels increase, insulin is immediately released from its granular stores in the pancreas. To ensure immediate release, insulin production is highly regulated (Hou et al., 2009). Specifically, mRNA transcripts are translated into an inactive protein called preproinsulin. This contains a terminal amino acid signalling sequence that is used to traffic it through the membrane of the endoplasmic reticulum (ER) where it is post-translationally modified. In the ER, the trafficking sequence of preproinsulin is proteolytically cleaved off. Preinsulin matures into insulin when three di-sulphate bonds form, allowing it to fold. This folding results in the generation of bioactive insulin which is stored in secretory granules, which accumulate in the cytoplasm ready for release when blood glucose levels rise.

Glucose in taken up into beta cells using the specific glucose transporter 2 (GLUT2). As blood glucose levels increase, more glucose is taken up into beta cells. Once inside the beta cells, glucokinase phosphorylates glucose allowing it to enter into glycolysis to produce adenosine triphosphate (ATP) in a rate-dependent manner (Figure 1.1). As intracellular glucose levels increase, more glucose enters glycolysis within beta cells, thus, increasing ATP levels in the cell. This changes the ATP:ADP ratio causing ATP-gated potassium channels to close, inhibiting potassium ions (K^+) from crossing the membrane, which, in turn, leads to depolarisation of the membrane due to an accumulation of K^+. As a consequence, voltage-gated calcium channels open allowing for an influx of

calcium ion (Ca^{2+}) into the cell (Figure 1.1). The increase in cytosolic Ca^{2+} initiates exocytosis of insulin-storing granules, allowing insulin to readily diffuse into the vessels that surround the highly vascularised islets. Insulin release is regulated in a biphasic manner (Rorsman et al., 2000); the initial amount of insulin released is dependent on the amount stored within secretory granules in the beta cell cytoplasm. The second round of insulin release is dependent on the length of time required for the synthesis and secret of *de novo* insulin (Henquin et al., 2002). Insulin is required until blood glucose levels return to normal, but *de novo* insulin synthesis is also needed to replenish the stores of insulin lost in the initial fast response phase from beta cells.

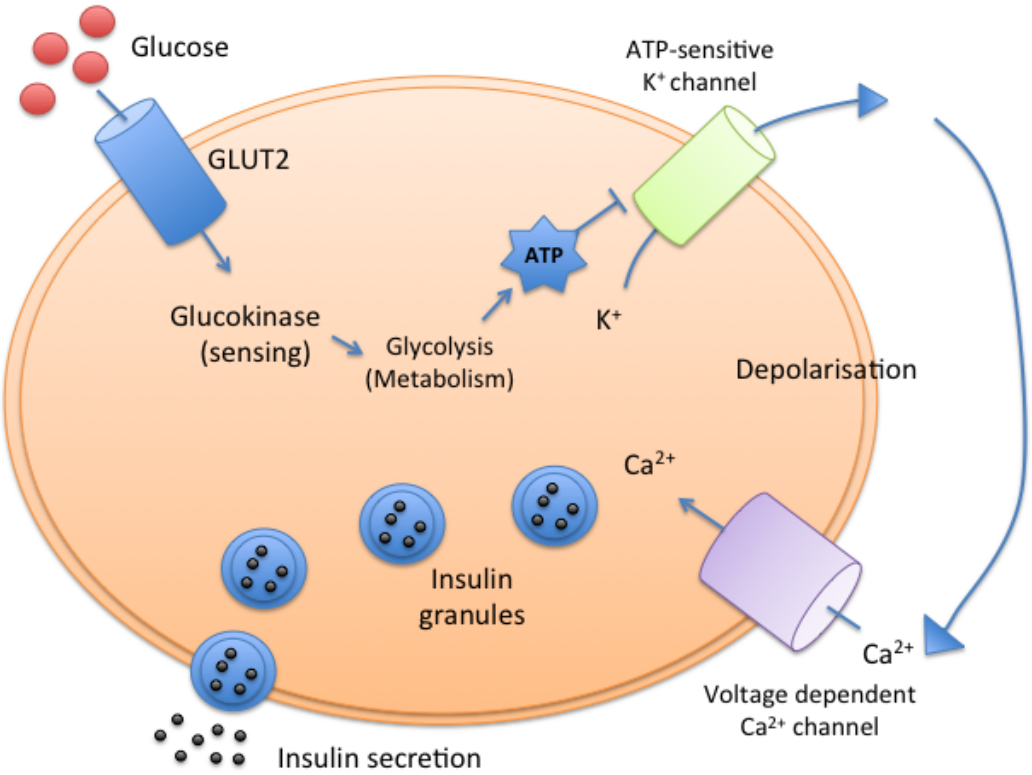

Figure 1.1: Pathway involved in glucose sensing and insulin release in Beta cells.

The 'classical' pathway' of insulin release involves the passive diffusion of glucose into the beta cells by glucose transporter 2 (GLUT2). Glucokinase 'senses' increases in glucose levels and metabolises glucose (by glycolysis) to generate ATP. This leads to the closure of ATP-sensitive K^+ channels, depolarising the plasma membrane causes opening voltage-dependent Ca^{2+} channels, which leads to an influx of extracellular Ca^{2+} and thus results in insulin exocytosis.

Once insulin is released into the circulation, it acts on specific insulin receptors, which signal via intercellular insulin receptor substrates-1 (IRS-1). Under basal conditions (normal physiological blood glucose levels), the IRS-1 complex is phosphorylated on serine (Ser)-307, which causes it to be inactive. Under hyperglycaemic conditions, insulin is released and binds to the insulin receptor;

the phosphorylation on Ser-307 is lost and allowing phosphorylation on tyrosine (Tyr)-608/628 (Figure 1.2) allowing signal transduction though phosphoinositide 3-kinase (PI3K)/protein kinase B (Akt).

The signalling cascade is initiated by insulin binding to the insulin receptor, which facilitates the translocation of glucose transporter 4 (GLUT4) positive vesicles to the cell membrane to allow the uptake of glucose from the blood stream (Figure 1.2). GLUT4 membrane channels are present on a number of peripheral cell types, including hepatocytes, skeletal muscle and adipocytes that utilise dietary glucose for energy metabolism or storage. Under basal conditions very few GLUT4 transporters are present on the cell surface, however, upon insulin release after a spike in blood glucose, a large number of GLUT4 transporters are trafficked to the cell membrane (James et al., 1988).

There are also other proteins involved in the regulation of insulin release. Glucagon-like-peptide-1 (GLP-1) is a potent incretinGLP hormone produced in the L-cells of the distal ileum and colon. Nutrients, including glucose, fatty acids, and dietary fiber, are all known to up regulate the transcription of the gene encoding GLP-1, and they can stimulate the release of this hormone. In the gut is has very distinct effects to those that are involved in insulin secretion (gut motility, inhibition of gastric acid secretion and inhibiting glucagon secretion) (Holst et al., 2007). As previously mentioned insulin secretion to occurs as a result of glucose metabolism. When glucose levels rise, the rate of glycolysis increases, which generates substrates (mainly pyruvate) for mitochondrial oxidative metabolism, the result of which is the generation of ATP, or more

correctly an increase in the ATP-to-ADP ratio. GLP-1 is proposed to modulate glucose stimulated insulin secretion by regulating the activity of several ion channels involved in K_{ATP}-dependent insulin secretion (MacDonald et al. 2002) (Figure 1.1). Indeed, GLP-1 receptor agonists are now part of a repertoire of drugs used to enhance glucose secretion (Garder et al 2011). Another is the dipeptidyl peptidase 4 (DPP-4) inhibitors these work by blocking the production of DPP-4, which is an enzyme that destroys incretin, therefore the hope is to increase the secretion of insulin (Deacon et al 2016)

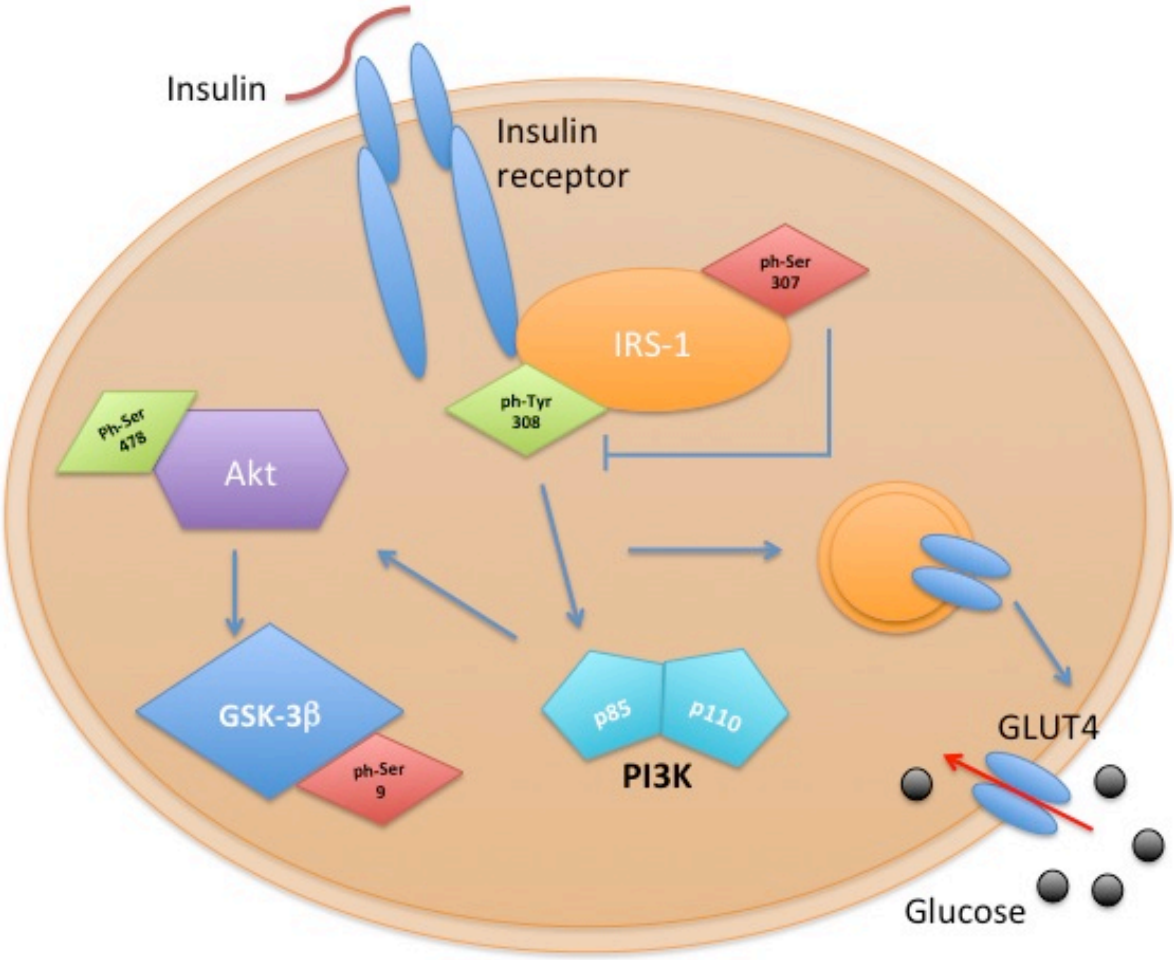

Figure 1.2. Schematic showing the mode of action of insulin signalling.

1.1.1 When it goes wrong: Diabetes

Diabetes mellitus is a chronic condition, in which patients can't maintain blood glucose homeostasis due to ineffective action or secretion of insulin. Diabetes is a very old disease and was first reported by the Egyptians around 3000 years ago. Thomas Willis first used the term "mellitus" which mean 'honey sweet' in 1675 after discovering the sweetness of urine and blood of patients with diabetes. It

was only in 1776 that the English physician Matthew Dobson confirmed that excessive sugar in the urine and blood was the cause of the sweetness (Ahmed 2002). It wasn't until much later that the role of the pancreas was elucidated by Joseph von Mering and Oskar Minkowski (1889); they conducted experiments with dogs who had their pancreas removed and demonstrated they had the same phenotype as diabetic patients (Mering & Minkowski, 1890). In 1923 Fredrick Banting and John MacLeod won the Noble Prize 'for the discovery of insulin' and its use for the treatment of diabetes (Majumdar, 2001). In 1936, the first distinction between type-1 (T1DM) and type-2 diabetes mellitus (T2DM) was made. T1DM is an autoimmune disease caused by the destruction and damage of beta cells in the pancreas resulting in insulin deficiency resulting in hyperglycaemia. Type-2 diabetes, formerly known as non-insulin dependant diabetes mellitus, and was first described as a metabolic syndrome in 1988. It is also associated with hyperglycaemia, but as a result of insulin-resistance of the tissues that utilise glucose and, hence, these patients are able to generate insulin, albeit, not in sufficient amounts to lower blood glucose.

It is estimated that in the UK 1 in 16 people of the general population have diabetes; this equates to around 4 million people as of December 2016. Around 10 % of the total patients with diabetes have T1DM, while the other 90 % have T2DM. There are also some more rare types of diabetes. Monogenetic diabetes account for around 1 to 5 percent of all cases of diabetes in young people (National Diabetes Statistics Report, 2014*).* Genetic testing can diagnose most forms of monogenic diabetes. If genetic testing is not performed, people with monogenic diabetes may appear to have one of the polygenic forms of diabetes.

Additionally, gestational diabetes is the most common form of maternity related condition and usually occurs in the second or third trimester. Indeed one study found that hypoglycaemia occurs in around 15 % of all pregnancies, this was a finding from a nine country, multi-centre study (Buckey et al. 2012). While maturity onset diabetes of the young often referred to MODY, is not related to obesity but the patients are young and have symptoms comparable to those of T2DM. Interestingly, this form of diabetes is more likely to be inherited than as and is caused by changes in a single gene GCL which encodes glucokinase mapped to chromosome 12q (Vaxillaire et al. 1995) (Sheild et al. 2010).

UK statistics report that 56 % of all adults with diabetes are female, suggesting that there may be a small, but significant, gender bias (National Diabetes Audit, 2014). The care burden of diabetes is financially significant with conservative estimates suggesting that diabetes directly and indirectly cost the UK currently £23.7 billion and that this is set to rise to £39.8 billion by 2035/6 (Hex et al., 2012).

1.1.2 Causes of diabetes

As previously mentioned both T1DM and T2DM share the common phenotype of hyperglycaemia, but the cause of the hyperglycaemia is very different. The classical model of T1DM suggests there is a strong genetic susceptibility (Pociot & Lernmark, 2016). All adults have a fixed number of beta cells. Specific environmental factors can trigger beta cell autoimmunity (Atkinson 2012) resulting in the development of islet reactive autoantibodies, the activation of autoreactive T-cells capable of destroying beta cells, and ultimately the

progressive loss of beta cells that cannot be replaced. As a consequence, insulin production is reduced and sufficient amounts of insulin cannot be secreted in response to elevations in blood glucose. Clinically, patients with T1DM are asymptomatic until they have lost ~80-90 % of their beta cell mass; only then is there significant perturbation of the system that results in elevated blood glucose levels. The environmental factor(s) that triggers beta cell autoimmunity remains very elusive, however, infectious agents are often cited. Rubella and enterovirus infection are the most commonly reported to having a relationship between beta cell autoimmunity and diabetes (Boettler & von Herrath, 2011). Other potential candidates are from dietary sources. The most predominant of these is the effect of breastfeeding and the early exposure to cows milk, but once again the idea is highly controversial. However, meta-analysis showed a small, but significant, correlation between short periods of breast feeding and cow's milk exposure before 3-4 months of age (Gerstein, 1994).

On the other hand, T2DM is characterised by peripheral insulin insensitivity (also called insulin resistance), leading to an increased insulin production and but ultimately in pancreatic beta cell failure. Insulin-resistance occurs when the signalling cascade activated by insulin through IRS-1 is blunted and as a result there is a reduction in PI3K/Akt signalling. It is now widely accepted that an increase in the phosphorylation of Ser-307 on IRS-1 is a mechanistic marker of peripheral insulin resistance in experimental models of diabetes (Figure 1.2). Unexpectedly, Wilson and colleagues have reported that mice with specific site-specific amino acid changes in Ser-307 developed more severe insulin resistance (Copps et al., 2010). This finding raises the question whether this

phosphorylation site is functionally the main driver of peripheral insulin resistance.

The cause of the receptor insensitivity is multifaceted, but largely due to excessive dietary intake of calories; there is also a strong correlation with both obesity and lack of exercise (Sigal et al., 2004). Large quantities of monounsaturated and polyunsaturated fats are harmful to rats and cause insulin resistance, while other studies demonstrate that saturated fats appear to have a more profound effect at eliciting insulin resistance (Storlien et al., 1991). Similarly, elevated levels of free fatty acids and triglyceride in the blood stream coupled with excess adipose tissue mass have been found to contribute to diminished insulin sensitivity (Lovejoy, 1999).

The liver is the central organ for lipid and glucose metabolism, both of which are in part regulated by insulin. Hepatic steatosis is a common finding in patients with T2DM, which is causally linked to features of the metabolic syndrome, liver cirrhosis, and cardiovascular. Excessive fat intake leads initially to hypercholesterolaemia, which is a common feature in patients with pre-diabetes. Indeed, clinically at this stage life style choices are very effective at correcting these abnormal test results. However, if left unchecked this compartment becomes overwhelmed and fat starts to become deposited in the liver (initially). Indeed, elevated circulating free fatty acid levels, in part related to diminished suppression of adipose tissue lipolysis by insulin, this results in increased delivery of free fatty acids to the liver (and ultimately liver accumulation). The synthesis of excess triglyceride in the liver is also driven by this supply of fatty

acids. The most severe consequences of this is the development of non-alcoholic fatty liver disease (NAFLD)/non-alcoholic steatohepatitis (NASH). Most patients with NAFLD/NASH are asymptomatic and typically identified when abnormal liver results are noted on routine laboratory assessment. In particular, the liver enzymes alanine aminotransferase (ALT) and aspartate aminotransferase (AST) are elevated. However, these enzymes may not be elevated in all cases of NAFLD, and the level of ALT/AST does not reliably predict the extent of inflammation and cirrhosis.

Indeed abdominal adiposity is very prevalent in patients with T2DM. Epidemiologic investigations have consistently shown an independent increased risk for diabetes associated with overweight and obesity, with clear dose response patterning across categories of increasing body mass. While the importance of increased body mass in diabetes etiology is unequivocal, it has been recognized for some time that the distribution of body fat provides additional resolution regarding diabetes risk (Hanley et al., 2008). There was a strong association between measures reflecting abdominal obesity and the incidence of type 2 diabetes, the pooled odds ratio was 2.14 (95% CI: 1.70–2.71; $p < 0.0001$) (Freemantle et al., 2008).

The dietary component fructose, which is commonly added to fast foods and used as sweeteners, is metabolised by the liver into triglycerides. This not only increases sugar intake, but also adds to the accumulation of triglycerides levels in the blood that can further lead to insulin insensitivity and renal dysfunction (Hwang et al., 1987).

1.1.3 Complications and co-morbidities of diabetes

The long-term effects of diabetes include neuropathy, retinopathy, cardiomyopathy and nephropathy. These complications are classified as microvascular problems and their prevalence is very high. It is estimated that annually 10 % of the NHS budget is spent on the treatment of diabetes, which equates to around £11 billion, and most of this budget is spent on treating the vascular complications of diabetes. Retinopathy is present in 13% of T1DM patients within 5 years, and 40% of patients with T2DM. The longer-term prognosis is worse, as 90% of patients with T1DM suffer from retinopathy after 10 to 15 years. Neuropathy is less well defined, but generally measured by loss of loss of fine touch and is present in around 7% of diabetic patients within 1 year, with up to 50% suffering neuropathy within 25 years. It appears that there is no difference in prevalence neuropathy between T1DM and T2DM.

1.2 Diabetic cardiomyopathy

1.2.1 Natural history of diabetic cardiomyopathy

The concept of diabetic cardiomyopathy (DCM) was first coined by Rubler *et al*. in 1972 who reviewed four autopsy cases of patients with diabetic glomerulosclerosis and no known cause of death (Rubler et al, 1972). The authors concluded that these patients had an underlying condition, diabetic cardiomyopathy, which contributed to their death. Diabetic cardiomyopathy is now known to be a potentially serious cardiac dysfunction induced by the alterations in structure and contractility of the myocardium in patients with severe diabetes. These fundamental changes stem from a lack of glycaemic control that affects the myocardium in the absence of hypertension, atherosclerosis or any other cardiomyopathies. Diabetic cardiomyopathy is now considered an important secondary complication of diabetes.

Diabetic cardiomyopathy occurs in approximately 12 % of all patients with T2DM and is slightly less common in patients with T1DM; however, the overall risk of a cardiovascular event is similar in both groups of patients (Martín-Timón et al., 2014). Using population-based studies it has been shown that the overall risk of heart failure is increased two fold by diabetes. The first stage of DCM is often an asymptomatic, but characterised by diastolic dysfunction (increased ventricular stiffness, left atrial enlargement, hypertrophy and elevated left ventricular end diastolic pressure). It is also a common feature however, that left ventricular function is preserved in these patients. The second stage of DCM is characterised by cardiac remodelling, severe left ventricular hypertrophy and the clinical emergence of heart failure. Although still controversial, some authors

report a strong association between length of time with diabetes and systolic cardiac dysfunction (Niemann et al., 2013).

1.2.2 Key mechanisms in diabetic cardiomyopathy

Although T1DM and T2DM differ in aetiology and metabolic profiles, both share many common features in the pathophysiology and the mechanisms, which drive diabetic cardiomyopathy. However, from here on the focus will be on the cardiomyopathy associated with T1DM. To date the progression DCM has not been fully characterised, but the pathophysiological of events associated with DCM include cell hypertrophy, interstitial fibrosis, inflammation and metabolic derangements (Westermann et al., 2007) (Ban & Twigg, 2008a).

1.2.3 Fibrosis in diabetic cardiomyopathy

Interstitial fibrosis is one of the key histological hallmarks of diabetic cardiomyopathy, resulting from both localised myocyte death and infiltration of immune cells. This leads to deposition of extracellular matrix (ECM) within the ventricle walls causing stiffness in the diabetic heart. Collagen type I and type III fibres accumulate in the epicardial and perivascular regions, whereas type IV fibres are predominantly found in the endocardium (Way et al. 2002). Glycated proteins undergo a series of chemical rearrangements to form complex compounds, which are referred to as advanced glycated end products (AGE). AGE's are increased in plasma of patients that are older, or have diabetes (hyperglycaemia) or renal failure (Singh et al., 2014). However, the accumulation of AGE in collagen reduces collagen turnover rate, and AGE-mediated cross-linking of collagen is responsible for increased stiffness of

arteries and the myocardium. Indeed, AGE accumulation in the myocardium is proportional to the levels of AGE seen in the serum. Soluble AGE also interacts with the receptor of AGE immunoglobulin's on both endothelial cells and myocardiocyte to up-regulate production of transforming growth factor-Beta (TGF-β), and nicotinamide adenine dinucleotide phosphate (NADPH) oxidases, which in turn increases cytoplasmic and extracellular reactive oxygen species (ROS), leading to cellular death and the need for production of ECM components (Wang et al., 2006) (Giacco & Brownlee, 2010). Low-grade chronic inflammation is a key driver of pathways involved in the re-modelling of the myocardium, which disrupts cardiac output (Festa & Haffner, 2005).

1.2.4 Inflammation in diabetic cardiomyopathy

Inflammation plays a key role in the development of diabetes (Rehman et al. 2016), and is thought to be one of the main contributors to the development of secondary microvascular complications. Pro-inflammatory signalling by cardiomyocytes occurs as an early response to hyperglycaemia, and is thought to be a protective response to noxious stimuli. Nuclear transcription factor-kappa beta (NF-κB) is a highly potent nuclear pro-inflammatory transcription factor that is involved in initiating the transcription cytokines, adhesion molecules and mediators under hyperglycaemic conditions (Basu et al., 2005). Activation of NF-*κ*B by hyperglycaemia is thought to be one of the key drivers of localised inflammation in heart (Lorenzo et al., 2011), but NF-*κ*B is also activated in numerous other cell types in response to hyperglycaemia. Diabetes can cause an augmented cytokine profile skewed toward a more pro-inflammatory phenotype

(interleukin (IL)-1β, IL-6 and IL-17a), however, the site of production of these cytokines is not known (King, 2008). *In vitro* studies have shown that cardiomyocytes and endothelial cells (which make up most of the cells of the heart) have the potential to produce pro-inflammatory cytokines in the presence of high glucose levels and this results in the up-regulation of adhesion molecules (ICAM-1 and VCAM-1) (Shanmugam et al., 2003). This may lead to an increase in the activation of immune cells and their subsequent recruitment and transmigration into the tissue causing localised inflammation and injury. The infiltration of immune cells, initially neutrophils and then monocytes can further increase localised inflammation in the heart, which can cause cell apoptosis and the development of fibrosis, which ultimately decreases the contractility of the myocardium (Mann, 2002).

1.2.5 Protein kinase C (PKC) in diabetic cardiomyopathy

Activation of the protein kinase C (PKC) pathway is one of the main mechanisms by which hyperglycaemia exerts negative effects on the heart. Hyperglycaemia causes the hydrolysis of phosphatidylinositol 4,5-bisphosphate (PIP_2) to diacylglycerol (DAG) and inositol trisphosphate (IP_3) by phospholipase C (PLC) (figure 1.3). IP_3 causes release of Ca^{2+} from the sarcoplasmic reticulum that can then activate PKC. Likewise, DAG can directly interact with PKC to increase its activation (Figure 1). Under hyperglycaemic conditions, PKC is constitutively activated. *In vitro* and *ex vivo* studies have shown that increased activation of PKC decreases Akt activation and increases the activation of the mitogen-activated protein kinase (MAPK) signal transduction pathway. Activated PKC and MAPK result in increases in permeability of the endothelium, monocyte

recruitment, chemokine activation, cardiomyocyte growth and in cardiac fibrosis (Geraldes & King, 2010a). PKC inhibition attenuates diastolic dysfunction, preserves contractility and reduces myocyte hypertrophy in rats with genetically induced diabetes heart failure (Connelly et al., 2009). Cardiac hypertrophy is prevalent in many cases of DCM, and commonly seen in biopsy specimen obtained from diabetic hearts. ERK1/2 activation secondary to poor glycaemic management results in activation of key signal transduction pathways of cardiac hypertrophy (Kehat & Molkentin, 2010). However, it is unknown how this contributes to the development of ventricular dysfunction (Dei Cas et al., 2013).

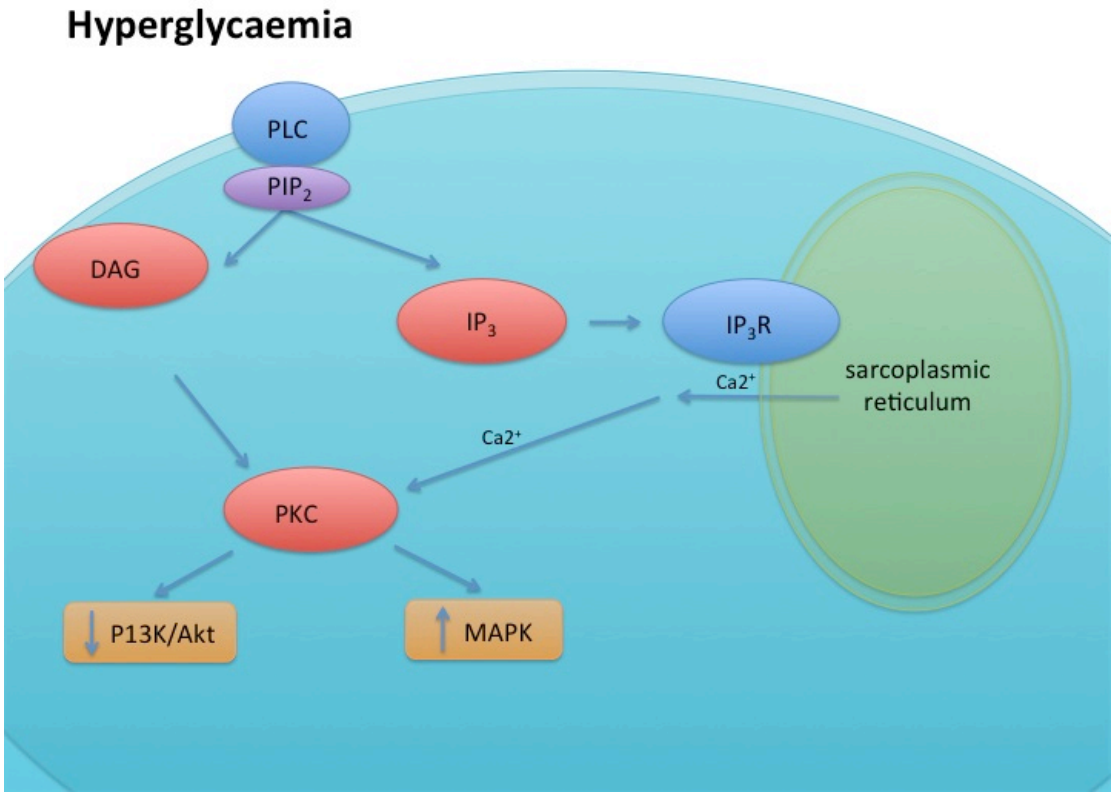

Figure 1.3. Schematic show how hyperglycaemia induces the activation of PKC.
Hyperglycaemia stimulates *de novo* synthesis of DAG and IP_3. DAG can then activate multiple isoforms of PKC. This will in turn affect the activity intracellular signaling pathways such as the MAP kinases (p38, JNK and ERK1/2) and PI3K/Akt pathways, altering key enzymes that determine cellular homeostasis. IP_3 facilitates the release of $Ca2^+$ from the sarcoplasmic reticulum by binding its receptor IP_3R, increasing cytosolic concentrations of calcium thus activating PKC by a secondary route.

1.2.6 Metabolic alterations in diabetic cardiomyopathy

Energetic imbalances within cells are often caused by lack of glycaemic regulation and can lead to mitochondrial uncoupling, which in turn generates excessive amounts of ROS. Small changes in the efficiency of ATP production can significantly compromise cellular function, including the ability of cardiomyocytes to contract and relax. Diabetes reduces the efficiency of energy production by enhancing fatty acid uptake at the expense of supressing glucose

oxidation. Glucose oxidation is inhibited at multiple metabolic steps in the diabetic hearts. Uptake of glucose is augmented by the down-regulation of GLUT4 and glucose transporter 1 (GLUT1), therefore, less substrate is available for oxidative phosphorylation (Boudina & Abel, 2010).

Any changes in glucose homeostasis particularly affects the cellular metabolism which is the main source of ATP production in the cell. Mitochondrial damage presents itself by loss of membrane potential which leads to a further increase in ROS production due to excessive proton leak (Ghosh et al., 2005). Proteomic analysis using 2D gels and mass spectrometry have shown that up to 24 cardiac proteins are altered in the hearts of diabetic rats, 12 of which are located in the mitochondria (Hamblin et al., 2007). Excessive proton leak allows free radicals to form superoxide anions that can combine with nitric oxide to form highly reactive and damaging peroxynitrite. ROS can cause damage to the endothelium, proteins, deoxyribonucleic acid (DNA) and lead to cell death (Stowe & Camara, 2009). The damage caused by excessive ROS formation can also induce vasoconstriction, increased leukocyte adherence and vessel wall inflammation, resulting in irreversible left ventricular remodelling and reduced cardiac output (Stowe & Camara, 2009). NADPH oxidase has emerged as the main source of ROS in the heart of diabetic rats with minor contributions from other sources, such as xanthine oxidase (Guo et al., 2007). Antioxidants can decrease the oxidative stress induced hyperglycaemia by a directly scavenging of ROS and by inhibiting cell proliferation (Farhangkhoee et al., 2003), but often they are not produced in sufficient amount to deal with the ROS overload in the diabetic heart.

1.3 Diabetic Nephropathy

1.2.1 Natural history of diabetic nephropathy

Clinically, diabetic nephropathy (DN) presents itself as elevated levels of albumin (≥ 30 mg/24 h) in the urine, referred to as microalbuminuria (Lim 2014). Patients presenting with microalbuminuria are referred to as having diabetic nephropathy. If patients do not receive specific interventions, around 80 % of patients with T1DM will go on to develop sustained microalbuminuria. Typically their annual albumin excretion rate increases 10 – 20 % per year to the stage of overt nephropathy, or clinical albuminuria (≥300 mg/24 h) over a period of 10 – 15 years. Again without specific interventions, patients with overt nephropathy have an annual decline in glomerular filtration rate (GFR) of 2-20 ml/min per year, however, the rate of decline is highly variable between individuals (Molitch et al. 2004).

Patients with T2DM can present with microalbuminuria or overt nephropathy shortly after diagnosis. This is partly due to the fact that their diabetes is usually present for many years before the diagnosis is made. Without specific interventions, 20-40 % of patients with microalbuminuria progress to overt nephropathy, but this can take up to 20 years. Of this population, less than 20 % will progress to ESRD. When patients enter ESRD GFR begins to decline, but the rate of decline in GFR is highly variable between individuals (Tapp et al., 2004). However, there is no difference in the annual decline in GFR between patients with T1DM and T2DM. Proportionally more patients with T1DM develop ESRD, this discrepancy may be in part due to patients with T2DM being associated with a higher risk of dying from coronary artery disease (CAD). Therefore, entering

preventative treatment plans and therapies for CAD may prevent many with earlier stages of DN from progressing to ESRD (Bruno et al., 2003). Indeed patients with T1DM also have a high risk of coronary heart disease (Slim et al. 2013). Interestingly, when compared to Caucasians, there is a 4-5 fold increased risk of developing T2DM for those patients that are of south Asian descent, compared with a white reference group (Hippisley-Cox et al., 2009). Collectively, DN is the main cause of patients receiving RRT (Bell et al., 2015).

The decline in renal function is associated with and may be explained by the following morphological (histological) changes in the kidney: Mesangial expansion, glomerular basement membrane thickening, glomerular sclerosis and tubulointerstitial injury. These morphological changes form the basis of a 5 stage classification strategy first introduced in the 1980s. However, in recent years, a new, 5-stage strategy of scoring has been developed that better mirrors the morphological changes that are specific for diabetic nephropathy. This scoring system postulates that the severity of tubulointerstitial injury represents an important factor in diagnosing the progression of DN. Therefore, depending on the severity of DN, interstitial and vascular modifications patients are graded into stages (Table 1.1). Although it is clinically useful to classify patients with DN, this classification does not give any indication of the factors driving these changes. This causes problems when targeting patients with specific therapies, as the underlying cause of these physical end-points is not clear (Tervaert et al., 2010). Again in 2014 Joint Committee on Diabetic Nephropathy has revised its classification of DN in line with the widespread use of key concepts, such as the estimated glomerular filtration rate (eGFR), proteinuria (urinary

albumin/creatinine ration) and chronic kidney disease (CKD) Table 2/3.

Table 1. Table describing the clinical scoring, description and inclusion criteria of 5-stage diabetic nephropathy. Adapted from Rohani *et al.*, 2014.

Class	Description	Inclusion Criteria
I	Mild or nonspecific LM changes and EM-proven GBM thickening	Biopsy does not meet any of the criteria mentioned below for class II, III, or IV
		GBM > 395 nm in female and >430 nm in male individuals 9 years of age and older· Podocyte hypertrophy
IIa	Mild mesangial expansion	Biopsy does not meet criteria for class III or IV
		Mild mesangial expansion in >25% of the observed mesangium
IIb	Severe mesangial expansion	Biopsy does not meet criteria for class III or IV
		Severe mesangial expansion in >25% of the observed mesangium
III	Nodular sclerosis (Kimmelstiel–Wilson lesion)	Biopsy does not meet criteria for class IV
		At least one convincing Kimmelstiel–Wilson lesion
IV	Advanced diabetic glomerulosclerosis	Global glomerular sclerosis in >50% of glomeruli
		Lesions from classes I through III

Table 2. Table describing the clinical scoring, set out as Classification of Diabetic Nephropathy 2014. Adapted from Haneda et al. 2015.

Classification of Diabetic Nephropathy 2014

Stage	Urinary albumin (mg/g Cr) Or urinaryprotein (g/g Cr)	GFR (eGFR) (mL/min/1.73 m2)
Stage 1 (prenephropathy)	Normoalbuminuria (<30)	≥30
Stage 2 (incipient nephropathy)	Microalbuminuria (30–299)§	≥30
Stage 3 (overt nephropathy)	Macroalbuminuria (≥300) or persistent proteinuria (≥0.5)	≥30
Stage 4 (kidney failure)	Any albuminuria/ proteinuria status	<30
Stage 5 (dialysis therapy)	Any status on continued dialysis therapy	

Table 3. Relationship between the 2014 categories for diabetic nephropathy stages and the chronic kidney disease severity categories. Adapted from Haneda et al 2015.

Albuminuria category		**A1**	**A2**	**A3**
	Quantitative urinary albumin estimation Urinary albumin/Cr ratio [mg/g Cr]	**Normoalbuminuria <30**	**Microalbuminuria 30–299**	**Macroalbuminuria ≥300 (or increased proteinuria) (≥0.50)**
GFR category (mL/min/1.73 m2)	≥90 60–89	Stage 1 (pre-nephropathy)	Stage 2 (incipient nephropathy)	Stage 3 (overt nephropathy)
	45–59 30–44			
	15–29 <15 (Dialysis therapy)	Stage 4 (kidney failure) Stage 5 (dialysis therapy)		

1.3.2 Key mechanisms driving in diabetic nephropathy

The mechanisms governing the development of diabetic nephropathy are very similar in models of T1DM and T2DM. Clinically, the pathophysiology is also very similar and as such the mechanisms driving both are very similar. Histologically, DN is well characterised; mesangial expansion as a result of increased ECM production and cell enlargement can be seen in the early stages. This is proceeded by thickening of the basement membrane, reduction in podocyte number and nodular lesions (Reidy et al., 2014). There are many processes involved in driving these changes, including PKC, excessive generation of ROS, fibrosis and low-grade chronic inflammation.

1.3.3 Protein kinase C (PKC) pathway in diabetic nephropathy

Failure of PKC to activate Akt and other downstream mediators has numerous cellular consequences that affect glucose metabolism, glycogen synthesis, cell proliferation, cell hypertrophy and may even lead to cell death. Akt is also an important mediator of the actions of insulin. Upon activation of insulin signalling, Akt regulates uptake of glucose into muscle, adipocytes, liver and other cells by causing the translocation of glucose transporters from intra cellular stores to the plasma membrane. Mice that genetically lack Akt develop insulin resistance and have other classical phenotypes that mimic T2DM, and go on to develop overt DN. There are 3 main isoforms of PKC, and it has been demonstrated that each contributes to the complication of DN (Geraldes & King, 2010b). Menne and colleagues have reported that diabetic PKC-$\alpha^{-/-}$ mice are resistant to the development of albuminuria and glomerular hyperfiltration stimulated by vascular endothelial growth factor (VEGF) (Menne et al., 2004). PKC-α is

associated with nicotinamide adenine dinucleotide phosphate (NADPH)-dependant superoxide production (Thallas-Bonke et al., 2008). Deletion of the PKC-β protects against DN by preventing renal hypertrophy, glomerular hyperfiltration, reduced production of ECM, TGF-β1 and ROS) (Koya et al., 2000). It has also been demonstrated that down-regulation of Akt due to hyperglycaemia contributes to p38 MAPK-mediated apoptosis, fibrosis which leads to development of DN (Rane et al., 2010).

1.3.4 Oxidative stress in diabetic nephropathy

Hyperglycaemia leads to an excess of available glucose to enter the mitochondrial respiratory chain complex to create ATP. Simply, most glucose that enters cells gets converted to pyruvate, which then enters the Kerbs cycle to generate ATP, NADH and flavin adenine dinucleotide ($FADH_2$). Both NADH and $FADH_2$ are generated in the cytosol and become electron donors for oxidative phosphorylation. Electrons from these molecules are transferred to molecular oxygen in the mitochondrial respiratory chain (complex I-IV) to generate ATP. Under normal physiological states, less that 1 % of molecular oxygen is converted to superoxide anion, which can cause pathological damage. However, in hyperglycaemic states there is an excess of free electrons at two sites in the electron transport chain: one at complex I, and the other at the interface between coenzyme Q and complex III. As a result, there is an excess of superoxide anions produced that can combine with other free radicals to produce damaging ROS (Bondeva & Wolf, 2014). Interestingly, glomerular mesangial cells, retinal capillary endothelial cells and neurons are known to be unable to regulate intracellular glucose levels in diabetes. This results in the generation of

excessive levels of superoxide within these cell types subjecting them to increased ROS-mediated oxidative stress and leads to functional decline.

ROS mediate cellular damage in a number of ways. Most of the effects directly target DNA causing single or double strand breaks, or by disrupting histones. Mitochondrial DNA is deficient in histones and is, therefore, more susceptible to damage from ROS. ROS-mediated damage caused to mtDNA is more extensive and more persistent than damage to nuclear DNA (Yakes & Van Houten, 1997). ROS can also induce cellular damage by disrupting the efficiency of numerous enzymes. The repetitive production of excessive ROS under hyperglycaemic conditions can damage various enzymes of the electron transport chain. This ultimately leads to reduced ATP production, effecting cytochrome C translocation, activation of caspases and predisposing the cell to undergo apoptosis or necrosis, which leads to loss of function and organ injury. The MAPK downstream mediators including c-Jun N-terminal kinase (JNK) is strongly up-regulated under oxidative stress in models of diabetes (Hirosumi et al., 2002). However, in mouse models of DN, JNK activation is dependent on the age of the mice; young diabetic mice showed little phosphorylation of JNK (activated), while old diabetic mice had increased levels of phosphorylation of JNK. This is consistent with other reports that older diabetic mice had higher oxidative stress levels in mesangial cells compared to young diabetic mice. This leads to cellular expansion and laying down of increased mesangial expansion (Wu et al., 2009). Importantly, it is postulated that elderly patients have increased levels of oxidative stress and as a result have worse clinical outcome compared to younger patients presenting with similar complaints. This could

suggest that conditions like diabetes, cause premature ageing (Ahima, 2009). Other downstream mediators of the MAPK pathways are also activated in response to oxidative stress, activating a number of key survival pathways mainly, apoptosis of immune cells, inflammation, growth/cell cycle arrest and cell differentiation (Son et al., 2011).

The polyol pathway is up-regulated as a result of hyperglycaemia; meaning glucose is utilised and converted to sorbitol in an NADPH-dependant manner. Sorbitol is enzymatically converted to fructose. This results in reduced availability of NADPH as an electron donor for oxidative phosphorylation and also for the regeneration of reduced glutathione (a potent antioxidant). Decreased levels of glutathione contribute to increased intracellular oxidative stress, which, in turn, increases cellular stress and apoptosis (Brownlee, 2001). Changes in the NADPH:NAD^+ ratio also have an inhibitory effect on glycolysis via the activation of PKC (Brownlee, 2001). Interestingly, fructose itself is directly nephrotoxic, leading to proteinuria, reduced GFR and increased proximal tubule injury (Beckerman & Susztak, 2014). Fructose is the end product of the polyol pathway, and under hyperglycaemic conditions more fructose is produced, which may be a contributing factor to renal dysfunction.

1.3.5 Fibrosis in diabetic nephropathy

Fibrosis is another common feature in DN. Expansion of the extracellular matrix is driven by hyperglycaemia. Podocytes display abnormal architecture including hypertrophy, which contributes to a decline in their function possibly contributing to the onset of DN. TGF-β1 is one of the key pro-fibrotic growth factors. Overexpression of TGF-β1 is responsible for apoptosis of podocytes

through the interaction of specific receptors (ALK5 and ALK1), which initiate a signalling cascade through the MAPK's. *In vitro* studies have shown that the diabetic milieu can activate p38 signalling in renal mesangial cells. Exposure to high glucose has also been demonstrated to induce the phosphorylation of p38 in mesangial cells (Wilmer et al., 2001), whilst glycated albumin can also induce phosphorylation of p38 in fibroblasts; both of these stimuli are key features in patients with DN (Daoud et al., 2001). Phosphorylation of p38 promotes the production of TGF-β1 and as a result the production of fibronectin. TGF-β1 signalling can then act in a positive feed back look to further activate p38, induce the synthesis of collagen and other ECM components by mesangial cells and fibroblasts (Chin et al., 2001). This suggests that activation of p38 may contribute to the development of renal interstitial fibrosis in DN, although other pathways may also contribute to renal dysfunction (Ban & Twigg, 2008b).

1.3.6 Local and systemic inflammation in diabetic nephropathy

Hyperglycaemia is a key driver of low-grade chronic inflammation in diabetic patients with DN (García-García et al., 2014). On of the key pro-inflammatory pathways that hyperglycaemia directly activates is the NF-κB pathway. Upon activation, NF-κB translocates to the nucleus, where it acts as a potent transcription factor for many pro-inflammatory cytokines (IL-1b and IL-6) and mediators (pro-caspase1). NF-κB can be found localised to the glomerulus, interstitial and tubular epithelial cells of the diabetic human kidney. Under hyperglycaemic condition, NK-κB activation is increased which correlates with

proteinuria and interstitial cell infiltration. Acute proteinuria is also known to further stimulate NK-κB which is regarded as a key driver of long-term proteinuria (Sanz et al., 2010). Recruitment of macrophages to the diabetic kidney produces a plethora of pro-inflammatory factors that contribute to the progression of DN. The high number of macrophages and over-production of macrophage-derived cytokines (IL-1β, TNF-α and IFN-γ) are responsible for increased vascular inflammation, leading to mesangial expansion and fibrosis, which eventually manifest in functional decline and urinary proteinuria.

The JAK/STAT pathways can be activated by both hyperglycaemia and ROS; transducing chemical signals from outside of the cell to regulate gene promoter activity (Chuang & He, 2010). JAK2 mRNA levels have been demonstrated to be inversely correlated with estimated GFR in patients with DN (Berthier et al., 2009). Treatment of inflammation in diabetes is a complicated field, as steroids are not only ineffective, but may indeed further increases blood glucose. In fact, long-term steroid treatment may lead to the development of diabetes (Hwang & Weiss, 2014).

1.4 The Blood brain barrier

There is now emerging evidence that there is a strong link between diseases of aging, chronic inflammation and cognitive decline. Indeed Alzheimer's disease is often referred to as diabetes type-3, indeed there is increasing evidence that the use of anti-diabetic drugs may have therapeutic benefit in treating Alzheimer's disease (Femminella et al., 2017).

1.4.1 The history of the BBB

The BBB is a specialised endothelial barrier with 3 main biological functions, (1) the barrier maintains homeostasis within the central nervous system (CNS), it carriers out the unique function by strictly limiting the passive diffusion of polar substances from the blood to the brain, (2) mediating the transport of nutrients to the brain parenchyma as well as the efflux of toxic metabolites from the brain and (3) regulating the migration of circulating immune cells into the brain. The German physiologists Paul Ehrlich and Edwin Goldman first investigated the BBB and found that water-soluble dyes injected into the peripheral circulation did not stain the brain or colour the cerebrospinal fluid (CSF), but stained other organs. This work later contributed to Paul Ehrlich winning the Nobel Prize for Medicine in 1908, for his contribution to chemotherapy. Later work by Broman and Friedemann in the early 1940's demonstrated that the brain could be stained when lipid soluble dyes where injected into the peripheral circulation, but this was by directed transport. They postulated that there were two protective barrier, the blood-CSF barrier at the chorid plexus and the BBB at the cerebral microvasculature that stopped the free movement of substance from the blood and interstitial fluids. Later work showed that the BBB has especially tight

junction in the endothelial capillaries. Some very elegant experiments from Stewart and Wiley (Stewart & Wiley, 1981) demonstrated the extreme tightness of the capillary network if the BBB compared to those in other peripheral organs. Whereby, they demonstrated the extreme tightness of brain endothelial cells was due to their proximity to the neuronal environment.

1.4.2 The structure of the blood brain barrier

The main component of the BBB is brain microvascular endothelial cells (BMEC). Compared to endothelial cells of the peripheral capillaries BMEC demonstrate extreme tightness, is this has been evidenced by a much higher transendothelial electrical resistance measurement of ~1500 Ω.cm^2 in *in vitro* systems while values as high as 5900 Ω.cm2 have been recorded *in vivo* (Srinivasan et al. 2015)(Butt et al., 1990), compared to 100-140 Ω.cm^2 in peripheral gastro intestinal tract epithelial barriers (Artursson et al., 2001). This enhanced tightness is due, in part, to the presence of strong adhesion molecules including adhesion junctions, tight junctions and other actin binding structures.

Adhesion junctions play a key role in the development and maintenance of the sealed endothelial as a barrier. The main component of this family is VE-cadherin, a Ca^{2+} regulated protein that mediates cell-cell adhesion via interactions with extracellular domains. The cytoplasmic portion of the VE-cadherin is both directly and indirectly linked to the actin cytoskeleton by scaffolding proteins catenins and members of the p120 family. This allows for the neighbouring cells to be anchored to each other through their cytoskeleton. VE-cadherin's and other family members. One key mechanism that regulates

strong interaction involves the phosphorylation of VE-cadherin that allows it to interact with β-catenin.

Similarly, tight junctions contribute directly to the tightness of the BBB. First discovered in 1960s by electron microscope, they were described as kissing points between two endothelial cells on their outer leaflet of the cell. Tight junctions have a complex proteomic composition that greatly depends on their location. Post capillary venules have very weak tight junction, to facilitate the rapid blood-tissue exchanges. While the tight junctions present in the BBB are the most restrictive and complex, which results in, limited passage of polar molecules. The tight junctions are formed by an array of transmembrane molecules including, claudins, occuldins and junction adhesion molecules, these molecules recruited by membrane-associated cytoplasmic proteins.

BBB disruption has been implicated in many diseases of the CNS (e.g. stroke, multiple sclerosis, cerebral infection, brain tumours, Parkinson's and Alzheimer's diseases). The most prominent mechanism(s) governing these disruptions have been associated with maintaining the integrity of tight junctions. The key feature that regulates BBB tightness tight junctions integrity is site-specific phosphorylation; in many disease settings these key regulatory phosphorylation's are lost. This can lead to tight junctions being degraded and disrupts their cellular translocation. A number of noxious stimuli including ROS, hypoxia, glutamate and amyloid-β peptide, have been shown to signal through RhoA and MAPK pathways to downregulate phosphorylation of occludin and claudin. More, recently there has been a strong association with both diabetes

and metabolic syndrome, and a loss of BBB integrity, which is not classically linked to the CNS.

1.5 Annexin-A1

1.5.1 Glucocorticoids in inflammation

Glucocorticoids are a class of corticosteroids produced in the adrenal gland that bind specifically to the glucocorticoid receptor. Glucocorticoids are involved in the regulation of glucose metabolism, synthesised in the adrenal cortex, but their most potent function is to reduce inflammation. Tissue from the adrenal gland was used to treat adrenal failure from as early as the 1930's. Research from Edward Kendall at the Mayo Clinic, and Tadeusz Reichstein in Zurich suggested that it was not one single chemical (or cortical hormone) that exerted these effects, instead, the effect was caused by a group of steroids (Sternberg & Judd, 2009) Early in the 1940's, it was understood that there were two types of steroids, those that caused sodium and fluid retention (mineralocorticoids) and those that counteracted shock and inflammation (glucocorticoids) (Neeck, 2002). In 1948, the first glucocorticoid, cortisone, was administered to a patient by rheumatologist Philip Hench to treat rheumatoid arthritis (Hench, kendall, Slocumb and Polley, 1950). The above discoveries won Kendal, Reichstein and Hench the Nobel Prize for Medicine or Physiology in 1950.

Much research has revolved around how glucocorticoids supress pro-inflammatory mediators and reduce excessive inflammation. Numerous synthetic glucocorticoids have been developed with varying potency and wide-ranging therapeutic indications. It is widely accepted that glucocorticoids work in a multifaceted manner, making them very interesting from a pharmacological point of view, however, they may result in significant side-effects ranging from headaches and gastric ulcers, to life threatening immunosuppression (Strehl &

Buttgereit, 2016). It was historically thought that the majority of the effects of glucocorticoids resulted from the direct or indirect reduction in the transcription of pro-inflammatory genes, but it is now widely accepted that many mediators are up-regulated upon delivery of these drugs. (Chatzopoulou et al., 2016). One such mediator was lipocortin-1, now known as annexin-A1 (ANXA1).

1.5.2 ANXA1 an anti-inflammatory mediator of glucocorticoids

ANXA1 was first characterised as secondary mediator of the anti-inflammatory effect of glucocorticoids hormones (Flower & Blackwell, 1979) such as preventing leukocyte migration into inflamed tissue (Solito and Parente, 2004). ANXA1 belongs to the large family of proteins called annexins (ANXA1-12).

By definition, annexins are proteins with a conserved structural region known as the 'annexin' repeat (a chain of around 70 amino acid residues), capable of binding in a Ca^{2+} dependant manner to negatively charged phospholipids (Gerke & Moss, 2002). ANXA1 is a 37-kDa protein comprising of a C-terminal core domain containing a Ca^{2+}/phospholipid binding site. This binding site contains four homologous repeats (numbered I – IV) of 5 α-helices each. This region is well conserved amongst all members of the annexin family; however, the N-terminal tail varies between annexin members. It is this specific sequence of 41 amino acids that gives ANXA1 its unique function compared to other annexins (Rosengarth et al., 2001). ANXA1 is widely distributed in numerous cell types including the endothelium, cardiomyocytes, glomerular fibroblasts and platelets, but the largest concentrations of ANXA1 are found in cells of myeloid and lymphoid lineage. Considering the potent anti-inflammatory effects of ANXA1, it

is not surprising that there are high levels of expression in these cells, and this explains why most of the research involving ANXA1 has been conducted in cells of this lineage.

Healthy volunteers administered glucocorticoids have increased ANXA1 expression on circulating monocytes and neutrophils (Goulding et al., 1990). Interestingly, ANXA1 levels are also modulated in diseases where glucocorticoids levels are altered. In diseases where cortisol is reduced, i.e. Addison's disease, patients exhibit lower levels of ANXA1 than healthy volunteers. On the contrary, in diseases presenting with excessive cortisol levels, i.e. Cushing's syndrome, ANXA1 levels are elevated (Mulla et al., 2005). These data suggest that the regulation of ANXA1 is under the control of the glucocorticoid receptor. The promoter of ANXA1 does not appear to have a canonical glucocorticoid response element, however, it has a partial consensus binding-site for the IL-6 response element (Solito et al., 1998). However, its does harbour a glucocorticoid response element half palindrome in the intron upstream the first not-translated exon (Solito et al., 1998).

Research by Solito *et al*. has elucidated some of the transcriptional mechanisms by which ANXA1 is expressed upon dexamethasone stimulation of the macrophage like cell-line U-937 (Solito et al., 1991). In mature macrophage-like U-937 cells, there were no time-dependant effects on ANXA1 mRNA production, but there was a considerable increase in ANXA1 release into the supernatant after dexamethasone administration, a process not observed in immature U-937 cells (Solito et al. 1991). The release of ANXA1 upon glucocorticoid stimulation

was controversial at the beginning, as ANXA1 does not contain a leader peptide for the secretion, but it is now accepted that the secreted form of ANXA1 could potentially elicit the anti-inflammatory effects of glucocorticoids. Glucocorticoid-stimulated ANXA1 production has subsequently been observed in macrophages, neutrophils, thymocytes, fibroblasts and squamous carcinoma cells (D'Acquisto et al., 2008).

ANXA1 has a number of phosphorylation sites. The most notable phosphorylation site is that of serine-27. Early experiments using mutant clones proved that phosphorylation of this site is needed to the conformational change allowing N-terminal domain release and for ANXA1 membrane aggregation. Later work demonstrated that PKC catalysed the phosphorylation of ANXA1 in cultured rat mesangial cells *in vitro,* but only in the presence of Ca^{2+} and phospholipids. However, phospholipids alone were not sufficient to support the phosphorylation. Further experiments on ^{32}P-labeled mesangial cells demonstrated that ANXA1 phosphorylation was increased by the addition of PKC activators such as angiotensin II. PKC phosphorylation of ANXA1 is essential for both cellular export and biological activity. Interestingly, dexamethasone induced signaling that causes the translocation of a serine phosphorylated-ANXA1 to the cytoplasmic membrane of human folliculostellate cells. These results suggest that glucocorticoids induce rapid serine-27 phosphorylation and membrane translocation of ANXA1 via a novel glucocorticoid receptor-dependent mechanism, which requires MAPK, PI3K and Ca^{2+} dependent PKC pathway (Perretti & D'Acquisto, 2009).

1.5.3 Mechanism of ANXA1 release and action

Under normal physiological conditions, ANXA1 is stored in granular vesicles of e.g. neutrophils. During cell activation (through pro-inflammatory or glucocorticoid stimulation), ANXA1 rapidly translocates to the cell surface where it is externalised and/or secreted. This effect has been shown to occur both in a dose- and time-dependant manner, upon dexamethasone stimulation (McLeod et al., 1995)

Translocation of ANXA1 to the cell membrane is highly regulated and involves a number of different mechanisms depending on the cell type, the most well studied being the neutrophil. ANXA1 can be rapidly released by weak activation signals, such as low concentrations of chemoattractants or upon adhesion to endothelial cell monolayers (Perretti et al., 1996). More often than not, these stimuli result in ANXA1 relocating to the outside leaflet of the plasma membrane, where it becomes tethered in a Ca^{2+}-dependent manner (Gerke et al., 2005). In macrophages, the ATP-binding cassette transporter has been demonstrated to facilitate the secretion of ANXA1, while in pituitary cells, the phosphorylation of Ser-27 is required for translocation of ANXA1 (Wein et al., 2004). It has also been shown that ANXA1 can be directly secreted from it storage granules and secreted via exocytosis.

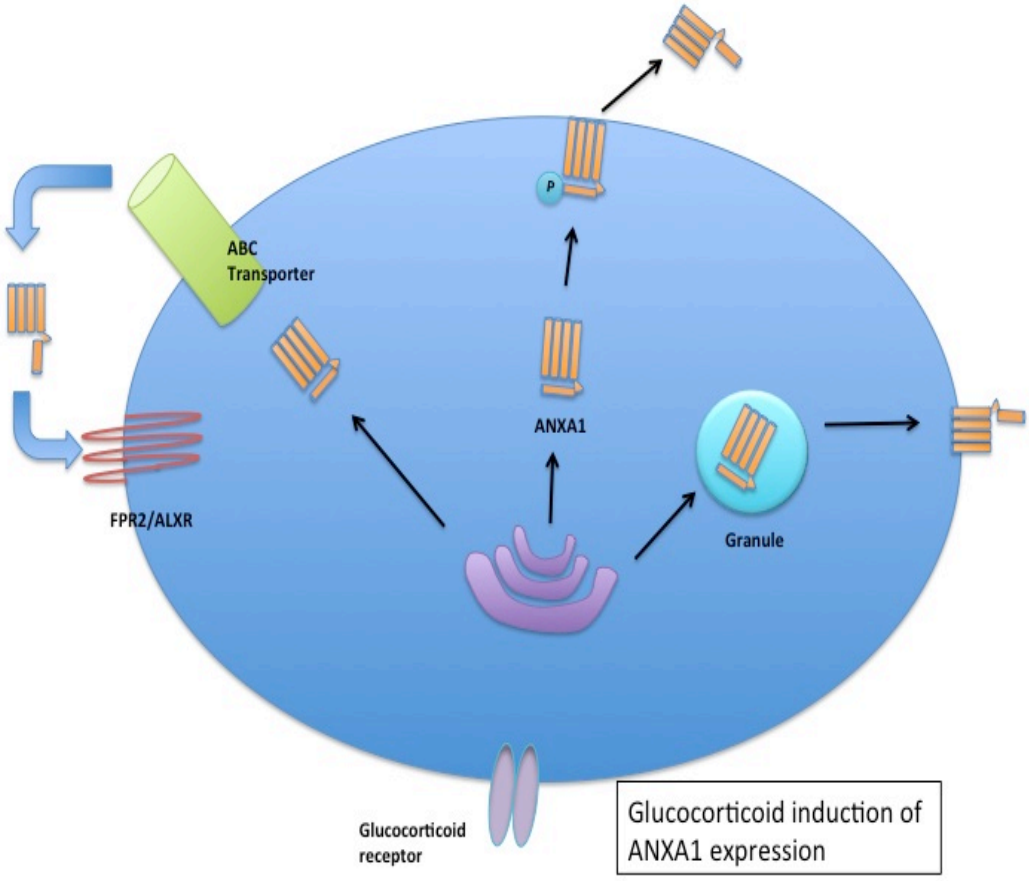

Figure 3. Potential mode of action of ANXA1 in activated cells

Upon cell activation, ANXA1 can be mobilised to the plasma membrane and then secreted, or externalised in one of three mechanisms depending on the cell type involved. Mechanisms involve; through the activation of the ATP-binding cassette (ABC) transporter (1); through the phosphorylation of the serine-27 residue followed by membrane localisation to specific lipid domains, before being moved to the outer leaflet of the plasma membrane to be secreted (2); through fusion of ANXA1 loaded granules to the plasma membrane allowing ANXA1 to be excreted by exocytosis (3). Once released, ANXA1 can act in an autocrine, paracrine or juxtacrine fashion to activate FPR2/ALXR signalling. Adapted from (Perretti & D'Acquisto 2009).

1.5.4 The ANXA1 receptor

ANXA1 acts in both autocrine and paracrine fashions exerting numerous potent functions, and ANXA1 also plays an important role as intracellular mediator. Initial studies demonstrated the presence of ANXA1 on the cell surface of both human and rodent peripheral blood leukocytes, and consequently, autocrine and

paracrine mechanisms of ANXA1 action have been intensively studied (Goulding et al., 1990). Among the most studied receptors in this area include the seven transmembrane G-couple protein receptor formyl peptide receptor (FPR) family (Perretti, 2003). This family of receptors was first identified on the cell surface of neutrophils as the receptor for the chemoattractant N-formylated peptide (from bacterial and host cell-derived mitochondrial protein degradation), however, further research of the FPR receptors has identified a wide range of ligands, including endogenous acute phase response molecules (serum amyloid A), endogenous lipids (resolvin-D_1, lipoxin A_4) and pathogenic molecules (β-amyloid) (Le et al., 2002). To date, 3 FPR subtypes have been characterised in humans: FPR1, FPR2 (also known as FPR like 1 or FRPL-1, lipoxin A_4 receptor and FPR3, all of which have a wide range of endogenous and exogenous ligands, with different affinities (Perretti, 2003). However, other species have more FPR subtypes, for example, mice have 7. These receptors are expressed on a wide variety of cell types, but are more abundant on immune cells such as leukocytes, neutrophils, but are also present on fibroblasts, endothelial cells, and stromal cells. It is now also clear that FPR's are also expressed in the microvascular endothelium (Solito et al., 2008). In the context of ANXA1 biology, the FPR2 has been most extensively studied. It has previously been demonstrated that ANXA1 can signal through this receptor; co-localisation studies have shown that the FPR2 and ANAX1 do in-fact co-localise during both normal physiological and in disease states (Neymeyer et al., 2015).

From a structural point of view, ANXA1 has to undergo a major conformational change following activation (phosphorylation of Ser-27) to allow its N-terminal

domain to be accessible to bind to its respective receptor (Figure 1.4C) (Bena et al., 2012). In its inactive form, (in the absence of calcium) the N-terminal domain of ANXA1 is 'buried' in the core domain. When extracellular concentrations of calcium exceed 1 mM, and upon membrane binding, the loop of repeat III folds into the D-helix resulting in a conformational change of ANXA1 (Figure 1.4A.B) (Rosengarth et al., 2001). This conformational change allows the hidden N-terminus to vacate the hydrophobic pocket of repeat III and to be exposed to interact with specific receptors (Migeotte et al., 2006)

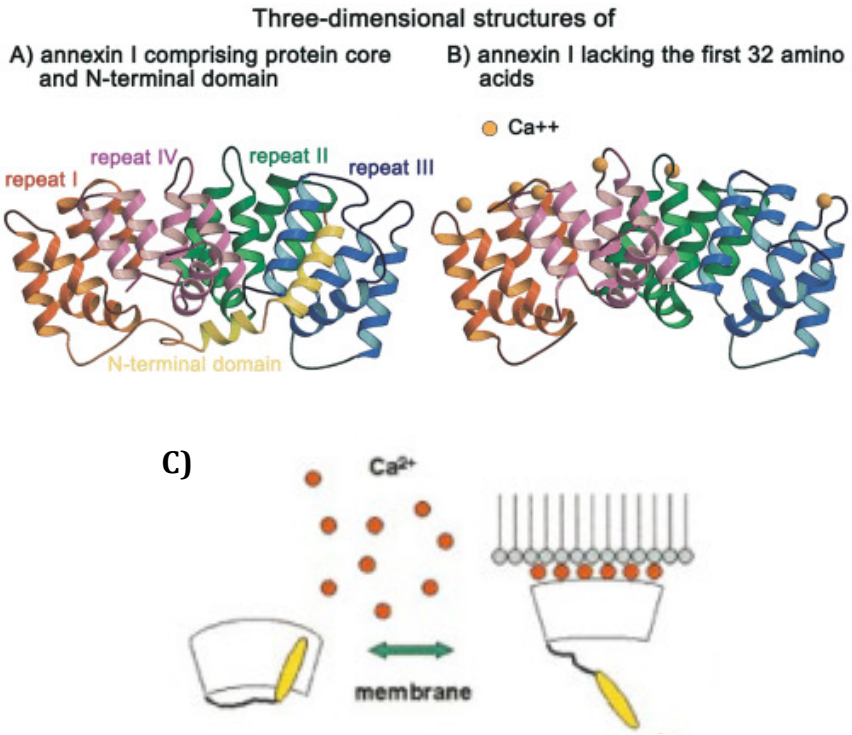

Figure 1.4. Crystallised structure of ANXA1 (A) and (B) and how the N-terminus is revealed in high Ca^{2+} (C). (Adapted from Migeotte et al, 2006).

1.5.5 Functions of ANXA1

Annexin-A1 has wide variety of biological effects ranging from cell-growth regulation, tumourigenesis, cell differentiation, and neuroendocrine regulation. The majority of studies have focused on the anti-inflammatory effects of ANXA1 in the periphery, and this research has been aided by the development of ANXA1$^{-/-}$ mice. These mice show an excessive inflammatory response in animal models of disease associated with inflammation. Moreover, the ability of glucocorticoids to reduce inflammation is attenuated in these mice. It is also important to note that ANXA1 has been shown to mimic most, if not all, of the anti-inflammatory effects of glucocorticoid in several inflammatory models (Kamal et al., 2005).

One of the most potent anti-inflammatory actions of ANXA1 is mediated by the proteolytic cleavage of the N-terminus, which releases a 24 amino acid peptide named the AC_{2-26}. This peptide prevents the phosphorylation and activation of phospholipase A_2. These findings have also been confirmed in *in vivo* studies using ANXA1$^{-/-}$ mice; during inflammatory conditions, demonstrating that both PLA_2 expression and activity are decreased (McArthur et al., 2010). Other inducible enzymes are targets of ANXA1, including inducible cyclooxygenase-2 (COX2) (Minghetti et al., 1999). COX-2 is important in the conversion of arachidonic acid into pro-inflammatory mediators such as prostaglandins (Vishwanath et al., 1993) (De Caterina et al., 1993). Inducible nitric oxide synthase is also regulated by ANXA1, which in turn is involved in the production of nitric oxide. ANXA1 has the ability to directly and indirectly affect the production and release of other pro-inflammatory mediators including

cytokines, histamine and ROS at the innate immune cell level, however, little is known about how ANXA1 can regulate pro-inflammatory mediators in other cell types (D'Acquisto et al., 2008).

Another striking feature of ANXA1 biology is its potent ability to halt the migration and extravasation of leukocytes into inflamed tissue. Immune cells migrate into the site of inflammation in a highly ordered and regulated manner (Luscinskas et al., 1996). Firstly, endothelial cells at the site of inflammation cause white blood cells to roll in a process mediated by selectins. The rolling cells undergo firm adhesion and arrest, mediated by integrins, allowing the cell to undergo paracellular and transcellular extravasation into the site of inflammation. Interestingly, upon leukocyte-endothelium adhesion ANXA1 is mobilised, inhibiting the ability of neutrophils to adhere and transmigrate to the site of inflammation. Full length ANXA1 and truncated ANXA1 (Ac2-26) have differential effects on these processes; full length ANXA1 inhibits firm adhesion of human PMNs, while Ac2-26 significantly attenuates capture and rolling without effect on firm adhesion (Hayhoe et al., 2006). These data suggest specific functions of both the full length ANXA1 and the cleaved N-terminus (Hayhoe et al., 2006). The mechanism by which ANXA1 inhibits these processes is not fully characterised, but it has been reported that ANXA1 causes L-selectin to be shed from the leukocyte membrane blocking rolling and firm adhesion (Solito et al., 2003). Co-immunoprecipitation experiments have shown that ANXA1 competes for the $\alpha_4\beta_1$ binding site in U-937 cells (Solito et al., 2000). As a result, ANXA1 inhibits the ability of PBMN'c to firmly adhere to the endothelium (de Coupade et al., 2003). These two differing anti-inflammatory properties could help explain

why ANXA1 and its truncated peptide are protective in models of myocardial ischaemia-reperfusion injury (La et al., 2001) and stroke (Gavins, Granger, & Perretti, 2006), as large immune cell infiltration to the ischaemic area is present upon reperfusion in both of these models and contributes to the extension of infarct size.

It has also been suggested that ANXA1 may negatively affect immune cell viability, which may explain some of its anti-inflammatory properties, and may also explain how glucocorticoids potentially elicit their potent anti-inflammatory effects. ANXA1 activates the caspase-3 signalling pathway (Parente & Solito, 2004), which is highly up-regulated during apoptosis. Programmed cell death is one of the mechanisms by which inflammatory cells mediate their anti-inflammatory actions and as a result these processes tightly regulated, and could explain how ANXA1 provides its anti-inflammatory effects and aids in the resolution of inflammation. Research suggests that ANXA1 can act as a clearance signal on apoptotic cells, promoting chemotaxis of macrophages and clearance of cellular debris from the site of injury; therefore, ANXA1 may aid in the resolution of inflammation and reduce further injury caused by changes in structure (Solito et al., 2003).

One other interesting role of ANXA1 is within the blood brain barrier; ANXA1 is expressed in BMEC, where it regulates BBB integrity. Most notably, ANXA$^{-/-}$ mice exhibit significantly increased BBB permeability as a result if disrupted inter-endothelial tight junctions. These findings support the view that ANXA1 stabilises tight junction through the interaction with the actin cytoskeleton

(Cristante et al., 2013). It is also important to note that in inflammatory states BBB integrity is lost. Activation of FPR2 by ANXA1 inhibits the small GTPase RhoA, which when activated destabilises the actin cytoskeleton, and enhances paracellular permeability (Cristante et al., 2013).

1.5.6 ANXA1 as a pharmacological agent

Pharmacologically, ANXA1 has been used in numerous models of acute and chronic inflammation. The N-terminus of ANXA1, the peptide Ac2-26, reduces inflammation and tissue-injury in acute models of inflammation *in vivo,* including cardiac ischaemia-reperfusion injury (La et al., 2001) (Zhang et al., 2011), neutrophil-dependant oedema (Perretti et al., 1993) and antigen-induced arthritis (Yang et al., 2004). Ac2-26 can promote locomotion of human primary cells, peripheral mono-nucleated cells and monocytes; this effect is, at least in part, due to a chemokinetic rather than chemotactic effect of the peptide. These data suggest that the cleavage of ANXA1 and the consequent generation of Ac2-26 during the resolution of inflammation may play an important role in the removal of blood-borne cells from the tissue. Tissue protective effects of Ac2-26 have been reported to be mediated primarily through ERK, but not the JNK or p38 pathways (Dalli et al., 2012). Thus, Ac2-26 may enhance the resolution of inflammation, and delivery systems are in development to achieve sustained slow release and a longer half-life of Ac2-26. In an *in vivo* model of colitis, treatment with polymeric nanoparticles containing Ac2-26 peptide has been found to promote epithelial wound healing (Leoni et al., 2015).

More recently, the full-length human recombinant (hr) ANXA1 has been demonstrated to have pharmacological potential *in vivo*. There is strong evidence suggesting that ANXA1 has a stronger binding affinity to it receptor than Ac2-26 (Solito et al., 2000). Moreover, the concentrations needed to elicit the same anti-inflammatory effects are some 20 times higher when using the Ac2-16 peptide compared to full length ANXA1 (Solito et al., 2000). There is strong sequence homology between the murine and human ANXA1 peptide, but specifically, there is near 100% homology in the N-terminus. The full length peptide has been shown to be effective in treating acute inflammatory condition, but also prolonged treatment with the full length hrANXA1 was able to reduce atherosclerotic plaque size in $LDLR^{-/-}$ mice on a high fat western diet (Kusters et al., 2015a). This proof of concept study suggests that not only is prolonged treatment with ANXA1 tolerated, but also that prolonged treatment does not result in severe adverse effects akin to those seen with prolonged steroid treatment.

1.5.7 ANXA1 and diabetes

To date little work has been conducted into ANXA1 and diabetes. ANXA1 is endogenously expressed in the islets of the pancreas, where it co-localises with insulin secretory granules (Ohnishi et al., 1994), and ANXA1 has been suggested to influence glucose-stimulated insulin secretion in an autocrine or paracrine manner (Ohnishi et al., 1995). Extracellular ANXA1 binding to a putative cell surface receptor increases insulin secretion in isolated rat pancreatic islets. In a Ca^{2+} independent fashion (Hong et al., 2002). However, insulin secretion is not altered when measured from pancreatic islets isolated from $ANXA1^{-/-}$ mice,

suggesting in the acute control of glucose-stimulated insulin release by ANXA1 signalling is redundant (Rackham et al., 2016). More recently, it has been demonstrated in islet graft that islet cells that are co-grafted with mesenchymal stromal cells improve graft survival and function. Additionally, when mesenchymal stromal cells that have be pre-cultured with ANXA1 and co-grafted with islet cells demonstrate an improvement in insulin secretion, one of the key measures of islet function. However, pre-incubating mesenchymal stromal cells with ANXA1 before co-graft with islet cells did not alter graft survival (Rackham et al., 2016).

Interestingly, ANXA1 seems to play a role in not only in the secretion of insulin but also in inhibiting the auto-phosphorylation of the insulin receptor, which is needed for successful transduction of insulin signalling. This effect was specific for insulin-stimulated tyrosine kinase activity and required the N-terminal end of the protein containing the a phosphorylation site on Tyrosine-21 (Melki et al., 1994). What makes this function curious is that insulin-sensitive cells such as hepatic cells or differentiated adipocytes do not express large amounts of ANXA1 (Karasik et al., 1988) (Wong etal., 1992). In contrast, endothelial cells contain high contain large concentrations of ANXA1, and process receptor-bound insulin, differently from most other cell types, resulting in receptor mediated transcytosis (Bottaro et al., 1989).

The key drivers of T2DM are diet-induced obesity and lack of exercise, leading to insulin resistance, subsequent hyperglycaemia and low-grade chronic inflammation. ANXA1 mRNA and ANXA1 protein levels are down- modulated in

HFD-induced insulin-resistance/type-2 diabetes in mice (Akasheh et al., 2013). Rand *et al.* discovered that ANXA1$^{-/-}$ mice fed a HFD gained more fat mass and had larger adipocyte size than their WT littermates fed the same diet, but critically there was no underlying alteration in inflammation arising from a HFD compared to WT littermates, measured by a range of pro-inflammatory cytokines (IL-6, IL-1β and IL-10). One of the key drivers of secondary complications in animal models of T2DM is chronic low-grade inflammation; therefore, reducing the concentration of an anti-inflammatory molecule (e.g. ANXA1) may well exaggerate the problem. In an *in vivo* model of insulin resistance (as a result of high fat diet) Yoon *et al*. found that ANXA1 expression was reduced in smooth muscle and the liver. Similarly, his finding was confirmed in an *ex vivo* proteomic analysis of palmitate-induced insulin resistance, which reported that both ANXA1 and FPR2 expression were decreased in smooth muscle cells (Yoon et al., 2015). Interestingly, in another study, mice given a HFD exhibited increased ANXA1 concentrations in adipose tissue compared to mice given a normal chow diet. This study demonstrated macrophage switching from M1 to M2 phenotype within the adipose tissue in mice fed on HFD mice, when compared to control chow fed mice. This suggests that ANXA1 may up-regulate the number in M2 (resolving) macrophages aiding resolution of inflammation (Börgeson et al., 2015). These two conflicting pieces of evidence suggest that there may be tissue-specific changes in ANXA1 expression.

There have also been a number of studies into patients who are classed as obese, reporting that there is a strong inverse relationship between increased weight, body mass index (BMI) and waist to hip ratio to levels of ANXA1 in the serum.

These data suggest that there may be a mechanism in obesity by which the active secreted form of ANXA1 is inactivated, or that ANXA1 expression is down-regulated. Furthermore, Petrani et al. compared plasma ANXA1 levels in patients with T2DM with no nephropathy and patients with T2DM who had nephropathy. This study found that plasma ANXA1 levels were lower in patients with T2DM and nephropathy compared to those with no nephropathy. (Pietrani et al., 2014).

1.6 Hypothesis

The hypothesis of this thesis is that ANXA1 play a key protective in diabetes. ANXA1 is well known for its anti-inflammatory and pro-resolving actions therefore, I postulate that ANXA1 levels may be modulated in diabetes and have an important function as an endogenously produced molecule. I postulate that AXNA1 maybe an endogenous mediator with protective properties against the development of microvascular complications in diabetes. Additionally, ANXA1 is known to play an important role in the regulation of the tightness of the BBB, here I hypothesis that the permeability of the BBB will be reduced do to the presence of T2DM, thus leaving the brain parenchyma vulnerable to infiltrating immune cells.

1.7 Aim of this thesis

There is a need for a better understanding of the pathophysiology of diabetes and for more specific interventions to treat the microvascular complications of diabetes.

To do this I have used plasma samples from healthy volunteers and patients with both T1DM and T2DM, as well as two murine models of inducible experimental diabetes investigate the role of ANXA1 in diabetes. Therefore the objectives of this thesis are:

- To measure the plasma levels of ANXA1 in patients with T1DM.
- To investigate the role of endogenous ANXA1 in the pathophysiology of type-1 diabetes in a STZ-induced model of type 1 diabetes in mice.
- To investigate if endogenous AXNA1 is protective against the development of microvascular complication (diabetic cardiomyopathy and diabetic nephropathy) in a STZ-induced model of T1DM in mice.
- Investigate if prophylactic treatment with human recombinant ANXA1 can be used to alter the diabetic phenotype, and prevent the development of microvascular complications in a STZ-induced model of T1DM in mice.
- Investigate if late therapeutic intervention with human recombinant ANXA1 after microvascular complications have developed can halt their progression in a STZ-induced model of T1DM in mice.
- To measure the plasma levels of ANXA1 in patients with T2DM.
- To investigate the role of endogenous ANXA1 in the pathophysiology of type-2 diabetes in a high-fat high-sugar model of obesity induced T2DM.

- To investigate if endogenous AXNA1 is protective against the development of microvascular complication (diabetic nephropathy) in a high- fat high-sugar model of obesity induced T2DM.
- Investigate if treatment with human recombinant ANXA1 can be used to alter the diabetic phenotype, and prevent the development of microvascular complications in a high- fat high-sugar model of obesity induced T2DM.
- To investigate if feeding a high-fat high-sugar diet alters the permeability of the blood brain barrier, and how endogenous AXNA1 regulated BBB integrity.
- If treatment with hrANXA1 to mice fed a high-fat high-sugar diet can restore BBB integrity and reduce BBB permeability.
- To investigate if feeding a high-fat high-sugar diet alters the peripheral T-cells population, and if treatment with hrAXNA1 can attenuate these changes.
- To investigate if isolated lymphocytes from mice fed a high-fat high-sugar diet have an altered ability to adhere to or transmigrate through a brain microvascular endothelial cell monolayer.

Overall, it is hoped that the finding of these studies will elucidate the role of endogenous ANXA1 in the pathophysiology of diabetes and its complication, and give insight into the potential of AXNA1 as a novel therapeutic intervention.

Chapter II:

The role of Annexin-A1 in the microvascular complications of type-1 diabetes mellitus.

2.1 Introduction

Type 1 diabetes is an autoimmune disease often diagnosed in childhood characterised by loss of insulin producing beta cells, which leads to hyperglycaemia (Atkinson, 2012). Even with strict glycaemic control, using rigorous insulin management, microvascular complications including diabetic nephropathy (Papadopoulou-Marketou et al., 2016) and diabetic cardiomyopathy (Bugger & Abel, 2014) develop over time. These microvascular complications associated with diabetes are key drivers of morbidity (and ultimately mortality) and, therefore, put a significant economic burden on health care providers. DN is the primary cause of death ~20 % of patients with T1DM and cardiovascular disease, which includes diabetic cardiomyopathy, accounts for ~40 % of all fatalities in T1DM (Martín-Timón et al., 2014). Both pathologies are characterised by an impairment in function (kidney: proteinuria (Bhattacharjee et al., 2016); heart: impairment in systolic contractility) (Niemann et al., 2013) caused by local inflammation (Downs & Faulkner, 2015) and loss of survival pathways (Rask-Madsen & King, 2013), the latter of which predisposes tissues to injury.

One of the key pathways driving both DN and cardiomyopathy are hypertrophy. Previous studies have shown that the activation of the mitogen-associated protein kinase (MAPK) mediators (p38, JNK and ERK1/2) are key drivers of hypertrophy, fibrosis and localised inflammation. Previous studies have demonstrated that inhibitions or genetic deletion of these key kinases protects the diabetic heart and kidney from functional decline. ANXA1 is an endogenous

mediator with anti-inflammatory and pro-resolving activities (Flower & Blackwell, 1979). The C-terminal core domain of ANXA1 harbours three calcium-binding phospholipid domain, which is conserved amongst all family members, while the N-terminus varies, giving each family member its unique functionality (Rosengarth et al., 2001). We know that PKC is unregulated in diabetes and directly activated key effects kinase of the MAPK pathway. Additionally, PKC is essential for the phosphorylation of serine-27, which allows both the release of the N-terminus but also its release from its intracellular stores, where it can act in both and autocrine and paracrine manner to elicit its biological effects.

Endogenous ANXA1 levels are modulated in many autoimmune diseases including multiple sclerosis (Cristante et al. 2013), cystic fibrosis (Bensalem et al. 2005), Crohn's disease (Sena et al., 2013) and rheumatoid arthritis (D 'acquisto et al. 2008). While, human recombinant ANXA1 (hrANXA1) or its N-terminal peptide (Ac2-26) have therapeutic benefits in many experimental models of chronic disease, including rheumatoid arthritis (Renshaw et al., 2010), atherosclerosis (Kusters et al., 2015b) and non-alcoholic steatohepatitis (Locatelli et al., 2014), and in acute inflammatory diseases including sepsis, renal and cardiac ischaemia reperfusion injury (La et al., 2001).

2.1.1 Specific aims

The role of endogenous ANXA1, or the potential efficacy of hrAXNA1 as a novel therapeutic in T1DM is unknown. Therefore, this study was designed to investigate:

(1) the plasma levels of endogenous ANXA1 in patients with T1DM with/without diabetic nephropathy;

(2) the role of endogenous ANXA1 in an murine model of T1DM and in the subsequent development of microvascular complications (diabetic nephropathy and diabetic cardiomyopathy);

(3) if prophylactic daily administration with hrANXA1 prevents diabetic nephropathy and diabetic cardiomyopathy in an murine model of T1DM; and

(4) if therapeutic intervention with hrANXA1 (after microvascular complications have developed) can halt the progression of diabetic nephropathy and/or cardiomyopathy in an murine model of T1DM.

2.2 Methods and Materials

2.2.1 Use of human subjects-ethical statement

The study was approved by the research ethics committee and was undertaken in adherence to the Declaration of Helsinki. All subjects gave written informed consent. Patients with T1DM were recruited from the Diabetes Outpatient clinic of Guy's and St Thomas Hospitals (London) ethical committee number 10/H0802/86. Healthy donors were recruited from the William Harvey Research Institute (London) and both covered by ethical approval. Non-fasting plasma was obtained from patients with T1DM, with /without a diagnosis of diabetic nephropathy and healthy donors.

2.2.2 Human study population

T1DM was defined as onset of diabetes a) before the age of 25 and b) the need for continued insulin therapy within 3 months of diagnosis. Patients with diabetic nephropathy (DN+) had a documented positive history of early morning urine albumin creatinine ratio (ACR) ≥3.5 mg/mmol on two occasions, arterial hypertension defined as treatment with on one or more anti-hypertensive agents and/or blood pressure (BP) ≥130/80 mmHg, and diabetic retinopathy (as proof of another microvascular complication associated with diabetes) but no other kidney or urinary tract disease. Patients without diabetic nephropathy (DN-) had a history of normal ACR (<2.5 mg/mmol in men and <3.5 mg/mmol in women), normal BP (<130/80 mmHg) on no antihypertensive agents and a duration of diabetes exceeding 20 years. All patients had preserved renal function (serum creatinine <150 μmol/L), and a positive diagnosis of diabetic

retinopathy. Healthy donors are defined as having no diagnosis of diabetes and no history of hypertension BP <135/80 mmHg.

2.2.3 Use of animals - ethical statement

The animal protocols followed in this study were approved by the Animal Welfare Ethics Review Board (AWERB) of Queen Mary University of London in accordance with the derivatives of both the Home Office guidance on the Operation of Animals (Scientific Procedures Act 1986) published by Her Majesty's Stationery Office and the Guide for the Care and Use of Laboratory Animals of the National Research Council. All research was conducted project licenses reference numbers PPL: 70/8350. This study was carried out on ten week-old male C57BL/6 mice and ANXA1$^{-/-}$ mice, weighing 25–30 g (Charles River Laboratories UK Ltd., Kent, UK). The animals were allowed to acclimatise to laboratory conditions for a period of at least one week before any experimental procedures were initiated. All animals had free access to a standard diet and water *ad libitum*.

2.2.4 Streptozotocin (STZ) induction of type-1 diabetes

Diabetes was induced in male 10-week-old wild-type (WT) C57BL/6 or ANXA1$^{-/-}$ mice using streptozotocin (45 mg/kg i.p. in 0.9 M citrate buffer) for 5 consecutive days while sham mice received vehicle only (0.9 M citrate buffer i.p.) for 5 consecutive days. Mice were deemed diabetic if blood glucose level was > 12 mmol/L; blood glucose level was determined from blood taken from the tail vein using a glucose analyser (Accu-Chek Compact System; Roche

Diagnostics, Basel, Switzerland).

2.2.5 Drug administration

Mice were randomly assigned treatment group and administered hrANXA1 (1 ug, 100 µl, Hepes 50mM; 140 mM NaCl; pH 7.0, i.p.) or while vehicle 100 µl, Hepes 50mM; 140 mM NaCl; pH 7.0, i.p.). Previous studies in both acute and chronic models have shown that a daily bolus of 1 µg hrANXA1 to be a therapeutically relevant dose (Pederzoli-Ribeil et al. 2010)(Patel et al. 2012).

2.2.6 Oral glucose tolerance test

Oral glucose tolerance test was preformed before termination of the experiment. Briefly, mice were fasted for 16 h prior to testing. Then given an oral bolus of glucose (1 g/kg, H_2O), blood glucose (tail vein puncture) was measured at 15 min intervals for a maximum of 120 min using a glucose analyser (Accu-Chek Compact System; Roche Diagnostics, Basel, Switzerland).

2.2.7 Assessment of cardiac function

Cardiac function was assessed in mice by echocardiography *in vivo*. At weeks 7 and/or 13 after STZ induction of diabetes, anesthesia was induced with 3% isoflurane and maintained at 0.5 to 0.7% for the duration of the procedure. Before assessment of cardiac function, mice were allowed to stabilise for at least 10 min. During echocardiography, the heart rate was obtained from ECG tracing and the temperature was monitored with a rectal thermometer. Two-dimensional (B-Mode) and M-mode echocardiography images were recorded

using a Vevo-770 imaging system (VisualSonics, Toronto, Ontario, Canada). Fractional area change (FAC) was assessed from two-dimensional trace of B-mode (Figure 2.1A and B) by tracing the LV in the parasternal short axis at the level of the papillary muscle and the measurement is derived using the Equation 1. Percentage ejection fraction (EF) and fractional shortening (FS) were calculated from the M-mode measurements using LV internal dimension (LVID) in diastolic (d) and systolic (s) phases (Figure 2.1C) in the parasternal short axis view at the level of the papillary muscles using equations 2 and 3 respectively.

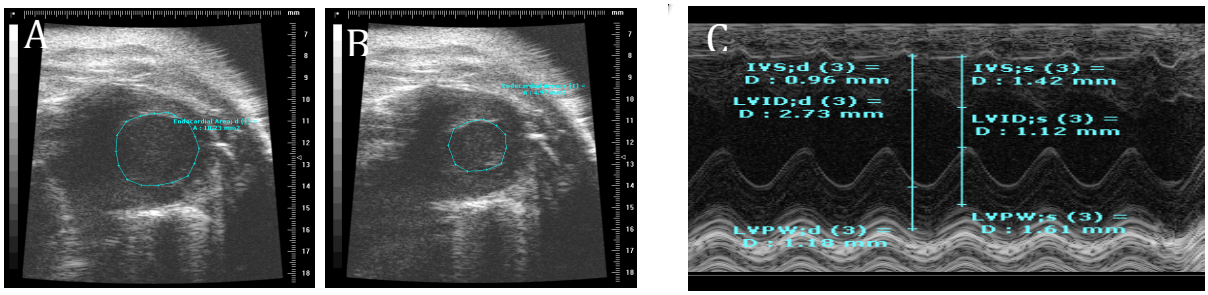

Figure 2.1. Typical echocardiograph M-mode and B-mode traces showing where measurements were taken.

A and B) Show typical B-mode traces in diastolic and systolic phase respectfully. Measurement of FAC are calculated by measuring around the left ventricle in B) diastolic C) systolic phases. A) Shows a typical M-mode trace from which EF and FS are assessed using 3 measurements between; intraventricular septum (IVS); left ventricle internal dimension (LVID) and left ventricle posterior wall (LVPW). Values are taken at the level of the papillary muscles in both systolic and diastolic phase.

$$FAC = 100 \times \left[\frac{LV\ end\ diastolic\ area - LV\ end\ systolic\ area}{LV\ end\ diastolic\ area}\right]$$

Equation 1: Equation for calculation of fractional area change.

Fractional area change is calculated using two measurements a) left ventricular end-diastolic area and b) left ventricular end-systolic area.

$$EF = 100 \times \left[\frac{LVID\ (d)^3 - LVID\ (s)^3}{LVID\ (d)^3}\right]$$

Equation 2: Equation for calculation of ejection fraction.

Ejection fraction is calculated using left ventricular internal dimension in both diastolic and systolic phases.

$$FS = 100 \times \left[\frac{LVID\ (d) - LVID(s)}{LVID\ (d)}\right]$$

Equation 3: Equation for calculation of fractional shortening.

Ejection fraction is calculated using left ventricular internal dimension in both diastolic and systolic phases.

2.2.8 Assessment of renal function

In the last week of the study, mice were placed in metabolic cages for 24 h to collect urine. Urinary creatinine and sodium was measured in a blinded fashion by a commercial veterinary testing laboratory (IDEXX Ltd, West Sussex, UK). Creatinine clearance was calculated using Equation 4 and was used as a measurement of renal filtration rate. Urinary albumin was measured using a mouse albumin ELISA kit as per manufacturers instructions (Bethyl Laboratories Inc., USA) and proteinuria was calculated using urinary albumin-to-creatinine ratio (ACR) (Equation 5). Tubular function was assessed using fractional excretion of sodium (Equation 6).

$$Creatinine\ Clearance = \frac{Urine\ creatinine}{Serum\ Creatinine} \times \frac{Urine\ volume}{Time\ (hours) \times 60}$$

Equation 4: Equation for the calculation of estimated creatinine clearance

Creatinine clearance is calculated using 4 measurements a) urine creatinine (µmol/L) b) serum creatinine (µmol/L) c) urine volume (ml) and d) then time the urine was collect for (hours).

$$ACR = \frac{Urine\ Albumin}{Urine\ Creatinine}$$

Equation 5: Equation for the calculation of albumin to creatinine ratio (ACR).

ACR is calculated by using 2 measurements a) urine albumin (mg/dL) and b) urine creatinine (mg/dL).

$$Fractional\ Excretion\ of\ Sodium\ = \frac{Urine\ sodium\ \div Serum\ Sodium}{Urine\ Creatinine\ \div Serum\ Creatinine}$$

Equation 6: Equation for the calculation of Fractional excretion of Sodium ($FENa^+$).

$FeNa^+$ is calculated by using 4 measurements a) urine sodium (mmol/L), b)serum sodium (mmol/L), c) urine creatinine (µmol/L) and d) serum creatinine (µmol/L).

2.2.9 Organ and blood collection

Mice were anaesthetised with a ketamine (100 mg/ml) and xylazine (20 mg/ml) mixture (2:1; 1.5 ml/kg, i.p.) and killed by cardiac exsanguination. Blood glucose was measured immediately using a glucometer (Accu-Chek Compact System; Roche Diagnostics, Switzerland). Organs were harvested and a section of kidney and heart was snap frozen and put in long-term storage for further processing and a section was of kidney was fixed in 10 % neutral-buffered for 48 h and transferred to 70 % ethanol for long term storage. Blood was collected and serum isolated; biochemical markers (urea, creatinine and sodium) were

measured in a blinded fashion by a commercial veterinary testing laboratory (IDEXX Ltd, West Sussex, UK) and serum insulin using a mouse ELISA kit (Abcam Plc., UK).

2.2.10 Sandwich ELISA for ANXA1

A homemade sandwich ELISA was used to measure serum and tissue levels of ANXA1. Briefly, ELISA-treated plates (Nunc MaxiSorp, ThermoScientific, UK) were incubated overnight with capture antibody 20µg/ml (mouse monoclonal antibody, generated in house) in bicarbonate buffer (25 mM $NaHCO_3$, 25 mM $Na2CO_3$, pH 9.6). The plate was then washed 3 times with bicarbonate buffer and blocked in blocking buffer (0.1 % BSA, PBS) for 1 h at 37 °C. Then 100 µl of sample and standard in assay diluent (Tween-20 0.05 % (v/v), PBS) where loaded and incubated for 1 h at 37 °C, then washed 5 times with wash buffer (0.9% (w/v) NaCl, 0.05 % (v/v) Tween-20, dH_2O). Following this wells where incubated with 1µg/ml of detecting antibody (rabbit polyclonal anti-ANXA1;Invitrogen, UK) for 1 h at 37 °C. After 5 washes, immuno-complexes were detected by adding the goat-anti-rabbit IgG with conjugated alkaline phosphatase for 30 min. After 5 washes, the substrate, p-Nitrophenyl phosphate (Sigma Aldrich, UK) was added and left for 30 min for full development of colour. The plate was then read absorbance at 405 nm and corrected at 540 nm as a reference wavelength, using a spectofluorimeter (Tecan Infinite M200 Pro, Tecan, Austria).

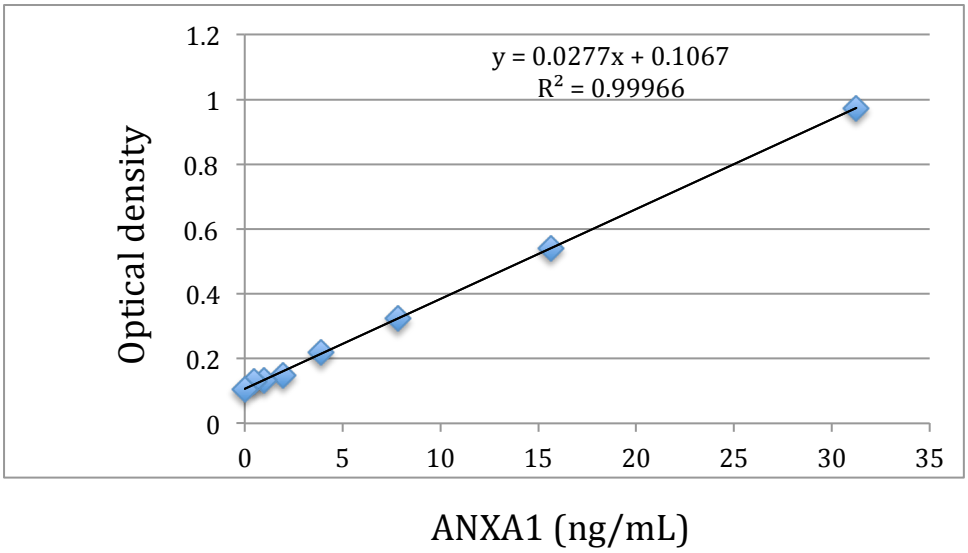

Figure 2.2. Standard curve using human recombinant ANXA1.

2.2.11 Western blot analysis

Semi-quantitative western blot analyses were carried out in mouse kidney, heart and liver tissues as described previously (Chen et al. 2014). Briefly, mouse tissue samples were homogenised and centrifuged at 4000 RPM for 5 min at 4 °C. Supernatants were removed and centrifuged at 14,000 RPM at 4 °C for 40 min to obtain the cytosolic fraction. The pelleted nuclei were re-suspended in extraction buffer and centrifuged at 14,000 RPM for 20 min at 4 °C. The resulting supernatants containing nuclear proteins were carefully removed, and protein content was determined on both nuclear and cytosolic extracts using a bicinchoninic acid (BCA) protein assay following the manufacturer's directions (Therma Fisher Scientific, Rockford, IL). Proteins were separated by 8 % sodium dodecyl sulphatepolyacrylamide gel electrophoresis (SDS-PAGE) and transferred to a polyvinyldenedifluoride (PVDF) membrane, blocked using 5 % milk and then incubated with a primary antibody dilution either 1:200 or 1:1000 (rabbit

anti-total p38; rabbit anti-pp38 (both 41kDa); rabbit anti-total JNK, rabbit anti-pJNK (both 46kDa); rabbit anti-total ERK1/2; mouse anti-pERK1/2(44/42 kDa); rabbit anti-ANXA1 (37 kDa); rabbit anti-total Akt; mouse anti-pAkt rabbit (63 kDA); anti β-actin (42 kDa). Bands where checked against their molecular weight using a rainbow ladder (Invitrogen, UK) to ensure positive identification. Blots were then washed 3 times for 5 min and incubated with a secondary antibody conjugated with horseradish peroxidase (dilution 1:10000) for 30 min at room temperature, washed 3 times for 15 min and developed with the ECL detection system. The bands were visualised by autoradiography. Densitometric analysis of the bands was performed using the Gel Pro Analyser 4.5, 2000 software (Media Cybernetics, Silver Spring, MD, USA). Each group was then adjusted against corresponding sham data to establish relative protein expression when compared with sham animals.

2.2.12 Histological analysis

Formulin fixed kidney samples were embedding in paraffin and processed to obtain 4 μm sections. After deparaffinisation and rehydrated through graded alcohols to distilled water.

Periodic Acid Schiffs: The sections were then incubated with saturated in Periodic Acid Schiff's (Sigma, UK) solution for 30 min washed in distilled water and counterstained with Harris hematoxylin (Sigma, UK).

Picrosirius Red: The sections were treated with phosphomolybdic acid (Polysciences, Warrington, PA), rinsed in distilled water and stained with picrosirius red (Polysciences, Warrington, PA) solution for 60 min. Sections were

then immediately immersed in hydrochloride acid for 2 min (Polysciences, Warrington, PA).

In both cases sections were then dehydrated through graded alcohols and cleared before mounting with coverslips. Images were acquired using a NanoZoomer Digital Pathology Scanner (Hamamatsu Photonics K.K. Japan) and analysed using the NDP Viewer software. The diameters of 20 randomly selected glomeruli were measured in all kidneys at magnification (200×) in a double-blinded manner. Additionally 10 randomly selected fields of view from each kidney were used to assess structural alteration of the proximal convoluted tubules at magnification (40×) in a double-blinded manner. Percentage of Sirius Red positive staining was calculated using ImageJ software in 10 randomly selected fields of view in all kidneys at magnification (x20) a double-blinded manner.

2.2.13 Statistical analysis

All data in the text and figures are presented as mean ± standard error mean (SEM) of n observations, where n represents the number of animals studied. All statistical analysis was calculated using GraphPad Prism 6 (GraphPad Software, San Diego, California, USA). Data without a repeated measurement was assessed by a one-way ANOVA or students t-test were appropriate. OGTT testing analysis was preformed using area under ROC-curve. A P-value of less than 0.05 was considered to be statistically significant.

2.3 Experimental plan and groups

2.3.1 The effect of endogenous ANXA1 on STZ-induced diabetes mellitus.

Table 2.1. Experimental groups used to study the effect of endogenous ANXA1 on experimental type-1 diabetes mellitus.

Group Name	Induction Protocol
WT + vehicle	0.9 M citrate buffer, i.p., days 1-5
ANXA1$^{-/-}$ + vehicle	0.9 M citrate buffer, i.p., days 1-5
WT + STZ	45 mg/kg, 0.9 M citrate buffer, i.p., days 1-5
ANXA1$^{-/-}$ + STZ	45 mg/kg, 0.9 M citrate buffer, i.p., days 1-5

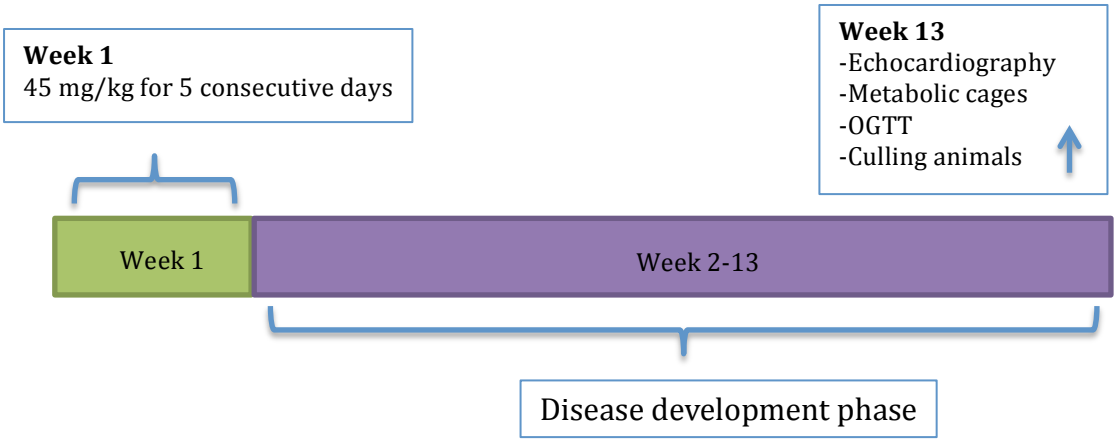

Figure 2.2: Summary of experimental protocol used to investigate the role of endogenous ANXA1 in STZ induced type-1 diabetes mellitus.

2.3.2 The effect of treatment with hrANXA1 on STZ-induced diabetes mellitus.

Table 2.2. Experimental groups used to study the effect of hrANXA1 on experimental type-1 diabetes mellitus.

Group Name	Induction Protocol	Treatment
Sham	Vehicle only	No treatment
STZ + vehicle	45 mg/kg, 0.9 M citrate buffer, i.p., days 1-5	100 µl Hepes buffer
STZ + daily hrANAXA1	45 mg/kg, 0.9 M citrate buffer, i.p., days 1-5	1 µg hrANXA1, 100 µl Hepes buffer, i.p., daily weeks 1-13
STZ + hrANAXA1 days 1-5	45 mg/kg, 0.9 M citrate buffer, i.p., days 1-5	1 µg hrANXA1, 100 µl Hepes buffer, i.p., days 1-5

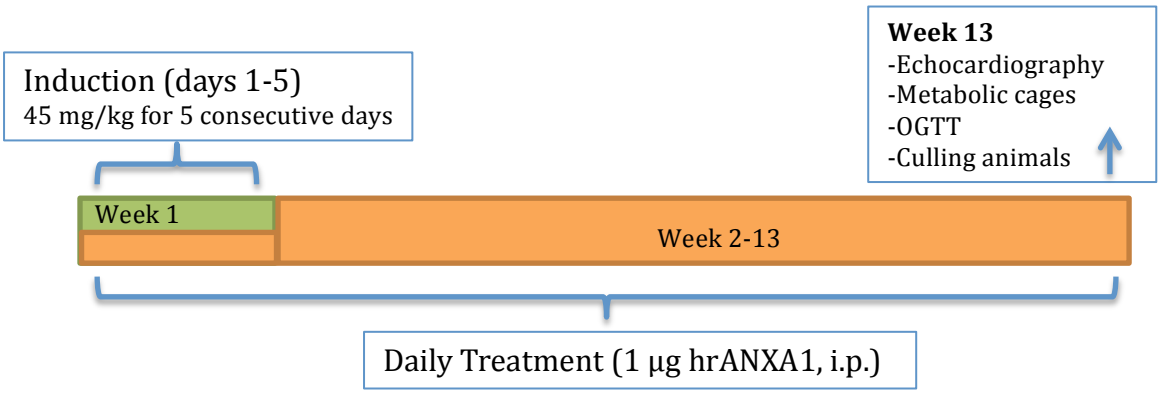

Figure 2.3. Summary of the experimental protocol used to investigate the effect of daily with hrANXA1on experimental diabetes.

2.3.3 Effect of late treatment with hrANXA1 (weeks 8-13) on STZ-induced diabetes mellitus.

Table 2.3. Experimental groups used to study the effect of late treatment with hrANXA1 (weeks 8-13) on experimental type-1 diabetes mellitus.

Group Name	Induction Protocol	Treatment
Sham	Vehicle only	No treatment
STZ + vehicle	45 mg/kg, 0.9 M citrate buffer, i.p., days 1-5	100 µl Hepes buffer
hrANXA1 weeks 7-13	45 mg/kg, 0.9 M citrate buffer, i.p., days 1-5	1 µg hrANXA1, 100 µl Hepes buffer, i.p., daily weeks 8-13

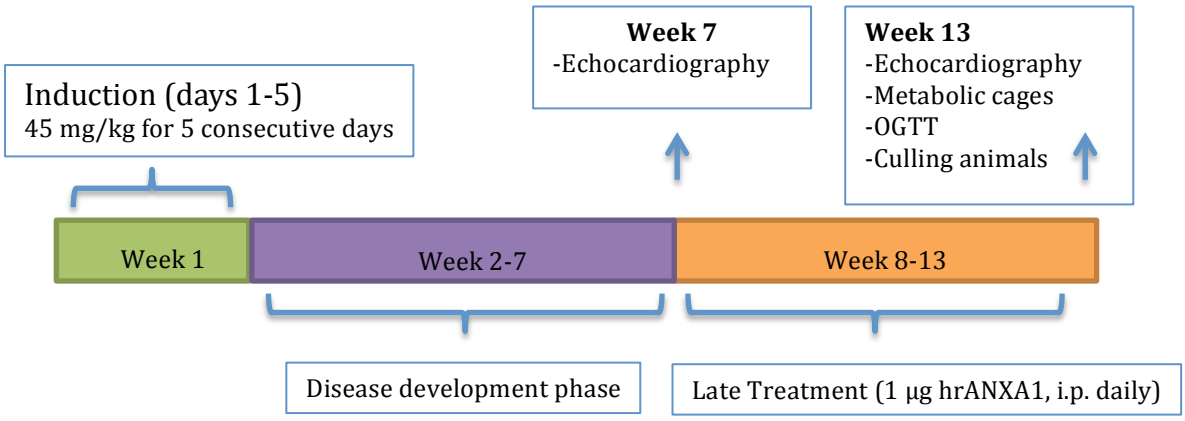

Figure 2.4. Summary of the experimental protocol used to investigate the effect of late treatment on STZ-induced type-1 diabetes mellitus.

2.4 Results

2.4.1. Quantification of plasma ANXA1 and C-reactive protein (CRP) levels in patients with type-1 diabetes.

To understand whether endogenous ANXA1 levels are modulated in T1DM a sandwich ELISA was preformed on plasma from healthy donors and patient's with T1DM with/without diabetic nephropathy. Compared to healthy donors, patients with diabetes with/without nephropathy had significantly elevated levels of plasma ANXA1 (Figure2.5A, $P<0.05$). There was no significant difference in age and sex between groups (Table 1). The patients with T1DM plus nephropathy had a significantly higher duration of diabetes (Table 1, $P<0.05$) and serum creatinine (Table 1, $P<0.05$).

Additionally, plasma CRP levels were measure by ELISA as a marker of systemic inflammation. When compared to patients with T1DM and no nephropathy, patients with T1DM plus nephropathy had elevated CRP levels (Figure 2.5B, $P<0.01$).

Table 2.4. Patient history of healthy donor and patients with type 1 diabetes with/without nephropathy.

Detail of patients included in the study. Number of patients per group, sex, age, diabetic duration and serum creatinine level, BMI and plasma CRP. Experimental groups: Healthy donors, patients with T1DM without diabetic nephropathy and patients with T1DM with diabetic nephropathy. Data analyzed by Student's t-test and expressed as mean ± SEM. *p<0.05 vs. Diabetic (no nephropathy).

	Healthy donors	Diabetic (no nephropathy)	Diabetic (plus nephropathy)
Patients (n)	20	20	22
Sex (F %)	9(45)	13(65)	11(50)
Age (year)	48.3±1.9	42.2±2.2	54.5±2.3
Diabetic duration (year)	n/a	30.5±2.2	38.7±2.1 *
Creatinine (mmol/L)	n/a	64.9±3.2	93.7±1229*
BMI (kg/m²)	n/a	26.8±0.9	26.3±0.8
Serum CRP (pg/m)	n/a	627.8±80.6	1469.2±225.2*

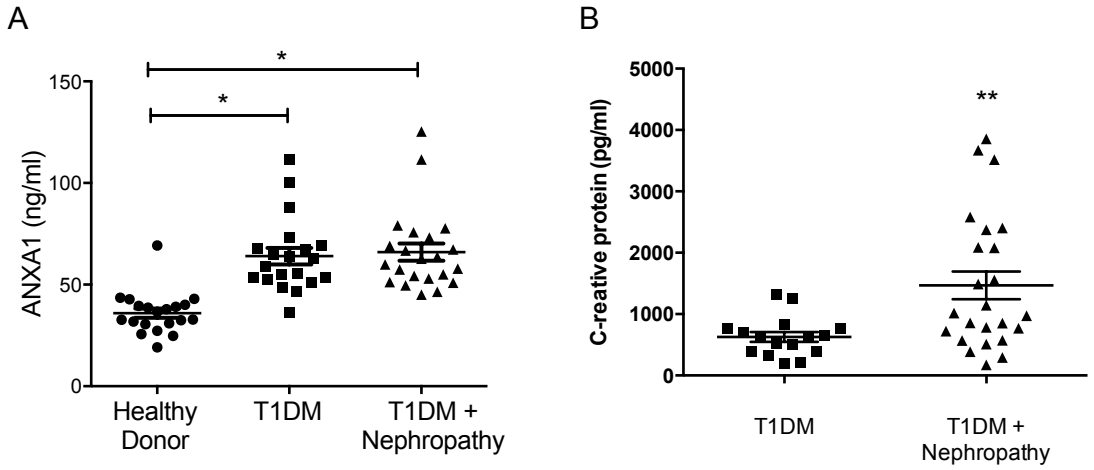

Figure 2.5 Changes in plasma levels of ANXA1 and CRP in patients with or without diabetic nephropathy.

ANXA1 levels (A) and CRP (B) were measured by sandwich ELISA in patient plasma. Groups analysed: Healthy donors (n=20), patients with T1DM without diabetic nephropathy (type 1 diabetes) (n=20) and patients with T1DM with diabetic nephropathy (T1DM + Nephropathy) (n=22). Data analysed by one-way ANOVA followed by a Bonferroni *post-hoc* test and expressed as mean ± SEM. *P<0.05, **P<0.01.

2.4.2. Correlation of BMI and CRP with AXNA1 in patients with type-1 diabetes.

Here I demonstrate that there is no significant correlation between with either body mass index (Figure 2.6A, ns) or plasma CRP (a marker of systemic inflammation) (Figure 2.6B, ns) with plasma ANXA1 levels in patients with T1DM with or without diabetic nephropathy. Additionally in our patient cohort of T1DM patients there is also no significant correlation with between plasma CRP levels and BMI (Figure 2.6C, ns).

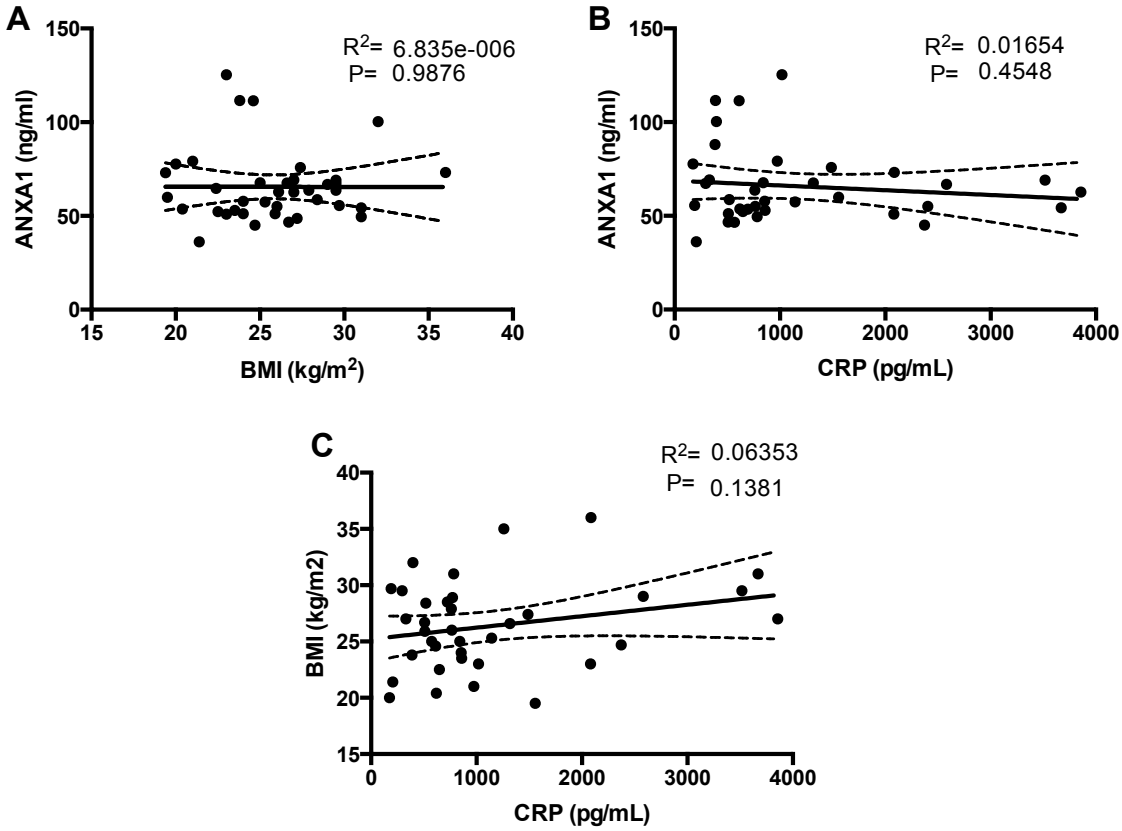

Figure 2.6. Correlation of type 1 diabetes with/without nephropathy between BMI/CRP and ANXA1 levels.

Correlation data show plasma ANXA1 vs. plasma CRP (A) and plasma ANXA1 vs. BMI (B) and BMI vs. plasma CRP (C) in patients with T1DM with/without nephropathy. Linear regressions were calculated and their significance estimated by a Fisher F test. $P<0.05$ was considered to be significant.

2.4.3. Protein levels of ANXA1 in a murine model of STZ-induced type-1 diabetes mellitus.

To understand whether endogenous ANXA1 levels are modulated as a result of STZ administration, a sandwich ELISA was performed in serum and both heart and kidney tissue from mice obtained at week 13 post STZ administration. When compared to sham WT-mice, WT-mice challenged with STZ demonstrated no significant difference in serum ANXA1 levels (Figure 2.7A, ns). When compared to WT-sham mice, WT-mice challenged with STZ demonstrated a significant decrease in ANXA1 levels in both the kidney (Figure 2.7B, $P<0.05$) and heart (Figure 2.7C, $P<0.05$).

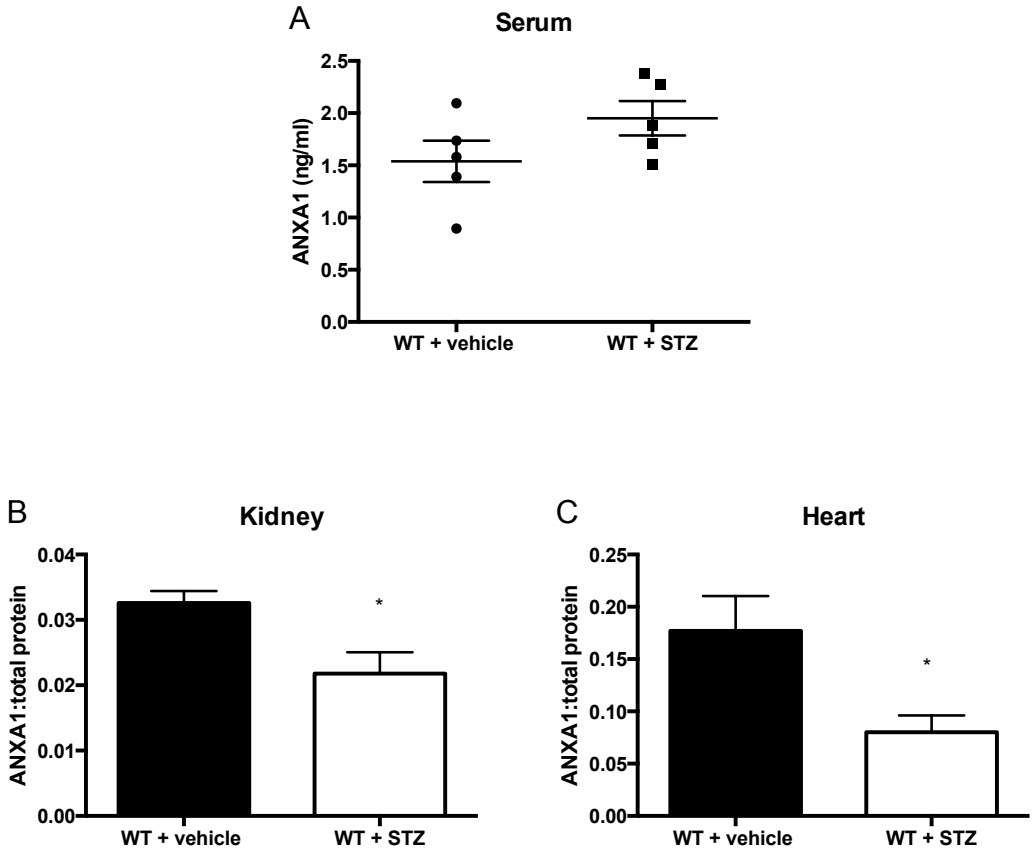

Figure 2.7. Changes in serum and tissue levels of ANXA1 in a mouse model of type-1 diabetes mellitus.

ANXA1 levels were measured by sandwich ELISA at week 13 after STZ administration in serum (A); kidney (B) and heart (C). Experimental groups: WT + vehicle (0.1 M citrate buffer, i.p. for 5 days) and WT + STZ (45 mg/kg, 0.1 M citrate buffer, i.p. for 5 days).). Data analysed by a students t-test, and expressed as mean ± SEM. n= 5 per group. *P<0.05.

2.4.4. The effect of endogenous ANXA1 on OGTT in a murine model of STZ-induced type-1 diabetes mellitus.

Wild-type (WT) mice not challenged with STZ (0.1 M citrate buffer, i.p. for 5 days) were subjected to an oral glucose tolerance test (OGTT) at week 13 after STZ administration. Within 15 min of glucose challenge, blood glucose rose from 8.8 mmol/L (fasting baseline) to 16.4 mmol/L (peak glucose) (Figure 2.8A), and returned to baseline within 60 min (Figure 2.8A). Similarly, ANXA1$^{-/}$ mice (not challenged with STZ) glucose challenge resulted in a rise in blood glucose rose from 8.9 mmol/L (fasting baseline) to 15.6 mmol/L (peak glucose) (Figure 2.8A), which returned to baseline within 60 min (Figure 2.8A).

When WT mice that had been challenged with STZ (45 mg/kg, 0.1 M citrate buffer, i.p. for 5 days) and then challenged with glucose 13 weeks later resulted in a rise in blood glucose from 9.8 mmol/L (fasting baseline) to 27.6 mmol/L (peak glucose) (Figure 2.8A), which did not return to baseline within 120 min (Figure 2.8A). Similarly, in ANXA1$^{-/-}$ mice that had been challenged with STZ 13 weeks prior to OGTT, glucose challenge resulted in a rise in blood glucose rose from 8.9 mmol/L (fasting baseline) to 32.1 mmol/L (peak glucose) (Figure 2.8A), which did not return to baseline within 120 min (Figure 2.8A).

To gain a better understanding of the dynamic changes in plasma glucose after OGTT, we analysed the area under the curve (AUC) of the rise in blood glucose over time. When compared to sham WT mice, WT mice challenged with STZ 13 weeks prior to OGTT exhibited a significant increase in the AUC (Figure 2.8B,

P<0.0001). Similarly, when compared sham ANXA1$^{-/-}$, ANXA1$^{-/-}$ mice challenged with STZ demonstrated a significant increase in AUC for blood glucose (Figure 2.8B, P<0.0001). Importantly, ANXA1$^{-/-}$ mice challenged with STZ had a significantly higher AUC compared to WT-mice challenged with STZ (Figure 2.8C, P<0.0001).

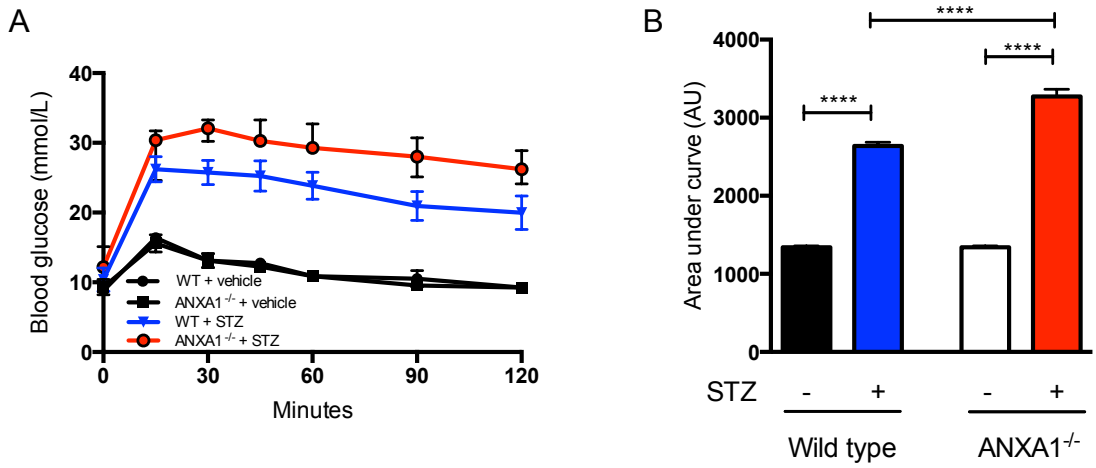

Figure 2.8. Comparison of oral glucose tolerance (OGTT) between WT and ANXA1$^{-/-}$ mice in a model of type-1 diabetes mellitus.

After 18 h of fasting, mice were given a 1 g/kg oral glucose bolus at time 0. Glucose levels were subsequently measured at 0, 15, 30, 45, 60, 90 and 120 minutes post oral glucose delivery (A) and the area under the curve of OGTT calculated (B). Experimental groups: WT + vehicle (0.1 M citrate buffer, i.p. for 5 days); WT + STZ (45 mg/kg, 0.1 M citrate buffer, i.p. for 5 days); ANXA1$^{-/-}$ + vehicle (0.1 M citrate buffer, i.p. for 5 days) and ANXA1$^{-/-}$ + STZ (45 mg/kg, 0.1 M citrate buffer, i.p. for 5 days). Data analysed by a one-way ANOVA followed by a Bonferroni *post-hoc* test, and expressed as mean ± SEM. n= 6-8 per group. ****P<0.0001.

2.4.5 The effect of endogenous ANXA1 on renal dysfunction in a murine model of STZ-induced type-1 diabetes mellitus.

One of the major microvascular complications associated with T1DM is diabetic nephropathy. Markers of renal function were assessed from serum and urine collected 13 weeks post STZ administration. When compared to sham WT-mice, WT mice challenged with STZ demonstrated a significant increase in the albumin-to-creatinine ratio (ACR) (Figure 2.9A, $P<0.001$), suggesting the development of proteinuria. Similarly, when compared to sham ANXA1$^{-/-}$ mice, ANXA1$^{-/-}$ mice challenged with STZ demonstrated a significant increase in the ACR (Figure 2.9A, $P<0.001$), suggesting an increase in proteinuria. Most notably, the degree of proteinuria was greater in ANXA1$^{-/-}$ mice challenged with STZ than in WT mice challenged with STZ (Figure 2.9A, $P<0.001$), suggesting that endogenous ANXA1 limited the degree of proteinuria associated with STZ challenge (T1DM).

When compared to sham WT mice, WT mice challenged with STZ demonstrated a significant increase in serum urea (Figure 2.9B, $P<0.001$), suggesting the presence of renal dysfunction. Similarly, when compared to sham ANXA1$^{-/-}$ mice, ANXA1$^{-/-}$ mice challenged with STZ demonstrated a significant increase in serum urea (Figure 2.9B, $P<0.001$). There was no significant difference in serum urea concentrations between WT and ANXA1$^{-/-}$ mice challenged with STZ (Figure 2.9B, ns).

When compared to WT mice not challenged with, WT mice challenged with STZ demonstrated a significant increase in creatinine clearance, suggesting renal hyperfiltration (Figure 3C, $P<0.005$). Similarly, when compared to sham ANXA1$^{-/-}$, ANXA1$^{-/-}$ mice challenged with STZ demonstrated a significant increase in creatinine clearance (Figure 3C, $P<0.005$). When compared to WT mice not challenged with STZ, ANXA1$^{-/-}$ mice challenged with STZ demonstrated a significant increase in creatinine clearance (Figure 3C, $P<0.001$), suggesting that the degree of hyperfiltration caused by STZ was limited by endogenous ANXA1.

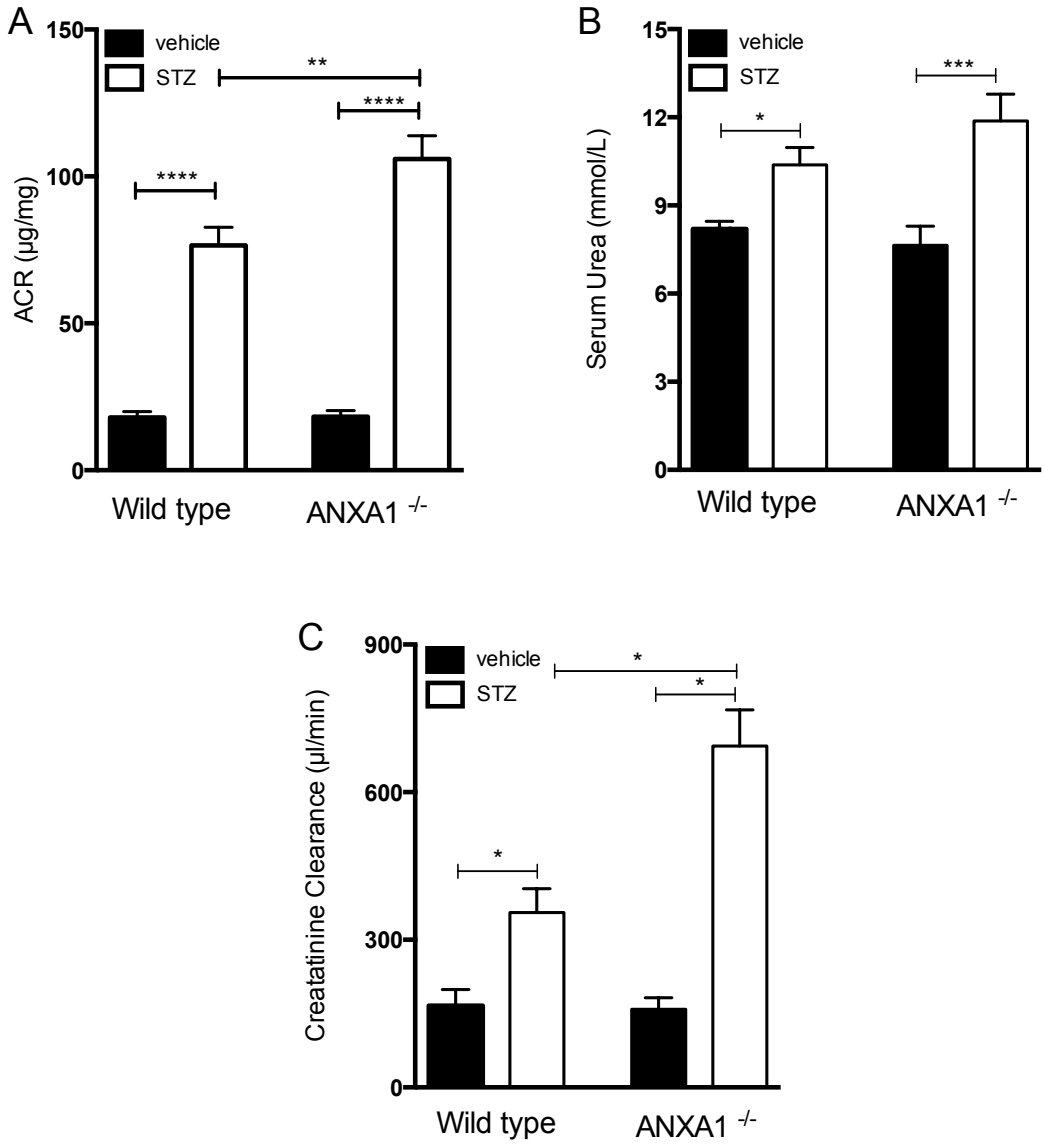

Figure 2.9. Changes in renal function in WT and ANXA1$^{-/-}$ mice in a model of type-1 diabetes mellitus.

Measurements of renal function in wild-type and ANXA1$^{-/-}$ mice: urine albumin-to-creatinine ratio (A); serum urea (B); and creatinine clearance (C), measured from serum and urine at week 13 post STZ administration. Experimental groups: WT + vehicle (0.1 M citrate buffer, i.p. for 5 days); WT + STZ (45 mg/kg, 0.1 M citrate buffer, i.p. for 5 days); ANXA1$^{-/-}$ + vehicle (0.1 M citrate buffer, i.p. for 5 days) and ANXA1$^{-/-}$ + STZ (45 mg/kg, 0.1 M citrate buffer, i.p. for 5 days). Data analysed by a one-way ANOVA followed by a Bonferroni *post-hoc* test, and expressed as mean ± SEM. n= 6-8 per group. *P<0.05, **P<0.01, ***P<0.001, ****P<0.0001.

2.4.6 The effect of endogenous ANXA1 on tubular function in a murine model of STZ-induced type-1 diabetes mellitus.

Tubular function was assessed by measured the fraction excretion of sodium from serum and urine samples collected 13 weeks post STZ administration. When compared to sham WT-mice, WT mice challenged with STZ demonstrated a significant increase in the fractional excretion of sodium (Figure 2.10A, $P<0.001$), suggesting an increase in tubular dysfunction. Similarly, when compared to sham ANXA1$^{-/-}$ mice, ANXA1$^{-/-}$ mice challenged with STZ demonstrated a significant increase in the fractional excretion of sodium (Figure 2.10A, $P<0.001$). Most notably, the degree of tubular dysfunction was greater in ANXA1$^{-/-}$ mice challenged with STZ than in WT mice challenged with STZ (Figure 2.10A, $P<0.001$), suggesting that endogenous ANXA1 limited the degree of tubular dysfunction associated with STZ challenge.

Tubular dysfunction can be observed histologically by visualising the brush borders of the convoluted proximal tubules using Periodic Acid Schiff's staining, which stains the of the basal lamina. Sham WT mice show no morphological alterations in their tubule structures, which include well-preserved brush borders in the S1-S2 of the proximal convoluted tubules (Figure 2.10A). However, WT mice challenged with STZ demonstrated some morphological alteration including tubular dilation, and a distinctive loss of the brush borders in the S1-S2 segment of the proximal convoluted tubules (Figure 2.10B). Similarly, sham ANXA1$^{-/-}$ mice also show no morphological alterations in their tubule structures, including well-preserved brush borders in the S1-S2 of the

proximal convoluted tubules (Figure 2.10C). . But ANXA1$^{-/-}$ mice challenged with STZ demonstrated showed a marked reduction in the brush borders of the S1-S2 of the proximal convoluted tubules, which was more advanced than that observed in the WT mice challenged with STZ (Figure 2.10D).

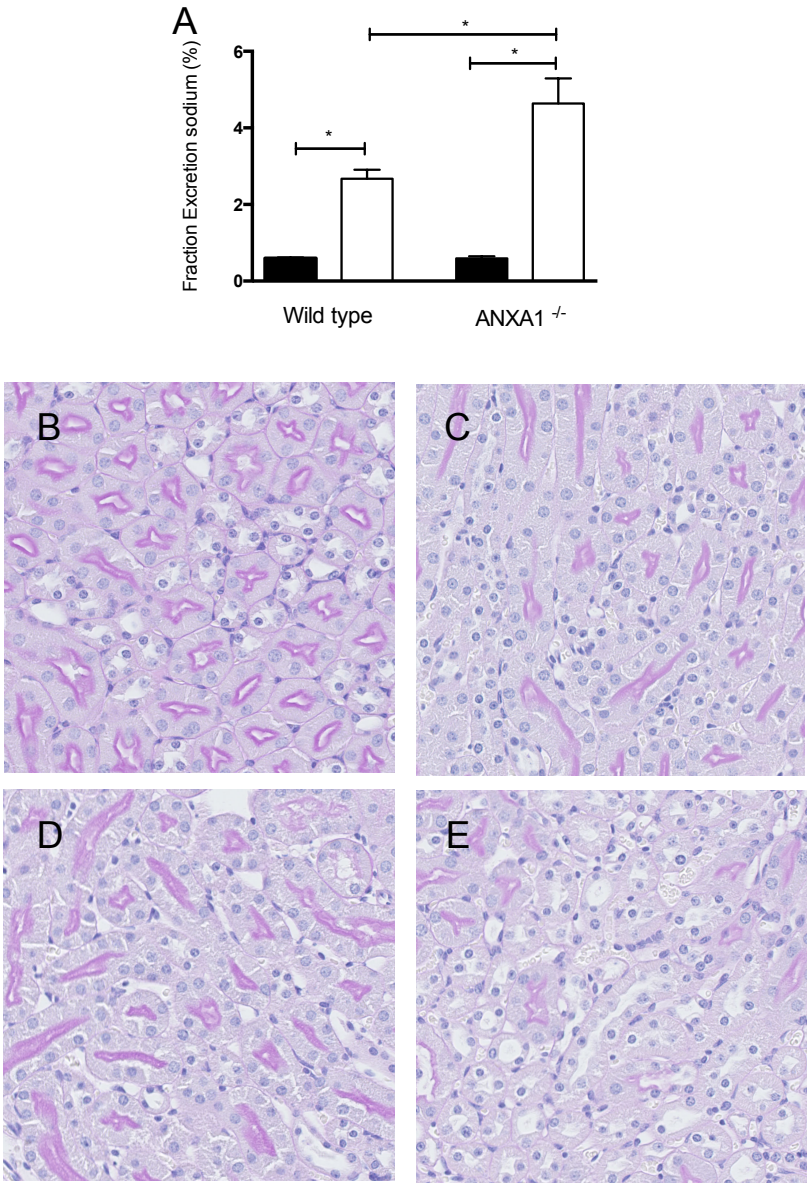

Figure 2.10. Changes in tubular function WT and ANXA1$^{-/-}$ mice in a model of type-1 diabetes mellitus. Measurements of renal function in wild-type and ANXA1$^{-/-}$ mice: fractional excretion of sodium measured from serum and urine (A) and Periodic acid Schiff's staining of the kidney (B-E); at week 13 post STZ administration. Experimental groups: WT + vehicle (0.1 M citrate buffer, i.p. for 5 days) (B); WT + STZ (45 mg/kg, 0.1 M citrate buffer, i.p. for 5 days) (C); ANXA1$^{-/-}$ + vehicle (0.1 M citrate buffer, i.p. for 5 days) (D) and ANXA1$^{-/-}$ + STZ (45 mg/kg, 0.1 M citrate buffer, i.p. for 5 days) (E). Data analysed by a one-way ANOVA followed by a Bonferroni *post-hoc* test, and expressed as mean ± SEM. n= 6-8 per group. *P<0.05.

2.4.7. The effect of endogenous ANXA1 on glomerular hypertrophy in a murine model of STZ-induced type-1 diabetes mellitus.

A classical hallmark of diabetic nephropathy is hypertrophy; to determine the extent of glomerular hypertrophy Periodic Acid Schiff's staining was used to stain the basal lamina around the glomerulus, so glomerular area could be calculated. When compared to sham WT-mice (Figure 2.11A), WT mice challenged with STZ demonstrated a significant increase in glomerular area (Figure 2.11B/E, $P<0.05$), suggesting the development of glomerular hypertrophy. Similarly, when compared to sham ANXA1$^{-/-}$ mice (Figure 2.11C), ANXA1$^{-/-}$ mice challenged with STZ demonstrated a significant increase in glomerular area (Figure 3D/E, $P<0.001$). Most notably, the degree of glomerular hypertrophy was greater in ANXA1$^{-/-}$ mice challenged with STZ than in WT mice challenged with STZ (Figure 3E, $P<0.05$), suggesting that endogenous ANXA1 limited the degree of glomerular hypertrophy associated with STZ challenge.

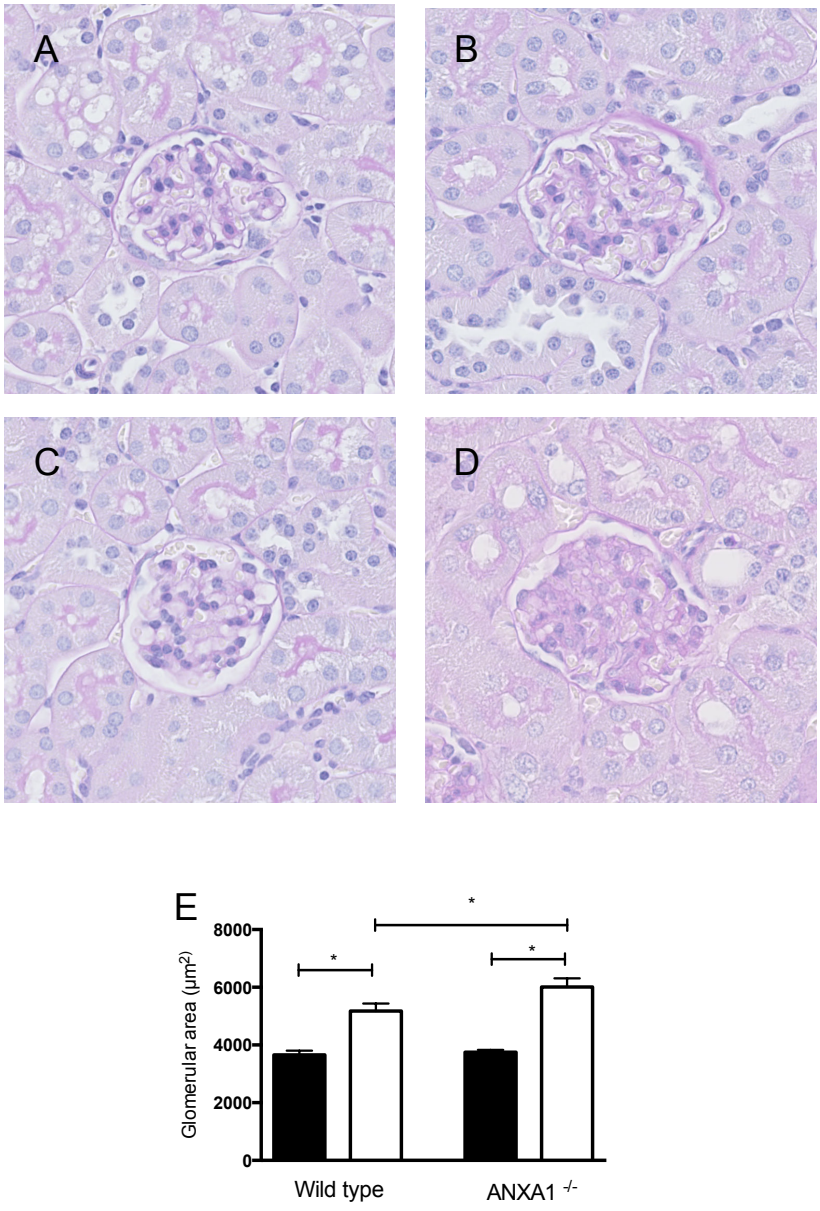

Figure 2.11. Changes glomerular hypertrophy in WT and ANXA1$^{-/-}$ mice in a model of type-1 diabetes mellitus. Quantification of glomerular hypertrophy in wild-type and ANXA1$^{-/-}$ mice measured after staining basement membranes with Periodic acid Schiff's at week 13 post STZ administration. Experimental groups: WT + vehicle (0.1 M citrate buffer, i.p. for 5 days) (A); WT + STZ (45 mg/kg, 0.1 M citrate buffer, i.p. for 5 days) (B); ANXA1$^{-/-}$ + vehicle (0.1 M citrate buffer, i.p. for 5 days) (C) and ANXA1$^{-/-}$ + STZ (45 mg/kg, 0.1 M citrate buffer, i.p. for 5 days) (D). Data analysed by a one-way ANOVA followed by a Bonferroni *post-hoc* test, and expressed as mean ± SEM. n= 6-8 per group. *P<0.05.

2.4.8. The effect of endogenous ANXA1 on renal fibrosis in a model of STZ-induced type-1 diabetes mellitus.

Another classical hallmark of diabetic nephropathy is interstitial fibrosis. To determine the extent of renal fibrosis Sirius Red staining was used to stain collagen I and III fibres. When compared to sham WT-mice (Figure 2.12A), WT mice challenged with STZ demonstrated a significant increase in Sirius Red staining (Figure 2.12B/E, $P<0.01$), suggesting the development of renal interstitial fibrosis. Similarly, when compared to sham ANXA1$^{-/-}$ mice (Figure 2.12C), ANXA1$^{-/-}$ mice challenged with STZ demonstrated a significant Sirius Red staining (Figure 2.12D/E, $P<0.001$). Most notably, the degree of renal interstitial fibrosis was greater in ANXA1$^{-/-}$ mice challenged with STZ than in WT mice challenged with STZ (Figure 2/12E, $P<0.05$), suggesting that endogenous ANXA1 limited the degree of renal interstitial fibrosis associated with STZ challenge.

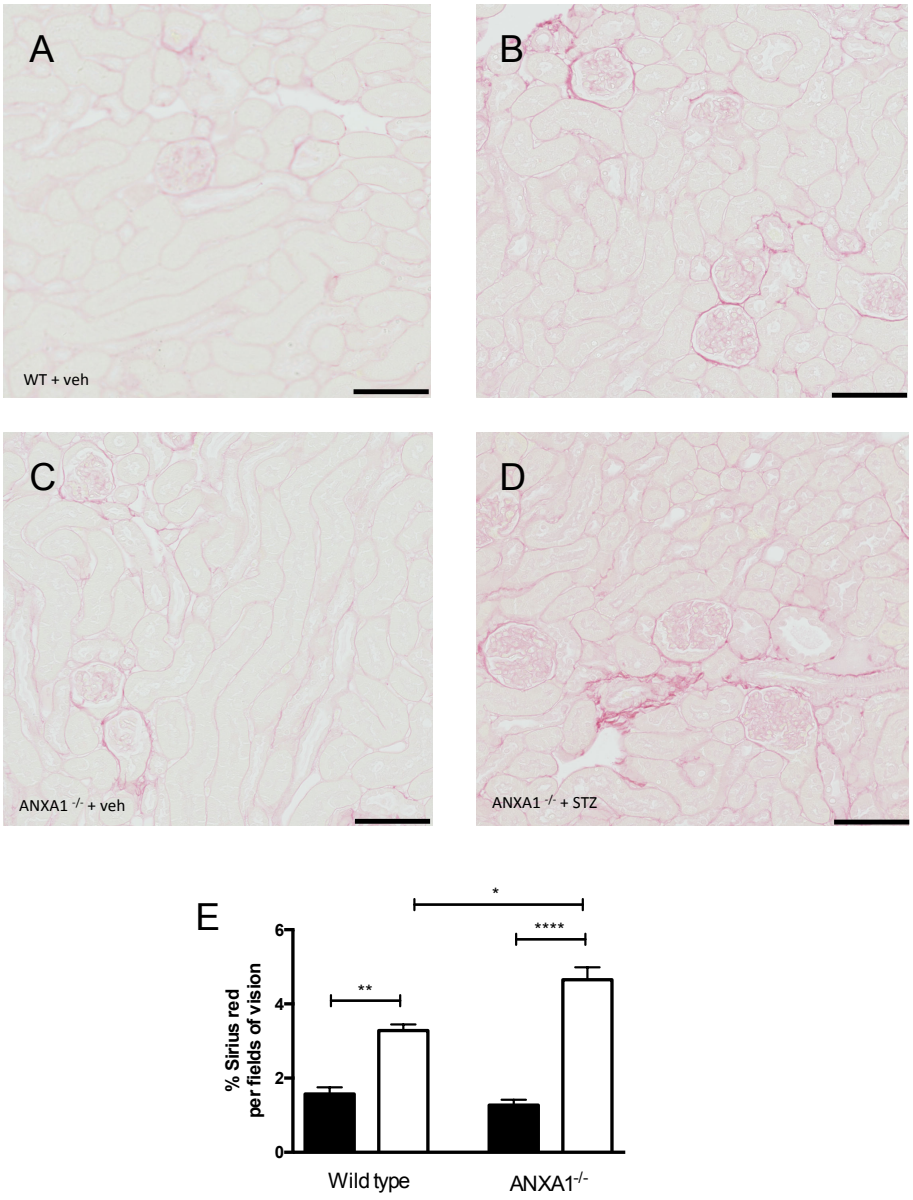

Figure 2.12. Changes renal fibrosis in WT and ANXA1$^{-/-}$ mice in a model of type-1 diabetes mellitus. Quantification of renal fibrosis (E) in wild-type and ANXA1$^{-/-}$ mice after staining with Sirius red at week 13 post STZ administration (A-D). Experimental groups: WT + vehicle (0.1 M citrate buffer, i.p. for 5 days) (B); WT + STZ (45 mg/kg, 0.1 M citrate buffer, i.p. for 5 days) (C); ANXA1$^{-/-}$ + vehicle (0.1 M citrate buffer, i.p. for 5 days) (D) and ANXA1$^{-/-}$ + STZ (45 mg/kg, 0.1 M citrate buffer, i.p. for 5 days) (E). Data analysed by a one-way ANOVA followed by a Bonferroni *post-hoc* test, and expressed as mean ± SEM. n= 6-8 per group. *P<0.05, **P<0.05. ****P<0.05.

2.4.9. The effect of endogenous ANXA1 on cardiac dysfunction in a murine model of STZ-induced type-1 diabetes mellitus.

One of the co-morbidities associated with T1DM is diabetic cardiomyopathy. To determine the effect of endogenous ANXA1 on the cardiac dysfunction caused by diabetes, left ventricular function was assessed using echocardiography 13 weeks post STZ administration. When compared to sham WT-mice, WT mice challenged with STZ demonstrated significant reductions in ejection fraction (Figure 2.14A, $P<0.001$), fractional shortening (Figure 2.14B, $P<0.001$) and fractional area change (Figure 2.14C, $P<0.0001$), indicating the development of systolic dysfunction. Similarly, when compared to sham ANXA1$^{-/-}$, ANXA1$^{-/-}$ mice challenged with STZ demonstrated significant reductions in ejection fraction (Figure 2.14A, $P<0.0001$), fractional shortening (Figure 2.14B, $P<0.0001$) and fractional area change (Figure 2.14C, $P<0.001$). Most notably the degree of systolic cardiac dysfunction was greater in ANXA1$^{-/-}$ mice challenged with STZ than in WT-mice challenged with STZ, indicating that endogenous ANXA1 limited the degree of cardiac dysfunction caused by STZ (Figure 2.14A, $P<0.01$).

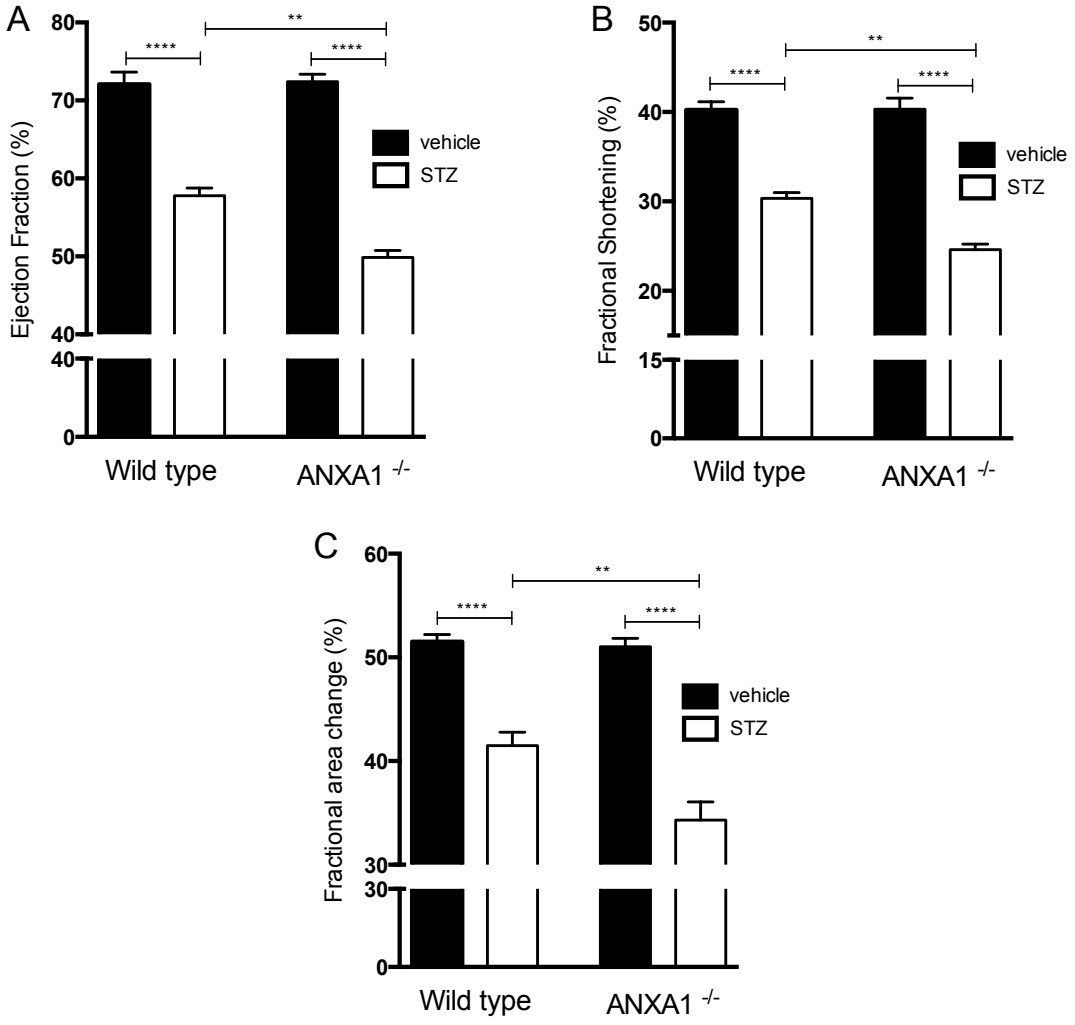

Figure 2.14. Changes in cardiac function in WT and ANXA1$^{-/-}$ mice in a model of type-1 diabetes mellitus.

Measurements of cardiac function in WT and ANXA1-/- mice: ejection fraction (A); fractional shortening (B); and fractional area change (C), measured by echocardiograph at week 13 post STZ administration. Experimental groups: WT + vehicle (0.1 M citrate buffer, i.p. for 5 days); WT + STZ (45 mg/kg, 0.1 M citrate buffer, i.p. for 5 days); ANXA1$^{-/-}$ + vehicle (0.1 M citrate buffer, i.p. for 5 days) and ANXA1$^{-/-}$ + STZ (45 mg/kg, 0.1 M citrate buffer, i.p. for 5 days). Data analysed by a one-way ANOVA followed by a Bonferroni *post-hoc* test, and expressed as mean ± SEM. n= 6-8 per group. *P<0.05, **P<0.01, ****P<0.0001.

2.4.10. Effect of endogenous ANXA1 on cardiac hypertrophy in a murine model of STZ-induced type-1 diabetes mellitus.

A classical hallmark of diabetic cardiomyopathy is cardiac hypertrophy; to determine the extent of cardiac hypertrophy measurements of intra ventricular diameter were calculated 13-weeks post STZ administration. When compared to sham WT-mice (Figure 2.15A), WT mice challenged with STZ demonstrated a significant increase in intra ventricular diameter (Figure 2.15A/E, $P<0.05$), suggesting the development of cardiac hypertrophy. Similarly, when compared to sham ANXA1$^{-/-}$ mice (Figure 2.15C), ANXA1$^{-/-}$ mice challenged with STZ demonstrated a significant increase in intra ventricular diameter (Figure 2.15D/E, $P<0.05$). However, the degree of cardiac hypertrophy between WT and ANXA1$^{-/-}$ mice challenged with STZ was not significantly different (Figure 3A, ns).

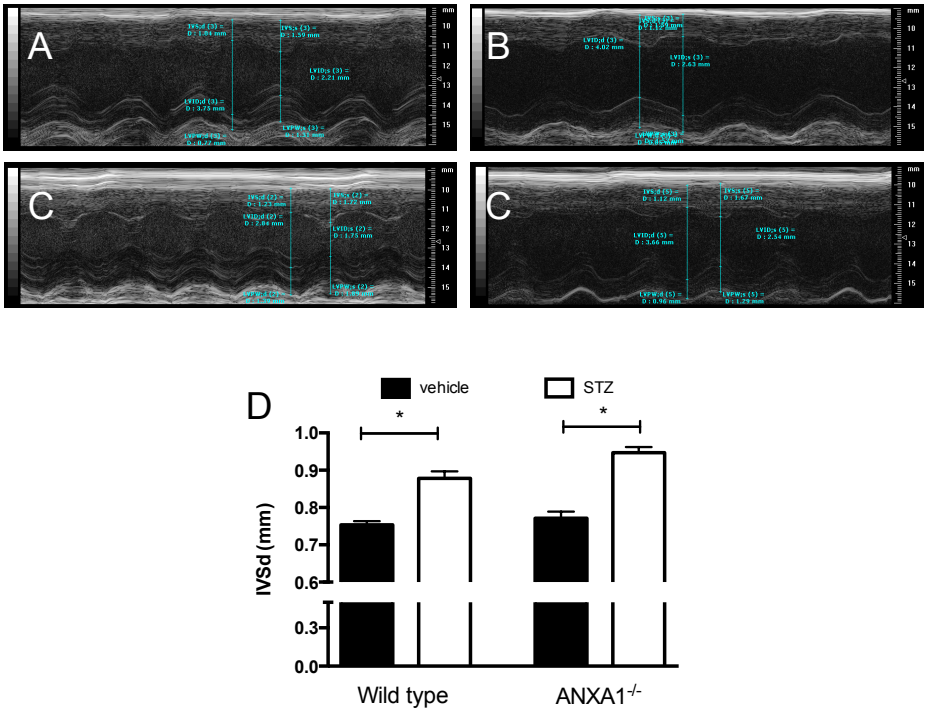

Figure 2.15. Quantification of intra ventricular septum diameter in WT and ANXA$^{-/-}$ mice in a model of STZ-induced type-1 diabetes mellitus.

Measurements of cardiac hypertrophy in WT and ANXA1-/- mice: intra ventricular septum diameter (IVSd) (D) measured by echocardiograph at week 13 post STZ administration. Experimental groups: WT + vehicle (0.1 M citrate buffer, i.p. for 5 days) (A); WT + STZ (45 mg/kg, 0.1 M citrate buffer, i.p. for 5 days) (B); ANXA1$^{-/-}$ + vehicle (0.1 M citrate buffer, i.p. for 5 days) (C) and ANXA1$^{-/-}$ + STZ (45 mg/kg, 0.1 M citrate buffer, i.p. for 5 days) (D). Data analysed by a one-way ANOVA followed by a Bonferroni *post-hoc* test, and expressed as mean ± SEM. n= 6-8 per group. *P<0.05.

2.4.11. Effect of endogenous ANXA1 on phosphorylation of p-38, JNK and ERK1/2 in kidneys from mice subjected to STZ-induced type-1 diabetes mellitus.

The potential underlying mechanisms behind the observed renal dysfunction were investigated by semi-quantitative western blot analysis of the mouse kidneys, 13 weeks post STZ administration. When compared to sham WT mice, kidneys from WT mice challenged with STZ exhibited a significant increase in the phosphorylation of JNK on Thr^{183}/Tyr^{185} (Figure 2.15B, $P<0.05$) and ERK1/2 on Thr^{202} and Tyr^{204} (Figure 2.15C, $P<0.001$) suggesting strong activation of downstream effectors of the MAPK signal transduction pathway. There was also a 3-fold increase in phosphorylation of p38 on Thr^{180}/Thr^{182} in mice challenged with STZ, but this increase was not statistically significant compared to WT nice not challenged with STZ (Figure 2.15B, ns).

When compared to sham $ANXA1^{-/-}$ mice, kidneys from $ANXA1^{-/-}$ mice challenged with STZ exhibited a significant increase in the phosphorylation of p38 on Thr^{180}/Thr^{182} (Figure 2.15A, $P<0.01$), JNK on Thr^{183}/Tyr^{185} (Figure 2.15B, $P<0.0001$) and ERK1/2 on Tyr^{202}/Tyr^{204} (Figure 2.15C, $P<0.0001$). When compared to WT mice challenged with STZ, kidney tissue from $ANXA1^{-/-}$ mice challenged with STZ exhibited increased levels of phosphorylation of p38 on Thr^{180}/Thr^{182} (Figure 2.15A, $P<0.01$), JNK on Thr^{183}/Tyr^{185} (Figure 2.15B, $P<0.0001$) and ERK1/2 on Tyr^{202}/Tyr^{204} (Figure 2.15C, $P<0.0001$).

Interestingly, when compared to WT mice not challenged with STZ, kidney tissue from ANXA1$^{-/-}$ mice not challenged with STZ exhibited elevated levels of phosphorylation of p38 on Thr^{180}/Thr^{182}, JNK on Thr^{183}/Tyr^{185}, although these 3- and 2-fold increases, respectively, were not significant (Figure 2.15A/B, ns). These data suggest there may be a degree of activation of these pathways in the kidneys of non-diabetic ANXA1$^{-/-}$ mice.

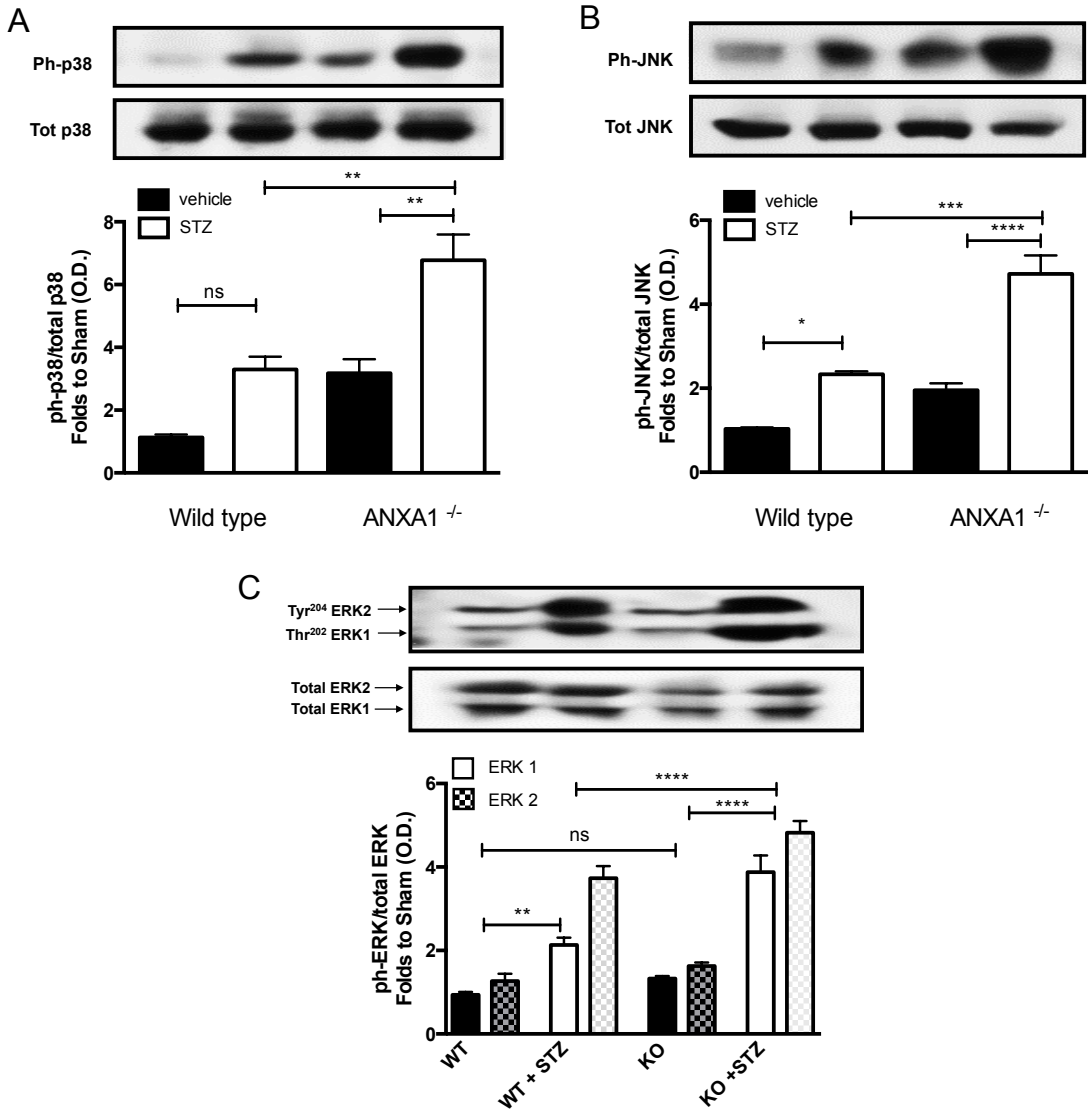

Figure 2.15. Effect of endogenous ANXA1 on phosphorylation of p38, JNK and ERK1/2 in kidneys of mice with STZ-induced type-1 diabetes mellitus.

Signalling in the kidney was assessed 13 weeks after STZ administration. Densitometric analysis of bands is expressed as a relative optical density (O.D.) of phosphorylated p38 ($pThr^{180}/Thr^{182}$) corrected to total p38 and normalised using the WT + vehicle band (A); phosphorylated JNK ($pThr^{183}/Thr^{185}$) corrected to total JNK and normalised using the WT + vehicle band (B); and phosphorylated ERK1/2 ($pThr^{202}/Tyr^{204}$) corrected to total ERK1/2 and normalised using the WT + vehicle band (C). Experimental groups: WT + vehicle (0.1 M citrate buffer, i.p. for 5 days); WT + STZ (45 mg/kg, 0.1M citrate buffer, i.p. for 5 days); $ANXA1^{-/-}$ + vehicle (0.1 M citrate buffer, i.p. for 5 days) and $ANXA1^{-/-}$ + STZ (45 mg/kg, 0.1 M citrate buffer, i.p. for 5 days). Representative images from one of three repeated experiments are shown in this Figure. Data analysed by a one-way ANOVA followed by a Bonferroni *post-hoc* test, and expressed as mean ± SEM. n= 3-4 per group per blot. **P*<0.05, **P<0.01, ***P<0.001, ****P<0.0001.

2.4.12. Effect of endogenous ANXA1 on phosphorylation of Akt in kidneys from mice subjected to STZ-induced type-1 diabetes mellitus.

When compared to WT mice not challenged with STZ, kidneys from WT mice challenged with STZ exhibited a significant decrease in the phosphorylation of Akt on Ser^{473} (Figure 2.16A, $P<0.001$). Similarly, when compared to $ANXA1^{-/-}$ mice not challenged with STZ, kidneys from $ANXA1^{-/-}$ mice challenged with STZ exhibited a significant decrease in the phosphorylation of AKT on Ser^{473} (Figure 2.16A, $P<0.001$).

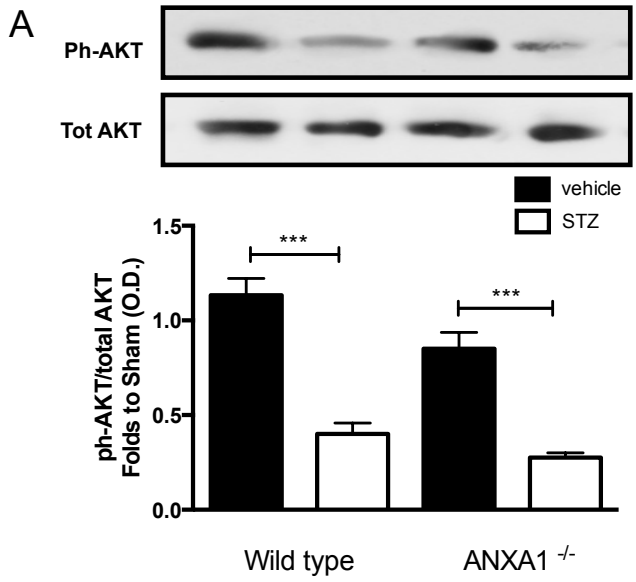

Figure 2.16. Effect of endogenous ANXA1 on phosphorylation of Akt in kidney of mice with STZ-induced type-1 diabetes mellitus.

Signalling in the kidney was assessed 13 weeks after STZ administration. Densitometric analysis of bands is expressed as a relative optical density (O.D.) of phosphorylated Akt ($pSer^{473}$) corrected to total Akt and normalised using the WT + vehicle band. Experimental groups: WT + vehicle (0.1 M citrate buffer, i.p. for 5 days); WT + STZ (45 mg/kg, 0.1M citrate buffer, i.p. for 5 days); $ANXA1^{-/-}$ + vehicle (0.1 M citrate buffer, i.p. for 5 days) and $ANXA1^{-/-}$ + STZ (45 mg/kg, 0.1 M citrate buffer, i.p. for 5 days). Representative images from one of three repeated experiments are shown in this Figure. Data analysed by a one-way ANOVA followed by a Bonferroni *post-hoc* test, and expressed as mean ± SEM. n= 3-4 per group per blot. ***P<0.001.

2.4.13. The effect of endogenous ANXA1 on phosphorylation of p-38, JNK and ERK1/2 in kidneys from mice subjected to STZ-induced type-1 diabetes mellitus.

The potential underlying mechanisms behind the observed cardiac dysfunction were investigated by semi-quantitative western blot analysis of the mouse heart, 13 weeks post STZ administration. When compared to WT mice not challenged with STZ, hearts from WT mice challenged with STZ exhibited a significant increase in the phosphorylation of p38 on Thr^{180}/Thr^{182} (Figure 2.17A, $P<0.05$), JNK on Thr^{183}/Tyr^{185} (Figure 2.17B, $P<0.05$), and ERK1/2 on Thr^{202}/Tyr^{204} (Figure 2.17A, $P<0.01$) suggesting activation of downstream effectors of the MAPK signal transduction pathway.

Similarly, when compared to $ANXA1^{-/-}$ mice not challenged with STZ, hearts from $ANXA1^{-/-}$ mice challenged with STZ exhibited a significant increase in the phosphorylation of p38 on Thr^{180}/Thr^{182} (Figure 2.17A, $P<0.001$), JNK on Thr^{183}/Tyr^{185} (Figure 2.17B, $P<0.0001$), and ERK1/2 on Thr^{202}/Tyr^{204} (Figure 2.17A, $P<0.0001$). When compared to WT mice challenged with STZ, hearts from $ANXA1^{-/-}$ mice challenged with STZ demonstrated a significant increase in the phosphorylation of p38 on Thr^{180}/Thr^{182} (Figure 2.17A, $P<0.001$), JNK on Thr^{183}/Tyr^{185} (Figure 2.17B, $P<0.0001$), and ERK1/2 on Thr^{202}/Tyr^{204} (Figure 2.17A, $P<0.0001$).

Interestingly, when compared to WT mice not challenged with STZ, hearts from $ANXA1^{-/-}$ mice challenged with STZ exhibited a significant increase in the

phosphorylation of p38 on Thr^{180}/Thr^{182} (Figure 2.17A, $P<0.01$), JNK on Thr^{183}/Tyr^{185} (Figure 2.17B, $P<0.01$), and ERK1/2 on Thr^{202}/Tyr^{204} (Figure 2.17A, $P<0.01$). This suggests that there may be a constitutive activation of these MAPK downstream mediators in $ANXA1^{-/-}$ mice.

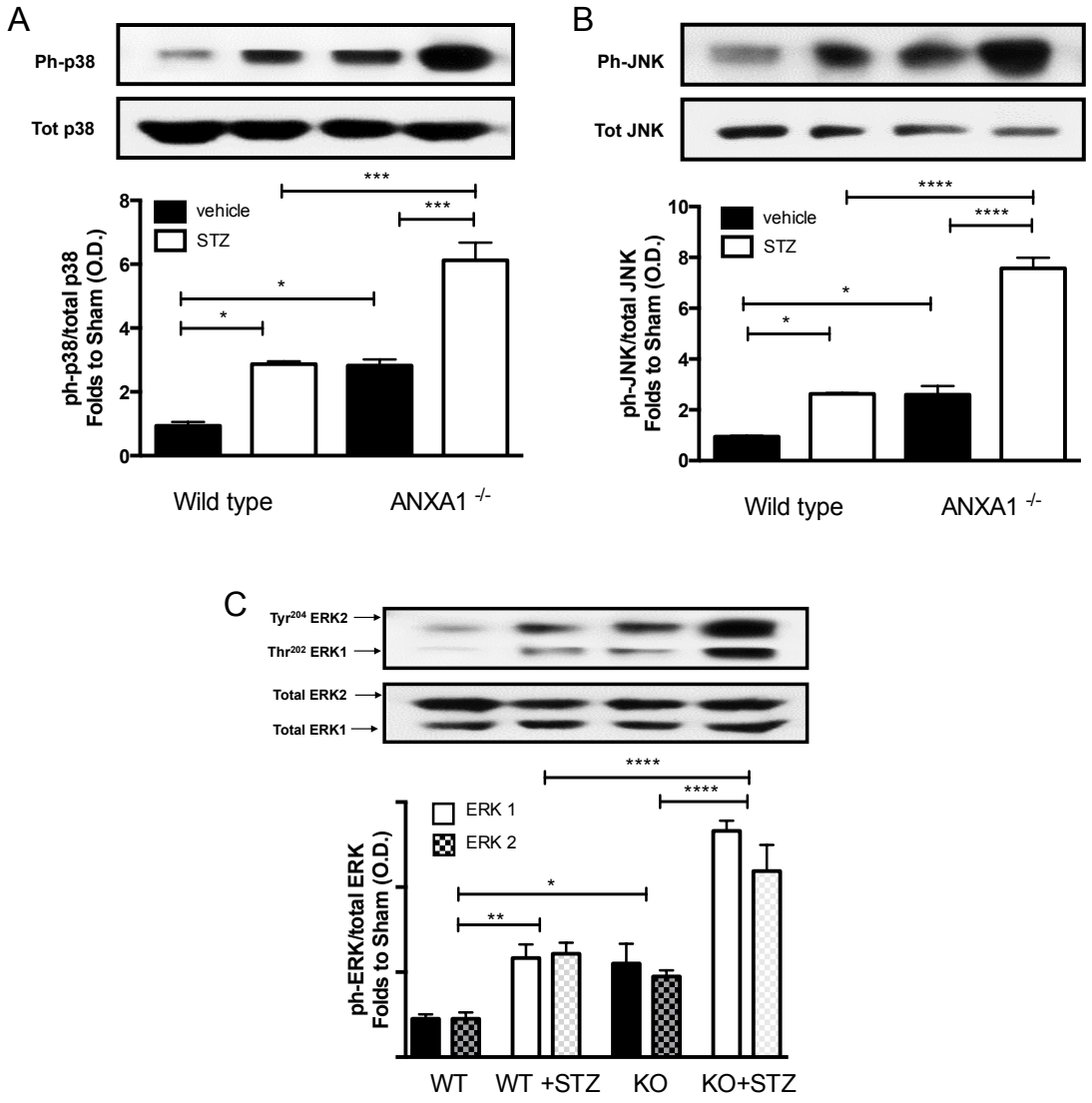

Figure 2.17. Effect of endogenous ANXA1 on phosphorylation of p38, JNK and ERK1/2 in hearts of mice with STZ-induced type-1 diabetes mellitus.

Signalling in the heart was assessed 13 weeks after STZ administration. Densitometric analysis of bands is expressed as a relative optical density (O.D.) of phosphorylated p38 ($pThr^{180}/Thr^{182}$) corrected to total p38 and normalised using the WT + vehicle band (A); phosphorylated JNK ($pThr^{183}/Thr^{185}$) corrected to total JNK and normalised using the WT + vehicle band (B); and phosphorylated ERK1/2 ($pThr^{202}/Ty^{204}$) corrected to total ERK1/2 and normalised using the WT + vehicle band (C). Experimental groups: WT + vehicle (0.1 M citrate buffer, i.p. for 5 days); WT + STZ (45 mg/kg, 0.1M citrate buffer, i.p. for 5 days); $ANXA1^{-/-}$ + vehicle (0.1 M citrate buffer, i.p. for 5 days) and $ANXA1^{-/-}$ + STZ (45 mg/kg, 0.1 M citrate buffer, i.p. for 5 days). Representative images from one of three repeated experiments are shown in this Figure. Data analysed by a one-way ANOVA followed by a Bonferroni *post-hoc* test, and expressed as mean ± SEM. n= 3-4 per group per blot. *P<0.05, **P<0.01, ***P<0.001, ****P<0.0001.

22.4.14. The effect of endogenous ANXA1 on phosphorylation of Akt in hearts from mice subjected to STZ-induced type-1 diabetes mellitus.

When compared to WT mice not challenged with STZ, hearts from WT mice challenged with STZ exhibited a significant decrease in the phosphorylation of Akt on Ser^{473} (Figure 2.18A, $P<0.01$). Similarly, when compared to $ANXA1^{-/-}$ mice challenged with STZ, heart tissue from $ANXA1^{-/-}$ mice challenged with STZ exhibited a significant decrease in the phosphorylation of Akt on Ser^{473} (Figure 2.18A, $P<0.05$).

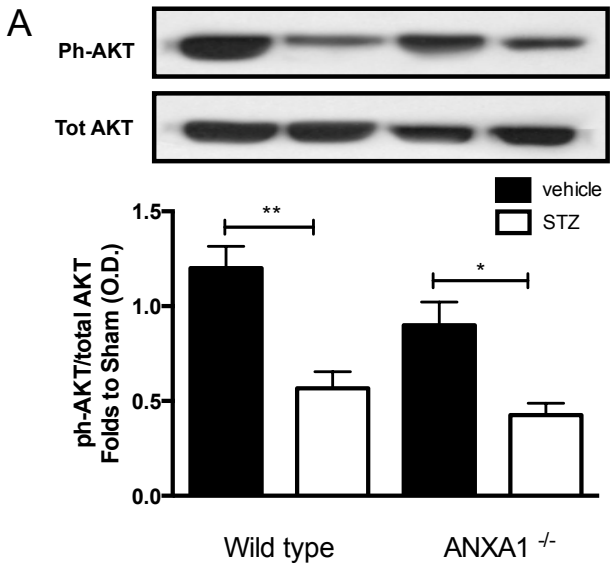

Figure 2.18. Effect of endogenous ANXA1 on phosphorylation of Akt in hearts of mice with STZ-induced type-1 diabetes mellitus.

Signalling in the heart was assessed 13 weeks after STZ administration. Densitometric analysis of bands is expressed as a relative optical density (O.D.) of phosphorylated Akt ($pSer^{473}$) corrected to total Akt and normalised using the WT + vehicle band. Experimental groups: WT + vehicle (0.1 M citrate buffer, i.p. for 5 days); WT + STZ (45 mg/kg, 0.1M citrate buffer, i.p. for 5 days); $ANXA1^{-/-}$ + vehicle (0.1 M citrate buffer, i.p. for 5 days) and $ANXA1^{-/-}$ + STZ (45 mg/kg, 0.1 M citrate buffer, i.p. for 5 days). Representative images from one of three repeated experiments are shown in this Figure. Data analysed by a one-way ANOVA followed by a Bonferroni *post-hoc* test, and expressed as mean±SEM. n= 3-4 per group. *P<0.05, **P<0.01.

2.4.15. The effect of administration of hrANXA1 on non-fasted blood glucose, serum insulin and OGTT in mice subjected to STZ-induced type-1 diabetes mellitus.

To determine the effect of administration of human recombinant (hr) ANXA1 on underlying diabetic phenotype, measurements were taken 13 weeks post STZ administration. When compared to sham WT-mice, WT-mice, challenged with STZ demonstrated a significant decrease in serum insulin (Figure 2.19A, $P<0.0001$), and a significant increase in non-fasted blood glucose levels (Figure 2.19B, $P<0.01$). When compared to WT-mice challenged with STZ, WT-mice challenged with STZ and treated with daily hrANXA1 (1 µg hrANXA1, 100 µl Hepes buffer, i.p., daily weeks 1-13) or with hrANXA1 days 1-5 (1 µg hrANXA1, 100 µl Hepes buffer, i.p., days 1-5) demonstrated not significant difference in serum insulin (Figure 2.19A, ns) or non-fasted blood glucose (Figure 2.19B, ns).

When compared to sham mice not challenged with STZ, mice challenged with STZ demonstrated a significant impairment in oral glucose tolerance (measured as AUC of OGTT; Figure 2.19D). When compared to WT-mice challenged with STZ, WT-mice challenged with STZ that had been treated with daily hrANXA1 or with hrANXA1 days 1-5 demonstrated no alteration on tolerance to oral glucose (Figure 2.19C), using AUC analysis (Figure 2.19D, ns). Leading to the conclusion that the treatment of mice challenged with hrAXNA1 during STZ administration did not effect the on set of a diabetic phenotype.

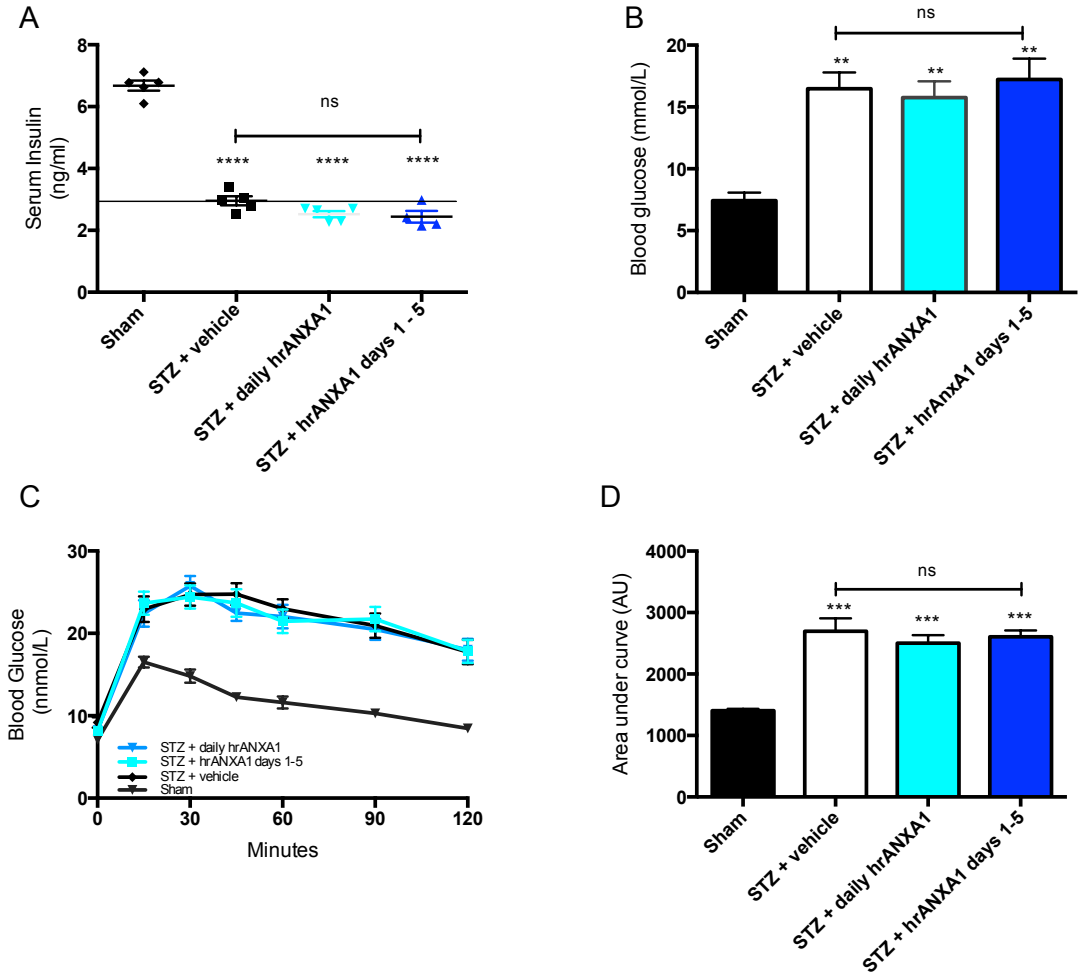

Figure 2.19. Effect of treatment with hrANXA1 on diabetic parameters in a model of STZ-induced type-1 diabetes mellitus.

Serum insulin measured by sandwich ELSIA at weeks 13 (A); non-fasted blood glucose measured 13 post STZ administration (B); OGTT was measured in life after 18 h of fasting, mice were then given a 1 g/kg oral glucose bolus at time 0. Glucose levels were subsequently measured at 0, 15, 30, 45, 60, 90 and 120 minutes post oral glucose delivery (C) and the area under the curve of OGTT calculated (D). Experimental groups: Sham (non-diabetic); STZ + vehicle (diabetic); STZ + daily hrANXA1 (diabetic + 1 µg hrANXA1, i.p., daily weeks 1-13) and STZ + hrANXA1 days 1-5 (diabetic + 1 µg hrANXA1, i.p., days 1-5). Data analysed by a one-way ANOVA followed by a Bonferroni *post-hoc* test, and expressed as mean ± SEM. n= 6-8 per group. **P<0.01, ***P<0.001, ****P<0.0001.

2.4.16. The effect of administration of hrANXA1 on renal dysfunction in mice subjected to STZ-induced type-1 diabetes mellitus.

To assess the effect of administration of hrANXA1 on renal function, parameters of renal function were assessed from serum and urine collection 13 weeks post administration of STZ. When compared to sham WT-mice, WT-mice challenged with STZ demonstrated a significant increase in ACR (Figure 2.20A, $P<0.0001$) and serum urea (Figure 2.20B, $P<0.001$) suggesting the development of proteinuria and renal dysfunction, respectively. When compared to sham WT-mice, mice challenged with STZ demonstrated a significant increase in urine flow (Figure 2.20C, $P<0.0001$) and creatinine clearance (Figure 2.20D, $P<0.001$) suggesting the development of renal hyperfiltration.

When compared to WT-mice challenged with STZ, WT-mice challenged with STZ and treated with daily hrANXA1 (weeks 1-13) demonstrated a reduction in ACR (Figure 2.20A, $P<0.01$) and serum urea (Figure 2.20B, $P<0.001$) suggesting less proteinuria and renal dysfunction, respectively. Similarly, when compared to WT-mice challenged with STZ, WT-mice challenged with STZ and treated with daily hrANXA1 (weeks 1-13) demonstrated a significant reduction in urine flow (Figure 2.20C, $P<0.0001$) and creatinine clearance (Figure 2.20A, $P<0.01$) suggesting a reduction in hyperfiltration. However, when compared to WT-mice challenged with STZ, mice challenged with STZ and treated with hrANXA1 (days 1-5) did not have significantly different ACR (Figure 2.20A, ns), serum urea (Figure 2.20B, ns), urine flow (Figure 2.00C, ns) and creatinine clearance (Figure 2.20D, ns).

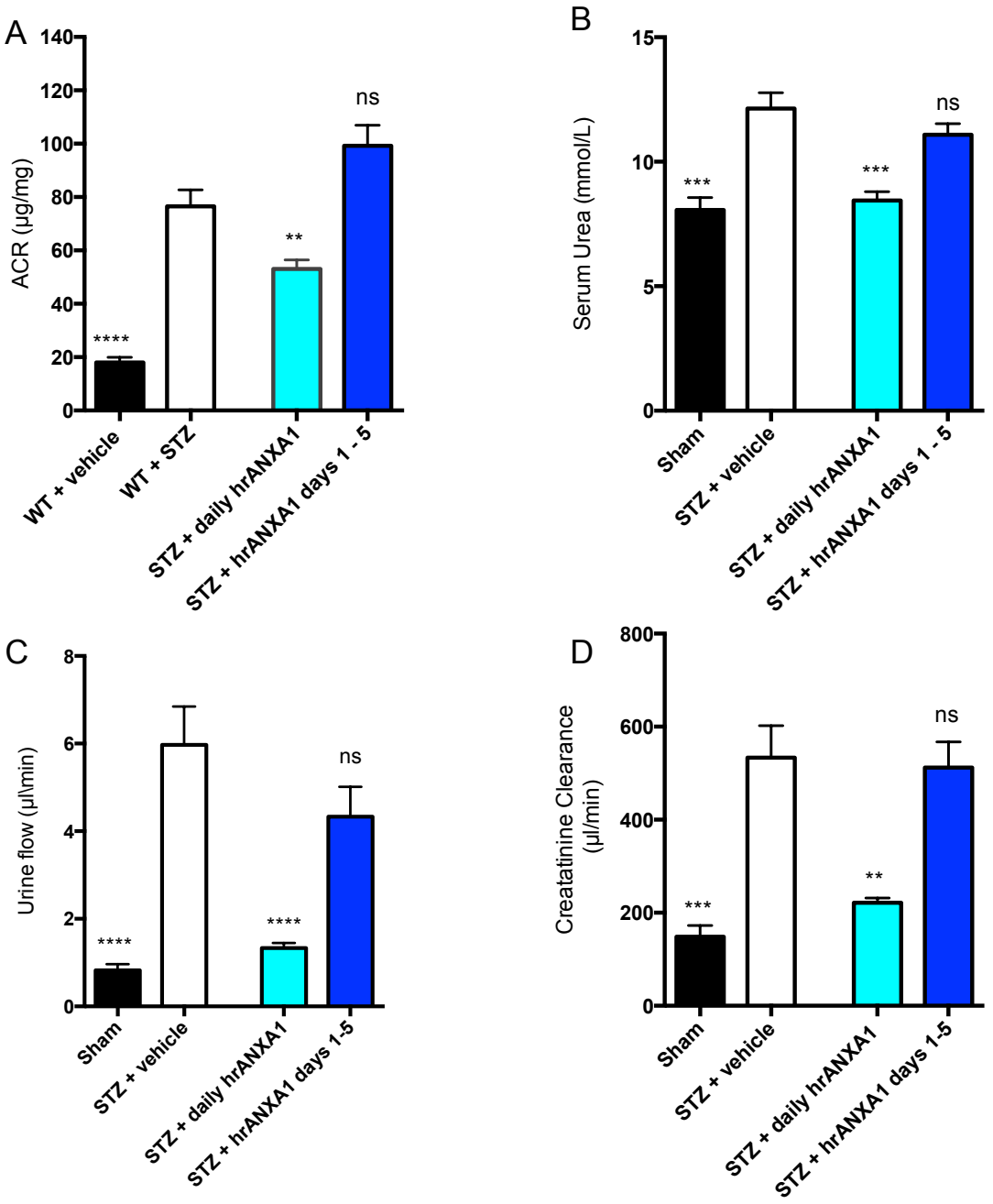

Figure 2.20. Effect of treatment with hrANXA1 on renal dysfunction caused by STZ-induced type-1 diabetes mellitus.

Measures of renal function urine albumin-to-creatinine ratio (A); serum urea (B); urine flow (C) and creatinine clearance (D measured from serum and urine at week 13 post STZ administration. Experimental groups: Sham (non-diabetic); STZ + vehicle (diabetic); STZ + daily hrANXA1 (diabetic + 1 µg hrANXA1, i.p., daily weeks 1-13) and STZ + hrANXA1 days 1-5 (diabetic + 1 µg hrANXA1, i.p., days 1-5). Data analysed by a one-way ANOVA followed by a Bonferroni *post-hoc* test, and expressed as mean ± SEM. n= 6-8 per group. **P<0.01, ****P<0.0001.

2.4.17. The effect of administration of hrANXA1 on the cardiac dysfunction in WT-mice subjected to STZ-induced type-1 diabetes mellitus.

To determine the effect of administration of hrANXA1 on the cardiac dysfunction caused by STZ administration, left ventricular function was assessed using echocardiography at 13 weeks post STZ administration. When compared WT-mice not challenged with STZ, WT-mice challenged with STZ demonstrated significant reductions in ejection fraction (Figure 2.21A, $P<0.0001$), fractional shortening (Figure 2.21B, $P<0.0001$) and fractional areas change (Figure 2.21C, $P<0.0001$), indicating the development of systolic contractile dysfunction.

When compared to WT-mice challenged with STZ, WT-mice challenged with STZ and treated with daily hrANXA1 (weeks 1-13) demonstrated a significant greater ejection fraction (Figure 2.21A, $P<0.0001$), fractional shortening (Figure 2.21B, $P<0.0001$) and fractional areas change (Figure 2.21C, $P<0.0001$) indicating that hrANXA1 has prevented the development of systolic contractile dysfunction. When compared to WT-mice challenged with STZ, WT-mice challenged with STZ and treated with hrANXA1 (days 1-5) demonstrated no significant difference in ejection fraction (Figure 11A, ns), fractional shortening (Figure 2.21B,ns) and fractional areas change (Figure 11C, ns).

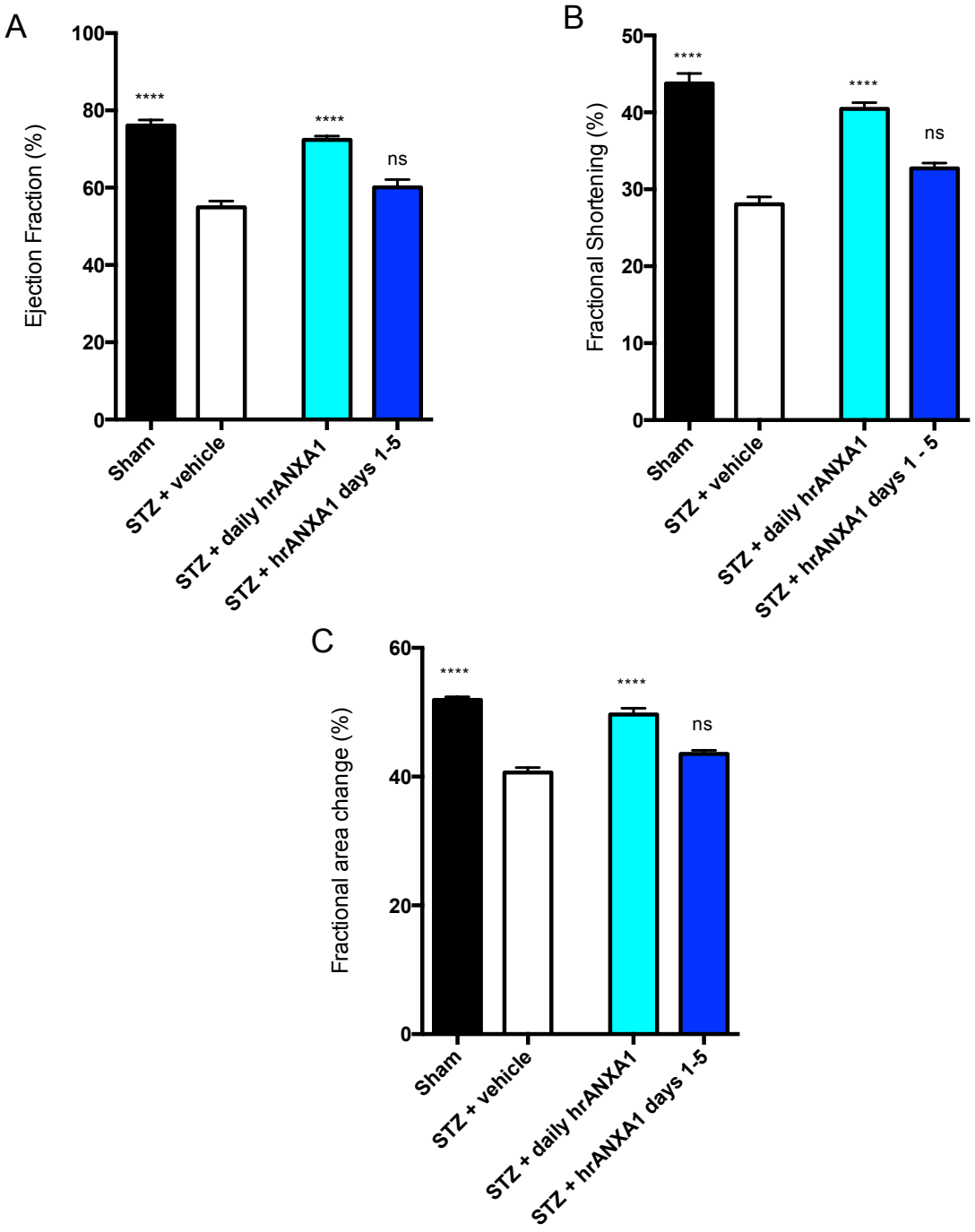

Figure 2.21. Effect of treatment with hrANXA1 on cardiac dysfunction caused by STZ-induced type-1 diabetes mellitus.

Measures of cardiac function ejection fraction (A); fractional shortening (B) and fractional area change (C) were measured by echocardiograph 13 weeks post STZ administration. Experimental groups: Sham (non-diabetic); STZ + vehicle (diabetic); STZ + daily hrANXA1 (diabetic + 1 µg hrANXA1, i.p., daily weeks 1-13) and STZ + hrANXA1 days 1-5 (diabetic + 1 µg hrANXA1, i.p., days 1-5). Data analysed by a one-way ANOVA followed by a Bonferroni *post-hoc* test, and expressed as mean ± SEM. n= 6-8 per group. ****P<0.0001.

2.4.18. The effect of late administration with hrANXA1 on non-fasted blood glucose, serum insulin and OGTT subjected to STZ-induced type-1 diabetes mellitus.

To determine the effect of late therapeutic administration of hrANXA1 on underlying diabetic phenotype, measurements were taken 13 weeks post STZ administration. When compared to WT-mice not challenged with STZ, WT-mice challenged with STZ demonstrated a significant reduction in insulin levels (Figure 2.22A, $P<0.0001$), and a significant increase in non-fasted blood glucose levels (Figure 2.22B, $P<0.01$). When compared to sham WT-mice, WT-mice challenged with STZ given late treatment with hrANXA1 (weeks 8-13) demonstrated no significant difference in serum insulin levels (Figure 2.22A, ns) or non-fasted blood glucose levels (Figure 2.22B, ns).

Similarly, when compared to sham WT-mice, WT-mice challenged with STZ demonstrated a significant impairment to oral glucose (Figure 2.22C) when AUC analysis of OGTT was performed (Figure 2.22D, $P<0.001$). When compared to WT- STZ, mice challenged with STZ and late treatment with hrANXA1 (weeks 8-13) demonstrated no difference in tolerance to oral glucose (Figure 2.22C,) when AUC analysis of OGTT was performed (Figure 2.22D, ns).

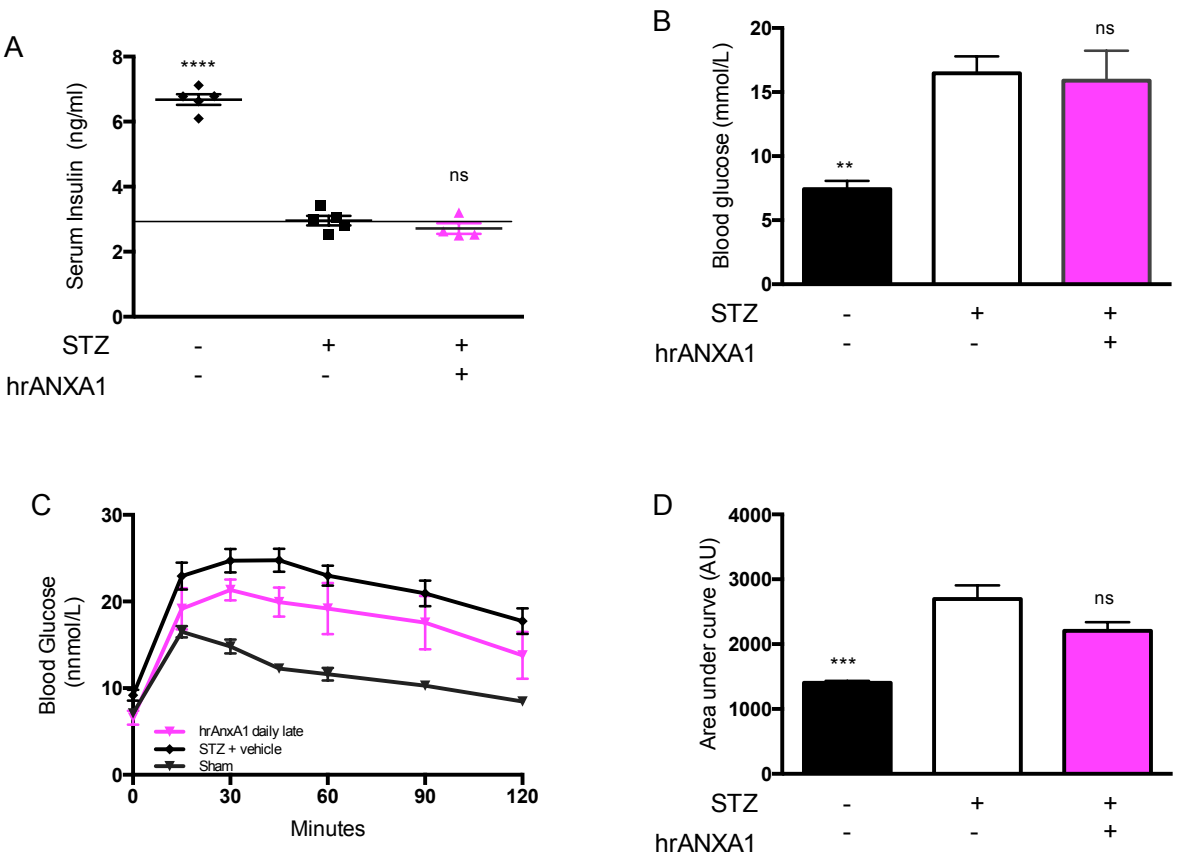

Figure 2.22. Effect of late treatment with hrANXA1 on diabetic parameters in a model of STZ-induced type-1 diabetes mellitus.

Serum insulin measured by sandwich ELSIA at weeks 13 (A); non-fasted blood glucose measured 13 weeks post STZ administration (B); OGTT was measured in life after 18 h of fasting, mice were then given a 1 g/kg oral glucose bolus at time 0. Glucose levels were subsequently measured at 0, 15, 30, 45, 60, 90 and 120 minutes post oral glucose delivery (C) and the area under the curve of OGTT calculated (D). Experimental groups: Sham (non-diabetic); STZ + vehicle (diabetic) and STZ + hrANXA1 (diabetic + 1 µg hrANXA1, i.p., daily weeks 8-13). Data analysed by a one-way ANOVA followed by a Bonferroni *post-hoc* test, and expressed as mean ± SEM. n= 6-8 per group. **P<0.01, ***P<0.001, ****P<0.0001.

2.4.19. The effect of late treatment with hrANXA1 on renal dysfunction in mice subjected to STZ-induced type-1 diabetes mellitus.

Renal function was assessed from serum and urine collected 13 weeks post STZ administration. When compared to sham WT-mice, WT-mice challenged with STZ demonstrated a significant increase in ACR (Figure 2.23A, $P<0.0001$), and serum urea (Figure 2.23B, $P<0.05$), suggesting the development of proteinuria and renal dysfunction. When compared to sham WT-mice, WT-mice challenged with STZ demonstrated a significant increase in urine flow (Figure 2.23C, $P<0.0001$), and creatinine clearance (Figure 2.23D, $P<0.001$), suggesting hyperfiltration in diabetic mice. .

When compared to WT-mice challenged with STZ, mice challenged with STZ and given late treatment with hrANXA1 from weeks 8-13 exhibited no significant changes in ACR (Figure 2.23A, ns). However, when compared to mice challenged with STZ, mice challenged with STZ and given late treatment with hrANXA1 demonstrated a significant decrease in serum urea (Figure 2.23B, $P<0.05$. Similarly when compared to mice challenged with STZ, mice challenged with STZ and given late treatment with hrANXA1 demonstrated a small reduction in urine flow (Figure 13C, ns), which was not significant, but a significant reduction in creatinine clearance (Figure 13D, $P<0.05$), suggesting a reduction in renal hyperfiltration.

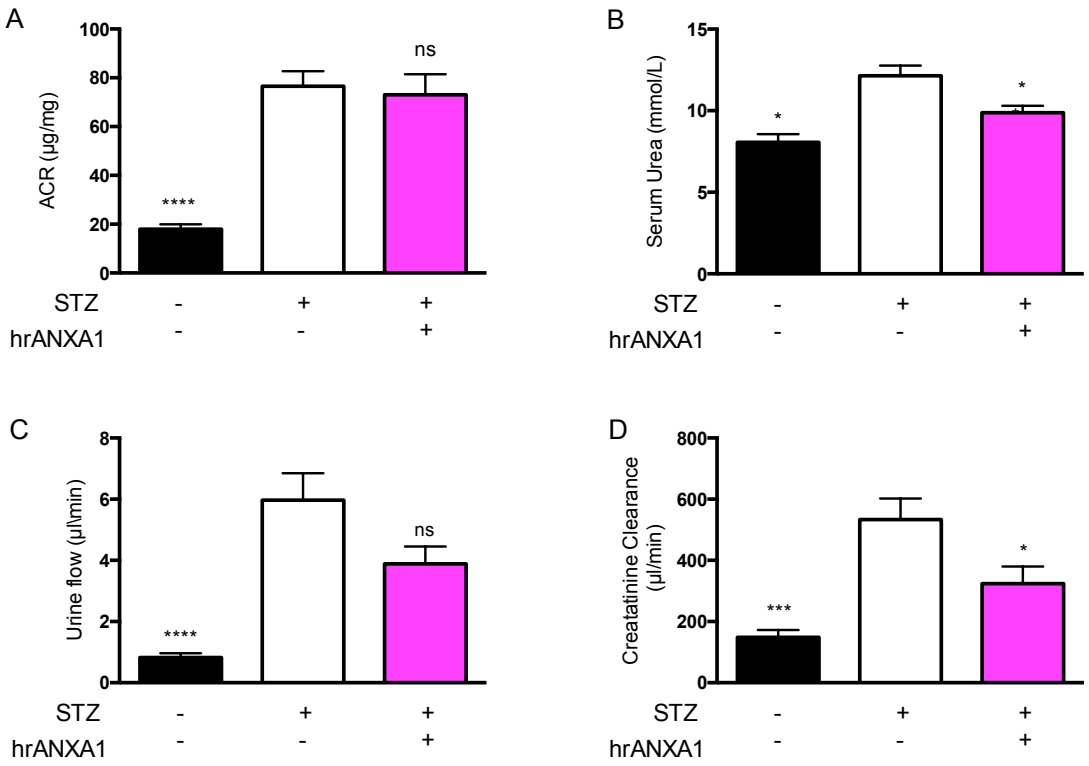

Figure 2.23. Effect of late treatment with hrANXA1 on renal dysfunction caused by STZ-induced type-1 diabetes mellitus.

Measures of renal function A) urine albumin-to-creatinine ratio; B) serum urea; C) urine flow and D) creatinine clearance where measured from urine and serum at week 13 post STZ administration. Experimental groups: Sham (non-diabetic); STZ + vehicle (diabetic) and STZ + hrANXA1 (diabetic + 1 µg hrANXA1, i.p., daily weeks 8-13). Data analysed by a one-way ANOVA followed by a Bonferroni *post-hoc* test, and expressed as mean ± SEM. n= 6-8 per group. *P<0.05, ***P<0.001, ****P<0.0001.

2.4.20. The effect of late treatment with hrANXA1 on cardiac dysfunction in mice subjected to STZ-induced type-1 diabetes mellitus.

To determine the effect of treatment with hrANXA1 on cardiac dysfunction caused by diabetes, left ventricular function was assessed using echocardiography 13 weeks post STZ administration. Sham WT-mice had no significant difference in ejection fraction (Figure 2.24A, $P<0.05$), fractional shortening (Figure 2.24B, $P<0.05$) and fractional areas change (Figure 2.24C, $P<0.05$) from week 7 to week 13. However, mice challenged with STZ demonstrated a time-dependent, significant decrease in ejection fraction (Figure 2.24A, $P<0.05$), fractional shortening (Figure 2.24B, $P<0.05$) and fractional area change (Figure 2.24C, $P<0.05$) at week 7 and week 13.

Interestingly, mice challenged with STZ and given late treatment with hrANXA1 had no significant difference in ejection fraction (Figure 2.24A, $P>0.05$), fractional shortening (Figure 2.24B, $P>0.05$) and fractional areas change (Figure 2.24C, $P>0.05$) when it was measured at week 7 (before treatment) and weeks 13 (end of treatment), suggesting that late therapeutic treatment with hrANXA1 can halt the progression of cardiac dysfunction in diabetic mice.

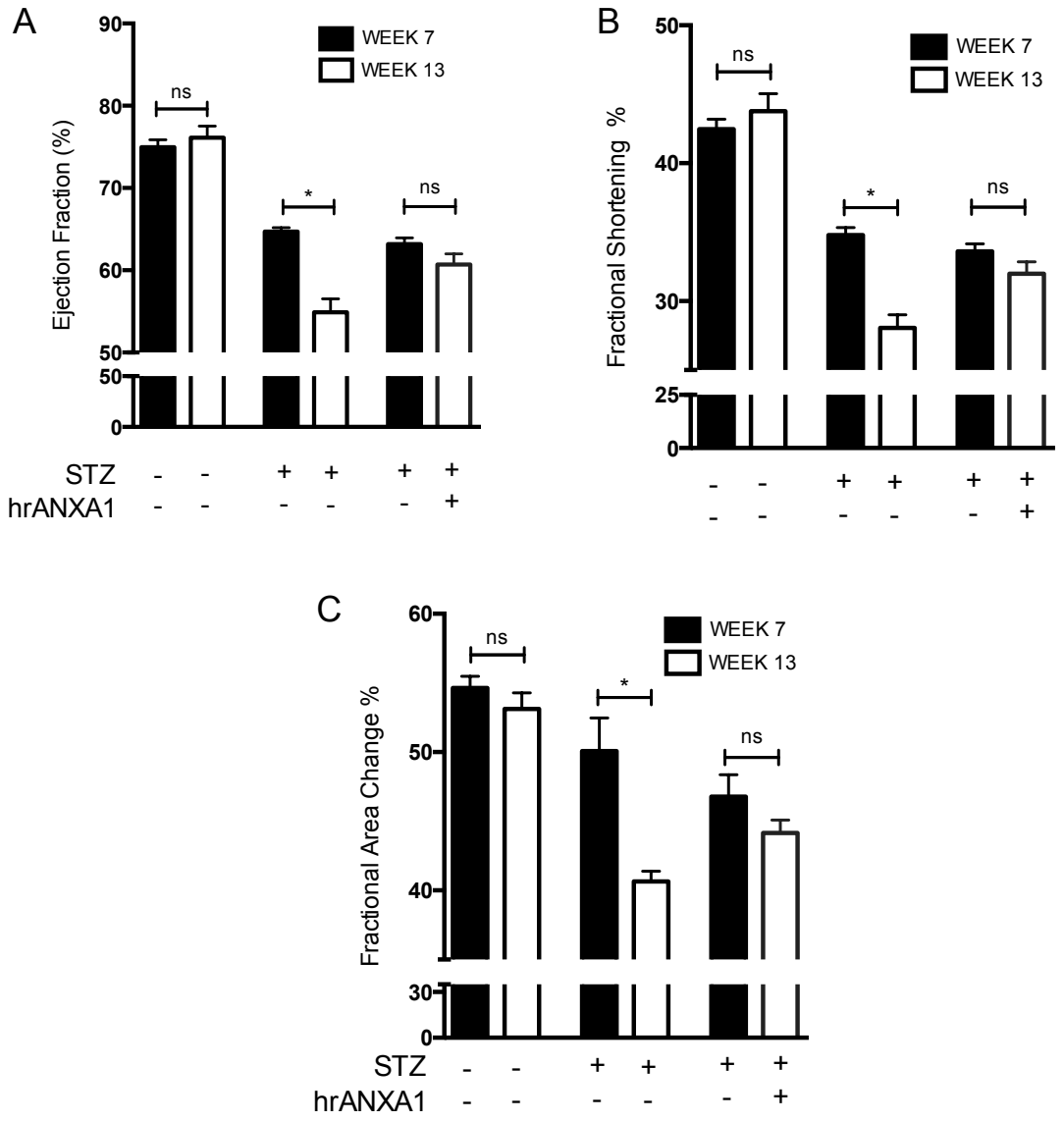

Figure 2.24. Effect of late treatment with hrANXA1 on cardiac dysfunction caused by STZ-induced type-1 diabetes mellitus.

Measurements of cardiac function in wild-type and ANXA1-/- mice: ejection fraction (A); fractional shortening (B); and fractional area change (C), measured by echocardiograph at week 7 and week 13 post STZ administration. Experimental groups: Sham (non-diabetic); STZ + vehicle (diabetic) and STZ + hrANXA1 (diabetic + 1 µg hrANXA1, i.p., daily weeks 8-13). Data analysed by a one-way ANOVA followed by a Bonferroni *post-hoc* test, and expressed as mean±SEM. n= 6-8 per group. **P*<0.05.

2.4.21. The effect of late treatment with hrANXA1 on the phosphorylation of p-38, JNK and ERK1/2 in kidneys from mice subjected to STZ-induced type-1 diabetes mellitus.

The potential underlying mechanisms behind the observed renal dysfunction were investigated by semi-quantitative western blot analysis of mouse kidneys 13 weeks post STZ administration. When compared to renal tissue obtained from sham mice, renal tissue from mice challenged with STZ exhibited a significant increase in phosphorylation of p38 on Thr^{180}/Thr^{182} (Figure 2.25A, $P<0.05$), JNK on Thr^{183}/Tyr^{185} (Figure 2.25B, $P<0.0001$) and ERK1/2 on Tyr^{202}/Tyr^{204} (Figure 2.25C, $P<0.001$) suggesting strong activation of downstream effectors of the MAPK signal transduction pathway.

When compared to mice challenged with STZ, kidney tissue from mice challenged with STZ and treated with daily hrANXA1 (weeks 1-13) exhibited a significantly lower degree of phosphorylation of p38 on Thr^{180}/Thr^{182} (Figure 2.25A, $P<0.05$), JNK on Thr^{183}/Tyr^{185} (Figure 2.25B, $P<0.0001$) and ERK1/2 on Tyr^{202}/Tyr^{204} (Figure 2.25C, $P<0.001$). Similarly, when compared to mice challenged with STZ, kidneys from mice challenged with STZ given late treatment (weeks 8-13) with hrANXA1 exhibited a significant decrease in the phosphorylation of JNK on Thr^{183}/Tyr^{185} (Figure 2.25B, $P<0.01$) and ERK1/2 on Tyr^{202}/Tyr^{204} (Figure 2.25B, $P<0.05$). However, when compared to mice challenged with STZ, kidneys from mice challenged with STZ treated with hrANXA1 (days 1-5) exhibited no difference in phosphorylation of p38 on

Thr^{180}/Thr^{182} (Figure 2.25A, P>0.05), JNK on Thr^{183}/Tyr^{185} (Figure 2.25B, P>0.05) and ERK1/2 on Tyr ^{202}/Tyr^{204} (Figure 2.25C, P>0.05).

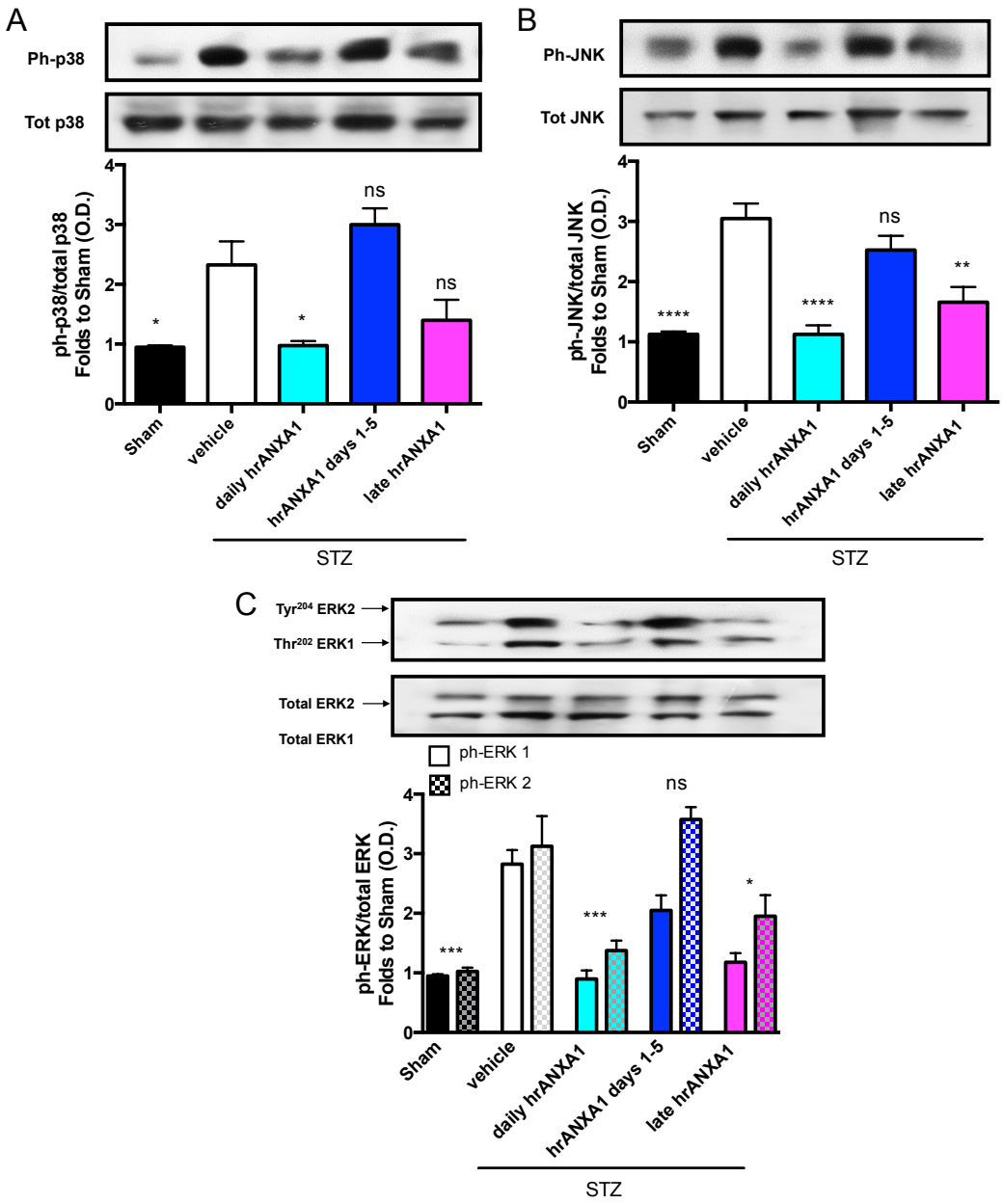

Figure 2.25. Effect of late treatment with hrANXA1 on the phosphorylation of p38, JNK and ERK1/2 in kidneys of mice with STZ-induced type-1 diabetes mellitus.

Signalling in the kidney was assessed 13 weeks after STZ administration. Densitometric analysis of bands is expressed as a relative optical density (O.D.) of phosphorylated p38 ($pThr^{180}/Thr^{182}$) corrected to total p38 and normalised using the WT + vehicle band (A); phosphorylated JNK ($pThr^{183}/Thr^{185}$) corrected to total JNK and normalised using the WT + vehicle band (B); and phosphorylated ERK1/2 ($pThr^{202}/Tyr^{204}$) corrected to total ERK1/2 and normalised using the WT + vehicle band (C). Experimental groups: Sham (non-diabetic); STZ + vehicle (diabetic), STZ + daily hrANXA1 (diabetic + 1 µg hrANXA1, i.p., daily weeks 1-13), STZ + hrANXA1 days 1-5 (diabetic + 1 µg hrANXA1, i.p., days 1-5) and STZ + hrANXA1 (diabetic + 1 µg hrANXA1, i.p., daily weeks 8-13). Representative images from one of three repeated experiments are shown in this Figure. Data analysed by a one-way ANOVA followed by a Bonferroni *post-hoc* test, and expressed as mean ± SEM. n= 3-4 per group. *P<0.05, **P<0.01, ***P<0.001, ****P<0.0001.

2.4.22. The effect of late treatment with hrANXA1 on the phosphorylation of Akt in kidneys from mice subjected to STZ-induced type-1 diabetes mellitus.

When compared to hearts obtained from sham mice, hearts from mice challenged with STZ exhibited a significant decrease in the phosphorylation of Akt on Ser^{473} (Figure 2.26, $P<0.01$). When compared to mice challenged with STZ, hearts from STZ-mice treated with daily hrANXA1 (weeks 1-13) exhibited a significantly greater degree of phosphorylation of Akt on Ser^{473} (Figure 2.26, $P<0.01$). However, when compared to mice challenged with STZ, hearts from mice challenged with STZ and treated with hrANXA1 (days 1-5) or given late treatment (weeks 8-13) with hrANXA1 exhibited no difference in the phosphorylation of Akt on Ser^{473} (Figure 2.26).

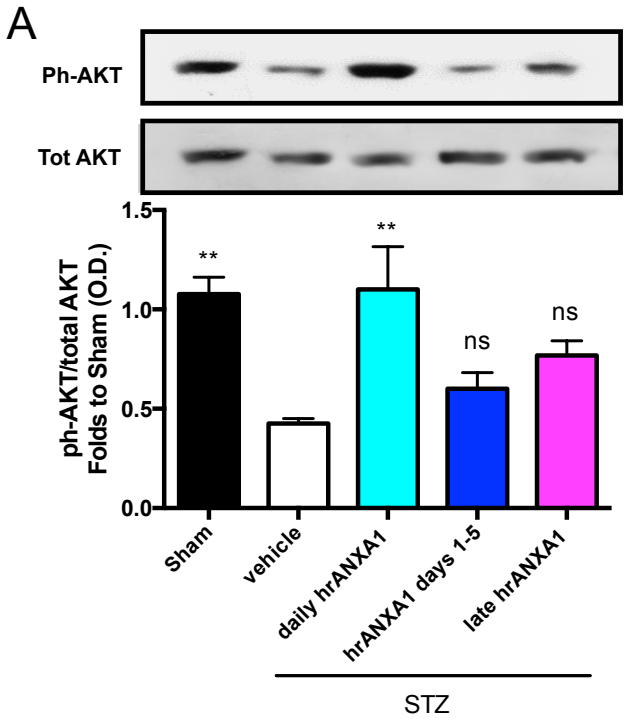

Figure 2.26. Effect of late treatment with hrANXA1 on phosphorylation of Akt in kidney of mice with STZ-induced type-1 diabetes mellitus.

Signalling in the kidney was assessed 13 weeks after STZ administration. Densitometric analysis of bands is expressed as a relative optical density (O.D.) of phosphorylated Akt ($pSer^{473}$) corrected to total Akt and normalised using the WT + vehicle band. Experimental groups: Sham (non-diabetic); STZ + vehicle (diabetic), STZ + daily hrANXA1 (diabetic + 1 µg hrANXA1, i.p., daily weeks 1-13), STZ + hrANXA1 days 1-5 (diabetic + 1 µg hrANXA1, i.p.., days 1-5)and STZ + hrANXA1 (diabetic + 1 µg hrANXA1, i.p., daily weeks 8-13). Representative images from one of three repeated experiments are shown in this Figure. Data analysed by a one-way ANOVA followed by a Bonferroni *post-hoc* test, and expressed as mean ± SEM. n= 3-4 per group. **P<0.01.

2.5 Discussion

The main finding of the clinical study outlined in this chapter is the discovery that patients with T1DM, with or without diabetic nephropathy had elevated plasma ANXA1 levels, when compared to healthy donors. Additionally, patients with diabetic nephropathy had significantly higher CRP level compared to those without nephropathy, suggesting greater systemic inflammation. Thus, I designed further experiments to gain a better insight into the biological importance of endogenous ANXA1, a known anti-inflammatory molecule, in T1DM. To do this, I used an animal model of STZ-induced T1DM in both WT and ANXA1$^{-/-}$ mice to model the human disease. The main findings of this experimental study were that (i) ANXA1 levels were lower in the kidneys and hearts, of mice administered STZ to induced diabetes (ii) ANXA1$^{-/-}$ mice with STZ-induced diabetes had a more severe diabetic phenotype compared WT-mice administrated STZ and (iii) ANXA1$^{-/-}$ mice with STZ-induced diabetes develop more severe cardiac dysfunction and renal dysfunction compared to WT-mice administrated.

I next wanted to investigate whether ANXA1 could be used as a potential new therapeutic agent. The main finding of this experimental, efficacy study were that (i) chronic treatment of diabetic mice with hrANXA1 (weeks 1-13) did not prevent the development of a diabetic phenotype, but prevented the development of both cardiac and renal dysfunction, (ii) therapeutic administration of hrANXA1 (weeks 8-13) after significant cardiac and renal dysfunction had developed halted the progression of both cardiac and renal

dysfunction seen in diabetic WT-mice treated with vehicle and (iii) administration of hrANXA1 during STZ induction of diabetes (days 1-5) did not protect against the development to diabetes or prevent the development of cardiac and renal dysfunction.

T1DM is characterised by elevated blood glucose level, which drives low-grade chronic inflammation, and this contributes to tissue/organ damage. Healthy donors have low levels of ANXA1 in plasma (Gavins & Hickey, 2012). Here we report that ANXA1 is elevated in patients with T1DM with/without nephropathy (Figure 1A). Additionally, we show that the diabetic patients have systemic inflammation and that the degree of inflammation is even higher in patients with impaired renal function (diabetic nephropathy). Elevated plasma CRP is a strongly associated with adverse outcome in myocardial infarction, stroke and coronary heart disease, which are common causes of death in patients with T1DM. I propose that the elevation in circulating ANXA1 is a compensatory mechanism to protect the tissue from the deleterious effects of hyperglycaemia, independent of the presence of diabetic nephropathy and not a consequence of systemic inflammation (Figure 1B). ANXA1 is found in many tissues, including heart and kidney but is also highly expressed in leukocytes, specifically neutrophils (Gavins & Hickey, 2012). Here I report that in the murine model of T1DM that in both the heart and kidney ANXA1 levels are lower, the hypothesis being that hyperglycaemia causes cellular activation and ANXA1 to be released from tissue stores. Solito *et al.* were the first showed that upon both stimulation with glucocorticoids (dexamethasone) and noxious stimuli (LPS) ANXA1 is released from its vesicular stores and released. Here we show using our patient

data that circulating (secreted) ANXA1 is elevated in plasma of diabetic patients. In our murine model we also show that circulating levels are increased in our diabetic mice (although not significantly) but importantly that tissue levels are decreased, supporting our hypothesis that ANXA1 is released in response to hyperglycaemia. ANXA1 is needed to be released so it can signal in both a autocrine and paracrine manner through the FPR repertoire of receptors.

When mice were challenged with STZ they developed a T1DM phenotype characterised by depleted serum insulin, elevated non-fasted blood glucose levels and impaired OGTT within 13 weeks. STZ enters pancreatic beta-cells via the glucose transporter GLUT2 and causes alkylation of DNA (Szkudelski 2001). DNA damage induces ADP-ribosylation, which leads to depletion of cellular NAD+ and ATP. Enhanced dephosphorylation of ATP after STZ administration supplies a substrate for xanthine oxidase resulting in the formation of superoxide radicals; eventually leading to beta cells destruction by necrosis (Szkudelski, 2001). In patients with T1DM, β-cell mass is irreversibly reduced by 70–80% at the time of diagnosis (Matveyenko & Butler, 2008), similarly, in murine experimental models of T1DM a diabetic phenotype is only evidenced with similar loss of beta cell mass (Akirav et al., 2008). This dramatic beta cells loss results in reduced insulin synthesis and, therefore, there is insufficient insulin secretion to regulate blood glucose levels, leading to persistent hyperglycaemia, and ultimately means an inability to deal with spikes in glucose for example after meals.

ANXA1 is endogenously expressed in islets (Gu et al., 2012), where it localises to the insulin secretory granules (Rackham et al., 2016). Ohnishi *et al.* reported that ANXA1 was involved in glucose-induced insulin secretion in rat pancreatic islets in both an autocrine and paracrine manner (Ohnishi et al., 1994)(Ohnishi et al., 1995). I found that baseline ANXA1$^{-/-}$ mice demonstrate no augmentation in OGTT compared to WT-mice, suggesting ANXA1$^{-/-}$ is not essential for 'normal' glucose-stimulated insulin release. This is consistent with Rachman *et al*. findings that isolated and cultured islets from ANXA1$^{-/-}$ mice demonstrate no augmentation in glucose-stimulated insulin release compared to islets from wild-type mice (Rackham et al., 2016). However, diabetic ANXA1$^{-/-}$ mice did have a more severe diabetic phenotype compared to diabetic WT-mice; evidenced by higher non-fasted blood glucose and a more severe impairments in OGTT. Interestingly, both diabetic WT and ANXA1$^{-/-}$ had their non-fasted serum insulin levels reduced to a similar degree. This finding suggests that endogenous ANXA1 limits the development of hyperglycaemia in an insulin-independent manner.

The first line treatment strategy for patients with T1DM is the rigorous management of blood glucose using insulin replacement. However, even patients with well-managed blood glucose develop microvascular complications overtime However, the pathogenesis and natural history of T1DM are largely understudied, especially in the context of the molecular mechanisms (Atkinson, 2012)(Papadopoulou-Marketou et al., 2016). These complications include diabetic cardiomyopathy and nephropathy. When compared to the general population, patients with T1DM have a 5.2-fold increased risk of a cardiovascular disease (Lee et al., 2015), and a 2.2-fold increase in risk of end-stage renal

disease (Chang et al., 2014). I have demonstrated that diabetic ANXA1$^{-/-}$ mice develop more severe cardiac and renal dysfunction compared to diabetic WT-mice within 13 weeks, suggesting that endogenous ANXA1 limits the development of end-organ injury/dysfunction in mice with STZ- induced diabetes.

As hypertrophy is an important contributor in diabetes-associated cardiac and renal dysfunction I evaluated both intra ventricular spectrum diameter a measure of concentric hypertrophy (heart) and glomerular size (kidney); and report that both are significantly increased in mice challenged with STZ. Notably, both glomerular hypertrophy, but not cardiac hypertrophy, was significantly further increased in diabetic ANXA1$^{-/-}$ mice when compared to diabetic WT-mice, suggesting that hypertrophy is not the lead cause of both cardiac and renal dysfunction. Cardiac hypertrophy is a common response to external stressors, including hyperglycaemia and oxidative stress (Festa & Haffner, 2005). Hypertrophy is a compensatory response to maintain cardiac output, however, when stressors persist (i.e. chronic hyperglycaemia in the case of T1DM), this compensatory process evolves into a decompensated state with profound changes contractile dysfunction, evidenced by reduced EF, FS and FAC and extracellular remodeling, evidence by IVSd. Similarly, renal hypertrophy is also a compensatory mechanism (Reidy et al., 2014); in the case of T1DM there is excessive renal hyperfiltration due to osmotic irregularities due to elevated blood glucose levels, putting stress on glomeruli and proximal tubules (Helal et al., 2012). Glomerular hypertension and hyperfiltration is in part due to activation of the renin angiotension system (Gross et al., 2005) and defects in the

SGLT2 sodium reabsorption pathways (Zhao et al., 2016). These two mechanisms combine and cause an increased pressure in the PCT and is a leading cause of hyperfiltration, indeed I clearly show evidence that mice with STZ-induced diabetes have hyperfiltration. This added stress manifests in other the structural loss of brush borders if the PCT and compensatory activation of pro-fibrotic mechanisms. Indeed I have demonstrated that ANXA1$^{-/-}$ have both a higher level of hyperfiltration, marked histological changes and increased fibrosis in the kidney after STZ-induction of T1DM.

Having found that endogenous ANXA1 limits the development of microvascular complications associated with diabetes, I wanted to investigate whether pharmacological intervention with exogenous hrANXA1 can attenuate the development of diabetic nephropathy and cardiomyopathy. Previously, both full length AXNA1 and Ac2-26 peptide (the N-terminal functional fragment of ANXA1) have been used *in vivo* both eliciting biological function. In this study we chose to use full-length human recombinant ANXA1. The rational being that studies have reported that the dose of full-length ANXA1 needed to induce biological function (inhibition of monocyte adherence to the endothelial) is up to 20 times less when using only the Ac2-26 peptide (Solito et al. 2000) and 14 times less to induce changes in gene expression in terms of molarity (Rodrigues-Lisoni et al., 2006).

Treatment of mice challenged with STZ with hrANXA1 (from week 1-13) did not alter the diabetic phenotype (reduced insulin levels, elevated blood glucose and impaired OGTT), but attenuated the cardiac dysfunction and the proteinuria

caused by diabetes; suggesting that ANXA1 reduces the cardiac and renal injury caused by hyperglycaemia and excessive oxidative stress (organ protection rather than reduction of diabetes). It should be noted that administration of ANXA1 for one week during the administration of STZ was also not sufficient to reduce the diabetic phenotype suggesting that ANXA1 does not reduce the destruction of pancreatic islet cells caused by STZ. Most notably, we also report that a late, therapeutic intervention (at week 8, when a diabetic phenotype and a moderate degree of cardiac and renal dysfunction had already occurred) halted the further decline in both cardiac and renal function seen in diabetic WT-mice. This evidence all supports the hypothesis that ANXA1 must activate protective pathways both as an endogenous mediator or when used exogenously as a pharmacological intervention.

What are the mechanisms by which ANXA1 elicits protection against cardiac and renal dysfunction associated with diabetes? I show here for the first time that the development of T1DM (caused by STZ) in mice are associated with (i) a reduction in endogenous ANXA1 levels in both the heart and the kidney (increased secretion), and (ii) a decline in cardiac and renal dysfunction. Thus, we speculated that endogenous ANXA1 protects both the heart and the kidney (and hence reduces organ injury/dysfunction) by acting on pro-survival and anti-inflammatory pathways.

Hyperglycaemia leads to activation (phosphorylation) of MAPK's p38, JNK and ERK1/2, which drives excessive inflammation, hypertrophy and fibrosis in the heart (Naito et al., 2003) and kidney (Komers et al., 2007)(Cheng et al., 2013) .

Pharmacological inhibition or genetic deletion of any of these three MAPKs reduces microvascular complications (diabetic nephropathy, cardiomyopathy and retinopathy) caused by T1DM in rodents (Du et al., 2010)(Singh et al., 2017). Indeed, we observed a significant increase in activated (phosphorylated) p38, JNK and ERK1/2 in diabetic WT-mice. Interestingly, ANXA1$^{-/-}$ mice even in the absence of diabetes (no STZ challenge), had constitutive activation (phosphorylation) of p38, JNK and ERK1/2 in the heart and kidney, suggesting endogenous ANXA1 inhibits their activation. The degree of activation of p38, JNK and ERK1/2 was further exacerbated when ANXA1$^{-/-}$ mice were challenged with STZ. As diabetic ANXA1$^{-/-}$ mice also had excessive renal hypertrophy and fibrosis, we speculate that the excessive activation of these known pro-inflammatory and pro-fibrotic signalling pathways are key drivers of the excessive pathology seen in ANXA1$^{-/-}$ mice. This hypothesis is supported by the following two findings: (i) treatment of diabetic WT-mice with hrANXA1 attenuated the activation of p38, JNK and ERK1/2 and the cardiac and renal dysfunction caused by diabetes; (ii) even when hrANXA1 was given therapeutically (week 8-13), this resulted in attenuated the activation of p38, JNK and ERK1/2 as well as the organ dysfunction caused by diabetes.

In addition to key mediators of the MAPK pathway another key pathway involved in tissue protection is the degree of activation of the Akt-survival pathway, which is, in part, regulated by the insulin receptor substrate (IRS-1) (Guo, 2014). Diabetic mice demonstrated a significant decrease in the phosphorylation of Ser^{473} on Akt (indicating a reduction in activity of the kinase) in the kidney and heart. One effect of this inhibition is that organs are less

resistant to stressor stimuli (hyperglycaemia) and subsequent organ injury. In contrast, treatment with hrANXA1 attenuated the decline in Akt-activation caused by diabetes. Akt is a member of the phosphoinositide-3-3kinase (PI3K) signal transduction pathway. Insulin signalling through IRS-1 regulates P13K activity, and P13K can activate Akt (phosphorylation on Ser^{473}). Activated Akt controls inflammatory and pro-survival responses (Cantley, 2002). Most notably, activation of the Akt-survival pathway reduces organ injury in many conditions associated with inflammation including sepsis-induced organ dysfunction (Chen et al., 2017)(Khan et al., 2013), haemorrhagic shock induced organ dysfunction (Yamada et al., 2017)(Sordi et al., 2017), myocardial infarction (Cai & Semenza, 2004), and diabetes (Chiazza et al., 2015). Specifically, in cardiac and renal ischemia/reperfusion injury treatment with the Ac2-16 (the N-terminal peptide of ANXA1) reduced tissue necrosis by activating (phosphorylating) pro-survival kinase Akt eliciting protection from reperfusion injury (Qin et al., 2013)(Facio et al., 2011).

In conclusion, I report for the first time that ANXA1 levels are elevated in plasma of patients with T1DM, and that this rise is independent of a the presence of diabetic nephropathy and systemic inflammation. I have also clearly demonstrated that endogenous ANXA1 plays a key protecting the heart and kidney from functional decline an animal model of T1DM. Specifically, I have shown that key mediators of the MAPK pathway (p38, JNK and ERK1/2) are constitutively activated in $ANXA1^{-/-}$ mice. Administration of hrANXA1 (days 1-5) did not alter the diabetic phenotype, while administration of hrANXA1 (weeks 1-13) attenuated both renal and cardiac dysfunction caused by STZ-induction of

diabetes. While late treatment (weeks 8-13), after significant renal and cardiac dysfunction has already developed, halted both cardiac and renal dysfunction. We propose that attenuation of activation of the MAPK pathway and restoration/activation of Akt-survival pathways mediates these effects. Thus, I propose that treatment with hrANXA1 may represent a novel new intervention that reduces cardiac and renal dysfunction (microvascular complication) caused by T1DM.

Chapter III: Assessing the role of annexin-A1 in type-2 diabetes

3.1 Introduction

Type-2 diabetes is a complex multifaceted metabolic disease that accounts for ~95 % of all cases of diabetes worldwide. Throughout the natural history of type 2 diabetes, obesity is highly linked to insulin resistance. The link between obesity and a state of low-grade chronic inflammation is said to be a key driver of insulin resistance. Insulin resistance occurs as a result if uncoupling of IRS-1 from the insulin receptor, and in turn signal transduction does not occur even in the presence of insulin, resulting in a reduction in glucose uptake in the peripheral tissue and, hence, hyperglycaemia.

Patients with T2DM are at a high risk of developing microvascular complications, including nephropathy, neuropathy and retinopathy, even if they manage their disease well (Habib & Brannagan, 2010). Diabetic nephropathy is divided into five stages, with the final one being end-stage renal disease (ESRD). However, from the time of onset it commonly takes over 20 years for patients to reach stage 5. Advanced diabetic nephropathy is now the most common cause of glomerulosclerosis and ESRD worldwide; and 30% of patients with diabetes will eventually develop nephropathy (Marshall, 2004).

One of the key features of diabetic nephropathy is endothelial dysfunction; with hypertension being present in many patients with T2DM. Currently there are no specific therapies available for the treatment of diabetic nephropathy. Indeed, management of hypertension and glucose is the only therapeutic strategies available to prevent diabetic nephropathy (Nakagawa et al., 2011). Another key pathway that is activated in diabetes is the RhoA/ROCK pathway. Drugs

targeting and small molecule inhibitors of RhoA have been targets for drug development in the last decade, however, clinical trails in many areas fail despite strong pre-clinical findings (Zhou & Li, 2012). Cristante *et al.* were the first to show that ANXA1 is an endogenous inhibitor of RhoA activity, signalling through FPR2 (Cristante et al., 2013).

3.1.1 Specific aims

The role of endogenous ANXA1, or the utility hrAXNA1 as a novel therapeutic in T2DM is unknown.

Therefore, this study was designed to investigate:

(1) the plasma levels of endogenous ANXA1 in patients with type-2 diabetes with/without diabetic nephropathy;

(2) the role of endogenous ANXA1 in a murine model of high fat diet induced T2DM and diabetic nephropathy;

(3) whether therapeutic intervention with hrANXA1 can halt the progression of diabetes and diabetic nephropathy in a murine model of high fat diet induced T2DM;

3.1 Methods and Materials

3.1.1. Use of human subjects-ethical statement

The study was approved by the research ethics committee and was undertaken in adherence to the Declaration of Helsinki. All subjects gave written informed consent. Patients with T2DM were recruited from the Diabetes Outpatient clinic of SISA Bassini Hospital, Cinisello (Italy) ethics committee number DGSAF 0021573-P-12/11/2013 and 0001217-P-19/1/2017). Healthy donors were recruited from the William Harvey Research Institute (London). Non-fasting plasma was obtained from patients with type 2. diabetes, with /without a diagnosis of diabetic nephropathy and healthy donors.

3.2.2 Use of Animals ethical statement

All animal protocols used in this study were approved by the Animal Welfare Ethics Review Board (AWERB) of Queen Mary University of London in accordance with the derivatives of both the Home Office guidance on the Operation of Animals (Scientific Procedures Act 1986) published by Her Majesty's Stationery Office and the Guide for the Care and Use of Laboratory Animals of the National Research Council. All research was conducted project licenses reference numbers PPL: 70/8350. This study was carried out on ten week-old male C57BL/6 mice and ANXA1$^{-/-}$ mice, weighing 25–30 g (Charles River Laboratories UK Ltd., Kent, UK). The animals were allowed to acclimatise to laboratory conditions for a period of at least one week before any experimental procedures were initiated. All animals had free access to food and water *ad libitum*.

3.2.3 Sandwich ELISA for ANXA1

ANXA1 levels were measured in healthy donors, patients with T2DM with or/without CKD, as previously described using a homemade sandwich ELISA (see 2.2.10).

3.2.4. HFD induction of type-2 diabetes

10-week old WT male C57BL/6 or ANXA1$^{-/-}$ mice were fed a normal chow diet (protein 23.5 %, fat 21.8 % and carbohydrate 54.7 %) or fed a high-fat high-sugar diet (HFD) (protein 14.9 %, fat 59.4 % and carbohydrate 25.7 %) for 10 weeks.

3.2.5. Drug administration

Before dietary manipulation, mice were randomly divided into treatment groups. Mice were then either treated with hrANXA1 (1 ug, 100 µl, Hepes 50mM; 140 mM NaCl; pH 7.0, i.p.) or vehicle (100 µl, Hepes 50mM; 140 mM NaCl; pH 7.0, i.p.) from weeks 5-10.

3.2.6. Oral glucose tolerance test

Oral glucose tolerance test was preformed before termination of the experiment. Briefly, mice were fasted for 6 h prior to testing. Having been given an oral bolus of glucose (2 g/kg, H_2O), blood glucose (tail vein puncture) was measured at 15 min intervals for a maximum of 120 min using a glucose analyser (Accu-Chek Compact System; Roche Diagnostics, Basel, Switzerland).

3.2.7. Assessment of renal function

In the last week of the study, mice were placed in metabolic cages for 24 h to collect urine. Urinary creatinine and sodium was measured in a blinded fashion by a commercial veterinary testing laboratory (IDEXX Ltd, West Sussex, UK). Urinary albumin was measured using a commercially available ELISA kits as per manufacturers instructions (Bethyl Ltd, Italy). Albumin-to-creatinine ratio was calculated using Equation 5.

3.2.8. Organ and blood collection

Mice were anaesthetised with a ketamine (100 mg/ml) and xylazine (20 mg/ml) mixture (2:1; 1.5 ml/kg, i.p.) and killed by cardiac exsanguination. Blood glucose was measured immediately using a glucometer (Accu-Chek Compact System; Roche Diagnostics, Switzerland). A section of liver, kidney and skeletal muscle was snap frozen and put in long-term storage for further processing and a section was of kidney was fixed in 10 % neutral-buffered for 48 h and transferred to 70 % ethanol for long term storage. A section of liver was snap frozen in isopropanol and stored. Blood was collected and serum isolated; biochemical markers (creatinine) were measured in a blinded fashion by a commercial veterinary testing laboratory (IDEXX Ltd, West Sussex, UK), serum insulin using a mouse ELISA kit (Abcam Plc., UK), serum triglyceride and cholesterol were measured using a enzymatic assays (Hospitex Diagnostics, Italy).

3.2.9. Western blot analysis

Western Blot analysis was preformed as described previously described (2.2.11.). Briefly, liver kidney and skeletal muscle was homogenised and protein extracted. Proteins were separated by SDS-PAGE, and transferred onto a PVDF membrane, blocked and incubated with primary antibody dilution either 1:200, 1:400 or 1:1000 (rabbit anti-total IRS-1; rabbit anti-pIRS-1 (180 kDa); rabbit anti-total Akt; rabbit anti-pAkt (63 kDa); rabbit anti-total GSK -3β; rabbit anti-p GSK -3β (47 kDa); rabbit anti-ANXA1 (37 kDa); rabbit anti- β-actin (42 kDa); rabbit anti-total RhoA rabbit anti-pRhoA (22 kDa); rabbit anti-total MYPT1 and rabbit anti-pMYPT1 (40 kDa)), then secondary horseradish peroxidase (dilution 1:10000), and visualised by autoradiography.

3.3.10. Histological analysis

Periodic acid Schiffs: Formulin fixed kidney samples were embedding in paraffin and processed to obtain 4 μm sections. After deparaffinisation and rehydratration (graded alcohols to distilled water), all sections were then incubated with saturated in Periodic Acid Schiff's (Sigma, UK) solution for 30 min washed in distilled water and counterstained with Harris hematoxylin (Sigma, UK) and finally dehydrated through graded alcohols and cleared before mounting with coverslips.

Oil Red O staining: Frozen liver samples were embedded in optimal cutting temperature compound (OCT), and cut in 10 μm sections. Section were brought to room temperature, fixed with 10 % buffer formulin for 5 min, washed with 60 % isopropanol, then saturated with Oil Red O (1% w/v, 60 % isopropanol) for 15

min, washed in 60 % isopropanol and rinsed in distilled water. Sections were then mounted using aqueous mount with coverslips. In both cases, images were acquired using a NanoZoomer Digital Pathology Scanner (Hamamatsu Photonics K.K. Japan) and analysed using the NDP Viewer software.

3.2.11. Statistical analysis

All data in the text and figures are presented as mean ± SEM of n observations, where n represents the number of animals studied. All statistical analysis was calculated using GraphPad Prism 6 (GraphPad Software, San Diego, California, USA). Data without a repeated measurement was assessed by a one-way ANOVA or students t-test were appropriate. OGTT testing analysis was preformed using area under ROC-curve. A P-value of less than 0.05 was considered to be statistically significant.

3.3. Experimental plan and groups.

3.3.1. The effect of treatment with hrANXA1 and endogenous ANXA1 in a model of HFD-induced insulin resistance.

Table 3.1. Experimental groups used to study the effect of treatment ANXA1 and endogenous ANXA1 in high fat diet induced insulin resistance.

Group Name	Diet	Treatment
WT + Veh	Chow	No treatment
WT + ANXA1	Chow	1 µg hrANXA1, 100 µl Hepes buffer, i.p., daily weeks 5-10
WT + HFD	HFD	100 µl Hepes buffer, i.p., daily weeks 5-10
WT + ANXA1	HFD	1 µg hrANXA1, 100 µl Hepes buffer, i.p., daily weeks 5-10
ANXA1$^{-/-}$ + Veh	Chow	No treatment
ANXA1$^{-/-}$ + Veh	HFD	100 µl Hepes buffer, i.p., daily weeks 5-10
ANXA1$^{-/-}$ +ANXA1	HFD	1 µg hrANXA1, 100 µl Hepes buffer, i.p., daily weeks 5-10

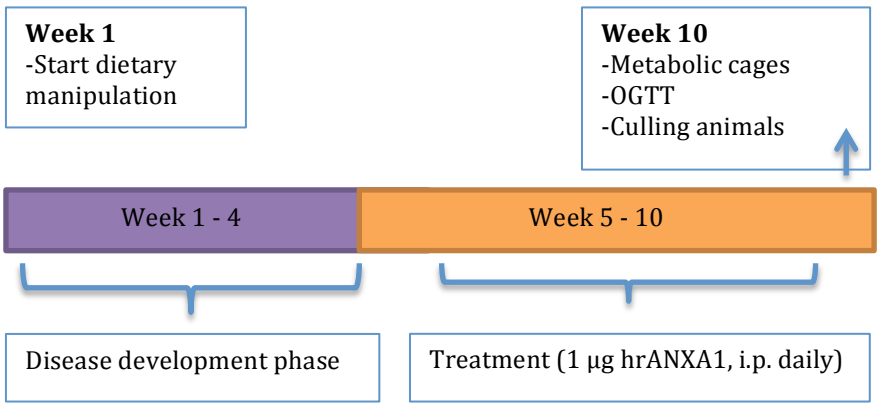

Figure 3.1. Summary of the experimental protocol used to investigate the effect of hrANXA1 treatment and endogenous ANXA1 in high fat diet induced insulin resistance.

3.4 Results

3.4.1. ANXA1 levels are elevated in patients with type-2 diabetes, independent of having diabetic nephropathy.

To understand whether endogenous ANXA1 levels are modulated in patients with T2DM, a sandwich ELISA was preformed on plasma obtained from either healthy volunteers or patients with T2DM with/without CKD. There was no significant factor different between test groups apart from those related to their diagnosis of CKD (urinary albumin). Compared to healthy donors, patients with T2DM had significantly elevated levels of plasma ANXA1 (Figure 3.2A, $P<0.01$). However, there was no difference in plasma ANXA1 levels between patients with T2DM and patients with T2DM plus CDK (Figure 3.2B, $P<0.01$). When we compared ANXA1 levels of patients at different stages of CDK 3-5, we found no significant difference in ANXA1 levels (Figure 3.2C, ns). We did, however, discover a strong, positive correlation between plasma ANXA1 levels and urinary albumin (Figure 3.2C, $P<0.05$).

	Healthy donors	Diabetic (no CKD)	Diabetic (CKD)
Patient (n)	28	19	130
Sex (F %)	16 (57)	5 (26)	20 (15)
Creatinine (mg/dL)	7.67±0.27	7.49±0.36	2.05±0.12
eGFR (ml/min)	na	32.98±3.98	28.59±1.23
Urinary albumin (mg/L)	na	45.05±36.75	233.99±41.62$^{\$}$
Fasting glucose (mg/dL)	127.86±8.25	128.41±8.3	139.82±4.29
BMI (kg/m^2)	27.39±0.74	27.18±0.73	30.23±0.58
Total cholesterol (mg/dL)	160.24±6.92	159.80±6.73	193.01±3.91*
HDL-c (mg/dL)	46.65±1.88	43.35±1.59	48.91±1.31
eLDL-c (mg/dL)	87.31±5.45	87.89±5.55	116.23±3.29*
TG (mg/dL)	151.17±12.37	142.63±11.22	139.27±9.59
CRP (mg/L)	na	0.075±0.02	0.47±0.11*

Table 3.4.1: Patient demographic included in the study.

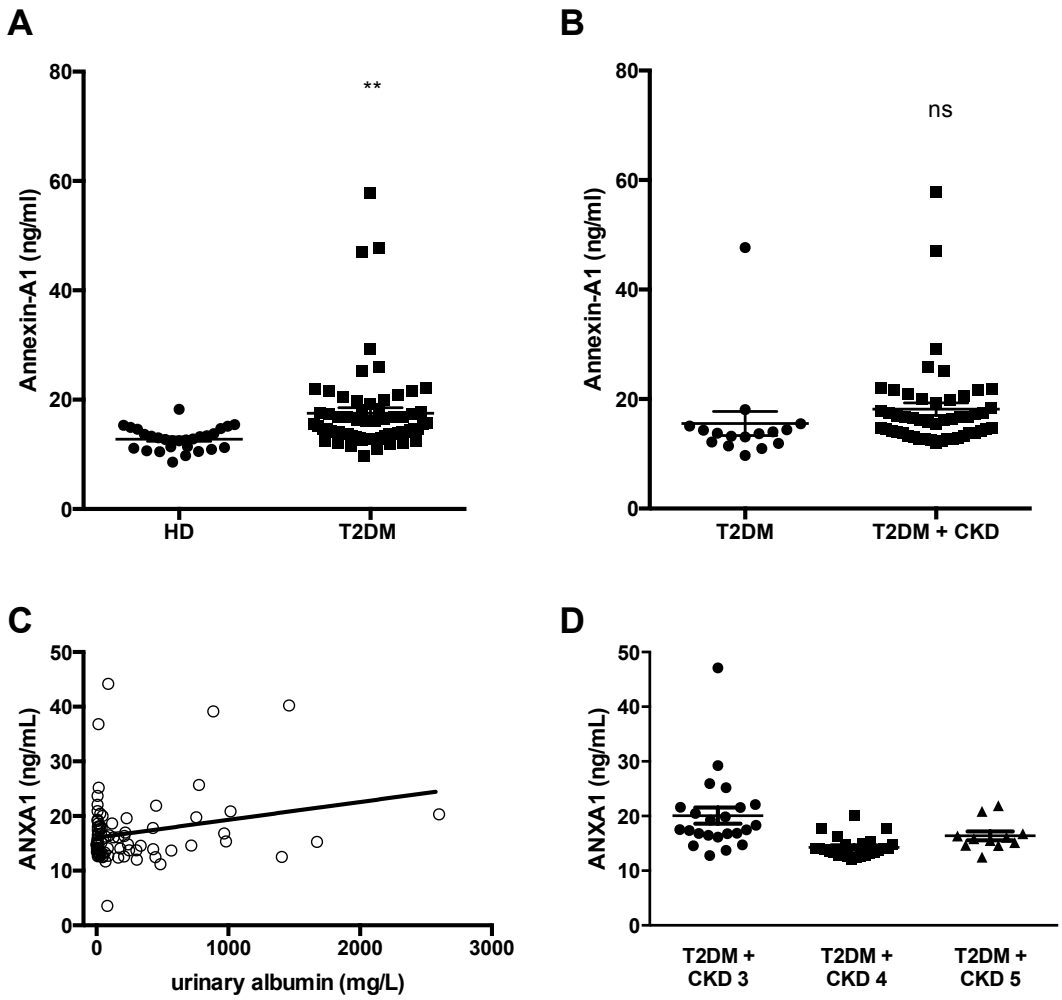

Figure 3.2 Changes in plasma levels of ANXA1 in patients with or without diabetic nephropathy.

ANXA1 levels were measured by sandwich ELISA in plasma of healthy controls and patients with type-2 diabetes (A); patients with type-2 diabetes and no CKD and patients with type-2 diabetes plus nephropathy (B); patients with type 2 diabetes plus stages of CKD 3-5 (C) and linear regression of AXNA1 vs. urinary albumin (D). Linear regressions were calculated by the least squares method and their significance were estimated by Fisher's *F* test. P<0.05 was considered significant. Data analysed by one-way ANOVA followed by a Bonferroni *post-hoc* test or an unpaired Student's t-test, and expressed as mean ±S EM. **P>0.01.

3.4.2. ANXA1 levels are strong correlated with increasing serum lipids but not systemic inflammation.

Increasing evidence suggests a strong link between T2DM and chronic low-grade inflammation. Here I demonstrate that in our cohort of patients with T2DM there is a not significant difference in plasma CRP levels (a marker of systemic inflammation) in patients with T2DM due to stage of CKD (Figure 3.3A, ns). There is a strong positive correlation between BMI and plasma ANXA1 (Figure 3.3B, $P<0.05$), however, there is no significant correlation between plasma CRP levels and plasma ANXA1 levels (Figure 3.3C, ns) in our cohort of patient with T2DM.

Although BMI is strongly associated with systemic inflammation, when serum lipid levels were correlated with plasma CRP, I found no significant correlation between plasma ANXA1 and total cholesterol (Figure 3.4A, ns), LDL-c (Figure 3.4A, ns) and HDL-c (Figure 3.4A, ns).

However, when serum lipid levels were correlated with ANXA1, there was a strong, positive correlation between ANXA1 and total cholesterol (Figure 3.5A, $P<0.05$), LDL-c (Figure 3.5B, $P<0.05$) and HDL-c (Figure 3.5C,$P<0.05$).

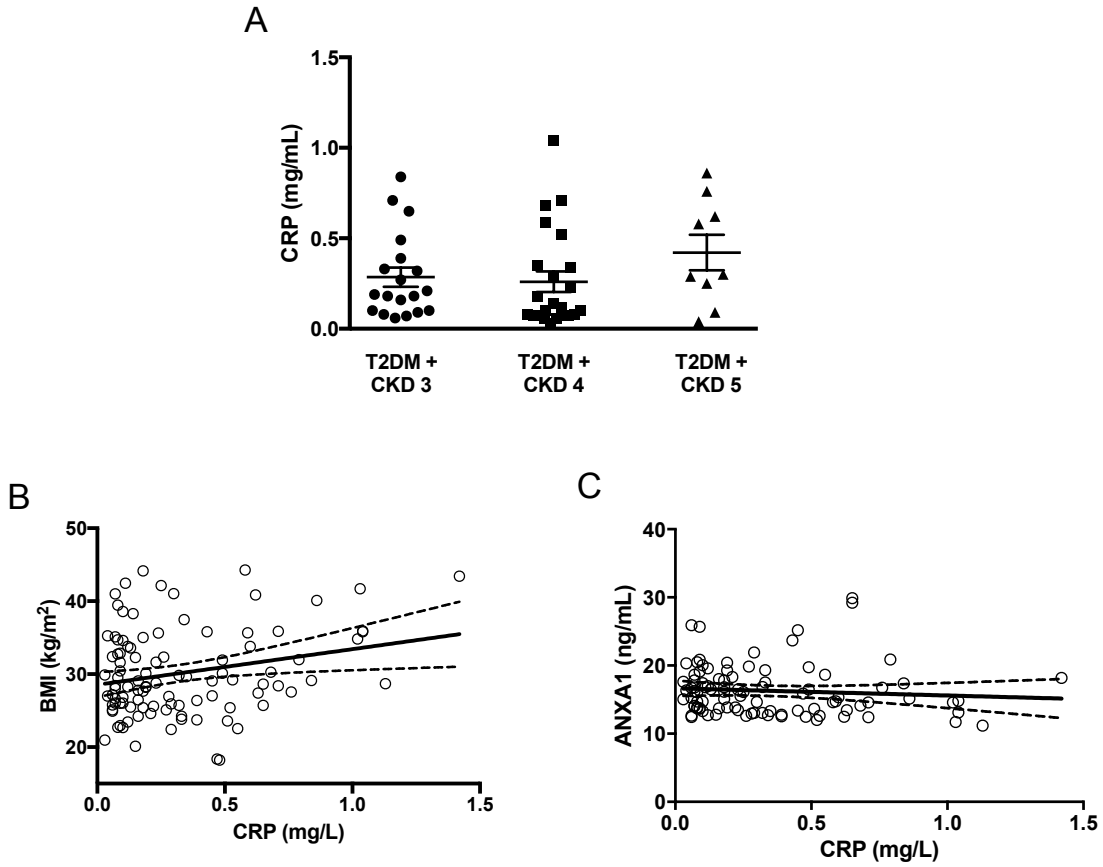

Figure 3.2. Measurement of systemic inflammation in patients with or without diabetic nephropathy.

Plasma CRP1 levels were in patients with type-2 diabetes with different stages of CKD (A); between BMI and plasma CRP (B) and plasma ANXA1 and plasma CRP (C). Linear regressions were calculated by the least squares method and their significance were estimated by Fisher's *F* test. $P<0.05$ was considered significant. Data analysed by one-way ANOVA followed by a Tukey's *post-hoc* test, and expressed as mean ± SEM.

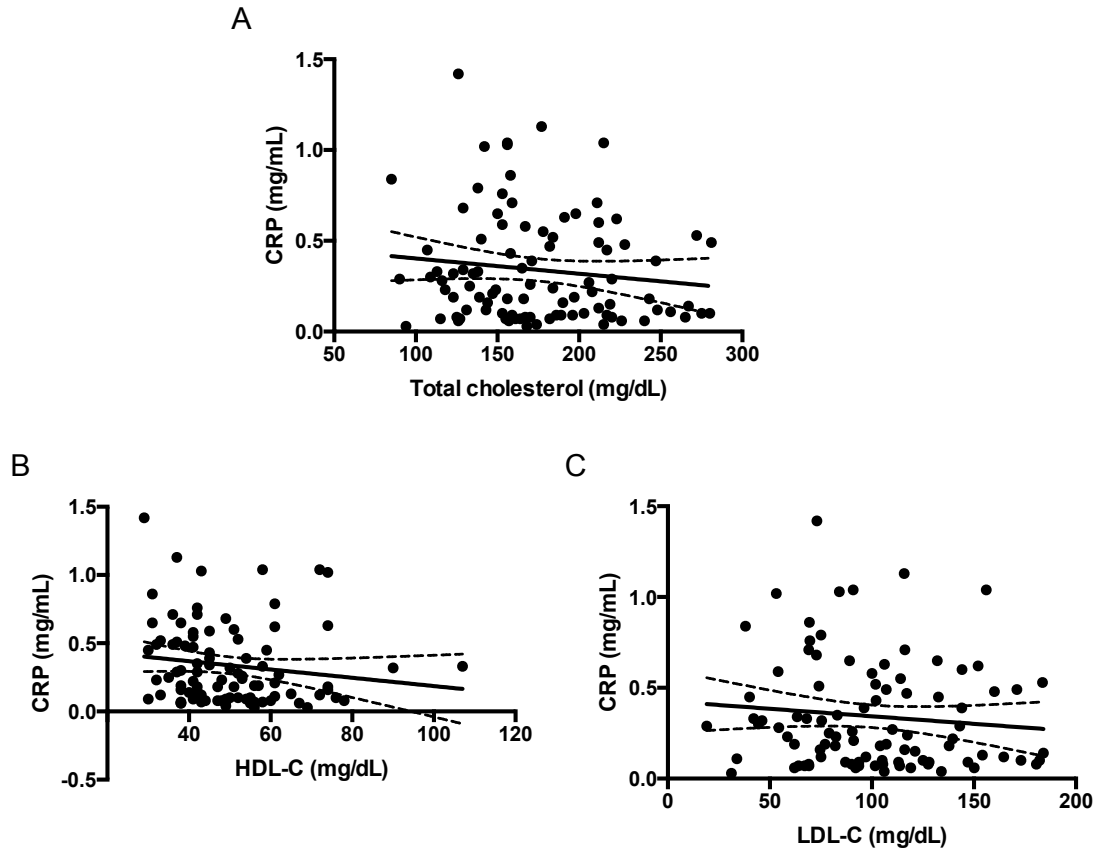

Fgure 3.3. The association between in plasma levels of plasma CRP and plasma lipids in T2DM patients with or without diabetic nephropathy.

Correlation data showing plasma CRP vs. total cholesterol (A), plasma CRP vs. LDL-c (B) and plasma CRP vs. HDL-c (C). Linear regressions were calculated by the least squares method and their significance were estimated by Fisher's *F* test. P<0.05 was considered significant.

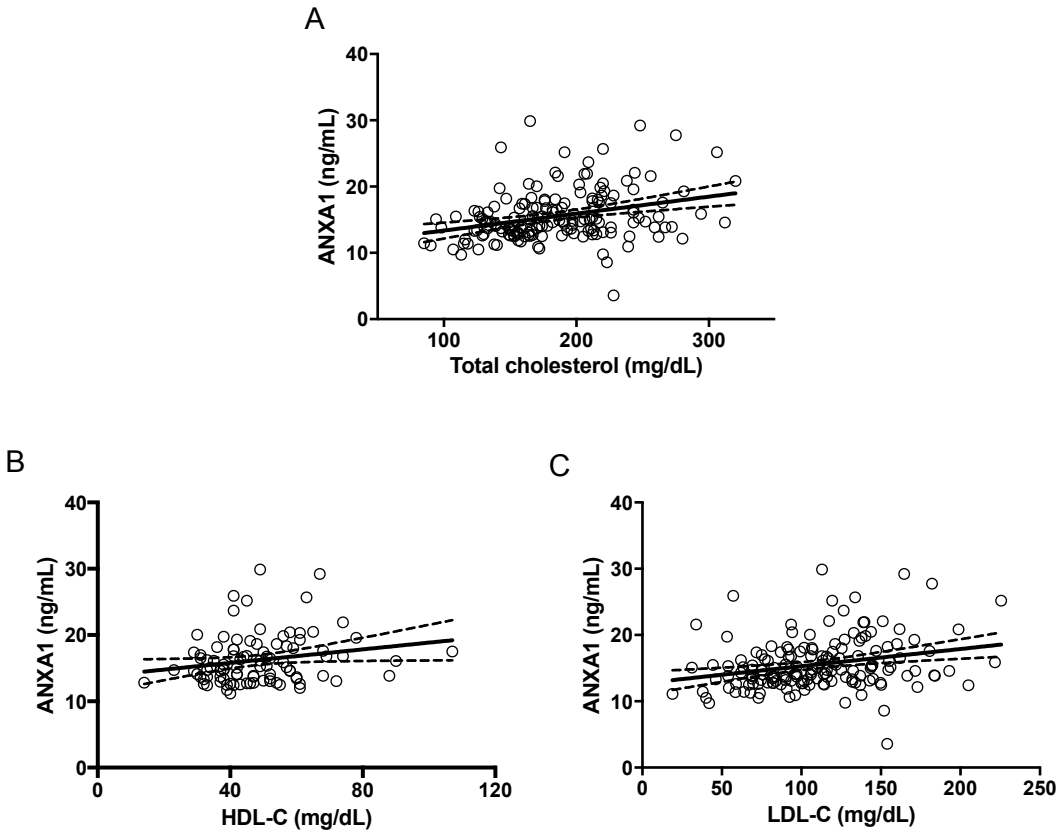

Figure 3.5 Association between in plasma levels of ANXA1 and plasma lipids in T2DM patients with or without diabetic nephropathy.

Correlation data showing plasma ANXA1 vs. total cholesterol (A), plasma ANXA1 vs. LDL-c (B) and plasma ANXA1 vs. HDL-c (C). Linear regressions were calculated by the least squares method and their significance were estimated by Fisher' *F* test. P<0.05 was considered significant.

3.4.3. The effect of treatment with hrANXA1 and the role of endogenous ANXA1 on body weights in a murine model of diet-induced insulin resistance.

Having found that there is a relationship between T2DM and plasma ANXA1 levels, I wanted to use a murine model of HFD-induced insulin resistance to investigate the role of endogenous ANXA1 and hrANXA1 (as a therapeutic). When compared to WT-mice fed on chow diet, WT-mice fed on HFD demonstrated a significant increase in body weight and fat mass (Table1). When compared to WT-mice fed on a HFD, WT-mice fed on HFD and treated with hrANXA1 demonstrated significantly less gains in either body weight or fat mass (Table1).

Similarly, when compared to ANXA1$^{-/-}$ mice fed on chow diet, ANXA1$^{-/-}$ mice fed a HFD demonstrated a significant increase in body weight and fat mass (Table 1). Interestingly, when compared to WT-mice fed on chow diet, ANXA1$^{-/-}$ mice fed on chow diet did not gain as much weight over the same period of dietary manipulation (Table 1, $P<0.05$). However, when compared to WT-mice fed on HFD, ANXA1$^{-/-}$ mice fed on HFD gained significantly more body weight and fat mass (Table 1).

	Wild Type				ANXA1 $^{-/-}$		
	Chow	**Chow + hrANXA1**	**HFD + Vehicle**	**HFD + hrANXA1**	**Chow**	**HFD + Vehicle**	**HFD + hrANXA1**
Body weight gain from baseline (g)	9.790±0.602*	9.857±0.674*	16.81±0.479	12.87±0.455*	4.550±0.276$^{\$@}$	13.89±0.772	7.00±0.447$^{\$}$
Kidney % of body weight	1.213±0.072	1.225±0.025	1.083±0.034	1.311±0.90	1.219±0.025$^{\$}$	0.814±0.008	0.931±0.002$^{\$}$
Liver % of body weight	3.325±0.144	3.475±0.094	3.191±0.098	3.156±0.111	4.069±0.0189$^{\$}$	3.212±0.185	3.395±0.144$^{\$}$
Epididimal fat % of body weight	1.963±0.163*	2.100±0.255*	3.570±0.291	2.867±0.253*	2.288±0.067$^{\$}$	5.609±0.246	4.361±0.007$^{\$}$
Inguinal fat % of body weight	1.250±0.128*	1.275±0.149*	2.320±0.243	1.833±0.212*	0.714±0.051$^{\$}$	1.842±0.096	1.370±0.094$^{\$}$

Table 1: The effect of hrANXA1 administration and the role of endogenous ANXA1 on body weight in a model of diet-induced insulin resistance

Effects of chronic exposure to a normal diet (chow) or a high-fat high-sugar diet (HFD) on body weight and kidney, liver, epididimal and inguinal fat masses. Experimental groups: WT or ANXA1$^{-/-}$ mice treated fed on normal diet (chow) or high-fat-high-sugar (HFD) with or without hrANXA1 (1 µg hrANXA1, i.p., 5 X per week). Data analysed by a one-way ANOVA followed by a Bonferoni *post-hoc* test, and expressed as mean ± SEM. n= 6-8 per group. **P<0.01, ***P<0.001 and ****P<0.0001 vs. WT + HFD. $^{\$}$P<0.05, $^{\$\$}$P<0.01 and $^{\$\$\$}$P<0.001 vs. ANXA1$^{-/-}$ + HFD. $^{@}$P<0.05 vs. WT + chow.

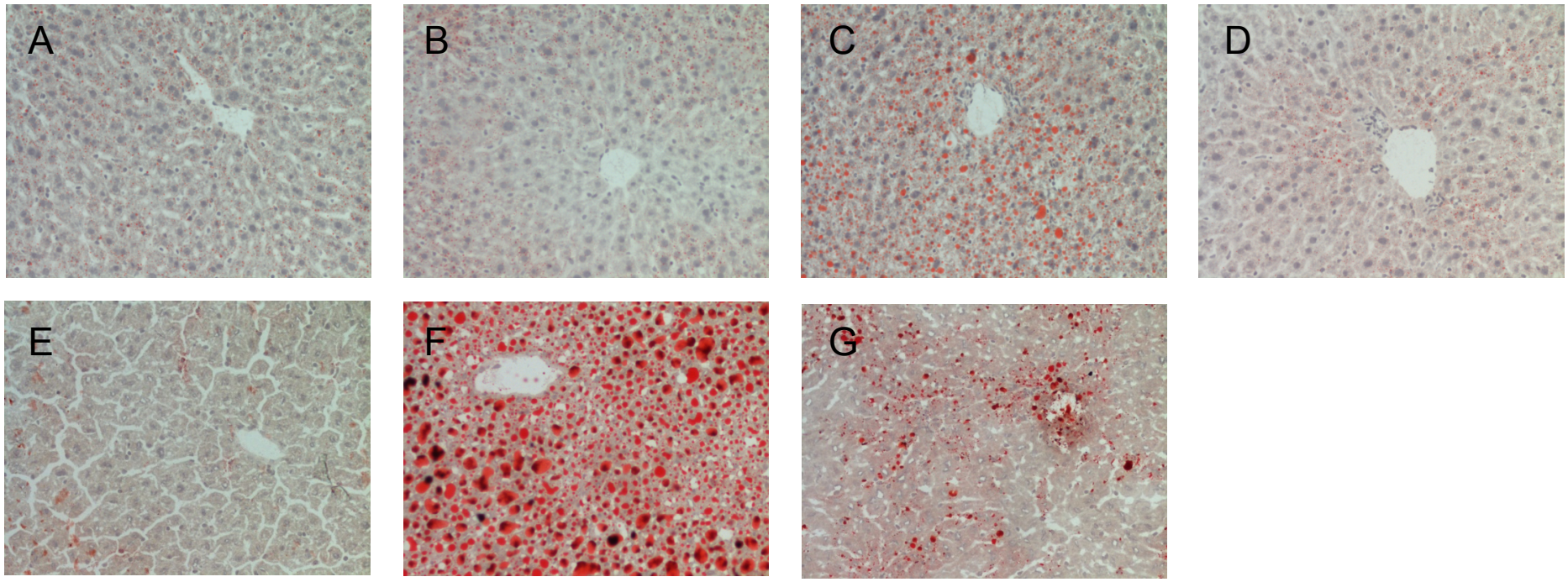

Figure 3.6. The effect of treatment with hrANXA1 and the role of endogenous ANXA1 on Oil Red-O staining in the liver.

Effects of chronic exposure to a normal diet (chow) or a high-fat high-sugar diet (HFD) on Oil Red-O staining in the liver after 10 weeks of dietary manipulation. Experimental groups: WT or ANXA1$^{-/-}$ mice treated fed on normal diet (chow) or high-fat-high-sugar (HFD) with or without hrANXA1 (1 μg hrANXA1, i.p., 5 X per week). Magnification X20. Scale bar.

3.4.4. The effect of treatment with hrANXA1 and the role of endogenous ANXA1 on Oil Red-O staining in a murine model of diet-induced insulin resistance.

To measure fat deposition in the liver, Oil Red-O staining was carried out in frozen liver sections. When compared to WT-mice fed on chow diet (Figure 3.6A), WT-mice fed on HFD demonstrated an increase in Oil Red-O positive staining in the liver (Figure 3.6C), suggesting a large deposition of fat. When compared to WT-mice fed on a HFD (Figure 3.6C), WT-mice fed on HFD and treated with hrANXA1 demonstrated less Oil Red-O positive staining in the liver (Figure 3.6D).

Similarly, when compared to ANXA1$^{-/-}$ mice fed on chow diet (Figure 3.6E), ANXA1$^{-/-}$ mice fed a HFD demonstrated an increase in Oil Red-O staining in the liver (Figure 3.6F). Similarly, when compared to ANXA1$^{-/-}$ mice fed on HFD (Figure 3.6F), ANXA1$^{-/-}$ mice fed on HFD and administrated hrANXA1 demonstrated less Oil Red-O positive staining (Figure 3.6G).

Interestingly, when compared to WT-mice fed on HFD (Figure 3.6C), ANXA1$^{-/-}$ mice fed on HFD demonstrated in increase in Oil Red-O positive staining (Figure 3.6F) suggesting an increase in the deposition of fat in the liver.

3.4.5. The effect of hrANXA1 administration and the role of endogenous ANXA1 on triglyceride and cholesterol level in the liver of a murine model of diet-induced insulin resistance.

To measure fat composition in the liver triglyceride and cholesterol levels were quantified in the liver using standard enzymatic reactions kits. When compared to WT-mice fed on chow diet, WT-mice fed on HFD demonstrated a significant increase in triglyceride level in the liver (Figure 3.7A, $P<0.001$), however there was no change in cholesterol level (Figure 3.7B, ns). When compared to WT-mice fed on a HFD, WT-mice fed on HFD and treated with hrANXA1 had significantly lower levels of triglycerides in the liver (Figure 3.7A, $P<0.001$).

Similarly, when compared to ANXA1$^{-/-}$ mice fed on chow diet, ANXA1$^{-/-}$ mice fed a HFD demonstrated a significant increase in triglyceride levels in the liver (Figure 3.7A, $P<0.0001$), but there was no change in cholesterol levels (Figure 3.7B, ns). Similarly, when compared to ANXA1$^{-/-}$ mice fed on HFD, ANXA1$^{-/-}$ mice fed on HFD and treated with hrANXA1 had significantly lower levels of triglycerides in the liver (Figure 3.7B, $P<0.01$).

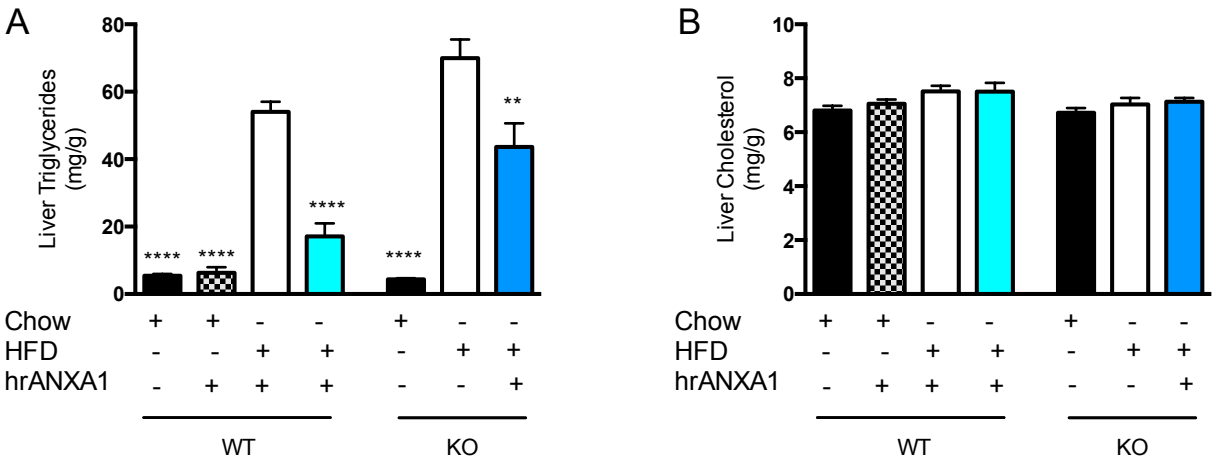

Figure 3.7. Effect of hrANXA1 administration and the role of endogenous ANXA1 on triglyceride and cholesterol level in the liver a model of diet-induced insulin resistance.

Effects of chronic exposure to a normal diet (chow) or a high-fat high-sugar diet (HFD) on triglyceride (A) and cholesterol (B) levels in the liver after 10 weeks of dietary manipulation. Experimental groups: WT or ANXA1$^{-/-}$ mice treated fed on normal diet (chow) or high-fat-high-sugar (HFD) with or without hrANXA1 (1 µg hrANXA1, i.p., 5 X per week). Data analysed by a one-way ANOVA followed by a Bonferroni *post-hoc* test, and expressed as mean ± SEM. n= 6 per group. **P<0.01, ***P<0.001 and ****P<0.0001 vs. WT + HFD. $^{\$}$P<0.05, $^{\$\$}$P<0.01 and $^{\$\$\$}$P<0.001 vs. ANXA1$^{-/-}$ + HFD.

3.4.6. The effect of hrANXA1 administration and the role of endogenous ANXA1 on triglyceride and cholesterol level in serum in a model of diet-induced insulin resistance.

To measure fat composition in the liver triglyceride and cholesterol levels were quantified in the serum using standard colorimetric assay.

When compared to WT-mice fed on chow diet, WT-mice fed on HFD demonstrated no change in serum triglyceride levels (Figure 3.8A, ns), however there was a significant increase in cholesterol level (Figure 3.8B, $P<0.01$). When compared to WT-mice fed on a HFD, WT-mice fed on HFD and treated with hrANXA1 had significantly lower levels of cholesterol in the serum (Figure 3.8B, $P<0.0001$).

Similarly, when compared to $ANXA1^{-/-}$ mice fed on chow diet, $ANXA1^{-/-}$ mice fed a HFD demonstrated a significant increase in serum triglyceride (Figure 3.8A, $P<0.01$) and cholesterol levels (Figure 3.8B, $P<0.001$). However, when compared to $ANXA1^{-/-}$ mice fed on HFD, $ANXA1^{-/-}$ mice fed on HFD and treated with hrANXA1 had similar levels of serum triglycerides (Figure 3.8A, ns) or cholesterol (Figure 3.8B, ns).

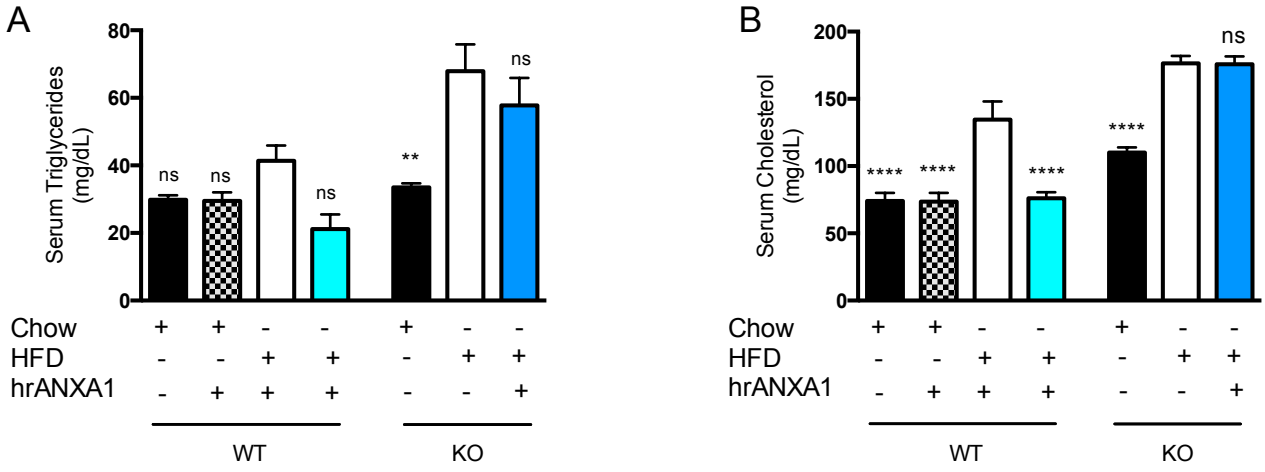

Figure 3.8. The effect of hrANXA1 administration and the role of endogenous ANXA1 on serum triglyceride and cholesterol levels a model of diet-induced insulin resistance.

Effects of chronic exposure to a normal diet (chow) or a high-fat high-sugar diet (HFD) on serum triglyceride and cholesterol levels after 10 weeks of dietary manipulation. Experimental groups: WT or ANXA1$^{-/-}$ mice treated fed on normal diet (chow) or high-fat-high-sugar (HFD) with or without hrANXA1 (1 µg hrANXA1, i.p., 5 X per week). Data analysed by a one-way ANOVA followed by a Bonferroni *post-hoc* test, and expressed as mean ± SEM. n= 6 per group. **P<0.01, ***P<0.001 and ****P<0.0001 vs. WT + HFD. $^{\$}$P<0.05, $^{\$\$}$P<0.01 and $^{\$\$\$}$P<0.001 vs. ANXA1$^{-/-}$ + HFD.

3.4.7. The effect of hrANXA1 administration and the role of endogenous ANXA1 on baseline diabetic parameters in a model of diet-induced insulin resistance.

When compared to WT-mice fed on chow diet, WT-mice fed on HFD demonstrated a significant increase in the serum insulin (Figure 3.9A, $P<0.001$) as well as the blood levels of (non-fasted) glucose (Figure 3.9B, $P<0.0001$). When compared to WT-mice fed on chow diet, WT-mice fed on HFD subjected to OGTT demonstrated a significant impairment in tolerance to oral glucose (Figure 3.9C/D, $P<0.01$). When compared mice fed on a HFD, mice fed on HFD and treated with hrANXA1 demonstrated significantly lower serum insulin (Figure 3.9A, $P<0.0001$) and blood glucose levels (Figure 3.9B, $P<0.0001$). Additionally, when compared to mice fed on HFD, mice fed on HFD and treated with hrANXA1 subjected to OGTT demonstrated a significant improvement in oral glucose tolerance (Figure 3.9C/D, $P<0.001$).

When compared to ANXA1$^{-/-}$ mice fed on chow diet, ANXA1$^{-/-}$ mice fed on HFD had elevated serum insulin (Figure 3.9A, $P<0.0001$) and blood glucose levels (Figure 3.9B, $P<0.0001$). When compared to ANXA1$^{-/-}$ mice fed on chow diet, ANXA1$^{-/-}$ mice fed on HFD demonstrated a significant impairment in oral glucose tolerance when subjected to OGTT (Figure 3.9C, $P<0.01$). When compared to ANXA1$^{-/-}$ mice fed on HFD, mice ANXA1$^{-/-}$ mice fed on HFD treated with hrANXA1 (to recover their phenotype to WT) had significantly lower serum insulin (Figure 3.9A, $P<0.05$) and blood glucose levels (Figure 3.9B, $P<0.05$). Similarly, when compared to ANXA1$^{-/-}$ mice fed on HFD, ANXA1$^{-/-}$ mice fed on HFD and treated

with hrANXA1 and subjected to an OGTT demonstrated an improvement in oral tolerance to glucose (Figure 3.9C, $P<0.01$).

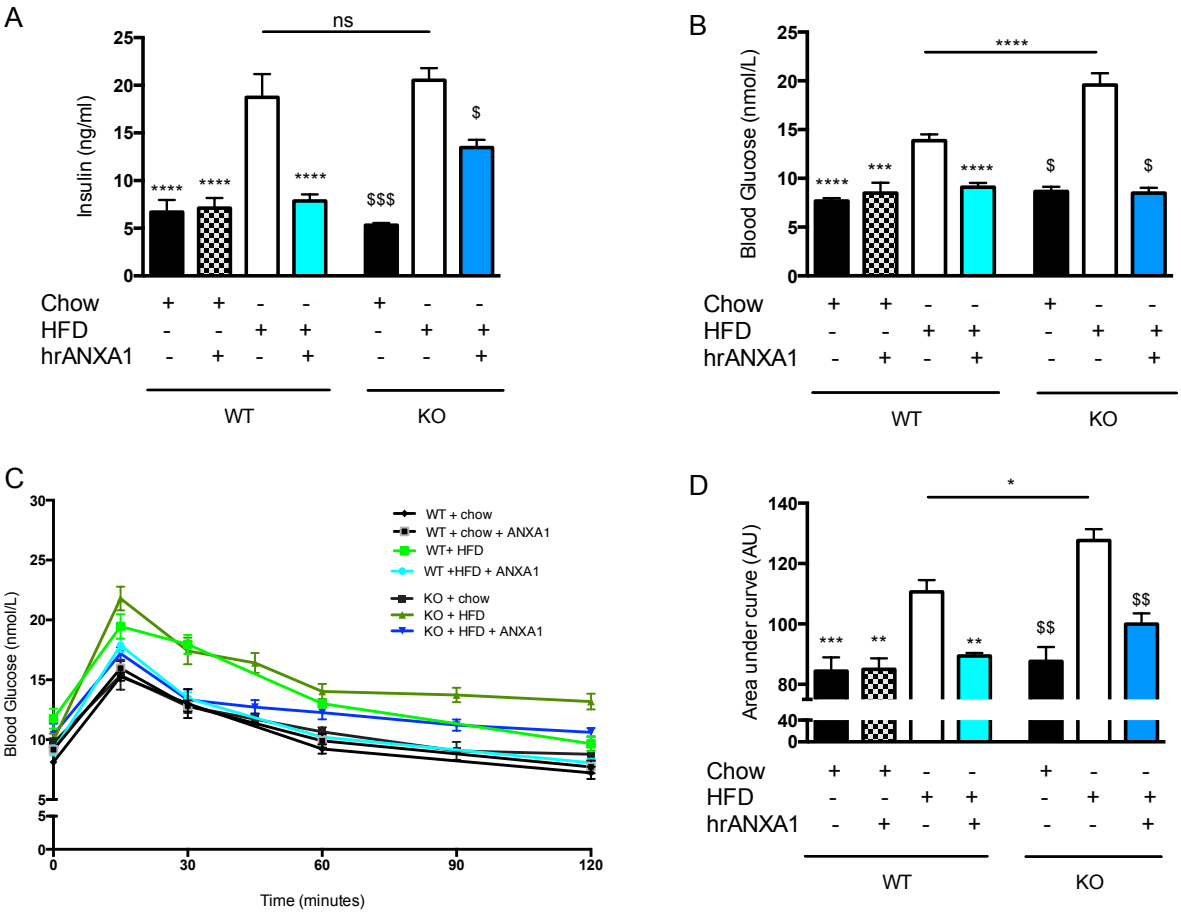

Figure 3.9. The effect of hrANXA1 administration and ANXA1$^{-/-}$ mice on diabetic parameters in a model of diet induced insulin resistance.

Effects of chronic exposure to a normal diet (chow) or a high-fat high-sugar diet (HFD) on serum insulin measured by sandwich ELSIA after 10 weeks of dietary manipulation (A); non-fasted blood glucose measured upon termination at week 10 (B); OGTT was measured after 6 h of fasting mice. Glucose levels measured at times 0, 15, 30, 45, 60, 90 and 120 post oral glucose delivery (C) and area under cure of OGTT (D). Experimental groups: WT or ANXA1$^{-/-}$ mice treated fed on normal diet (chow) or high-fat-high-sugar (HFD) with or without hrANXA1 (1 µg hrANXA1, i.p., 5 X per week). Data analysed by a one-way ANOVA followed by a Bonferroni *post-hoc* test, and expressed as mean ± SEM. n= 6-8 per group. **P<0.01, ***P<0.001 and ****P<0.0001 vs. WT + HFD and $^{\$}$P<0.05, $^{\$\$}$P<0.01 and $^{\$\$\$}$P<0.001 vs. ANXA1$^{-/-}$ + HFD.

3.4.8. The effect of treatment with hrANXA1 and role of endogenous ANXA1 on insulin signalling pathways, in the liver, in a murine model of diet-induced insulin resistance.

To assess the potential mechanisms (insulin resistance), which account for the rise in blood glucose and insulin levels caused by HFD, a semi-quantitative western blot analysis of key elements of the insulin signalling pathways was performed in the liver. When compared to liver tissue obtained from WT-mice fed on chow diet, liver tissue from WT-mice fed on HFD demonstrated a significant increase in the phosphorylation of insulin receptor substrate-1 (IRS-1) on Ser^{307} (Figure 3.10A, $P<0.0001$) and significant decreases in the phosphorylation of Akt on Ser^{473} (Figure 3.10B, $P<0.0001$) and GSK-3β on Ser^{9} (Figure 3.10C, $P<0.001$). Taken together, these findings suggest that WT-mice fed a HFD had a significant impairment in the insulin-signalling pathway indicative of insulin resistance (in the liver).

When compared to liver tissue from WT-mice fed on HFD, liver tissue from mice fed on HFD and treated with hrANXA1 demonstrated a significant lower degree of phosphorylation of IRS-1 on Ser^{307} (Figure 3.10A, $P<0.0001$), and exhibited a significant higher degree of phosphorylation of Akt on Ser^{473} (Figure 3.10B, $P<0.0001$) and GSK-3β on Ser^{9} (Figure 3.10C, $P<0.0001$), suggesting a restoration of normal insulin signalling. Indeed, the degree of phosphorylation of IRS-1 on Ser^{307}, Akt on Ser^{473} and GSK-3β on Ser^{9} in liver samples obtained from mice fed on HFD and treated with hrANXA1 was not different from that seen in mice fed standard chow.

Similarly, when compared to liver tissue obtained from ANXA1$^{-/-}$ mice fed on chow diet, liver tissue from ANXA1$^{-/-}$ mice fed on HFD showed a significant increase in the phosphorylation of IRS-1 on Ser^{307} (Figure 3.10A, P<0.0001) and significant decreases in the phosphorylation of Akt on Ser^{473} (Figure 3.10B, P<0.0001) and GSK-3β on Ser^{9} (Figure 3.10C, P<0.001). When compared to liver tissue obtained from ANXA1$^{-/-}$ mice on HFD, liver tissue from ANXA1$^{-/-}$ mice fed on HFD but treated with hrANXA1 (to restore their phenotype to WT) exhibited a significant lower degree of phosphorylation of IRS-1 on Ser^{307} (Figure 3.10A, P<0.0001), and a higher degree of phosphorylation of Akt on Ser^{473} (Figure 3.10B, P<0.0001) and GSK-3β on Ser^{9} (Figure 3.10C, P<0.0001). Thus, treatment of ANXA1$^{-/-}$ mice with hrANXA1 restored the impairment in insulin signalling observed in the liver of ANXA1$^{-/-}$ mice treated with vehicle.

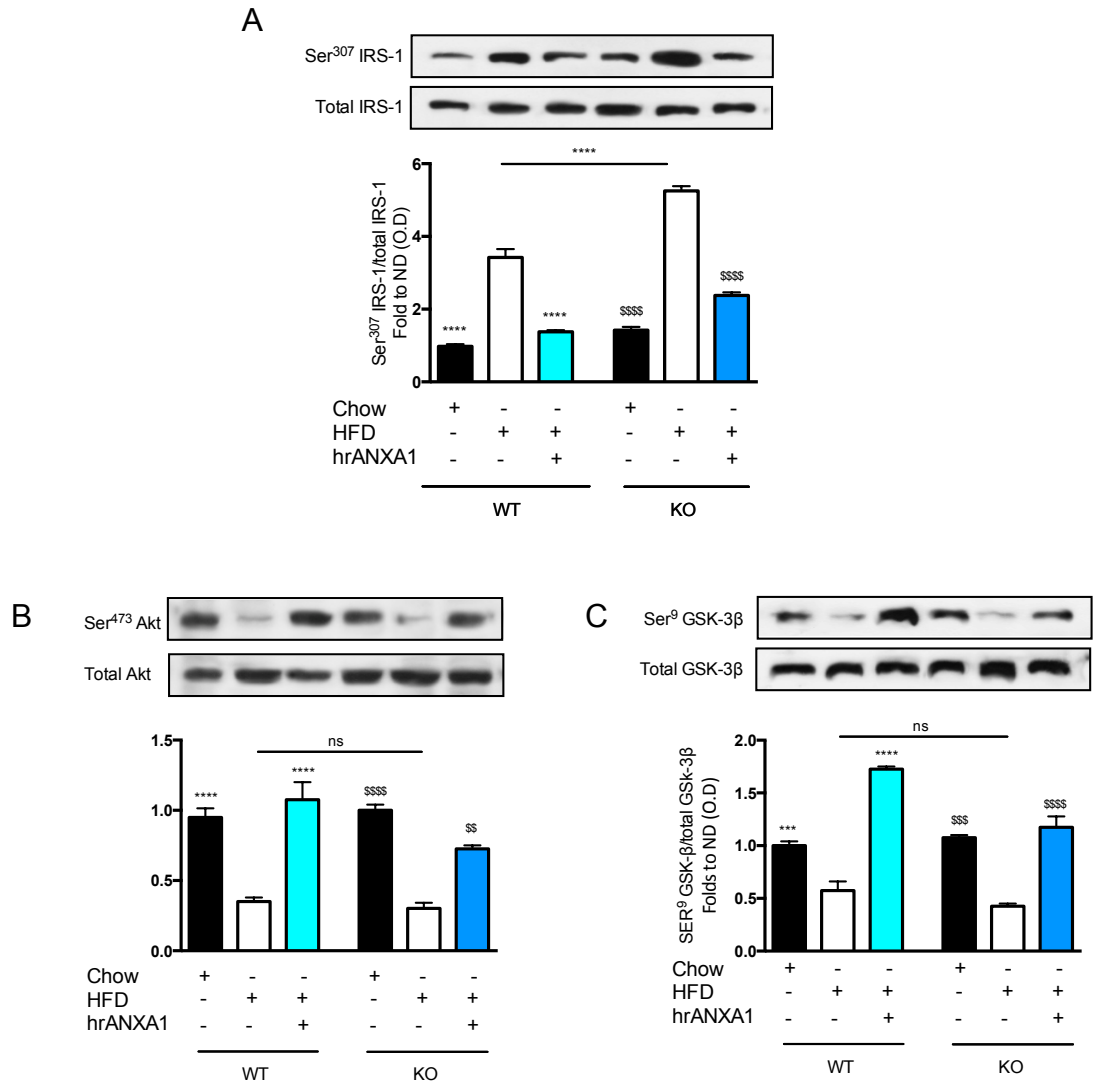

Figure 3.10 The effect of hrANXA1 administration and ANXA1$^{-/-}$ mice on insulin signalling the liver in a model of diet induced insulin resistance.

Signalling in the kidney was assessed after 10 weeks of dietary manipulation. Densitometric analysis of bands is expressed as a relative optical density (O.D.) of phosphorylated IRS-1 (pSer^{307}) corrected to total IRS-1, phosphorylated Akt (pSer^{473}) corrected to total Akt (A) and phosphorylated GSK-3β (pSer^{9}) corrected to total GSK-3β (B) and normalised using the WT + chow band. and normalised using the WT + chow band. Experimental groups: WT or ANXA1$^{-/-}$ mice treated fed on normal diet (chow) or high-fat-high-sugar (HFD) with or without hrANXA1 (1 µg hrANXA1, i.p., 5 X per week). Representative images from one of three repeated experiments are shown in this Figure. Data analysed by a one-way ANOVA followed by a Bonferroni *post-hoc* test, and expressed as mean ± SEM. n= 6-8 per group. ****P<0.0001 vs. WT + HFD and $^{\$\$}$ P<0.01 and $^{\$\$\$\$}$ P<0.001 vs. ANXA1$^{-/-}$ + HFD.

3.4.9. The effect of hrANXA1 administration and role of endogenous ANXA1 on insulin signalling pathways, in skeletal muscle, in a murine model of diet-induced insulin resistance.

To further assess the potential mechanisms (insulin resistance), which account for the rise in blood glucose and insulin levels caused by HFD, a semi-quantitative western blot analysis of key elements of the insulin signalling pathways was preformed in skeletal muscle. When compared to skeletal muscle obtained from WT-mice fed on chow diet, skeletal muscle from WT-mice fed on HFD showed significant increases in the phosphorylation of insulin receptor substrate-1 (IRS-1) on Ser^{307} (Figure 3.11A, $P<0.0001$) and significant decreases in phosphorylation of Akt on Ser^{473} (Figure 3.11B, $P<0.0001$) and GSK-3β on Ser^{9} (Figure 3.11C, $P<0.001$). Taken together, these findings suggest that WT-mice fed a HFD had a significant impairment in the insulin-signalling pathway indicative of insulin resistance (in skeletal muscle).

When compared to skeletal muscle from WT-mice fed on HFD, skeletal muscle from mice fed on HFD and treated with hrANXA1 demonstrated a significantly lower degree of phosphorylation of IRS-1 on Ser^{307} (Figure 3.11A, $P<0.0001$) as well as a significantly higher degree of phosphorylation of Akt on Ser^{473} (Figure 3.11B, $P<0.0001$) and GSK-3β on Ser^{9} (Figure 3.11C, $P<0.0001$), suggesting a restoration of normal insulin signalling. Indeed, the degree of phosphorylation of IRS-1 on Ser^{307}, Akt on Ser^{473} and GSK-3β on Ser^{9} in skeletal muscle samples obtained from mice fed on HFD and treated with hrANXA1 was not different from that seen in mice fed standard chow.

Similarly, when compared to skeletal muscle obtained from ANXA1$^{-/-}$ mice fed on chow diet, skeletal muscle from ANXA1$^{-/-}$ mice fed on HFD demonstrated a significant increase in the phosphorylation of IRS-1 on Ser^{307} (Figure 3.11A, $P<0.0001$); and significant decreases in the phosphorylation of Akt on Ser^{473} (Figure 3.11B, $P<0.0001$) and GSK-3β on Ser^{9} (Figure 3.11C, $P<0.001$). When compared to skeletal muscle obtained from ANXA1$^{-/-}$ mice on HFD, skeletal muscle from ANXA1$^{-/-}$ mice fed on HFD and administrated hrANXA1 (to restore their phenotype to WT) exhibited a significantly lower degree of phosphorylation of IRS-1 on Ser^{307} (Figure 3.11A, $P<0.0001$), and significantly higher degree of the phosphorylation of Akt on Ser^{473} (Figure 3.11B, $P<0.0001$) and GSK-3β on Ser^{9} (Figure 3.11C, $P<0.0001$). Thus, treatment of ANXA1$^{-/-}$ mice with hrANXA1 also restored the impairment in insulin signalling observed in the skeletal muscle of ANXA1$^{-/-}$ mice treated with vehicle.

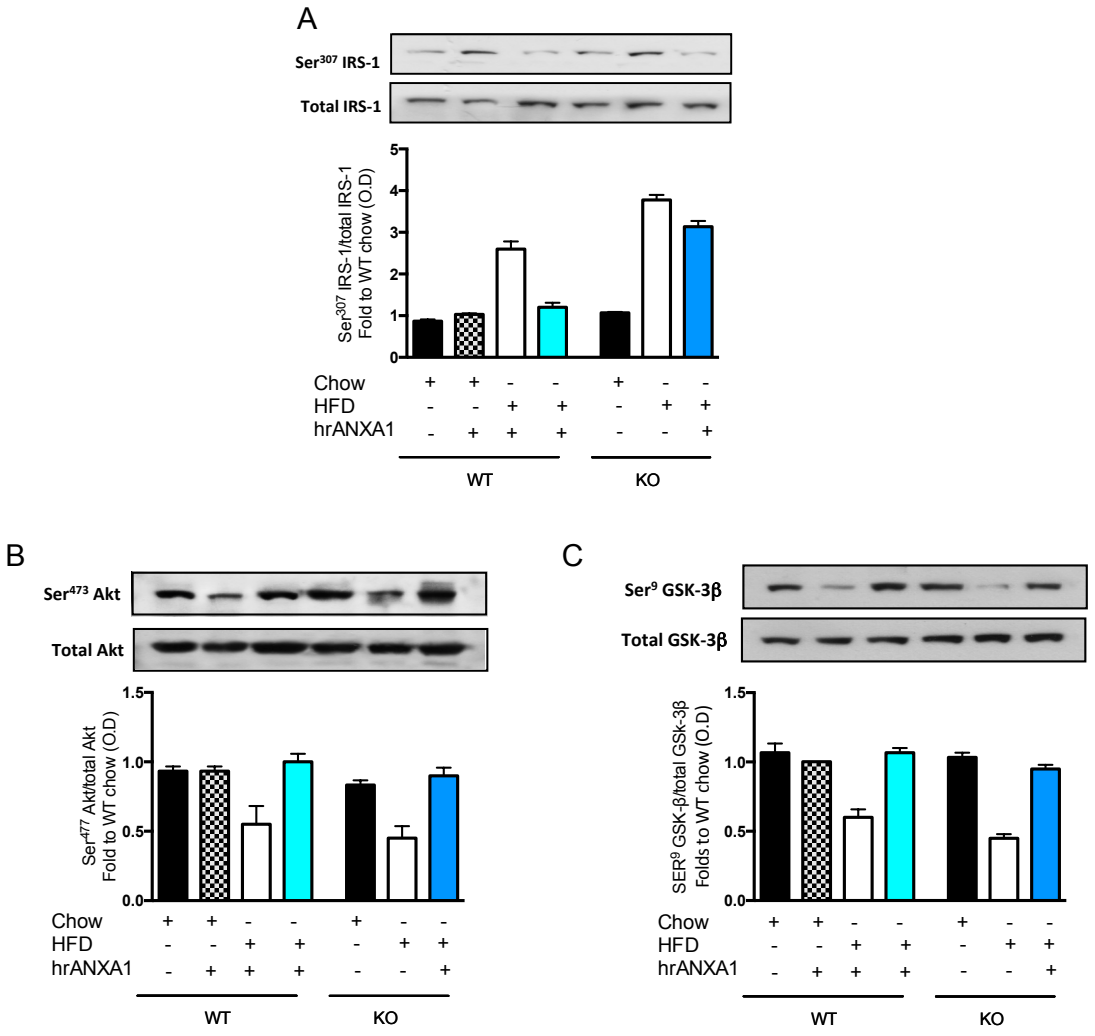

Figure 3.11. The effect of hrANXA1 administration and ANXA1$^{-/-}$ mice on insulin signalling skeletal muscle in a model of diet induced insulin resistance.

Signalling in the kidney was assessed after 10 weeks of dietary manipulation. Densitometric analysis of bands is expressed as a relative optical density (O.D.) of phosphorylated IRS-1 (pSer^{307}) corrected to total IRS-1, phosphorylated Akt (pSer^{473}) corrected to total Akt (A) and phosphorylated GSK-3β (pSer^{9}) corrected to total GSK-3β (B) and normalised using the WT + chow band and normalised using the WT + chow band. Experimental groups: WT or ANXA1$^{-/-}$ mice treated fed on normal diet (chow) or high-fat-high-sugar (HFD) with or without hrANXA1 (1 µg hrANXA1, i.p., 5 X per week). Representative images from one of three repeated experiments are shown in this Figure. Data analysed by a one-way ANOVA followed by a Bonferroni *post-hoc* test, and expressed as mean ± SEM. n= 6-8 per group. ****P<0.0001 vs. WT + HFD and $^{\$\$}$P<0.01 and $^{\$\$\$\$}$P<0.001 vs. ANXA1$^{-/-}$ + HFD. Quantification of bands for WT-mice fed a chow diet and treated with hrANAXA1 was carried out, but, not shown in the representative image, only in histogram.

3.4.10. The effect of hrANXA1 administration and role of endogenous ANXA1 on renal dysfunction in a model of diet-induced insulin resistance.

One of the major complications associated with T2DM is diabetic nephropathy. Thus, renal function was assessed by measuring relevant biomarkers of proteinuria and renal dysfunction in serum and urine collected after 10 weeks of dietary manipulation. When compared to WT-mice fed on chow diet, WT-mice fed a HFD demonstrated a significant increase in ACR (Figure 3.12A, $P<0.0001$) indicating the presence of proteinuria. When compared to WT-mice fed a HFD, WT-mice fed on a HFD and treated with hrANXA1 showed a lower ACR (Figure 3.12A, $P<0.05$), suggesting prevention by hrANXA1 of the development of proteinuria. Similarly, renal function was assessed in ANXA1$^{-/-}$ mice after 10 weeks of dietary augmentation. When compared to ANXA1$^{-/-}$ mice fed on chow diet, ANXA1$^{-/-}$ mice fed on a HFD demonstrated a significant increase in ACR (Figure 3.12A, $P<0.001$), indicating the development of proteinuria. When compared to ANXA1$^{-/-}$ mice, ANXA1$^{-/-}$ mice fed on HFD and administrated hrANXA1 (to recover their phenotype to WT) had a lower ACR (Figure 3.12A, $P<0.01$). Interestingly, when compared to WT-mice fed on HFD, ANXA1-/- mice fed on HFD demonstrated a significant increase in ACR (Figure 3.12A, $P<0.05$) suggesting the development of a more severe degree of proteinuria.

When compared to WT-mice fed on chow diet, WT-mice fed on a HFD exhibited a small increase in serum creatinine, which was not significant (Figure 3.12B, ns). Similarly, when compared to ANXA1$^{-/-}$ mice fed on chow diet, ANXA1$^{-/-}$ mice fed

on HFD showed a small increase in serum creatinine, which was not significant (Figure 3.12B, ns).

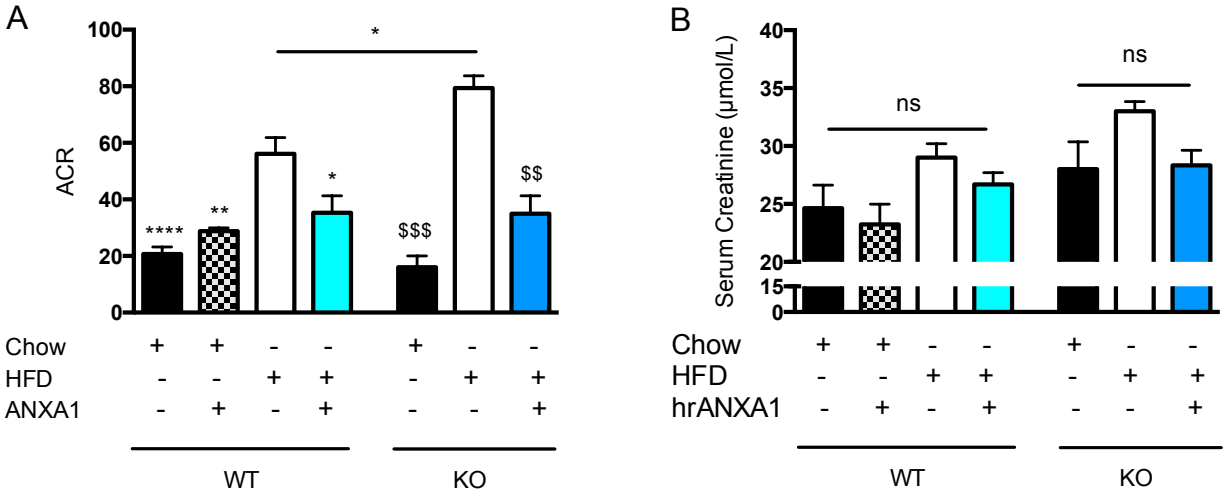

Figure 3.12. The effect of hrANXA1 administration and ANXA1$^{-/-}$ mice on renal dysfunction in a model of diet induced insulin resistance.

Effects of chronic exposure to a normal diet (chow) or a high-fat high-sugar diet (HFD) urine albumin-to-creatinine ratio (A); serum creatinine (B) were measured from urine and serum after 10 weeks of dietary manipulation. . Experimental groups: WT or ANXA1$^{-/-}$ mice treated fed on normal diet (chow) or high-fat-high-sugar (HFD) with or without hrANXA1 (1 µg hrANXA1, i.p., 5 X per week). Data analysed by a one-way ANOVA followed by a Bonferroni *post-hoc* test, and expressed as mean ± SEM. n= 6-8 per group. *P<0.05 **P<0.01 ****P<0.0001 vs. WT + HFD and $^{\$\$}$P<0.01 and $^{\$\$\$}$P<0.001 vs. ANXA1$^{-/-}$ + HFD.

3.4.11. The effect of hrANXA1 administration and role of endogenous ANXA1 on eNOS signalling in the kidney in a model of diet-induced insulin resistance.

To further investigate the potential mechanisms behind the reduction in insulin sensitivity and renal dysfunction, a semi-quantitative western blot analysis was performed in renal tissue. When compared to renal tissue obtained from WT-mice fed on chow diet, renal tissue from WT-mice fed on HFD exhibited a significantly lower degree of phosphorylation of eNOS on Ser^{1177} (Figure 3.13, $P<0.05$). When compared to renal tissue obtained from WT-mice fed on HFD, renal tissue from mice fed on HFD treated with hrANXA1 exhibited a higher degree of phosphorylation of eNOS on Ser^{1177} (Figure 3.13, $P<0.05$).

When compared to kidney tissue obtained from $ANXA1^{-/-}$ mice fed on chow diet, renal tissue from $ANXA1^{-/-}$ mice fed on HFD exhibited a significant reduction in the phosphorylation of eNOS on Ser^{1177} (Figure 3.13, $P<0.05$) However, renal tissue obtained from $ANXA1^{-/-}$ mice fed on HFD that were given hrANXA1 (to recover their phenotype to WT) exhibited a significantly higher degree of phosphorylation of eNOS on Ser^{1177} (Figure 3.13, $P<0.001$).

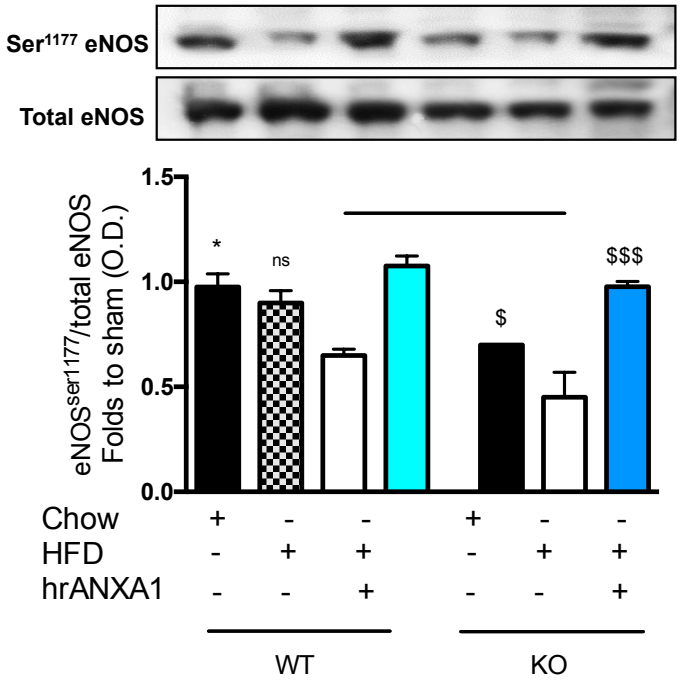

Figure 3.13. The effect of hrANXA1 administration and ANXA1$^{-/-}$ mice on eNOS signalling the kidney in a model of diet-induced insulin resistance.

Signalling in the kidney was assessed after 10 weeks of dietary manipulation. Densitometric analysis of bands is expressed as a relative optical density (O.D.) of phosphorylated eNOS (pSer^{1177}) corrected to total and normalised using the WT + chow band. Experimental groups: Wild-type or ANXA1$^{-/-}$ mice treated fed on normal diet (chow) or high-fat-high-sugar (HFD) with or without hrANXA1 (1 µg hrANXA1, i.p., 5 X per week). Representative images from one of three repeated experiments are shown in this Figure. Data analysed by a one-way ANOVA followed by a Bonferroni *post-hoc* test, and expressed as mean ± SEM. n= 3-4 per group. *P<0.05, **P<0.01, ****P<0.0001 vs. WT+ HFD and $^{\$\$\$}$P<0.001, $^{\$\$\$\$}$P<0.001 vs. ANXA1$^{-/-}$ + HFD. Quantification of bands for WT-mice fed a chow diet and treated with hrANAXA1 was carried out, but not shown in the representative image, only in histogram.

3.4.12. The effect of diet-induced insulin resistance on endogenous levels of ANXA1.

ANXA1 levels were measured in skeletal muscle using a semi-quantitative western blot analysis after 10 weeks of dietary manipulation. When compared to skeletal muscle obtained from WT-mice fed on chow diet, skeletal muscle from WT-mice fed on HFD exhibited a significant decrease in the levels of ANXA1 protein (Figure 3.14A, $P<0.0001$). When compared to WT-mice fed on HFD, the amount of ANXA1 protein in skeletal muscle from WT-mice fed on HFD and treated with hrANXA1 was significantly higher (Figure 3.14B, $P<0.001$). ANXA1 levels were also measured in the liver using a semi-quantitative western blot analysis after 10 weeks of dietary manipulation. When compared to liver tissue obtained from WT-mice fed on chow diet, liver tissue from WT-mice fed on HFD exhibited a significant decrease in ANXA1 protein (Figure 3.14B, $P<0.0001$). When compared to WT-mice fed on HFD, the amount of ANXA1 protein in the liver from WT-mice fed on HFD and treated with hrANXA1 was significantly higher (Figure 3.14B, $P<0.001$). Similarly, endogenous ANAXA1 levels were measured in the kidney using semi-quantitative western blot analysis after 10 weeks of dietary manipulation. When compared to renal tissue obtained from WT-mice, renal tissue obtained from WT-mice fed on a HFD exhibited a significant decrease in ANXA1 (Figure 3.14C, $P<0.01$). When compared to WT-mice fed on HFD, the amount of ANXA1 protein in kidneys from WT-mice fed on HFD and treated with hrANXA1 were significantly higher (Figure 3.14C, $P<0.0001$).

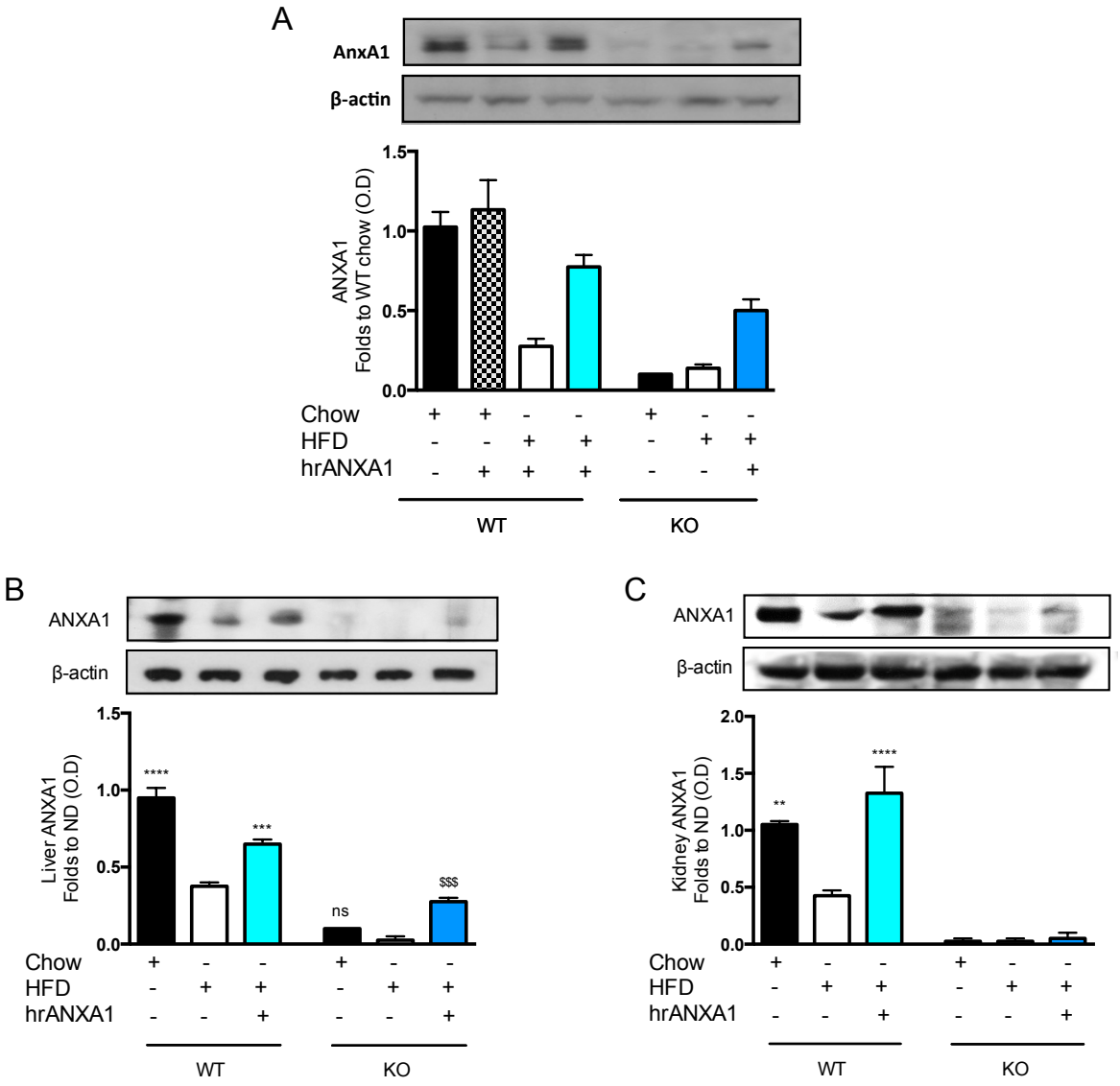

Figure 3.14. Tissue levels of ANXA1 in a model of diet induced insulin resistance.

ANXA1 levels were measured by western blot analysis in skeletal muscle (A), liver (B) and kidney (C). Densitometric analysis of bands is expressed as a relative optical density (O.D.) of ANXA1 corrected to β-actin and normalised using the WT + chow band. Experimental groups: WT or ANXA1$^{-/-}$ mice treated fed on normal diet (chow) or high-fat-high-sugar (HFD) with or without hrANXA1 (1 μg hrANXA1, i.p., 5 X per week). Representative images from one of three repeated experiments are shown in this Figure. Data analysed by a one-way ANOVA followed by a Bonferroni *post-hoc* test, and expressed as mean ± SEM. n= 3-4 per group. ***P<0.001, ****P<0.0001 vs. WT+ HFD and $^{\$\$\$}$P<0.001 vs. ANXA1$^{-/-}$ + HFD. Quantification of bands for WT- mice fed a chow diet and treated with hrANAXA1 was carried out, but not shown in the representative image, only in histogram 3.14A.

3.4.12. The effect of hrANXA1 administration and role of endogenous ANXA1 on RhoA and MYPT1 signalling, in skeletal muscle, in a murine model of diet-induced insulin resistance.

When compared to skeletal tissue obtained from WT-mice fed on chow diet, skeletal muscle from WT-mice fed on HFD exhibited a significantly lower degree of phosphorylation of RhoA on Ser^{188} (Figure 3.15A, $P<0.01$) and a significant increase in the phosphorylation of MYPT1 on Thr^{853} (Figure 3.15B, $P<0.0001$). The observed alterations in phosphorylation of RhoA on Ser^{188} and of MYPT1 on Thr^{853} caused by HFD in skeletal muscle were abolished by treatment of WT-mice fed on HFD with hrANXA1 (Figure 3.15A/B).

When compared to WT-mice fed on chow diet, skeletal muscle from $ANXA1^{-/-}$ mice fed on chow diet exhibited a significantly lower degree in the (inhibitory) phosphorylation of RhoA on Ser^{188}, which was associated with a significant increase in the phosphorylation of MYPT1 on Thr^{853} (Figure 3.15B, $P<0.0001$). When compared to skeletal muscle obtained from $ANXA1^{-/-}$ mice fed on chow diet, skeletal muscle from $ANXA1^{-/-}$ mice fed on HFD showed no significant change in the phosphorylation of RhoA on Ser^{188} (Figure 3.15A, ns) or MYPT1 on Thr^{853} (Figure 315B, ns). However, when compared to skeletal muscle obtained from $ANXA1^{-/-}$ mice on HFD, skeletal muscle from $ANXA1^{-/-}$ mice on HFD and administrated hrANXA1 exhibited a significant increase in the phosphorylation of RhoA on Ser^{188} (Figure 3.15A, $P<0.0001$) and significant lower degree of phosphorylation of MYPT1 on Thr^{853} (Figure 3.15B, $P<0.0001$).

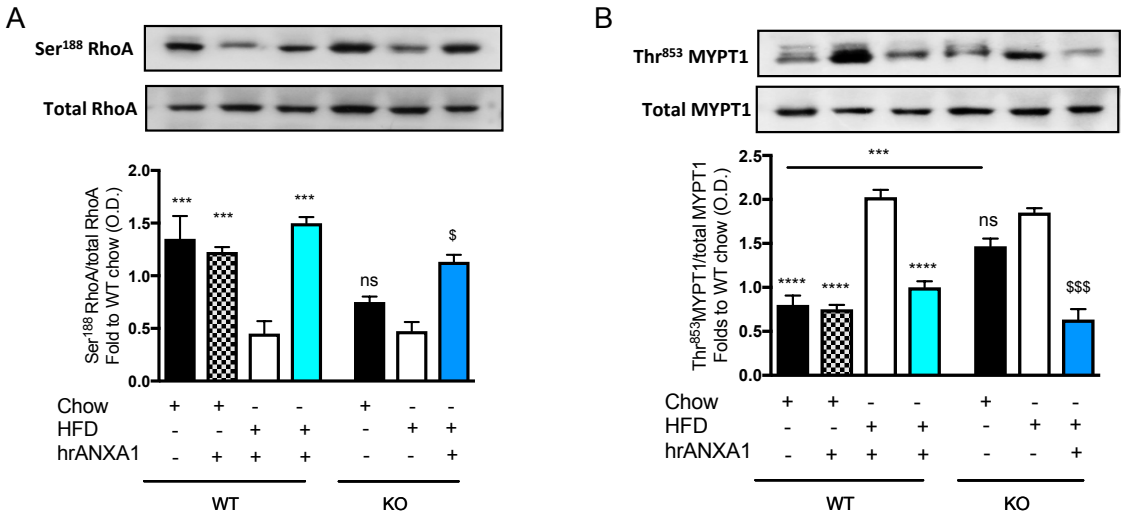

Figure 3.15. The effect of hrANXA1 administration and ANXA1$^{-/-}$ mice on RhoA and MYPT1 signalling, in skeletal muscle, in a model of diet-induced insulin resistance.

Signalling in skeletal muscle was assessed after 10 weeks of dietary manipulation. Densitometric analysis of bands is expressed as a relative optical density (O.D.) of A) phosphorylated RhoA (pSer^{4188}) corrected to total RhoA and B) phosphorylated MYPT1 (pThr853) corrected to total MYPT1 and normalised using the WT + chow band. Experimental groups: Wild-type or ANXA1$^{-/-}$ mice treated fed on normal diet (chow) or high-fat-high-sugar (HFD) with or without hrANXA1 (1 µg hrANXA1, i.p., 5 X per week). Representative images from one of three repeated experiments are shown in this Figure. Data analysed by a one-way ANOVA followed by a Bonferroni *post-hoc* test, and expressed as mean ± SEM. n= 3-4 per group. *P<0.05, **P<0.01, ****P<0.0001 vs. WT+ HFD and $^{\$\$\$}$P<0.001, $^{\$\$\$\$}$P<0.001 vs. ANXA1$^{-/-}$ + HFD. Quantification of bands for WT-mice fed a chow diet and treated with hrANAXA1 was carried out, but not shown in the representative image, only in histogram.

3.4.13. The effect of hrANXA1 administration and role of endogenous ANXA1 on RhoA and MYPT1 signalling, in the liver, in a murine model of diet-induced insulin resistance.

When compared to liver tissue obtained from WT-mice fed on chow diet, liver tissue from WT-mice fed on HFD exhibited a significantly lower degree of inhibitory phosphorylation of RhoA on Ser^{188} (Figure 3.16A, $P<0.01$) and a significant increase in the phosphorylation of MYPT1 on Thr^{853} (Figure 3.16B, $P<0.0001$). The observed alterations in phosphorylation of RhoA on Ser^{188} and of MYPT1 on Thr^{853} caused by HFD in the liver were abolished by treatment of WT-mice fed on HFD with hrANXA1 (Figure 3.16, $P<0.05$).

When compared to WT-mice fed on chow diet, livers from $ANXA1^{-/-}$ mice fed on chow diet exhibited a decrease in the phosphorylation of RhoA on Ser^{188} (Figure 3.16A, $P<0.0001$) suggesting that RhoA is constitutively active in ANXA1 mice. This was associated with a significant increase in the phosphorylation of MYPT1 on Thr^{853} (Figure 3.16B, $P<0.0001$). When compared to liver tissue obtained from $ANXA1^{-/-}$ mice fed on chow diet, liver tissue from $ANXA1^{-/-}$ mice fed on HFD had no significant change in the phosphorylation of RhoA on Ser^{188} (Figure 3.16A, ns) or MYPT1 on Thr^{853} (Figure 3.16B, ns). However, when compared to liver tissue obtained from $ANXA1^{-/-}$ mice on HFD, liver tissue from $ANXA1^{-/-}$ mice on HFD and treated with hrANXA1 exhibited a significant increase in the phosphorylation of RhoA on Ser^{188} (Figure 3.16A, $P<0.0001$) and significantly lower degree of phosphorylation of MYPT1 on Thr^{853} (Figure 3.16B, $P<0.0001$).

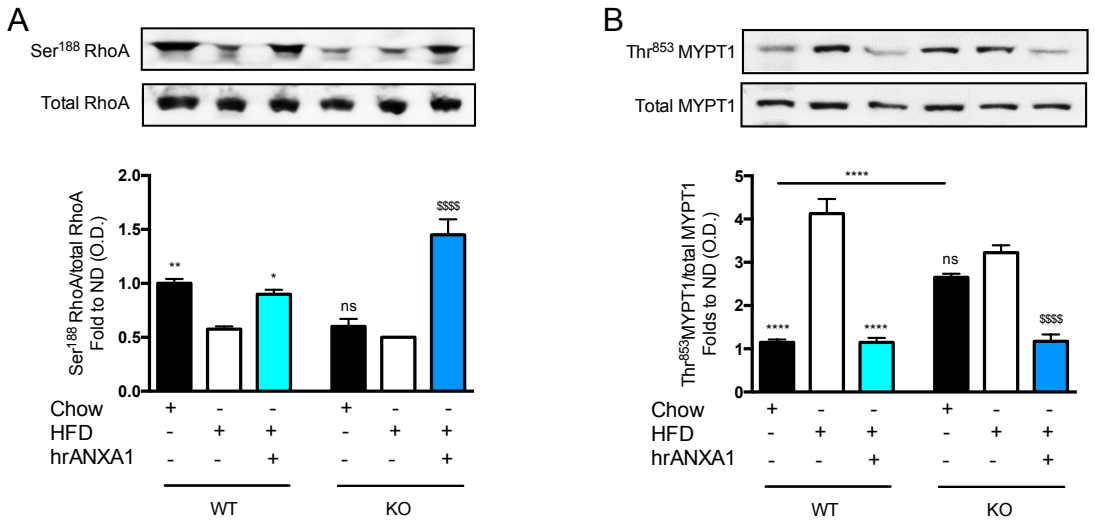

Figure 3.16. The effect of hrANXA1 administration and ANXA1$^{-/-}$ mice on RhoA and MYPT1 signalling in the liver in a model of diet-induced insulin resistance.

Signalling in the liver was assessed after 10 weeks of dietary manipulation. Densitometric analysis of bands is expressed as a relative optical density (O.D.) of A) phosphorylated RhoA (pSer^{4188}) corrected to total RhoA and B) phosphorylated MYPT1 (pThr853) corrected to total MYPT1 and normalised using the WT + chow band. Experimental groups: Wild-type or ANXA1$^{-/-}$ mice treated fed on normal diet (chow) or high-fat-high-sugar (HFD) with or without hrANXA1 (1 µg hrANXA1, i.p., 5 X per week). Representative images from one of three repeated experiments are shown in this Figure. Data analysed by a one-way ANOVA followed by a Bonferroni *post-hoc* test, and expressed as mean ± SEM. n= 3-4 per group. *P<0.05, **P<0.01, ****P<0.0001 vs. WT+ HFD and $^{\$\$\$}$P<0.001, $^{\$\$\$\$}$P<0.001 vs. ANXA1$^{-/-}$ + HFD.

3.4.14. The effect of hrANXA1 administration and role of endogenous ANXA1 on RhoA and MYPT1 signalling in the kidney in a murine model of diet-induced insulin resistance.

When compared to kidney tissue obtained from WT-mice fed on a chow diet, renal tissue from WT-mice fed on a HFD exhibited a significantly lower degree of phosphorylation of RhoA on Ser^{188} (Figure 3.17A, $P<0.0001$) and a significant increase in the phosphorylation of MYPT1 on Thr^{853} (Figure 3.17B, $P<0.0001$). When compared to kidney tissue obtained from WT-mice fed on HFD, renal tissue from mice fed on HFD treated with hrANXA1 exhibited a significant increased in the phosphorylation of RhoA on Ser^{188} (Figure 3.17A, $P<0.0001$) and a significantly lower degree of phosphorylation of MYPT1 on Thr^{853} (Figure 3.17B, $P<0.0001$).

When compared kidney tissue from WT-mice fed on chow diet, renal tissue from $ANXA1^{-/-}$ mice fed on chow diet exhibited a significantly lower degree of phosphorylation of RhoA on Ser^{188} (Figure 3.17A, $P<0.0001$) and an increase in the phosphorylation of MYPT1 on Thr^{853} (Figure 3.17B, $P<0.001$). When compared to renal tissue obtained from $ANXA1^{-/-}$ mice fed on chow diet, renal tissue from $ANXA1^{-/-}$ mice fed on HFD exhibited no significant change in the phosphorylation of RhoA on Ser^{188} (Figure 3.17A, ns) or MYPT1 on Thr^{853} (Figure 3.17B, ns). However, renal tissue obtained from $ANXA1^{-/-}$ mice fed on HFD that were given hrANXA1 to recover their phenotype to WT exhibited a significant increase in the phosphorylation of RhoA on Ser^{188} (Figure 3.17A, $P<0.001$) and a lower degree of phosphorylation of MYPT1 on Thr^{853} (Figure 3.17B, $P<0.001$).

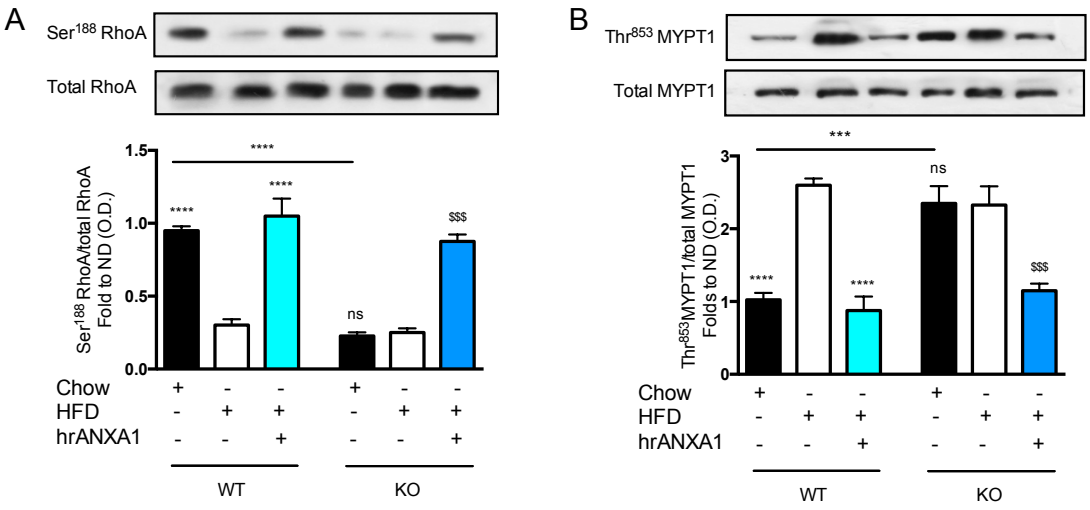

Figure 3.17. The effect of hrANXA1 administration and ANXA1$^{-/-}$ mice on RhoA and MYPT1 signalling the kidney in a model of diet-induced insulin resistance.

Signalling in the kidney was assessed after 10 weeks of dietary manipulation. Densitometric analysis of bands is expressed as a relative optical density (O.D.) of A) phosphorylated RhoA (pSer^{4188}) corrected to total RhoA and B) phosphorylated MYPT1 (pThr853) corrected to total MYPT1 and normalised using the WT + chow band. Experimental groups: Wild-type or ANXA1$^{-/-}$ mice treated fed on normal diet (chow) or high-fat-high-sugar (HFD) with or without hrANXA1 (1 µg hrANXA1, i.p., 5 X per week). Representative images from one of three repeated experiments are shown in this Figure. Data analysed by a one-way ANOVA followed by a Bonferroni *post-hoc* test, and expressed as mean ± SEM. n= 3-4 per group. *P<0.05, **P<0.01, ****P<0.0001 vs. WT+ HFD and $^{\$\$\$}$P<0.001, $^{\$\$\$\$}$P<0.001 vs. ANXA1$^{-/-}$ + HFD.

3.5. Discussion

The main findings of this chapter are that (i) ANXA1 levels are elevated in patients with T2DM. This elevation in ANXA1 was independent of the presence of an impairment in renal function (CKD), but correlated positively with the degree of proteinuria (urinary albumin) measured in these patients; (ii) there is a strong positive correlation between the increase BMI and plasma CRP levels indicting a link between obesity and systemic inflammation and (iii) there are strong correlations between plasma ANXA1 and total cholesterol, HDL-c and LDL-c. These findings led me to want to investigate a) the role of endogenous ANXA1 in a murine model of HFD-induced insulin resistance and diabetic nephropathy, and b) whether treatment with hrANXA1 reverses insulin resistance and diabetic nephropathy and may, hence, be a potential new therapeutic agent for patients with T2DM.

The main findings the murine study in this chapter are that (i) ANXA1$^{-/-}$ mice fed on a HFD develop more severe peripheral insulin resistance compared to WT mice fed a HFD, while therapeutic administration with hrANXA1 prevented the development of peripheral insulin resistance in both WT and ANXA1$^{-/-}$ mice; (ii) ANXA1$^{-/-}$ mice have more severe renal dysfunction and hepatic steatosis when challenged with a HFD, while the therapeutic administration of hrANXA1 reduced both renal dysfunction and hepatic steatosis caused by a HFD; (iii) WT mice fed on a high fat diet have lower levels of ANXA1 in the kidney, liver and skeletal muscle; (iv) genetic deletion of ANXA1 leads to the constitute activation of the small GTPase RhoA, allowing for increased MYTP1 activity in the kidney,

liver and skeletal muscle and (v) therapeutic administration of hrANXA1 attenuated the activation of the small GTPase RhoA and subsequent activation of MYPT1 in the kidney, liver and skeletal muscle.

Healthy people have low circulating levels of ANXA1 in the blood. Here I have shown that patients with T2DM have elevated levels of plasma ANXA1. CKD is a pro-inflammatory condition, however, I show that ANXA1 levels are not further elevated in patients with T2DM and CKD, suggesting that the rise of in ANXA1 is independent of an impairment in renal function and/or systemic inflammation. Three additional lines of evidence support this; (i) the rise in AXNA1 is independent of a diagnosis of CKD, as there is not difference in ANXA1 levels at progressive stages of CKD; (ii) and there is not progressive increase in CRP level with increasing stages of CKD and (iii) there is no correlation between increasing CRP levels and ANXA1 in patients with T2DM with/without CKD. Taken together, these observations suggest that endogenous ANXA1 may play an important role in the pathophysiology of T2DM, and that the rise in plasma ANAX1 in patients with T2DM is not dependent on either an impairment in renal function or the presence of significant systemic inflammation.

One of the biggest risk factors for the development of T2DM is obesity; indeed an increase in body mass index (BMI) is a strong predictor of the risk of suffering a cardiovascular event(s) and for subsequent adverse outcomes. In accordance with many others, I show in this chapter that there is a strong positive correlation between increased BMI and serum CRP levels, suggesting that there is link between BMI (obesity in the broadest terms) and low-grade inflammation

in T2DM. Consistent with our finding, Kosicka *et al.* have shown that as BMI and hip-to-waist ratio increase so does the level of system inflammation (plasma CRP level) when they studied the role of ANXA1 in obesity (Kosicka et al., 2013). Here we show for the first time that plasma ANXA1 is strongly correlated with increases in total plasma cholesterol, and with HDL-c and LDL-c (Figure 3.5). This is a particularly striking observation when we consider that most of the patients included in this study are on medication aimed at lowering circulating cholesterol levels. This interesting finding is made more striking by the fact that none of the circulating makers of hypercholesterolaemia are correlated with CRP. Indeed, independently, both elevated CRP and circulating cholesterol levels are associated with adverse cardiovascular events. Here I show that in patients with T2DM both plasma ANXA1 are linked to both elevated cholesterol and the presence of urinary proteinuria. Therefore, our working hypothesis is that ANXA1 is secreted from intracellular stores upon cell activation (driven by hyperglycaemia, hypercholesterolemia and uraemia) and is a surrogate plasma marker for the development of renal dysfunction in patients T2DM.

While, lifestyle factors and genetic predisposition provide us with predictive indications as to who is at risk of developing T2D, the pathophysiology of the progression of microvascular complications is incompletely defined due to its complexity, and involvement of multiple signalling pathways and processes. Using a murine model of HFD-induced insulin resistance I report in this chapter that ANXA1 plays a key protective role in T2DM. Two lines of evidence suggest this: (i) ANXA1$^{-/-}$ mice develop a more severe diabetic phenotype when fed a HFD; and (ii) therapeutic administration of hrANXA1 to mice fed on a HFD

reduces the severity of diabetes (e.g. improved OGTT, reduced blood glucose and reduced serum insulin). The observed improvement in glucose tolerance seen in mice fed on HFD is in part mediated by alterations in insulin signalling. The IRS-1/Akt/GSK-3β cascade is a key regulator of glucose transportation, glycogen synthesis and glycolysis. Peripheral insulin resistance is attributed to an increase in the phosphorylation of Ser^{307} on insulin receptor substrate-1 (IRS-1); this uncouples IRS-1 from the insulin receptor blunting the ability of insulin to signal through its receptor. This means that even when insulin binds to the IR, there is a decrease in the phosphorylation of $Tyr^{608/628}$, which are needed for PI3-kinase docking and signal transduction (Gual et al., 2005). This results in blunted GLUT4 translocate to the cell surface to facilitate glucose uptake in peripheral organs, leading to hyperglycaemia (Chiazza et al., 2015). I demonstrate in this chapter that mice fed a HFD have increased phosphorylation of Ser^{307}, which is attenuated by hrANXA1 restabilising the insulin receptor allowing normal signal transduction and glucose homeostasis, inhibiting IRS-1 uncoupling from the insulin receptor.

One of the key downstream mediators of the insulin-signalling cascade is Akt. I demonstrate in this chapter that mice fed a HFD have a reduced phosphorylation of of Akt on Ser^{473} resulting in a reduction in Akt activity. Activated Akt controls inflammatory and pro-survival responses (Cantley, 2002). We have previously shown that one consequence of inhibition of Akt is that organs are less resistant to stressor stimuli (hyperglycaemia/hyperlipidaemia) and subsequently develop organ injury. Most notably, activation of the Akt-survival pathway reduces organ injury/dysfunction in many conditions associated with severe inflammation

including sepsis (Chen et al., 2017)(Khan et al., 2013), haemorrhagic shock (Yamada et al. 2017)(Sordi et al. 2017), renal ischaemia reperfusion (Patel et al., 2012) and diabetes (Chiazza et al., 2015). Here I demonstrate that the prevention of the decline in Akt activity by hrANXA1 reduces both kidney (proteinuria) and liver injury (hepatic steatosis) in animals challenged with HFD, supporting previous evidence that a loss of Akt activity predisposes organ to injury. Most notably, both full length ANXA1 and Ac2-16 (the N-terminal peptide of ANXA1) reduce a) ischaemia-reperfusion injury (heart/kidney) and b) the liver injury associated with non-alcoholic steatohepatitis by activating Akt (Qin et al., 2013)(Facio et al., 2011) (Locatelli et al., 2014).

Another function of activated Akt is to inhibit GSK-3β (Ser^9 phosphorylation), thus activating glycogen synthase, which converts glucose to glycogen for storage in the liver effectively reducing circulating blood glucose levels. Here I demonstrate that mice fed on a HFD have decreased activation of GSK-3β, which results in a reduction in glycogen synthesis, which may be one of the reasons for the observed hyperglycaemia. In contrast, mice treated with hrANXA1 demonstrated a restoration of phosphorylation of GSK-3β allowing for enzymatic conversion of glucose to glycogen.

The observed improvements in insulin sensitivity seen in mice fed on a HFD treated hrANXA1 have also translated into an improved lipid profile. Previous studies have documented that hyperinsulinaemia due to chronic exposure to a HFD can induce greater lipid accumulation (liver), which is consistent with the pathogenic features observed in clinical T2DM (Cusi, 2010)(Semple et al.,

2009)(Chiazza et al., 2015). Indeed, the livers of mice fed on a HFD had excessive lipid accumulation and hepatic steatosis, which was more severe in ANXA1$^{-/-}$ mice. Similarly, Akasheh *et al.* who report increased adiposity in ANXA1 deficient mice fed a HFD, albeit on a different genetic background (Akasheh et al., 2013). Indeed, excessive fat in the liver can directly contribute to the exacerbation of the degree of peripheral insulin resistance. Here I clearly show that the lack of endogenous ANXA1 dramatically increased lipid deposition caused by HFD in the liver and that these mice also display a more severe diabetic phenotype. This is consistent with other reports confirming that excessive lipid accumulation and hepatic steatosis are key drives of peripheral insulin resistance (Garg & Misra, 2002). Most notably, I show in this chapter that treatment with hrAXNA1 can not only reduce lipid accumulation, but that it can restore insulin receptor sensitivity resulting in normal glucose-stimulated insulin responses.

Secondary to peripheral insulin resistance, hyperglycaemia leads to the development of microvascular complications. Indeed, diabetic nephropathy is the leading cause of end-stage renal disease and in patients needing renal replacement therapy. The data presented here demonstrate that ANXA1$^{-/-}$ mice fed a HFD have more severe renal dysfunction (proteinuria) compared to WT-mice fed on a HFD, strongly suggesting that ANXA1 protects the kidney from the harmful effects of having T2DM phenotype. Moreover, renal impairment was confirmed histologically with evidence of mild glomerular hypertrophy, loss of brush borders in the proximal convoluted tubules and glomerular membrane and ECM thickening, all of which are histological hallmarks of diabetic nephropathy (Tervaert et al., 2010). Most notably, treatment of mice subjected to

HFD with hrANXA1 prevented the development of all of these histological alterations and translated into improved renal function.

Clinically, patients with T2DM have endothelial dysfunction, which is associated with an increased cardiovascular risk (Huang, 2009). Several lines of evidence suggest that decreased endothelial nitric oxide synthase (eNOS) phosphorylation is a molecular mechanism linking metabolism and vascular dysfunction: (i) eNOS phosphorylation is diminished in diabetes, hypercholesterolemia (Musicki et al. 2010) and atherosclerosis (Li et al., 2013)(Blair et al., 1999)(Ponnuswamy et al., 2012); (ii) statins and PPAR agonist increase eNOS phosphorylation (Rikitake & Liao, 2005); and (iii) signalling molecules such as insulin, IGF-1 and leptin increase eNOS phosphorylation. Here I demonstrate that mice fed on a HFD have decreased eNOS phosphorylation, and that this decrease in eNOS phosphorylation was prevented by treatment with hrANXA1. Decreased eNOS phosphorylation results in less enzymatic conversion of L-arginine to nitric oxide (NO), which is a key regulator of vascular tone. Reduced NO increases decreased vascular tone and leads to increased constriction (Campia et al., 2014), which could cause hypertension within the nephron leading to functional decline due to hyperfiltration and proteinuria. Activation of Akt is known to modulate eNOS activity through phosphorylation of eNOS at Ser^{1177}. Indeed, the present study shows that mice fed a HFD have decreased Akt and eNOS phosphorylation, suggesting a common link to these pathways. Indeed treatment with hrAXNA1 restored Akt signalling and increased eNOS phosphorylation in mice fed a HFD.

Many studies have described the central role of RhoA signalling in diabetes and specifically in diabetic kidney disease (Gojo et al., 2007) (Massey et al., 2003) (Miao et al., 2002) (Tang et al., 2006). Although the effects of RhoA inhibitors have been investigated in many clinical trials, albeit with limited success (Komers, 2013). In this study, I demonstrate that endogenous ANXA1 is a key regulator of RhoA activity. ANXA1$^{-/-}$ mice on a chow diet have decreased inhibitory phosphorylation of RhoA at Ser^{188} making the small GTPase constitutively active, which, in turn, drives the down-stream activation of MYPT1. This is consistent with a previous report from Christante *et al.* who demonstrated for the first time that ANXA1 signals in an autocrine/paracrine action via FPR2 to inhibit the activity of the small GTPase RhoA. When mice are fed a HFD, the tissue expression (kidney, liver and skeletal muscle) of ANXA1 is decreased. Therefore, I speculate that the loss of ANXA1 signalling through FRP2 allows for the activation of the small RhoA GTPase (Cristante et al., 2013). Importantly, from a pharmacological point of view, the G protein-coupled receptor FPR2 represents a novel target for the microvascular complications of diabetes. This is reinforced by our experiments in ANXA1$^{-/-}$ mice, in which, even in the absence of endogenous ANXA1 we could restore normal signalling events, but treating with exogenous hrANXA1 leading to phenotypic rescue (improved diabetic phenotype and reduced organ injury).

MYPT1 is a key regulator of vascular tone within vascular smooth muscle, and is directly under the regulatory control of RhoA. Activated (phosphorylated) MYPT1 actively phosphorylates myosin delaying its ability to relax, therefore, inducing a prolonged contraction (Brozovich et al., 2016). Hypertension is a key

co-morbidity of diabetes, and a key driver of renal dysfunction. One of the key therapies for treating CKD and diabetic nephropathy is inhibition of the renin-angiotensin system. Indeed, we report that mice fed on a HFD have increased phosphorylation of MYPT1, which was attenuated by treatment with hrANXA1. This evidence coupled with the decrease in eNOS phosphorylation leads to the working hypothesis that the microvascular compactions seen in mice fed a HFD are driven at least in part by hypertension. Indeed, here we have identified an endogenous molecule that can regulate two key pathways involved in maintaining vascular tone (i) regulation of eNOS activation and (ii) regulation if MYPT1 activity both of which are deregulated in diabetes.

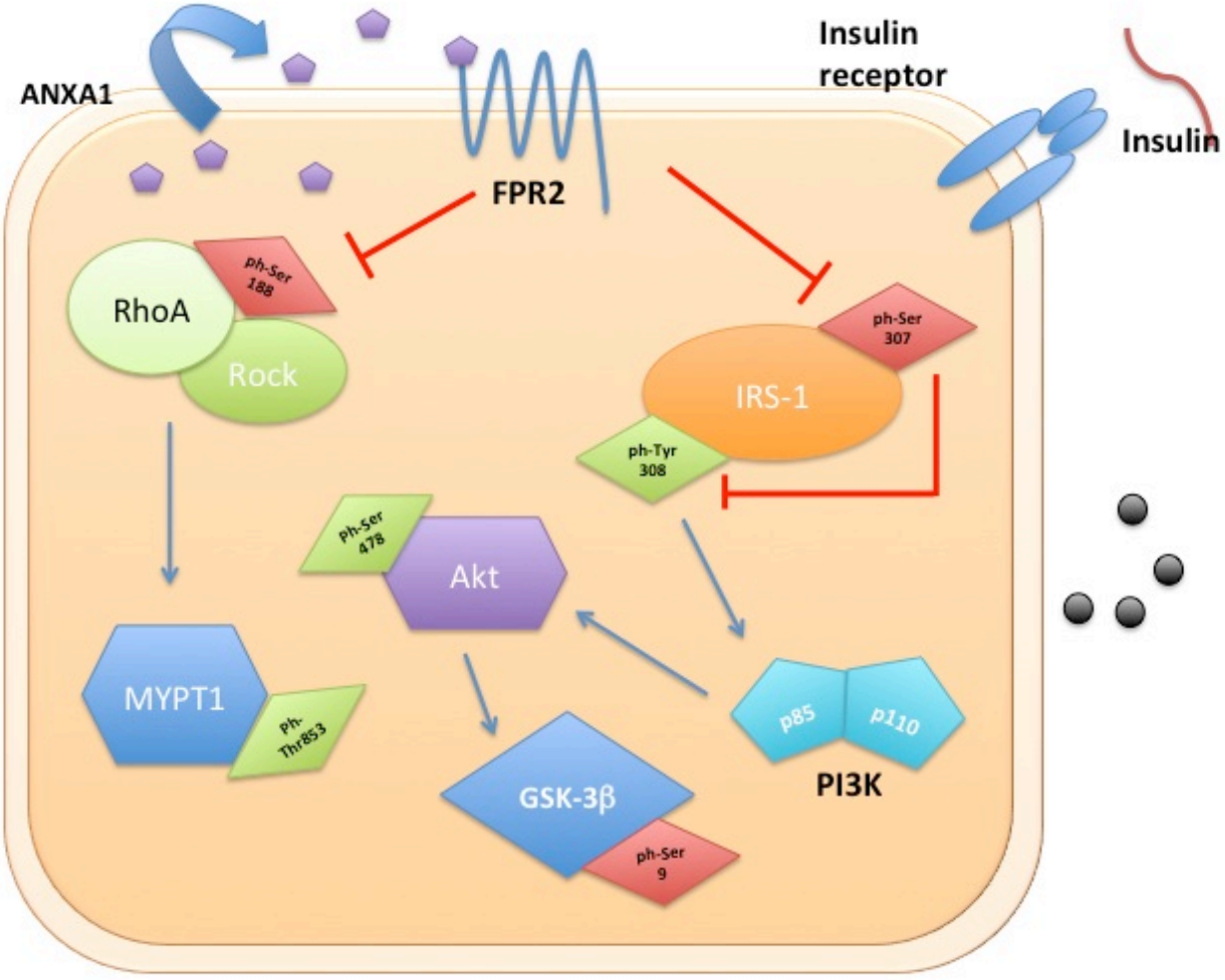

Figure 3.18. . Schematic of the mode of action of ANXA1 in a murine model of type-2 diabetes. When blood glucose levels are increased, insulin is released and binds to the insulin receptor, this allows for signalling transduction through the IRS-1. For signal transduction to occur tyrosine-308 must be phosphorylated. This then allows signal transduction through PI3K to activated Akt by phosphorylating serine-478, which in turn activates GSK-3β, which coverts glucose to glycogen. In T2DM, cellular levels of ANXA1 are depleted, and there is increased phosphorylation of serine-307 on IRS-1 which inhibits the tyrosine phosphorylation needed for signal transduction upon insulin binding, here I propose that ANXA1 signalling through the FPT2 receptor blocks the inhibitory phosphorylation of serine-307 on IRS-1, allowing normal insulin signalling events to occur. ANXA1 signalling through FPR2 inhibits the small GTPase RhoA, allowing it to activate MYPT1. In type-2 diabetes cellular levels of ANXA1 are depleted, meaning that RhoA is constitutively activated. In both cases when exogenous ANXA1 is given it restored signalling through FPR2 restoring normal signalling events.

Chapter IV:
Annexin-A1 linking peripheral inflammation and the blood brain barrier.

4.1. Introduction

The classical complications of T2DM are well known and include diabetic nephropathy, retinopathy and neuropathy. Hyperglycaemia and dyslipidaemia are the key drivers of these pathologies of the microvasculature (Chawla et al., 2016). It is well documented that endothelial dysfunction is a driver of many pathologies including hypertension, atherosclerosis and subsequently leads to increased incidence of both myocardial infarction and stroke (Deanfield et al. 2007). Uncontrolled blood glucose as is the case in diabetes is correlated with endothelial dysfunction, indeed both hyper and hypoglycaemia has been shown to be detrimental to the endothelium.

The brain is a unique organ and is subject to immune privilege and has a specialised barrier, the blood brain barrier (BBB), which has extreme tightness. The extreme tightness of the BBB stops the passage of immune cells and other large particles into the brain parenchyma. Specialised tight junctions are found in the BBB, and in-part mediate the tight junctions; they do this by creating 'kissing points' between cells and the intracellular actin cytoskeleton. Disruption of these unique structures causes the BBB to become more permeable and allows immune cells and large particle to cross into the brain. Cristante published for the first time that ANXA1$^{-/-}$ mice have increased BBB permeability and that these effects are mediated through FPR2 signalling to activate RhoA (Cristante et al., 2012). Indeed, increased BBB permeability and increased immune cell infiltration in the central nervous system plays a major role in many neurological conditions including, multiple sclerosis, Alzheimer's disease and Parkinson's

disease. Each of these diseases of the CNS is associated with increased peripheral and central inflammation resulting in neurological decline.

It is now widely accepted that metabolic stress can alter immune cells behaviour particularly how they interact with the endothelial to mediate migration into sites of inflammation. Indeed, diabetes is classically known as being a disease of low-grade chronic inflammation, often associated with increased monocyte number in the adipose tissue. However, emerging evidence now suggests that there may also be alterations in T-lymphocytes populations in diabetes, and that these may exacerbate endothelium damage. Recently, Yang and colleagues have demonstrated that ANXA1 deficient mice have an augmented T-cells population characterised by an increase in RORγt and decreased Th17 cells (Yang et al, 2013).

4.1.1. Specific aims

The role of ANXA1, in regulating BBB permeability is unknown in T2DM, as is the role of ANAX1 in T-cell differentiation in T2DM and their ability to extravasate. Therefore, this study was designed to investigate:

(1) if the BBB is more permeable in mice fed a HFD and if endogenous ANXA1 regulates BBB tightness;

(2) if feeding mice a HFD changes the number of $CD4^+$ T-cells populations;

(3) If isolated lymphocytes from mice fed a HFD have an altered ability to adhere to and transmigrate through a BMEC mono-layer; and

(4) if therapeutic intervention with hrANXA1 alters different CD4+ T0cells ability to adhere to and transmigrate through a BMEC mono-layer.

4.2. Methods and materials

4.2.1. Use of animals - ethic statement

The animal protocols followed in this study were approved by the Animal Welfare Ethics Review Board (AWERB) of Queen Mary University of London in accordance with the derivatives of both the Home Office guidance on the Operation of Animals (Scientific Procedures Act 1986) published by Her Majesty's Stationery Office and the Guide for the Care and Use of Laboratory Animals of the National Research Council. All research was conducted project licenses reference numbers PPL: 70/8350. This study was carried out on 10 week-old male C57BL/6 mice and ANXA1$^{-/-}$ mice, weighing 25–30 g (Charles River Laboratories UK Ltd., Kent, UK). The animals were allowed to acclimatise to laboratory conditions for a period of at least one week before any experimental procedures were initiated. All animals had free access to food and water *ad libitum*.

4.2.2. HFD induction of type-2 diabetes

10-week old WT male C57BL/6 or ANXA1$^{-/-}$ mice were fed a normal chow diet (protein 23.5 %, fat 21.8 % and carbohydrate 54.7 %) or fed a high-fat high-sugar diet (HFD) (protein 14.9 %, fat 59.4 % and carbohydrate 25.7 %) for 10 weeks.

4.2.3. Drug administration

Before dietary manipulation mice were randomly divided into treatment groups. Mice fed a HFD were administered either hrANXA1 (1 ug, 100 µl, Hepes 50mM;

140 mM NaCl; pH 7.0, i.p.) or vehicle (100 µl, Hepes 50mM; 140 mM NaCl; pH 7.0, i.p.).

4.2.4. T-cells isolation and expansion

Lymph nodes (inguinal, mesenteric, axillary, brachial, superficial and deep cervical, lumbar, and sacral) of C57BL/6 and ANXA1$^{-/-}$ mice were isolated and passed through 70 µm mesh and re-suspended in PBS (5 ml) and centrifuged at 1800 RPM at 5 min 4 °C. To expand cells, 1 x10^6 cells are plated on pre coated plates with coating buffer (50 mM Tris; pH 8,5; 1 µg/mL anti-CD3; 5 µg/mL anti-CD28), cells were then cultured in RPMI medium (10 % fetal bovine serum; 2nM glutamine; 10 mM HEPES; 1mM sodium pyruvate; gentamycin; 50 µM β-mercaptoethanol; 10 ng/mL IL-2) for 4 days.

4.2.5. T-cell migration in static condition

bEND5 cells were plated on laminin-coated transwells (Sigma Aldrich Plc. UK) and 48 h prior to adhesion/migration assay and grown at 37°C in 10 % CO_2 humidity in Dulbecco's modified Eagles medium (DMEM + 10 % fetal bovine serum; 100 U/L penicillin; 100 mg/L streptomycin; 2nM glutamine) before assay according to Rohnelt *et al.* 1997. 1 x 10^6 activated and expanded lymphocytes (as previously described) were put in contact with bEND5 endothelial cells for 4 hours at 37 °C. After 4 hours cells were isolated from bottom compartment and adhered cells detached from bEND5 cell mono-layer with trypsin.

4.2.6. Membrane and intracellular FACS staining

Isolated lymphocytes were fixed at room temperature for 10 min with 2 % PFA in FACS buffer (PBS + 0.2 % BSA + 0.2 % sodium azide) for intracellular markers cells were permeabilised with permeabilsation buffer for 30 min at 37 °C (BD Biosciences, UK) and were then stained with intracellular markers (FoxP3 and RORγt), and for surface markers (CD4, CD8, CD25) with fluorescently conjugated primary antibodies (1:100 or 1:200, eBioscience/BioLegend) at room temperature for 60 min in FACS buffer. All samples were then assessed by flow cytometry using a LSRFortessa II (BD Biosciences) and analysed using FlowJo.

4.2.7. Statistical analysis

All data in the text and figures are presented as mean ± SEM of n observations, where n represents the number of animals studied. All statistical analysis was calculated using GraphPad Prism 6 (GraphPad Software, San Diego, California, USA). Data without a repeated measurement was assessed by a one-way ANOVA or students t-test were appropriate. OGTT testing analysis was preformed using area under ROC-curve. A P-value of less than 0.05 was considered to be statistically significant.

4.3. Results

4.3.1. The effect of hrANXA1 administration and the role of endogenous ANXA1 on BBB permeability in mice fed a HFD.

Previous reports by Cristante *et al*. have shown that ANXA1$^{-/-}$ mice have enhanced BBB permeability under physiological conditions compared to WT littermates. I*n vivo*, BBB permeability was assessed in both WT and ANXA1$^{-/-}$ mice. Chow fed ANXA1$^{-/-}$ mice injected with Evan's blue dye (i.v.) had a significantly greater dye content in the brain when measured by spectrophotometric analysis compared to WT mice, confirming that AXNA1$^{-/-}$ mice have greater BBB leakage. When compared to WT mice fed a chow diet, WT mice fed a HFD had more Evan's blue dye in the brain, which could be reversed with treatment with hrANXA1.

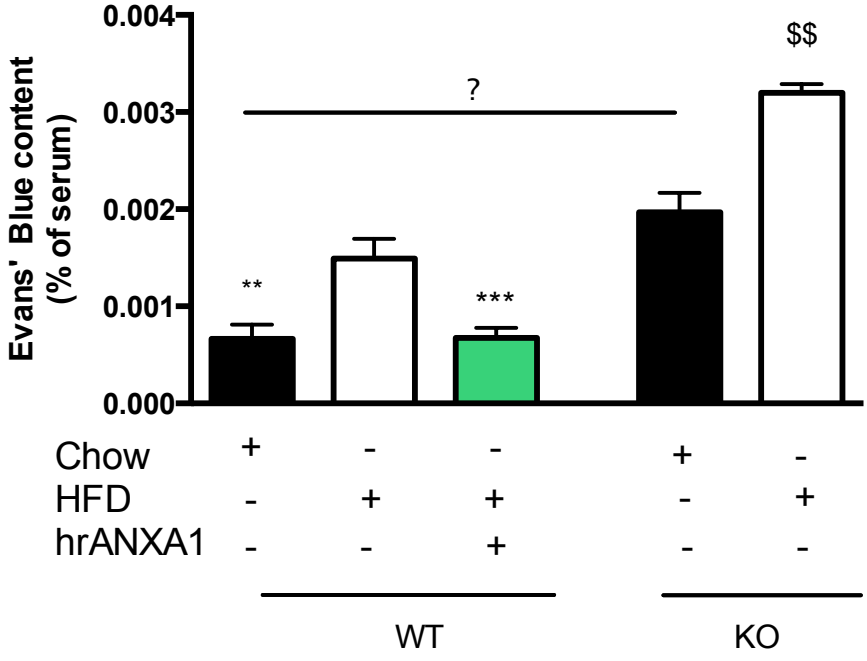

Figure 4.1. Effect of hrANXA1 administration and the role of endogenous ANXA1 on BBB permeability.

Effects of chronic exposure to a normal diet (chow) or a high-fat high-sugar diet (HFD) on paracellular permeability assessed by Evan's blue leakage into the brain after 10 weeks of dietary manipulation. Experimental groups: WT or ANXA1$^{-/-}$ mice treated fed on normal diet (chow) or high-fat-high-sugar (HFD) with or without hrANXA1. Data analysed by a one-way ANOVA followed by a Bonferroni *post-hoc* test, and expressed as mean±SEM. n= 6 per group.

4.3.2. The role of endogenous ANXA1 on specific $CD4^+$ lymphocyte populations from mice fed a HFD.

Previous reports have shown that ANXA1 plays a central role in the differentiation of lymphocytes. Here we investigate the role endogenous ANXA1 on T-cell subsets in HFD-fed mice isolated from the draining lymph nodes. When compared to chow-fed WT mice, chow-fed $ANXA1^{-/-}$ mice have more $CD4^+$ cells (Figure 4.2A). Subsets of $CD4^+$ T-cell preform different biological functions. When compared to chow-fed WT mice, chow-fed $ANXA1^{-/-}$ mice have a significantly larger population of $CD4^+0$ (Figure 4.2B, $P<0.05$), while the number of $CD4^+FoxP3^+$ T-cells remains unchanged (Figure 4.2C, $P<0.05$). When compared to chow-fed WT mice, HFD-fed WT mice have a significantly smaller population of $CD4^+FoxP3^+$ T-cells, while the population of $CD4^+ROR\gamma t^+$ T-cells remains unchanged. Similarly, when compared to chow-fed $ANXA1^{-/-}$ mice, HFD-fed $ANXA1^{-/-}$ mice have a significantly smaller population of $CD4^+FoxP3^+$ T-cells, while the population $CD4^+ROR\gamma t^+$ T-cells remains unchanged.

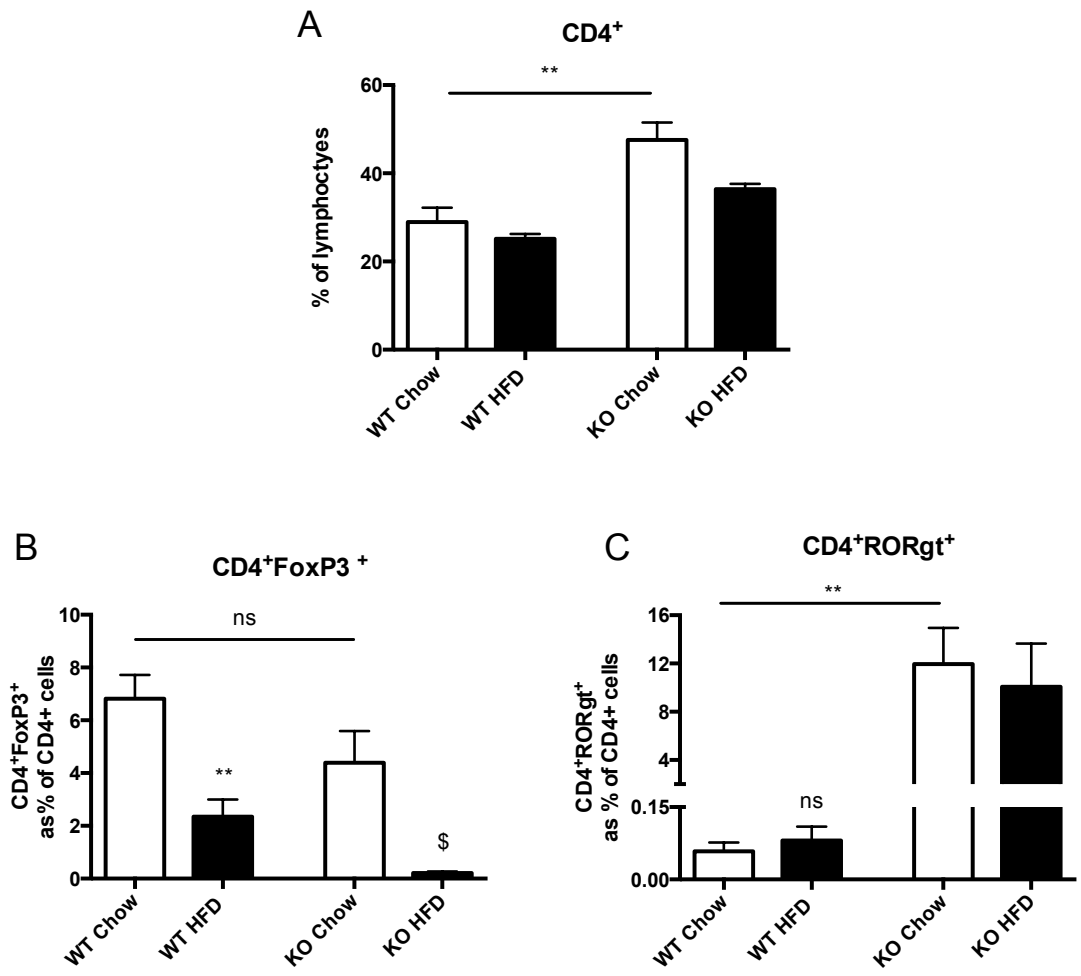

Figure 4.2. The role of endogenous ANXA1 on specific CD4+ lymphocyte populations.
Effects of chronic exposure to a normal diet (chow) or a high-fat high-sugar diet (HFD) on specific CD4+ lymphocytes after 10 weeks of dietary manipulation. $CD4^+$ cells (A), $CD4^+FoxP3^+$ cells as a % of $CD4^+$ cells (B) and $CD4^+RORgt^+$ cells (C) as a % of $CD4^+$ cells. Experimental groups: WT or $ANXA1^{-/-}$ mice treated fed on normal diet (chow) or high-fat-high-sugar (HFD). Data analysed by a one-way ANOVA followed by a Bonferroni *post-hoc* test, and expressed as mean ± SEM. n= 6-8 per group.

4.3.3. The role of endogenous ANXA1 on the ratio of $CD4^+FoxP3^+$ to $CD4^+ROR\gamma t^+$ lymphocytes from mice fed a HFD.

T-cells were isolated from draining lymph nodes and specific CD4+ T-cells populations quantified. The ratio of specific subsets of $CD4^+$ T-cell; TReg ($CD4^+FoxP3^+$) to Th17 ($CD4^+ROR\gamma t^+$) was calculated. When compared to chow-fed WT mice, chow-fed $ANXA1^{-/-}$ mice have a lower $CD4^+FoxP3^+$ to $CD4^+ROR\gamma t^+$ T-cell ratio (Figure 4.3, $P<0.001$). Likewise, when compared to chow-fed WT mice, HFD-fed WT mice have a lower $CD4^+FoxP3^+$ to $CD4^+ROR\gamma t^+$ T-cell ratio (Figure 4,2,$P<0.01$). Similarly, when compared to chow-fed $ANXA1^{-/-}$ mice, HFD-fed $ANXA1^{-/-}$ mice have a lower $CD4^+FoxP3^+$ to $CD4^+ROR\gamma t^+$ T-cell ratio, but this does not reach statistical significance (Figure 4.3, ns). Collectively, these results suggesting that both feeding a HFD and ANXA1 depletion ($ANXA1^{-/-}$ mice) lowers the number of TReg cells compared to Th17.

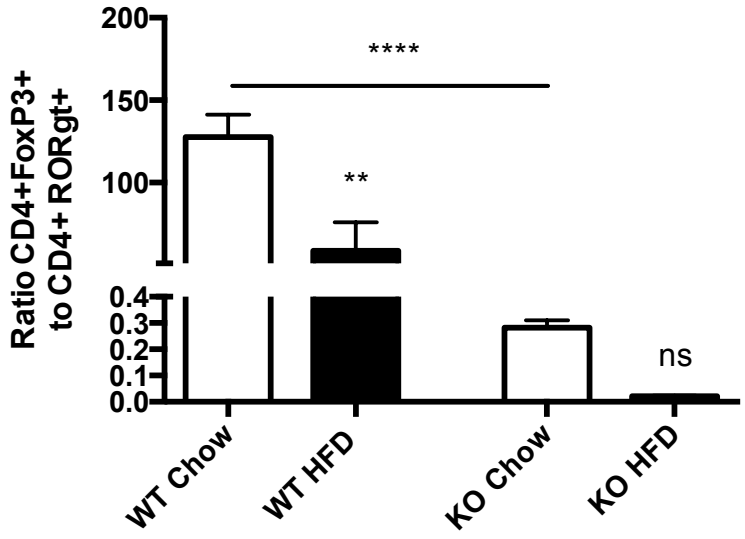

Figure 4.3. The role of endogenous ANXA1 on the ratio of $CD4^+FoxP3^+$ to $CD4^+ROR\gamma t^+$ lymphocytes from mice fed a HFD.

The effects of chronic exposure to a normal diet (chow) or a high-fat high-sugar diet (HFD) on the ratio of $CD4^+FoxP3^+$ to $CD4^+ROR\gamma t^+$ lymphocytes after 10 weeks of dietary manipulation. Experimental groups: WT or $ANXA1^{-/-}$ mice treated fed on normal diet (chow) or high-fat-high-sugar (HFD). Data analysed by a one-way ANOVA followed by a Bonferroni *post-hoc* test, and expressed as mean ± SEM. n= 6 per group.

4.3.4. The effect of treatment with hrANXA1 on specific $CD4^+$ lymphocyte populations in mice fed a HFD.

T-cells from mice fed a HFD and treated with hrANXA1 were isolated from draining lymph nodes and specific CD4+ T-cells populations quantified. Overall the $CD4^+$ population of T-cells was not altered by feeding of a HFD (Figure 4.4A, ns) or by treating HFD-fed mice with hrANXA1 (Figure 4.4A, ns). Similarly, the $CD4^+CD25^+$ and $CD4^+CD25^-$ T-cells populations were not altered by feeding in a HFD (Figure 4.4B/C) or by treating HFD-fed mice with hrANXA1 (Figure 4.4B/C). However, when compared to mice fed a chow diet, mice HFD-fed mice have a decreased population of CD^+FoxP3^+ T-cells (Figure 4.4D, $P<0.05$) and increased population of $CD4^+RORgt^+$ T-cells (Figure 4.4E, $P<0.01$), which was attenuated by hrANXA1

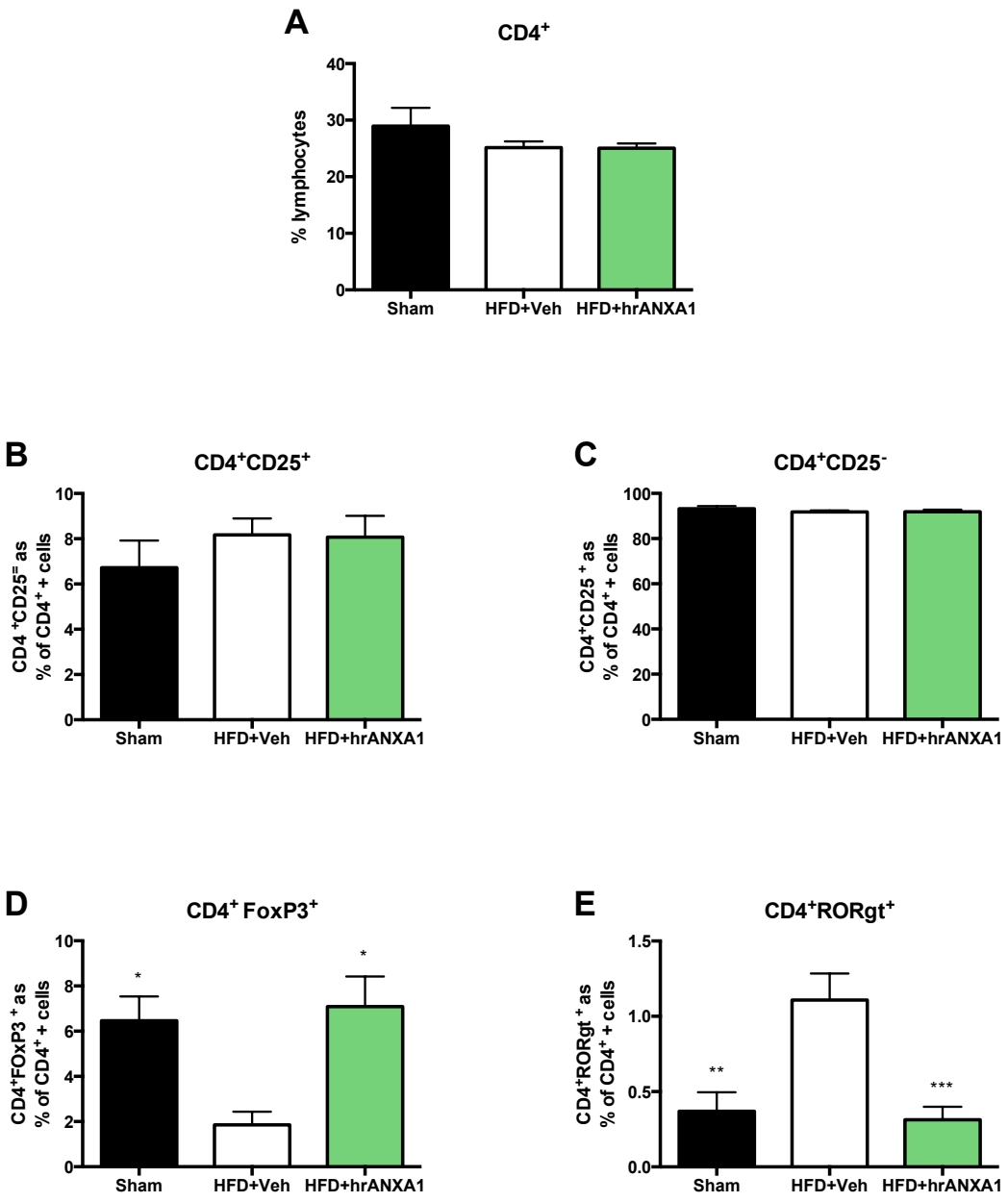

Figure 4.4. The effect of treatment with hrANXA1 on specific CD4⁺ lymphocyte populations in mice fed a HFD.

Effects of chronic exposure to a normal diet (chow) or a high-fat high-sugar diet (HFD) on specific $CD4^+$ lymphocyte populations after 10 weeks of dietary manipulation. $CD4^+$ cells (A), $CD4^+CD25^+$ (B) $CD4^+CD25^-$ cells (C) $CD4^+ROR\gamma t^+$ cells (D) and $CD4^+FoxP3^+$ cells (E) as a % of $CD4^+$ cells. Experimental groups: WT or $ANXA1^{-/-}$ mice treated fed on normal diet (chow) or high-fat-high-sugar (HFD) with or without hrANXA1. Data analysed by a one-way ANOVA followed by a Bonferroni *post-hoc* test, and expressed as mean ± SEM. n= 6 per group.

4.3.5. The effect of treatment with hrANXA1 on the ratio of $CD4^+FoxP3^+$ to $CD4^+ROR\gamma t^+$ lymphocytes from mice fed a HFD.

We next compared the ratio of TReg ($CD4^+FoxP3^+$) to Th17 ($CD4^+ROR\gamma t^+$) subsets of CD4+ T-cells. When compared to chow-fed mice, HFD-fed mice have a lower $CD4^+FoxP3^+$ to $CD4^+ROR\gamma t^+$ T-cell ratio (Figure 4.5, $P<0.05$), which could be attenuated by treating HFD-fed with hrANXA1 (Figure 4.5, $P<0.05$).

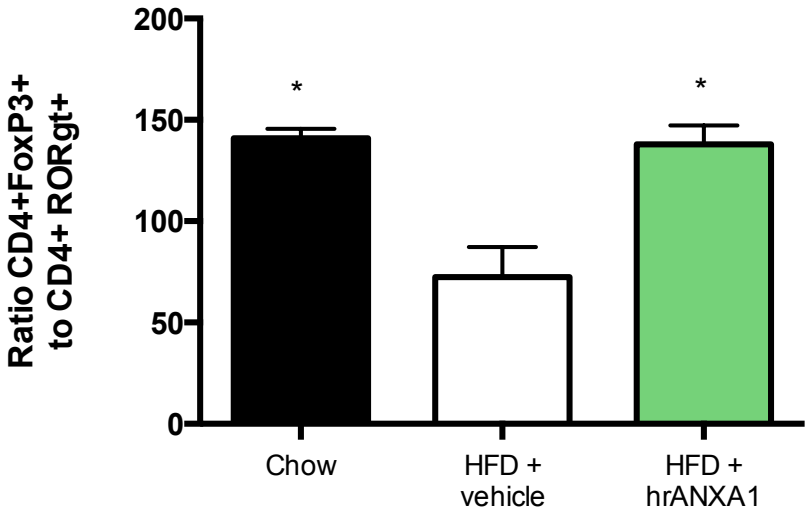

Figure 4.5. The effect of treatment with hrANXA1 on the ratio of $CD4^+FoxP3^+$ to $CD4^+ROR\gamma t^+$ lymphocytes from mice fed a HFD.

The effects of chronic exposure to a normal diet (chow) or a high-fat high-sugar diet (HFD) on the ratio of $CD4^+FoxP3^+$ to $CD4^+ROR\gamma t^+$ lymphocytes after 10 weeks of dietary manipulation. Experimental groups: WT or $ANXA1^{-/-}$ mice treated fed on normal diet (chow) or high-fat-high-sugar (HFD) with or without hrANXA1. Data analysed by a one-way ANOVA followed by a Bonferroni *post-hoc* test, and expressed as mean ± SEM. n= 6 per group.

4.3.6. The effect of treatment with hrANXA1 on lymphocytes ability to adhere and transmigrate through an endothelial monolayer *ex vivo*.

Using an *ex vivo* model of paracellular permeability we assessed the ability of activated lymphocytes to firstly adhere to and then migrate through a monolayer of brain derived endothelial cells. When compared to lymphocytes from chow-fed mice, lymphocytes isolated from HFD-fed mice and put in contact with a endothelial monolayer demonstrated an increased number of lymphocytes adhered to the endothelial cell monolayer (Figure 4.6, $P<0.001$) and also an increased number of transmigrated lymphocytes through the endothelial cell monolayer (Figure 4.5, $P<0.01$) after 4 h of incubation. When compared to lymphocytes isolated from mice from HFD-fed mice, lymphocytes from HFD-fed mice that were treated with hrANXA1 had less lymphocytes adhered to the endothelial cell monolayer (Figure 4.6, $P<0.01$) but did was not difference in the number that transmigrated through the endothelial cell monolayer (Figure 4.6, ns).

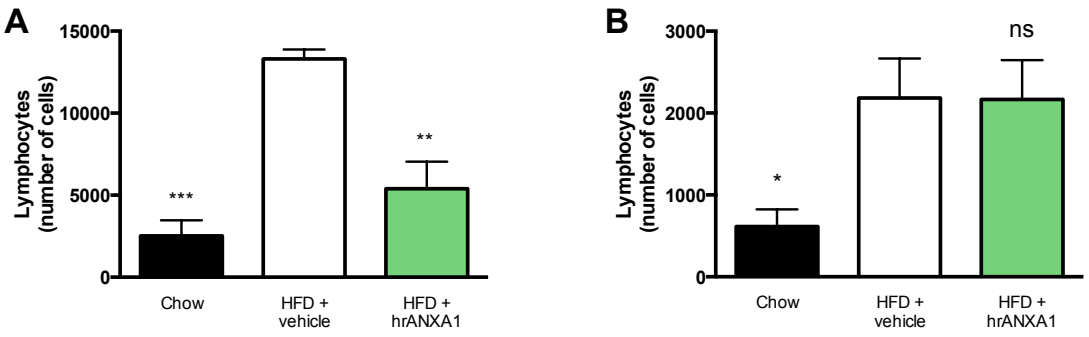

Figure 4.6. The effect of treatment with hrANXA1 on lymphocytes ability to adhere and transmigrate through an endothelial monolayer *ex vivo*.

Effects of chronic exposure to a normal diet (chow) or a high-fat high-sugar diet (HFD) on lymphocytes ability to adhere (A) and transmigrate (B) through an endothelial monolayer. Experimental groups: WT or ANXA1$^{-/-}$ mice treated fed on normal diet (chow) or high-fat-high-sugar (HFD) with or without hrANXA1. Data analysed by a one-way ANOVA followed by a Bonferroni *post-hoc* test, and expressed as mean ± SEM. n= 6 per group.

4.3.7. The effect of treatment with hrANXA1 on specific $CD4^+$ lymphocyte populations in mice fed a HFD that adhere to a brain endothelial monolayer *ex vivo*.

Quantification of specific $CD4^+$ T-cells populations was carried out in cells that were adhered to the brain endothelial monolayer after 4 h of incubation. When compared to lymphocytes isolated chow-fed mice, lymphocytes isolated from HFD-fed mice and put in contact with endothelial monolayer had a larger $CD4^+$ population of adhered lymphocytes (Figure 4.7A, $P<0.001$), which was attenuated by hrAXNA1. (Figure 4.7A, $P<0.01$).

When compared to lymphocytes isolated from chow-fed mice, lymphocytes isolated from HFD-fed mice and put in contact with endothelial monolayer had a increased $CD4^+CD25^+$ (Figure 4.7B, $P<0.05$) and decreased $CD4^+CD25^-$ T-cell populations (Figure 4.7C, $P<0.05$), which was attenuated by hrAXNA1.

When compared to lymphocytes isolated chow-fed mice, lymphocytes isolated from HFD-fed mice and out in contact with endothelial monolayer had an increased $CD4^+FoxP3^+$ (Figure 4.7D, $P<0.05$) and $CD4^+ROR\gamma t^+$ (Figure 4.7E, $P<0.05$) T-cell populations of adhered lymphocytes, which was attenuated by hrAXNA1.

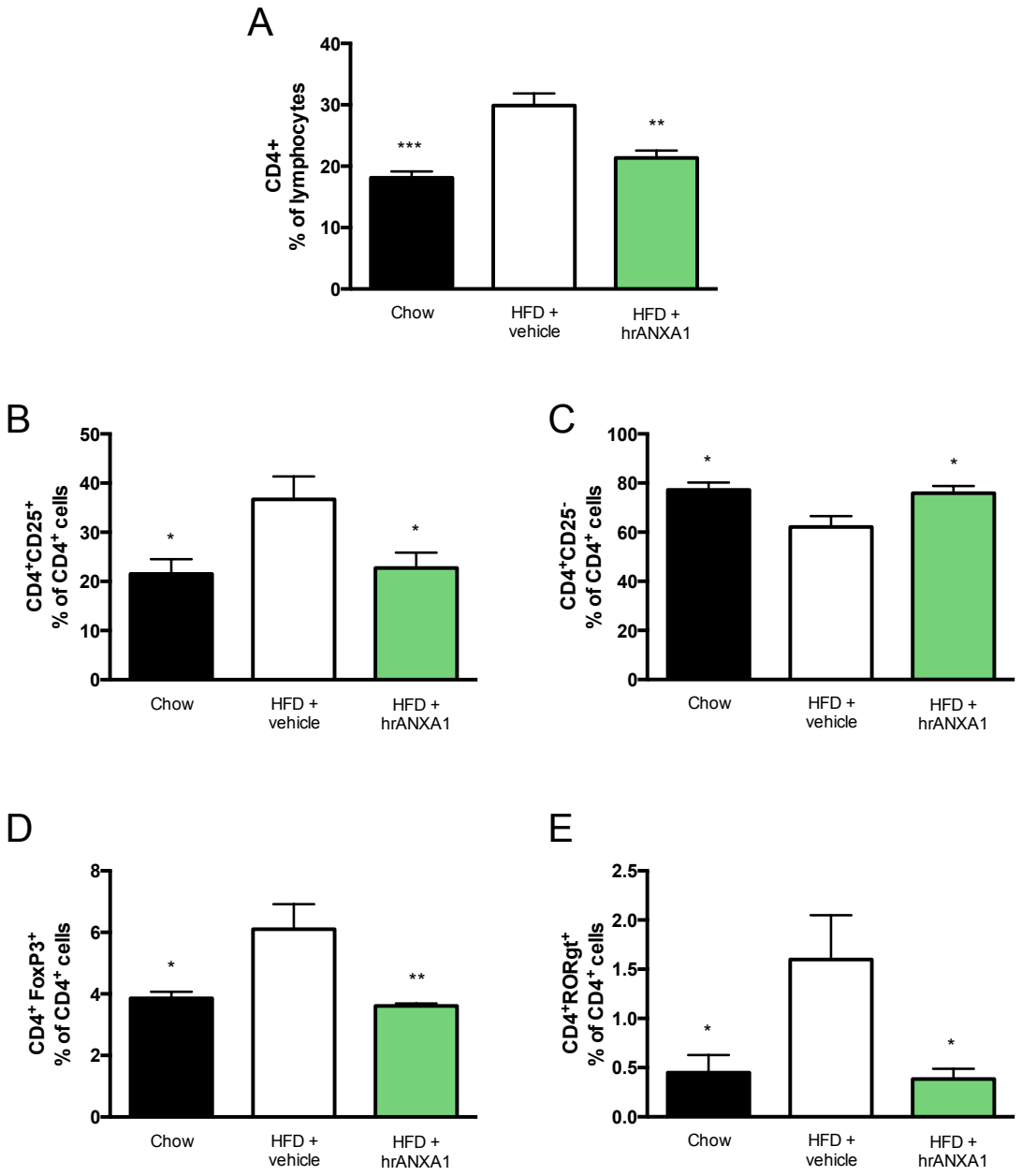

Figure 4.7. The effect of treatment with hrANXA1 on specific CD4⁺ lymphocyte populations in mice fed a HFD that adhere to a brain endothelial monolayer *ex vivo*.

Effects of chronic exposure to a normal diet (chow) or a high-fat high-sugar diet (HFD) on specific $CD4^+$ lymphocyte populations ability to adhere to a brain endothelial monolayer. $CD4^+$ cells (A), $CD4^+CD25^-$ (B) $CD4^+CD25^+$ cells (C) $CD4^+FoxP3^+$ cells (D) $CD4^+ROR\gamma t^+$ cells and (E) as a % of $CD4^+$ cells. Experimental groups: WT or $ANXA1^{-/-}$ mice treated fed on normal diet (chow) or high-fat-high-sugar (HFD) with or without hrANXA1. Data analysed by a one-way ANOVA followed by a Bonferroni *post-hoc* test, and expressed as mean ± SEM. n= 6 per group.

4.3.8. The effect of treatment with hrANXA1 on specific $CD4^+$ lymphocyte populations in mice fed a HFD that transmigrate through a brain endothelial monolayer *ex vivo*.

Quantification of specific $CD4^+$ T-cells populations was carried out in lymphocytes that transmigrated through the brain endothelial monolayer after a 4 h incubation. When compared to lymphocytes isolated chow-fed mice, lymphocytes isolated from HFD-fed mice and put in contact with an endothelial monolayer had an increased $CD4^+$ population of transmigrated lymphocytes (Figure 4.8A, $P<0.05$). When compared to lymphocytes isolated from HFD-fed mice, lymphocytes isolated from HFD-fed mice and treated with hrANXA1 did not prevent the increase in $CD4^+$ cells that transmigrated through the brain endothelial monolayer (Figure 4.8A, ns).

When compared to lymphocytes isolated from chow-fed mice, lymphocytes isolated from HFD-fed mice and put in contact with an endothelial monolayer had a increased $CD4^+CD25^+$ (Figure 4.8B, $P<0.05$) and decreased $CD4^+CD25^-$ (Figure 4.8C, $P<0.05$) T-cell populations of transmigrated lymphocytes. When compared to lymphocytes isolated from HFD-fed mice, lymphocytes isolated from HFD-fed mice and treated with hrANXA1 did not alter the population of $CD4^+CD25^+$ (Figure 4.8B, ns) and $CD4^+CD25^-$, (Figure 4.8C, ns) T-cell populations that transmigrated through the brain endothelial monolayer.

When compared to lymphocytes isolated chow-fed mice, lymphocytes isolated from HFD-fed mice and out in contact with endothelial monolayer had an

increased $CD4^+FoxP3^+$ (Figure 4.8D, $P<0.5$) and $CD4^+ROR\gamma t^+$ (Figure 4.8E, $P<0.05$) T-cell populations of transmigrated lymphocytes. When compared to lymphocytes isolated chow-fed mice, lymphocytes isolated from HFD-fed mice and treated with hrANXA1 attenuated the increases in both $CD4^+FoxP3^+$ (Figure 4.8D, $P<0.05$) and $CD4^+ROR\gamma t^+$ (Figure 4.8E, $P<0.01$) ability to transmigrated through the brain endothelial monolayer,

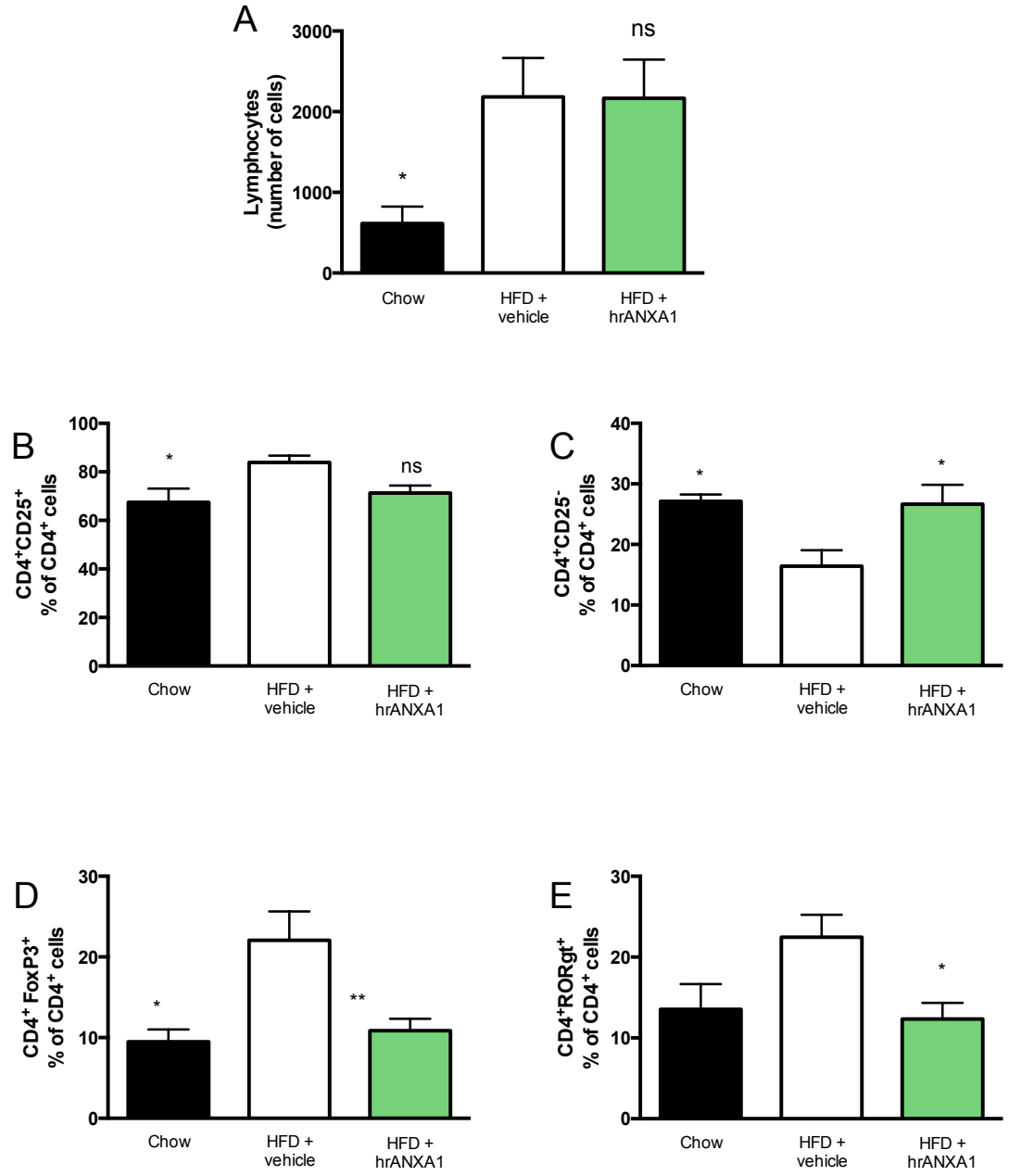

Figure 4.8. The effect of treatment with hrANXA1 on specific CD4⁺ lymphocyte populations in mice fed a HFD that transmigrate through a brain endothelial monolayer *ex vivo*.

Effects of chronic exposure to a normal diet (chow) or a high-fat high-sugar diet (HFD) on specific CD4⁺ lymphocyte populations after 10 weeks of dietary manipulation. Experimental groups: WT or ANXA1$^{-/-}$ mice treated fed on normal diet (chow) or high-fat-high-sugar (HFD) with or without hrANXA1. Data analysed by a one-way ANOVA followed by a Bonferroni *post-hoc* test, and expressed as mean ± SEM. n= 6 per group.

4.3.9. The effect of treatment with hrANXA1 on the ratio of $CD4^+FoxP3^+$ to $CD4^+RORgt^+$ lymphocytes from mice fed a HFD that adhere to and transmigrate through a brain endothelial monolayer *ex vivo*.

We next compared the ratio of TReg ($CD4^+FoxP3^+$) to Th17 ($CD4^+ROR\gamma t^+$) subsets of CD4+ T-cells that adhered to a monolayer of brain endothelial cells after 4 h of incubation. When compared to lymphocytes isolated to from chow-fed mice, lymphocytes isolated from HFD-fed mice had a decrease in the ratio $CD4^+ROR\gamma t^+$: $CD4^+FoxP3^+$ T-cells that adhered to the brain endothelial monolayer (Figure 4.9A, $P<0.01$). When compared to lymphocytes isolated to from HFD-fed mice, lymphocytes isolated from HFD-fed mice and treated with hrANXA1 attenuated the decrease in the ratio of $CD4^+ROR\gamma t^+$: $CD4^+FoxP3^+$ T-cells that adhered to the brain endothelial monolayer (Figure 4.9A, $P<0.05$).

When compared to lymphocytes isolated to from chow-fed mice, lymphocytes isolated from HFD-fed mice had an increase in the ratio of $CD4^+ROR\gamma t^+$: $CD4^+FoxP3^+$ T-cells that transmigrated through the brain endothelial monolayer (Figure 4.9B, $P<0.05$). When compared to lymphocytes isolated to from HFD-fed mice, lymphocytes isolated from HFD-fed mice and treated with hrANXA1 attenuated the increase in the ratio of $CD4^+ROR\gamma t^+$: $CD4^+FoxP3^+$ T-cells that transmigrated through the brain endothelial monolayer (Figure 4.9B, $P<0.01$).

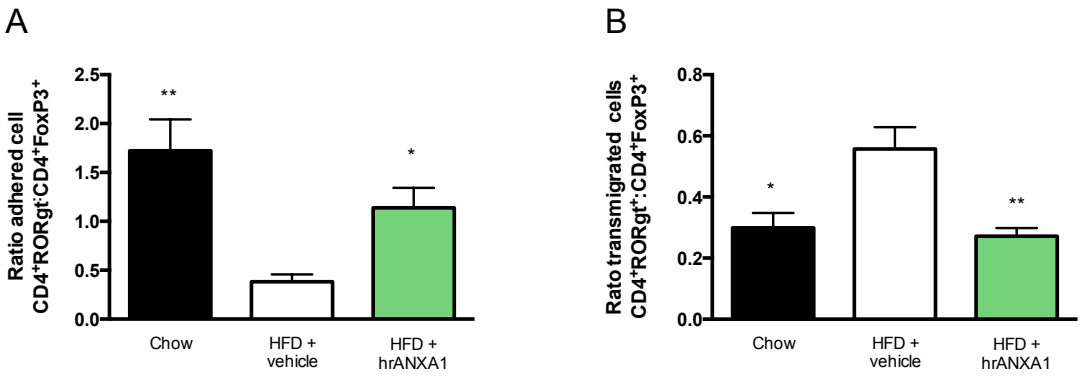

Figure 4.9. The effect of treatment with hrANXA1 on the ratio of $CD4^+ROR\gamma t^+$ to $CD4^+FoxP3^+$ lymphocytes from mice fed a HFD that adhere to and transmigrate through a brain endothelial monolayer *ex vivo*.

Effects of chronic exposure to a normal diet (chow) or a high-fat high-sugar diet (HFD) on the ratio of $CD4^+CD25^-$ to $CD4^+CD25^+$ (A/B) and $CD4^+FoxP3^+$ to $CD4^+ROR\gamma t^+$ (C/D) that had adhered to (A/C) or transmigrated through (C/D) a brain endothelial monolayer. Experimental groups: WT or $ANXA1^{-/-}$ mice treated fed on normal diet (chow) or high-fat-high-sugar (HFD) with or without hrANXA1. Data analysed by a one-way ANOVA followed by a Bonferroni *post-hoc* test, and expressed as mean ± SEM. n= 6 per group.

4.4 Discussion

ANXA1 mediates a broad range of effects within the immune system (Perretti & D'Acquisto 2009) and is known to play a key role in the regulation of BBB permeability (Cristante et al. 2013). The main findings of this chapter are that (i) mice fed a HFD have a more permeable BBB, and the degree of permeability is further augmented in ANXA1$^{-/-}$ mice fed a HFD; while treatment with hrANXA1 attenuates the increase in BBB permeability caused by HFD; (ii) ANXA1$^{-/-}$ mice have an altered T-cell profile characterised by an increase in CD4^{+}RORγt^{+} T-cells; (iii) WT mice fed a HFD have a decreased population of FoxP3^{+}CD4^{+} cells and an increased population of RORγt^{+} T-cells, which was attenuated by treatment with hrANXA1; (iv) lymphocytes from mice fed a HFD had increased ability to adhere to and transmigrate through a bEND5 endothelial monolayer *ex vivo,* while treatment with hrANXA1 reduced lymphocyte ability to adhere, but not to transmigrate through a bEND5 endothelial monolayer *ex vivo*; and (v) lymphocytes from mice fed a HFD have elevated number of both FoxP3^{+} and RORγt^{+} T-cells that adhered to and transmigrated through a bEND5 endothelial monolayer *ex vivo,* which was attenuated by hrANXA1.

BBB tightness is highly regulated. One of the main components responsible for its extreme tightness are tight junction. Disruption of BBB integrity has been implicated in many neurological conditions such as multiple sclerosis, Alzheimer's disease, cognitive decline and aging. Recently, there have been controversial reports about the effect of diabetes on BBB integrity, but the general consensus is that there is a loss of BBB integrity in diabetes (Hawkins et

al., 2006)(Acharya et al., 2013)(Starr et al., 2003)(Huber et al., 2006). Indeed the data presented in this chapter confirms that there is increased leakage of Evan's blue dye in to the brains of WT-mice fed a HFD. Additionally, our data also confirms that BBB permeability is significantly increased in chow-fed ANXA1$^{-/-}$ mice compared to WT littermate fed a chow diet. Most notably, when ANXA1$^{-/-}$ mice are fed a HFD, there is a significant increase in BBB permeability compared to chow-fed ANXA1$^{-/-}$ mice. This key finding indicates that endogenous ANXA1 plays a pivotal role in the regulation of BBB integrity. Previously, Cristante *et al*. demonstrated that this increase in permeability in ANXA1$^{-/-}$ mice could be reserved by treatment with hrAXNA1 24 h prior to Evan's Blue injection. In agreement with this finding when HFD-fed WT mice were given chronic treatment (weeks 5-10) with hrANXA1 BBB permeability was reduced compared to HFD-fed WT mice treated with vehicle. The data presented here adds evidence to the hypothesis that ANXA1 given exogenously can be used to increase and/or restore BBB integrity.

Endogenous ANXA1 stabilises tight junctions, which is critical to ensuring the tightness of the endothelial of the BBB. Critical to this process is the ability of ANXA1 to regulate cellular polarity and consequently the formation of tight and adhesion junction (Cristante et al., 2013). ANXA1 interacts with cytosolic, rather than fibular actin; binding predominantly to soluble G-actin (Cristante et al., 2013). Additionally, activation of the small GTPase RhoA is known to initiate a signaling pathway resulting in the destabilisation of the actin cytoskeleton, ultimately enhancing paracellular permeability (Terry et al., 2010). Central to these actions is the ability ANXA1's to signal in both an autocrine and paracrine

manner via FPR2 to inhibit the small GTPase RhoA (Perretti & D'Acquisto, 2009) (Cristante et al., 2013). I have shown in chapter III that the GTPase RhoA is constitutively activated in ANXA1$^{-/-}$ mice and that feeding mice a HFD leads to a further increase in RhoA activation. This data suggests that activation of RhoA is the mechanism by which the initial leakage of the BBB is caused and the mechanism by which treatment with hrAXNA1 restored BBB integrity. Suggesting that a type-2 diabetic phenotype (elevated blood glucose leading to shedding of intracellular ANXA1) could cause activation of RhoA allowing for actin rearrangements and ultimately de-stabilising tight junctions and causing increased BBB permeability.

One consequence of having a more permeable BBB is that molecules and cells that should be blocked from migrating into the brain parenchyma penetrate in. Here I investigated whether mice fed a HFD have altered peripheral T-cell populations and whether these lymphocytes would have an increased ability to penetrate through an endothelial monolayer. Specifically, I have used flow cytometry to identify specific populations of CD4^{+} T-cells isolated from lymph nodes from mice fed a HFD. Both Th17 and TReg cells express specific transcription factors that can be used to identify them as specific populations. Th17 expresses the unique transcription factor RORγt, while TReg cells express FoxP3 in high quantities.

I clearly demonstrate that chow-fed ANXA1$^{-/-}$ mice have an increased Th17 (CD4^{+}RORγt^{+}) T-cell population compared to chow-fed WT-mice, suggesting a

role for endogenous ANXA1, in the regulation of both expansion and differentiation of Th17 T-cells. Our data is consistent with Yang *et al.* who previously shown that PBMC's from ANXA1$^{-/-}$ mice have increased mRNA for the transcriptional factor RORγt and IL-17 (Yang et al., 2013), suggesting they have an increased Th17 population. I demonstrate that in mice fed a HFD there is no overall change in CD4^{+} T-cell lymphocyte number or in general regulatory T-cells (CD4^{+}CD25^{+}), however, there is a specific change in the number of terminally differentiated populations; specifically a decrease in TReg (CD4^{+}FoxP3^{+}) and subsequent increase in Th17 (CD4+RORγt) T-cell populations. I propose that as cellular levels of ANXA1 are decreased in T2DM, the lack of ANXA1 allowed for a class-switching event from TReg to Th17, or allowed the expansion of the Th17 population (Figure 4.10A/B). Moreover, when hrANXA1 was given exogenously, the the class-switching phenomenon, or expansion of the Th17 population was blocked and restore T-cell population size to those seen in WT-mice fed on a chow diet (Figure 4.10C). Previous *ex vivo* studies using isolate CD4^{+} T-cells and *in vivo* studies in mice have shown that glucocorticoids promote a Th2 cells response, however, here we show that endogenous ANXA1 limits the expansion of the Th17 population, while therapeutic administration of hrANXA1 to HFD prevents the expansion of Th17 cells, and promotes maintenance of the TReg population.

ANXA1 is a well-known mediator of glucocorticoid action. Most of the work regarding ANXA1 biology has predominantly been carried out in polymorphonuclear leukocytes, as these are the cell type that expresses most ANXA1. Here I show that lymphocytes from mice fed a HFD exhibit increased

adhesion to and migration through a brain endothelial monolayer compared to mice fed a chow diet, suggesting that these lymphocytes are in a more activated state. Hyperglycaemia is a well characterised activator of immune cells; after activation lymphocytes up-regulate adhesion molecules, which allow them to adhere more readily, and to roll and transmigrate through the endothelium (Morigi et al., 1998). These results demonstrate a lymphocyte specific change, as the endothelial monolayer is grown in basic medium, suggesting that the increased ability to migrate in intrinsic to changes in the lymphocytes due to exposure to high glucose/high lipids *in vivo*.

After glucocorticoid stimulation or cellular activation, ANXA1 is released form its cellular store where is inhibits leukocyte to bind to endothelium. Here we demonstrate that treatment with exogenous hrANXA1 plays a role in the adhesion, but not in the migration of the total population of lymphocytes through the brain endothelial monolayer (Figure 4.6). Interestingly, real-time *in vivo* analysis of activated PBMNC's in cremaster muscle microcirculation of ANXA1$^{-/-}$ mice demonstrated a subtle yet significant increase in leukocyte emigration, but not rolling or adhesion (Chatterjee et al., 2005), these results suggest that endogenous ANXA1 may block the process of migration in the cremaster muscle microcirculation. The results represents a subtle difference in the role of endogenous ANXA1 compared to therapeutic administration of ANXA1 or its N-terminal fragments. Here we show that exogenously given hrANXA1 inhibits the first step in extravasation, while endogenous ANXA1 inhibits transmigration at least on the total population of lymphocytes. The next curious finding is I looked at the ability of terminally differentiated CD4^{+} T-cells to adhere to and

transmigrate through a brain endothelium monolayer I found that Th17 and TReg cells from mice fed a HFD's have an increased ability to adhere to and transmigrate through a brain endothelial monolayer. One interesting finding is that treatment with hrANXA1 decreased Th17 and TReg T-cells from both adhering to and migrating through a brain endothelial monolayer. This result represents a distinct difference to that seen in the whole population of $CD4^+$ lymphocytes where treatment with hrANXA1 inhibited only adhesion.

ANXA1 is known to interact and block the binding site of the $\alpha_4\beta_1$ integrin VLA_4 in leukocytes. This integrin is elevated in monocytes, leukocytes and lymphocytes from diabetic patients (Stulc et al., 2012)(Noda et al., 2012). VLA_4 as has also been implicated in diseases such as multiple sclerosis, were immune cells infiltration in to the brain is a key driver of disease progression. VLA_4 is one of the essential integrins by which T-cells gain access to the brain, and is a current therapeutic target. The aim is to block VLA_4 resulting in reduced T-cells infiltrating into the brain from the peripheral system. ANXA1 has been shown to directly block the $\alpha_4\beta_1$ subunit of VLA_4 effectively blocking leukocytes ability to adhere to the endothelium (Solito et al., 2000). Here I speculate that a similar mechanism could be involved in the inhibition of lymphocyte adhesion and migration through the endothelium of the BBB. Three lines of thought support this hypothesis, (i) only activated lymphocytes express VLA_4; (ii) hrANXA1 has been shown to bind to the $\alpha_4\beta_1$ of integrin VLA_4, and (iii) we show that hrANXA1 blocks adhesion and migration in terminally differentiated activated Th17 and TReg cells.

Indeed little work has been has been conducted on the cross talk between the infiltrating cells and the resident cells (neurons, microglia, astrocytes and oligodendrocytes). However, there is an emerging bulk of literature that points towards an increase in central inflammation and cognitive decline (Cunningham & Hennessy 2015), indeed there is also strong evidence of cognitive decline in patients with obesity and/or diabetes (Cunningham & Hennessy 2015)(Nguyen et al., 2014)(Kodl & Seaquist, 2008)(Bruce et al., 2003). Specifically, it will be very important to understand how different subsets of T-cells interact with different cell types in the brain parenchyma, and if these drive different phenotypic effects. The results presented in the chapter demonstrate that therapeutically treatment with hrNXA1 is a double-edged sword, not only does it restore BBB tightness and integrity, but it inhibits T-cells ability to adhere, and transmigrate through the BBB into the brain, in murine model of T2DM.

The results presented in this chapter suggest a central role for ANXA1 in both BBB functionality and lymphocyte extravasation through the BBB for these specific reasons; (i) *in vivo*, ANXA1$^{-/-}$ mice have a more permeable BBB, (ii) feeding mice a HFD increases BBB permeability, while treatment with hrAXNA1 restores BBB tightness; (iii) diabetes enhances lymphocytes ability to adhere to and transmigrate through a brain endothelial mono-layer; (iv) treatment with hrANXA1 inhibited lymphocyte ability to adhere to the brain endothelial mono-layer the first critical step in extravasation.

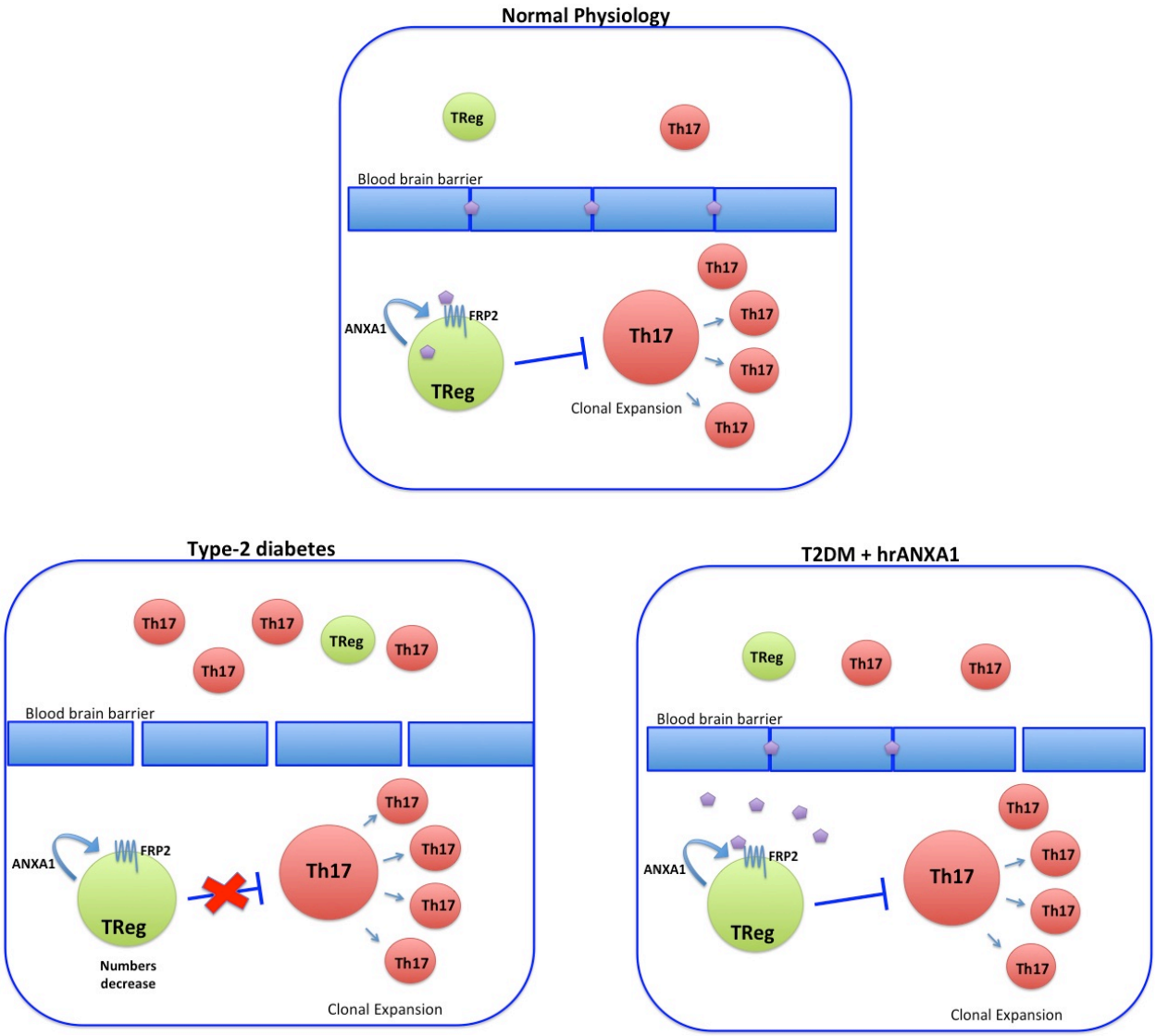

Figure 4.10. Schematic showing the central role of ANXA1 in linking peripheral inflammation and the BBB integrity.

(A) Under normal physiological conditions intracellular AXNXA1 signaling within TReg cells with the cell surface receptor FPR2. This signaling allows TReg cells to inhibit the clonal expansion of Th17 cells. Additionally, ANXA1 in endothelial cells inhibits RhoA activity allowing for the formation of stable tight junctions and BBB integrity to be maintained. (B) Under diabetic conditions, intracellular ANXA1 levels decrease in TReg cells, and there is no signaling through FPR2. This allows for the clonal expansion of TReg cells increasing their number. Additionally, at the level of the BBB, ANXA1 levels are depleted, RhoA is activated and actin destabilisation occurs allowing for weakening of the tight junctions and a loss of BBB integrity.

Chapter V:

General Discussion

5.1. General Discussion

The secondary complications of diabetes represent a great burden to health care providers, including the NHS. Indeed, the treatment of diabetes annually costs £10 billion, which accounts for 10 % of the NHS budget, and some 80 % of this cost is spent on the complications of diabetes. In a report published by Diabetes UK, cardiovascular events and kidney related costs rank in the top 3 most expensive costs associated with diabetes (NHS, 2014). Due to the huge increase in costs, there is an even greater need for a better understanding of the pathophysiology of the microvascular complication of diabetes.

In this thesis, I have used serum samples from patients with both T1DM and T2DM to measure ANXA1 levels to understand whether the levels of in this known anti-inflammatory protein are modulated in both T1DM and T2DM. I then used two murine models to diabetes (i) STZ-induced T1DM and (ii) HFD-induced T2DM to gain a better insight into the role of endogenous ANXA1 in the pathophysiology of diabetes and also to evaluate whether the administration hrANXA1 is of potential therapeutic benefit. Both of these animal models are well established and have been used extensively in pre-clinically studies in rodents, mostly mice and rats. Thus, these models represent affordable and reliable methods to gain a better insight into the pathophysiology of and to evaluate novel interventions for diabetes.

I demonstrate in this thesis that AXNA1 levels are elevated in patients with both T1DM and T2DM. Previously Solito *et al*. have shown that ANXA1 needs to be

shed upon cellular activation to have a biological function. Here I postulate that ANXA1 is shed from its cellular stores secondary to an elevation of either glucose and/or lipids in the blood allowing ANXA1 to act on its cell surface receptor FPR2. This conclusion is supported by the following, three observations: (i) patients with both T1DM and T2DM plus a diagnosis of diabetic nephropathy/CKD did not cause a further rise in ANXA1 but did cause a further increase in CRP levels. This suggests that ANXA1 is not shed in response to increased chronic inflammation, but rather that ANXA1 release occurs in response to excessive glucose or lipid load in the plasma. This was confirmed by the lack of correlation between ANXA1 and CRP levels in patients with both T1DM and T2DM; (ii) in patients with T2DM plasma cholesterol levels correlated with an increase in plasma ANXA1, but there was no correlation with plasma CRP, and (iii) in the murine models of both T1DM and T2DM there was elevated ANXA1 levels in the sera, while in the tissue there was a decrease ANXA1 levels, suggesting that ANXA1 had been released/shed (in response to a stimuli) from it cellular stored into the circulation. This shedding or release of ANXA1 is essential for ANXA1 to signal in both an autocrine and paracrine manner through FPR2.

One of the limitations of these observations is that I used CRP as a marker of systemic inflammation. Classically, CRP is an acute-phase protein, which serves as an early marker of inflammation or infection. The main weakness of using CRP as a marker of inflammation is that it is very unspecific. Although, CRP does have strong predictive value for adverse incidents in cardiovascular disease; CRP levels that are above 3 mg/L confer a 1.58 increase in relative risk of an adverse

event (Buckley et al., 2015) (Ridker et al., 2000). Here I show that CRP was elevated in patients with both T1DM and T2DM, but was further elevated in patients with diabetic nephropathy.

Having found that ANXA1 levels were elevated in patients with both T1DM and T2DM, I subjected ANXA1$^{-/-}$ mice to experimental models of T1DM and T2DM in order to (i) get a better insight into the role of endogenous ANXA1 in these disease states and (ii) to evaluate the efficacy of hrANXA1 in experimental diabetes. In the clinical setting, patients will be on the best standard of care, meaning that they will be on medication to manage their diabetes. Patients with T1DM will be on insulin replacement therapy to regulate blood glucose levels, while patients on T2DM will most likely be on a lipid lowering agents (for example a statin) and/or a blood pressure lowering agent. The main limitations of these *in vivo* animal models is that the mice were not treated for their 'diabetes'. There are also good reasons for not managing the diabetic phenotype, as hyperglycaemia is one of the key drivers of the microvascular complications and must, therefore, be allowed to persist. In the STZ-induced model of T1DM, if I treated with insulin to lower blood glucose levels the mice would appear to have no diabetic phenotype indeed this is well established the insulin therapy prevents the development of microvascular complications by reducing the glycaemic load (Havel et al., 2000). Additionally, the length of time required to develop microvascular complications would be much more if I had used insulin to achieve rigorous glycaemic control. In chapter 2, I show that after 6 weeks after induction of T1DM with STZ, I can document the development of cardiac (reduced ejection fraction) and renal dysfunction (proteinuria). Additionally, in

the HFD-induced T2DM models, if mice were treated with a lipid-lowering agent again the driving stimulus for peripheral insulin resistance would be lost. However, using this model (with no conventional treatment), I can document the development of renal dysfunction (proteinuria) within 10 weeks of commencing the HFD.

Endogenously ANXA1 appears to be a tissue protective protein. In chapter II I show that ANXA1$^{-/-}$ mice administered STZ have a more severe diabetic phenotype by week 13, which in turn results in a greater degree of cardiac and renal dysfunction. In chapter III I show that ANXA1$^{-/-}$ mice fed a HFD also have a more severe diabetic phenotype, which was associated with increased liver injury and renal dysfunction. Then in chapter IV, I show that ANXA1$^{-/-}$ mice have a major permeability defect in their BBB, which was further augmented in ANXA1$^{-/-}$ mice fed a HFD. These 3 studies show that ANXA1 acts on a diverse range of pathways, but ultimately, all evidence suggests that ANXA1 acts to in a tissue-protective manner to maintain normal physiology.

One of the most striking findings of this thesis was that the diabetic phenotype was more severe in ANXA1$^{-/-}$ mice when challenged with STZ or when fed a HFD, suggesting that ANXA1 maybe involved in the secretion of insulin. However, under normal physiological conditions ANXA1$^{-/-}$ mice displayed normal glucose-stimulated insulin secretion, suggesting that the increased severity of the diabetic phenotype is independent of insulin secretion. Studied using isolated islet from ANXA1$^{-/-}$ mice demonstrated in support of the finding here that ANXA1$^{-/-}$ do not have a defect in glucose-stimulated insulin secretion (Rackham

et al., 2016). Indeed, this would appear to be the case in chapter II as in the STZ-induced model there is no insulin produced, therefore these effects are independent of insulin secretion. Additionally, in chapter II, I report that treatment with hrANXA1 does not affect the diabetic phenotype in the STZ-model; mice treated with hrANXA1 still had an augmented OGTT, suggesting that in a system devoid of insulin, ANXA1 has little effect. Yet, in chapter III, I report that mice fed a HFD and treated with ANXA1 have an improved diabetic phenotype; mice treated with hrANXA1 displayed lower plasma insulin and glucose levels, and an improved OGTT. From the outset this may seem like a dichotomy in findings between the two studies. However, when the induction mode of each model is assessed the picture becomes clearer. Streptozotocin is a chemical, which specifically targets beta cells for destruction. It does this by causing alkylation of DNA leading cells death by necrosis. Beta cells are on of a number of cell types that once destroyed cannot be replaced; therefore it is not surprising that when mice are given hrANXA1 after STZ-induced of diabetes it did not improve their diabetic phenotype. This is because there is no method by which the mice can increase insulin production to sufficient levels to lower blood glucose. In contrast, mice fed a HFD are under metabolic alteration due to over consumption of dietary fats and sugar. This leads to an augmentation in signaling events ultimately resulting in peripheral insulin resistance. Therefore, if the HFD-fed mice are given a therapeutic i.e. hrANXA1 that has the ability to modulate the IRS-1 pathway and desensitise the insulin receptor then there will be a improvement if diabetic phenotype. Indeed, this what I report in chapter III, mice fed a HFD and treated with hrAnXA1 have an improved diabetic phenotype as a result of restoration of signaling through IRS-1.

In this thesis I undertook an in-depth mechanistic analysis of the pathways by which endogenous ANXA1 exerts its protective effects; whether this was in limiting the development of cardiac or renal dysfunction (chapter II and III), liver injury (chapter III) or by increasing BBB tightness (chapter IV). I have demonstrated that AXNA1 plays a central role in regulating many biological pathways; and a key role in modulating the phosphorylation states of numerous targets proteins. For example, I show in chapter II that ANXA1$^{-/-}$ mice have increased phosphorylation of the MAPK's p38, JNK and ERK1/2, while, in chapter III, I have shown that ANXA1$^{-/-}$ mice have decreased phosphorylation of RhoA. These changes in phosphorylation state result in activation of these proteins. Indeed, activation of all these proteins is associated with negative outcomes in many disease states. The development of a diabetic phenotype was also associated with a decrease in the intracellular levels of ANXA1 resulting in reduced intracellular signaling through FPR2. The outcome of this was activation of the MAPK's, and RhoA, again suggesting that intracellular signaling of ANXA1 through FPR2 is key to normal physiology. Interestingly, in chapter III when HFD-fed mice where treated with hrANXA1, intracellular ANXA1 levels were maintained at a physiological level. However, the mechanism behind this increase is unknown; the increase could be due to an increase in transcription, or increased uptake the i.p bolus. Additionally, as well as increasing intracellular ANXA1 concentration, the aberrant signaling events seen in diabetic mice, either T1DM and T2DM, are ameliorated.

One of the key pathways investigated in this thesis is activation of Akt. I show that mice subjected to STZ-induced T1DM (chapter II) and in mice challenged with HFD to induce diabetes T2DM (chapter III), that the phosphorylation of Ser^{473} on Akt is decreased. This means that the kinase is less active, leaving organs more vulnerable to stressor stimuli. Indeed, in both models of T1DM and T2DM, I have shown that when Akt activity is decreased organs are more susceptible to injury and develop dysfunction over time. Additionally, when mice were treated with hrANXA1, the phosphorylation of Ser^{473} on Akt was maintained at a higher level, increasing/restoring its kinase activity. Indeed, the data presented here are consistent with other studies which have shown that treatment with ANXA1 or Ac2-26 restore Akt signalling (Qin et al., 2013) (Facio et al., 2011).

I have shown that patients with diabetes have elevated CRP, indeed there are many other epidemiological studies that have demonstrated that CRP is related to cardiovascular risk; however few show a relationship with insulin resistance. There is a lot of *in vivo* and *in vitro* evidence that suggests a clear link between CRP and insulin resistance. CRP can suppress insulin-induced NO production, inhibit eNOS and Akt phosphorylation and also initiate the phosphorylation of Ser^{307} on IRS-1 (Tanigaki et al., 2009), all of which are key features of insulin resistance in man. An elegant paper by Jin-Wen Xu *et al.* demonstrated that many of that actions of CRP could be blocked using a RhoA-dependent kinase inhibitor (Y27632), or by a JNK inhibitor (SP6000125) (Xu et al., 2007). Indeed, I show in the murine models that ANXA1 is key endogenous inhibitor of both RhoA activity and JNK. Additionally, I have shown that treatment with hrANXA1 can also

prevented the increase in RhoA and JNK activity resulting from feeding a HFD; this results in increased phosphorylation of IRS-1 and eNOS and an ultimately an improved diabetic phenotype and limit the development of microvascular complications.

In chapter IV, I have changed focus away from treating the conventional microvascular complications of diabetes and an attempt to link changes in peripheral T-cell biology with the central nervous system. These preliminary data show that endogenously AXNA1 is a key regulator of BBB integrity, and that the specialised endothelium of the BBB is altered in mice fed a HFD. Additionally, these results show that ANXA1 is a key regulator of both Th17 and TReg differentiation in the peripheral system. I have also shown that Th17 and TReg cells more readily adhere to and transmigrate through a brain microvascular endothelium. I have also demonstrated that when mice are treated with hrANXA1 the negative effect of a HFD can be ameliorated.

The main limitation of this study are that I have not conducted any mechanistic studies into the mechanisms by which diabetes affects ANXA1 levels and its interactions with tight junctions to increased BBB permeability. Based on findings in chapter II and III, I show that ANXA1 levels are depleted in the tissue (kidney, liver and skeletal muscle), I speculate that ANAX1 levels are depleted in the endothelium of the BBB of mice fed a HFD; this leads to a destabilisation of the actin cytoskeleton and reduces tight junction integrity increasing BBB permeability. The consequence of this is a increased influx of immune cells into the brain parenchyma.

5.1.2 Clinical relevance of my findings.

Indeed the results presented in this thesis I believe have translatable worth. Therapeutically, giving ANXA1 could be an add on therapy to conventional insulin treatment in type-2 diabetes. Three lines of evidence would support this; (i) ANAX1 is effective at lowering blood glucose, (ii) it can lower the lipid in serum, and (iii) it also restores the signaling by directly inhibiting the inhibitory phosphorylation of IRS-1.

There is a strong case that treatment with ANXA1 protects multiple organs from development of complications that arise from diabetes. I have shown that the heart does not develop left ventricular dysfunction, the liver does not develop hepatic steatosis, and the kidneys do not develop diabetic nephropathy. There is also a strong case that by restoring the BBB from becoming more permeable you could reduce the risk of age related disease of the central nervous system.

One alternative strategy could be to developed a dual therapy with insulin. Using the same delivery route (sub cutaneous) is the ideal method for a slow release protein therapy. Therefore, with good insulin management you are also boosting your levels of a naturally occurring endogenous anti-inflammatory and tissue protective protein.

Here I have presented a novel therapeutic agent that has lipid-lowering properties, which are mediated through a new pathway, FPR2. If an oral formulation of an agonist to the FPR2 could be developed there would be a huge commercial market, if these findings could be confirmed in man.

5.2. Future Perspectives

1. One of the main questions that remain to be answered is whether ANXA1$^{-/-}$ mice have a hypertensive phenotype. Activation of MYPT1 is associated with a slowing of the relaxation of the myosin light chain of smooth muscle. This can lead to increased contraction in resistance vessels. Along the same lines, it would be interesting to know whether WT mice fed a HFD develop hypertension. Two lines of evidence suggest that this may be the case: (i) WT mice fed HFD have activated MYPT1 (increasing vasoconstriction) and (ii) WT mice fed a HFD have decreased eNOS activity (reducing vasodilation). Hypertension can be measured using one of two techniques: (i) traditionally tail cuff measurements of blood pressure are taken, but they have significant limitations. The main one being that that the animal is conscious and that the stress of fitting the cuff often tends to result in hypertension resulting in an overestimation of the reading; (ii) *in vivo* telemetry can be used to insert a telemetry probe into the carotid and the mouse then recovers for anaesthsia goes back to it cage. The advantage of this technique is that you get a continuous measurement of blood pressure, which allows for diurnal variation, which can be very important.

2. At the levels of the BBB it would be useful to assess RhoA activation in the microvasculature of the brain. Our hypothesis is that RhoA activation is causing actin destabilisation, which reduces the tightness of the tight junctions. Initially, it would be useful to use whole brain protein extracts to measure RhoA activation in mice from each of the test groups. However, tight

junctions are only present of the endothelial so a more specific technique could be to isolate specifically the brain microvascular endothelial cells. This would allow for the specific determination of if RhoA is activated in the endothelial.

3. In diabetic mice it would be interesting to assess the quality of the tight junctions. This could be achieved by doing immunofluorescence of frozen brain sections, measuring the expression of ANXA1, occludin, F-actin, ZO-1, and claudin 5 and laminin. This could give indication of the structural integrity of the BBB, which would compliment the *in vivo* data suggesting that the BBB from diabetic mice is more permeable.

4. It would also be very interesting to look for the presence of infiltrating immune cells in the brain of mice in different treatment groups. This could be done, using immunofluorescence or by FAC sorting brain homogenates. This would allow for the investigation of which sub-sets of T-cells more actively migrate into the brain parenchyma in mice fed a HFD, and if treatment with hrANXA1 has the same effect *in vivo* as it does *in vitro*.

References

Acharya, N.K. et al., 2013. Diabetes and hypercholesterolemia increase blood-brain barrier permeability and brain amyloid deposition: beneficial effects of the LpPLA2 inhibitor darapladib. *Journal of Alzheimer's disease : JAD*, 35(1), pp.179–98.

Ahima, R.S., 2009. Connecting obesity, aging and diabetes. *Nature Medicine*, 15(9), pp.996–997.

Ahmed, A.M., 2002. History of diabetes mellitus. *Saudi medical journal*, 23(4), pp.373–8.

Akasheh, R.T. et al., 2013. Increased Adiposity in Annexin A1-Deficient Mice R. Ahmad, ed. *PLoS ONE*, 8(12), p.e82608.

Akirav, E., Kushner, J.A. & Herold, K.C., 2008. Beta-cell mass and type 1 diabetes: going, going, gone? *Diabetes*, 57(11), pp.2883–8.

Diabetes UK, 2014. THE COST OF DIABETES. Publishes online at http://www.diabetes.co.uk/cost-of-diabetes.html

Artursson, P., Palm, K. & Luthman, K., 2001. Caco-2 monolayers in experimental and theoretical predictions of drug transport. *Advanced drug delivery reviews*, 46(1–3), pp.27–43.

Atkinson, M.A., 2012. The pathogenesis and natural history of type 1 diabetes. *Cold Spring Harbor perspectives in medicine*, 2(11).

Ban, C.R. & Twigg, S.M., 2008a. Fibrosis in diabetes complications: pathogenic mechanisms and circulating and urinary markers. *Vascular health and risk management*, 4(3), pp.575–96.

Ban, C.R. & Twigg, S.M., 2008b. Fibrosis in diabetes complications: pathogenic mechanisms and circulating and urinary markers. *Vascular health and risk management*, 4(3), pp.575–96.

Basu, S. et al., 2005. Type 1 Diabetes Is Associated With Increased Cyclooxygenase- and Cytokine-Mediated Inflammation. *Diabetes Care*, 28(6), pp.1371–1375.

Beckerman, P. & Susztak, K., 2014. Sweet debate: fructose versus glucose in diabetic kidney disease. *Journal of the American Society of Nephrology : JASN*, 25(11), pp.2386–8.

Bena, S. et al., 2012. Annexin A1 interaction with the FPR2/ALX receptor: identification of distinct domains and downstream associated signaling. *The Journal of biological chemistry*, 287(29), pp.24690–7.

Bensalem, N. et al., 2005. Down-regulation of the anti-inflammatory protein annexin A1 in cystic fibrosis knock-out mice and patients. *Molecular & cellular proteomics : MCP*, 4(10), pp.1591–601.

Berthier, C.C. et al., 2009. Enhanced expression of Janus kinase-signal transducer and activator of transcription pathway members in human diabetic nephropathy. *Diabetes*, 58(2), pp.469–77.

Bhattacharjee, N. et al., 2016. Mechanistic insight of diabetic nephropathy and its pharmacotherapeutic targets: An update. *European Journal of Pharmacology*, 791, pp.8–24.

Blair, A. et al., 1999. Oxidized low density lipoprotein displaces endothelial nitric-oxide synthase (eNOS) from plasmalemmal caveolae and impairs eNOS activation. *The Journal of biological chemistry*, 274(45), pp.32512–9.

Boettler, T. & von Herrath, M., 2011. Protection against or triggering of Type 1 diabetes? Different roles for viral infections. *Expert review of clinical immunology*, 7(1), pp.45–53.

Bondeva, T. & Wolf, G., 2014. Reactive oxygen species in diabetic nephropathy: friend or foe? *Nephrology, dialysis, transplantation : official publication of the European Dialysis and Transplant Association - European Renal Association*, 29(11), pp.1998–2003.

Börgeson, E. et al., 2015. Lipoxin A4 Attenuates Obesity-Induced Adipose Inflammation and Associated Liver and Kidney Disease. *Cell metabolism*, 22(1), pp.125–37.

Bottaro, D.P., Bonner-Weir, S. & King, G.L., 1989. Insulin receptor recycling in vascular endothelial cells. Regulation by insulin and phorbol ester. *The Journal of biological chemistry*, 264(10), pp.5916–23.

Boudina, S. & Abel, E.D., 2010. Diabetic cardiomyopathy, causes and effects. *Reviews in endocrine & metabolic disorders*, 11(1), pp.31–9.

Brownlee, M., 2001. Biochemistry and molecular cell biology of diabetic complications. *Nature*, 414(6865), pp.813–820.

Brozovich, F.V. et al., 2016. Mechanisms of Vascular Smooth Muscle Contraction and the Basis for Pharmacologic Treatment of Smooth Muscle Disorders. *Pharmacological Reviews*, 68(2).

Bruce, D.G. et al., 2003. Cognitive impairment, physical disability and depressive symptoms in older diabetic patients: the Fremantle Cognition in Diabetes Study. *Diabetes research and clinical practice*, 61(1), pp.59–67.

Bruno, G. et al., 2003. Progression to overt nephropathy in type 2 diabetes: the Casale Monferrato Study. *Diabetes care*, 26(7), pp.2150–5.

Buckley, B.S. et al., 2012. Gestational diabetes mellitus in Europe: prevalence, current screening practice and barriers to screening. A review. *Diabetic Medicine*, 29(7), pp.844–854.

Bugger, H. & Abel, E.D., 2014. MolecuBugger, H., & Abel, E. D. (2014). Molecular mechanisms of diabetic cardiomyopathy. Diabetologia, 57(4), 660–71. doi:10.1007/s00125-014-3171-6lar mechanisms of diabetic cardiomyopathy. *Diabetologia*, 57(4), pp.660–71.

Butt, A.M., Jones, H.C. & Abbott, N.J., 1990. Electrical resistance across the blood-brain barrier in anaesthetized rats: a developmental study. *The Journal of physiology*, 429, pp.47–62.

Cai, Z. & Semenza, G.L., 2004. Phosphatidylinositol-3-Kinase Signaling Is Required for Erythropoietin-Mediated Acute Protection Against Myocardial Ischemia/Reperfusion Injury. *Circulation*, 109(17).

Campia, U. et al., 2014. The vascular endothelin system in obesity and type 2 diabetes: Pathophysiology and therapeutic implications. *Life Sciences*, 118(2), pp.149–155.

Cantley, L.C., 2002. The Phosphoinositide 3-Kinase Pathway. *Science*, 296(5573), pp.1655–1657.

De Caterina, R. et al., 1993. Macrophage-specific eicosanoid synthesis inhibition and lipocortin-1 induction by glucocorticoids. *Journal of applied physiology (Bethesda, Md. : 1985)*, 75(6), pp.2368–75.

Chang, Y.-T. et al., 2014. Diabetes and end-stage renal disease synergistically contribute to increased incidence of cardiovascular events: a nationwide follow-up study during 1998-2009. *Diabetes care*, 37(1), pp.277–85.

Chatterjee, B.E. et al., 2005. Annexin 1-deficient neutrophils exhibit enhanced transmigration in vivo and increased responsiveness in vitro. *Journal of Leukocyte Biology*, 78(3), pp.639–646.

Chatzopoulou, A. et al., 2016. Glucocorticoid-Induced Attenuation of the Inflammatory Response in Zebrafish. *http://dx.doi.org/10.1210/en.2015-2050*.

Chawla, A., Chawla, R. & Jaggi, S., 2016. Microvasular and macrovascular complications in diabetes mellitus: Distinct or continuum? *Indian journal of endocrinology and metabolism*, 20(4), pp.546–51.

Chen, J. et al., 2014. Gender Dimorphism of the Cardiac Dysfunction in Murine Sepsis: Signalling Mechanisms and Age-Dependency. *PLOS ONE*, 9(6), p.R158.

Chen, J. et al., 2017. IκB Kinase Inhibitor Attenuates Sepsis-Induced Cardiac Dysfunction in CKD. *Journal of the American Society of Nephrology : JASN*, 28(1), pp.94–105.

Cheng, X. et al., 2013. Both ERK/MAPK and TGF-Beta/Smad signaling pathways play a role in the kidney fibrosis of diabetic mice accelerated by blood glucose fluctuation. *Journal of diabetes research*, 2013, p.463740.

Chiazza, F. et al., 2015. Targeting the NLRP3 Inflammasome to Reduce Diet-Induced Metabolic Abnormalities in Mice. *Molecular Medicine*, 21(1), p.1.

Chin, B.Y. et al., 2001. Stimulation of pro-alpha(1)(I) collagen by TGF-beta(1) in mesangial cells: role of the p38 MAPK pathway. *American journal of physiology. Renal physiology*, 280(3), pp.F495-504.

Chuang, P.Y. & He, J.C., 2010. JAK/STAT signaling in renal diseases. *Kidney international*, 78(3), pp.231–4.

Connelly, K.A. et al., 2009. Inhibition of Protein Kinase C- by Ruboxistaurin Preserves Cardiac Function and Reduces Extracellular Matrix Production in Diabetic Cardiomyopathy. *Circulation: Heart Failure*, 2(2), pp.129–137.

Copps, K.D. et al., 2010. Irs1 serine 307 promotes insulin sensitivity in mice. *Cell metabolism*, 11(1), pp.84–92.

de Coupade, C., Solito, E. & Levine, J.D., 2003. Dexamethasone enhances interaction of endogenous annexin 1 with L-selectin and triggers shedding of L-selectin in the monocytic cell line U-937. *British journal of pharmacology*, 140(1), pp.133–45.

Cristante, E. et al., 2013. Identification of an essential endogenous regulator of blood-brain barrier integrity, and its pathological and therapeutic implications. *Proceedings of the National Academy of Sciences of the United States of America*, 110(3), pp.832–41.

Cunningham, C. & Hennessy, E., 2015. Co-morbidity and systemic inflammation as drivers of cognitive decline: new experimental models adopting a broader paradigm in dementia research. *Alzheimer's research & therapy*, 7(1), p.33.

Cusi, K., 2010. The Role of Adipose Tissue and Lipotoxicity in the Pathogenesis of Type 2 Diabetes. *Current Diabetes Reports*, 10(4), pp.306–315.

D'Acquisto, F., Perretti, M. & Flower, R.J., 2008. Annexin-A1: a pivotal regulator of the innate and adaptive immune systems. *British journal of pharmacology*, 155(2), pp.152–69.

D 'acquisto, F. et al., Glucocorticoid treatment inhibits annexin-1 expression in rheumatoid arthritis CD4 þ T cells.

Dalli, J. et al., 2012. Annexin A1 N-terminal derived Peptide ac2-26 exerts chemokinetic effects on human neutrophils. *Frontiers in pharmacology*, 3, p.28.

Deacon, C.F. & Lebovitz, H.E., 2016. Comparative review of dipeptidyl peptidase-4 inhibitors and sulphonylureas. *Diabetes, Obesity and Metabolism*, 18(4), pp.333–347.

Deanfield, J.E., Halcox, J.P. & Rabelink, T.J., 2007. Endothelial Function and Dysfunction. *Circulation*, 115(10).

Dei Cas, A. et al., 2013. Diabetes and chronic heart failure: from diabetic cardiomyopathy to therapeutic approach. *Endocrine, metabolic & immune disorders drug targets*, 13(1), pp.38–50.

Downs, C.A. & Faulkner, M.S., 2015. Toxic stress, inflammation and symptomatology of chronic complications in diabetes. *World journal of diabetes*, 6(4), pp.554–65.

Du, Y. et al., 2010. Effects of p38 MAPK inhibition on early stages of diabetic retinopathy and sensory nerve function. *Investigative ophthalmology & visual science*, 51(4), pp.2158–64.

Facio, F.N. et al., 2011. Annexin 1 mimetic peptide protects against renal ischemia/reperfusion injury in rats. *Journal of Molecular Medicine*, 89(1), pp.51–63.

Farhangkhoee, H. et al., 2003. Heme oxygenase in diabetes-induced oxidative stress in the heart. *Journal of Molecular and Cellular Cardiology*, 35(12), pp.1439–1448.

Femminella, G.D. et al., 2017. Antidiabetic Drugs in Alzheimer's Disease: Mechanisms of Action and Future Perspectives. *Journal of diabetes research*, 2017, p.7420796.

Festa, A. & Haffner, S.M., 2005. Inflammation and cardiovascular disease in patients with diabetes: lessons from the Diabetes Control and Complications Trial. *Circulation*, 111(19), pp.2414–5.

Flower, R.J. & Blackwell, G.J., 1979. Anti-inflammatory steroids induce biosynthesis of a phospholipase A2 inhibitor which prevents prostaglandin generation. *Nature*, 278(5703), pp.456–9.

Freemantle, N. et al., 2008. How strong is the association between abdominal obesity and the incidence of type 2 diabetes? *International journal of clinical practice*, 62(9), pp.1391–6.

Gall, M.A. et al., 1997. Risk factors for development of incipient and overt diabetic nephropathy in patients with non-insulin dependent diabetes mellitus: prospective, observational study. *BMJ (Clinical research ed.)*, 314(7083), pp.783–8.

García-García, P.M. et al., 2014. Inflammation in diabetic kidney disease. *World journal of diabetes*, 5(4), pp.431–43.

Garber, A.J., 2011. Long-acting glucagon-like peptide 1 receptor agonists: a review of their efficacy and tolerability. *Diabetes care*, 34 Suppl 2(Supplement 2), pp.S279-84.

Garg, A. & Misra, A., 2002. Hepatic Steatosis, Insulin Resistance, and Adipose Tissue Disorders. *The Journal of Clinical Endocrinology & Metabolism*, 87(7), pp.3019–3022.

Gavins, felicity nicola, Granger, N.D. & perretti, mauro, 2006. Impact of the annexin 1 system on focal cerebral ischaemia-reperfusion injury in mice.

The FASEB Journal, 20(4), pp.A285–A285.
Gavins, F.N.E. & Hickey, M.J., 2012. Annexin A1 and the regulation of innate and adaptive immunity. *Frontiers in immunology*, 3, p.354.
Geraldes, P. & King, G.L., 2010a. Activation of protein kinase C isoforms and its impact on diabetic complications. *Circulation research*, 106(8), pp.1319–31.
Geraldes, P. & King, G.L., 2010b. Activation of protein kinase C isoforms and its impact on diabetic complications. *Circulation research*, 106(8), pp.1319–31.
Gerke, V., Creutz, C.E. & Moss, S.E., 2005. Annexins: linking Ca2+ signalling to membrane dynamics. *Nature Reviews Molecular Cell Biology*, 6(6), pp.449–461.
Gerke, V. & Moss, S.E., 2002. Annexins: From Structure to Function. *Physiol Rev*, 82(2), pp.331–371.
Gerstein, H.C., 1994. Cow's milk exposure and type I diabetes mellitus. A critical overview of the clinical literature. *Diabetes care*, 17(1), pp.13–9.
Ghosh, S. et al., 2005. Cardiomyocyte apoptosis induced by short-term diabetes requires mitochondrial GSH depletion. *American journal of physiology. Heart and circulatory physiology*, 289(2), pp.H768-76.
Giacco, F. & Brownlee, M., 2010. Oxidative stress and diabetic complications. *Circulation research*, 107(9), p.1058.
Gojo, A. et al., 2007. The Rho-kinase inhibitor, fasudil, attenuates diabetic nephropathy in streptozotocin-induced diabetic rats. *European Journal of Pharmacology*, 568(1–3), pp.242–247.
Goulding, N. et al., 1990. Anti-inflammatory lipocortin 1 production by peripheral blood leucocytes in response to hydrocortisone. *The Lancet*, 335(8703), pp.1416–1418.
Gross, J.L. et al., 2005. Diabetic Nephropathy: Diagnosis, Prevention, and Treatment. *Diabetes Care*, 28(1), pp.164–176.
Gu, Z. et al., 2012. Effect of aging on islet beta-cell function and its mechanisms in Wistar rats. *AGE*, 34(6), pp.1393–1403.
Gual, P., Le Marchand-Brustel, Y. & Tanti, J.-F., 2005. Positive and negative regulation of insulin signaling through IRS-1 phosphorylation. *Biochimie*, 87(1), pp.99–109.
Guo, S., 2014. Insulin signaling, resistance, and the metabolic syndrome: insights from mouse models into disease mechanisms. *Journal of Endocrinology*, 220(2), pp.T1–T23.
Guo, Z. et al., 2007. Downregulation of NADPH oxidase, antioxidant enzymes, and inflammatory markers in the heart of streptozotocin-induced diabetic rats by N-acetyl-L-cysteine. *American journal of physiology. Heart and circulatory physiology*, 292(4), pp.H1728-36.
Habib, A.A. & Brannagan, T.H., 2010. Therapeutic strategies for diabetic neuropathy. *Current neurology and neuroscience reports*, 10(2), pp.92–100.
Hamblin, M. et al., 2007. Alterations in the diabetic myocardial proteome coupled with increased myocardial oxidative stress underlies diabetic cardiomyopathy. *Journal of molecular and cellular cardiology*, 42(4), pp.884–95.
Haneda, M. et al., 2015. A new classification of Diabetic Nephropathy 2014: a report from Joint Committee on Diabetic Nephropathy. *Clinical and Experimental Nephrology*, 19(1), pp.1–5.
Hanley, A.J.G. & Wagenknecht, L.E., 2008. Abdominal adiposity and diabetes risk:

the importance of precise measures and longitudinal studies. *Diabetes*, 57(5), pp.1153–5.
Havel, P.J. et al., 2000. E ffects of Streptozotocin-Induced Diabetes and Insulin Treatment on the Hypothalamic Melanocortin System and Muscle Uncoupling Protein 3 Expression in Rats. *DIABETES*, 49.
Hawkins, B.T. et al., 2006. Increased blood?brain barrier permeability and altered tight junctions in experimental diabetes in the rat: contribution of hyperglycaemia and matrix metalloproteinases. *Diabetologia*, 50(1), pp.202–211.
Hayhoe, R.P.G. et al., 2006. Annexin 1 and its bioactive peptide inhibit neutrophil-endothelium interactions under flow: indication of distinct receptor involvement. *Blood*, 107(5), pp.2123–30.
Helal, I. et al., 2012. Glomerular hyperfiltration: definitions, mechanisms and clinical implications. *Nature Reviews Nephrology*, 8(5), pp.293–300.
Hench, P.S. et al., 1950. Effects of cortisone acetate and pituitary ACTH on rheumatoid arthritis, rheumatic fever and certain other conditions. *Archives of internal medicine (Chicago, Ill. : 1908)*, 85(4), pp.545–666. Available at: http://www.ncbi.nlm.nih.gov/pubmed/15411248 [Accessed July 14, 2016].
Henquin, J.-C. et al., 2002. Signals and Pools Underlying Biphasic Insulin Secretion. *Diabetes*, 51(Supplement 1), pp.S60–S67.
Hex, N. et al., 2012. Estimating the current and future costs of Type 1 and Type 2 diabetes in the UK, including direct health costs and indirect societal and productivity costs. *Diabetic medicine : a journal of the British Diabetic Association*, 29(7), pp.855–62.
Hippisley-Cox, J. et al., 2009. Predicting risk of type 2 diabetes in England and Wales: prospective derivation and validation of QDScore. *BMJ (Clinical research ed.)*, 338(mar17_2), p.b880.
Hirosumi, J. et al., 2002. A central role for JNK in obesity and insulin resistance. *Nature*, 420(6913), pp.333–336.
Holst, J.J., 2007. The Physiology of Glucagon-like Peptide 1. *Physiological Reviews*, 87(4), pp.1409–1439.
Hong, S.-H. et al., 2002. Effect of annexin I on insulin secretion through surface binding sites in rat pancreatic islets. *FEBS Letters*, 532(1), pp.17–20.
Hou, J.C., Min, L. & Pessin, J.E., 2009. Insulin granule biogenesis, trafficking and exocytosis. *Vitamins and hormones*, 80, pp.473–506.
Huang, P.L., 2009. eNOS, metabolic syndrome and cardiovascular disease. *Trends in Endocrinology & Metabolism*, 20(6), pp.295–302.
Huber, J.D., VanGilder, R.L. & Houser, K.A., 2006. Streptozotocin-induced diabetes progressively increases blood-brain barrier permeability in specific brain regions in rats. *American journal of physiology. Heart and circulatory physiology*, 291(6), pp.H2660-8.
Hwang, I.S. et al., 1987. Fructose-induced insulin resistance and hypertension in rats. *Hypertension*, 10(5), pp.512–516.
Hwang, J.L. & Weiss, R.E., 2014. Steroid-induced diabetes: a clinical and molecular approach to understanding and treatment. *Diabetes/metabolism research and reviews*, 30(2), pp.96–102.
James, D.E. et al., 1988. Insulin-regulatable tissues express a unique insulin-sensitive glucose transport protein. *Nature*, 333(6169), pp.183–5.
Juutilainen, A. et al., 2008. Similarity of the Impact of Type 1 and Type 2 Diabetes

on Cardiovascular Mortality in Middle-Aged Subjects. *Diabetes Care*, 31(4).
Kamal, A.M., Flower, R.J. & Perretti, M., 2005. An overview of the effects of annexin 1 on cells involved in the inflammatory process. *Memórias do Instituto Oswaldo Cruz*, 100, pp.39–48.
Karasik, A. et al., 1988. Lipocortins 1 and 2 as substrates for the insulin receptor kinase in rat liver. *The Journal of biological chemistry*, 263(24), pp.11862–7.
Kehat, I. & Molkentin, J.D., 2010. Molecular pathways underlying cardiac remodeling during pathophysiologic stimulation. *Circulation*, 122(25).
Khan, A.I. et al., 2013. Erythropoietin attenuates cardiac dysfunction in experimental sepsis in mice via activation of the β-common receptor. *Disease models & mechanisms*, 6(4), pp.1021–30.
King, G.L., 2008. The Role of Inflammatory Cytokines in Diabetes and Its Complications. *Journal of Periodontology*, 79(8s), pp.1527–1534.
Kodl, C.T. & Seaquist, E.R., 2008. Cognitive dysfunction and diabetes mellitus. *Endocrine reviews*, 29(4), pp.494–511.
Komers, R. et al., 2007. Renal p38 MAP kinase activity in experimental diabetes. *Laboratory Investigation*, 87(6), p.548.
Komers, R., 2013. Rho kinase inhibition in diabetic kidney disease. *British journal of clinical pharmacology*, 76(4), pp.551–9.
Kosicka, A. et al., 2013. Attenuation of plasma annexin A1 in human obesity. *FASEB journal : official publication of the Federation of American Societies for Experimental Biology*, 27(1), pp.368–78.
Koya, D. et al., 2000. Amelioration of accelerated diabetic mesangial expansion by treatment with a PKC beta inhibitor in diabetic db/db mice, a rodent model for type 2 diabetes. *FASEB journal : official publication of the Federation of American Societies for Experimental Biology*, 14(3), pp.439–47.
Kusters, D.H.M. et al., 2015a. Pharmacological Treatment with Annexin A1 Reduces Atherosclerotic Plaque Burden in LDLR-/- Mice on Western Type Diet. *PloS one*, 10(6), p.e0130484.
Kusters, D.H.M. et al., 2015b. Pharmacological Treatment with Annexin A1 Reduces Atherosclerotic Plaque Burden in LDLR-/- Mice on Western Type Diet. *PloS one*, 10(6), p.e0130484.
La, M. et al., 2001. Annexin 1 peptides protect against experimental myocardial ischemia-reperfusion: analysis of their mechanism of action. *FASEB journal : official publication of the Federation of American Societies for Experimental Biology*, 15(12), pp.2247–56.
Le, Y., Murphy, P.M. & Wang, J.M., 2002. Formyl-peptide receptors revisited. *Trends in Immunology*, 23(11), pp.541–548.
Lee, S.I. et al., 2015. Cardiovascular disease and type 1 diabetes: prevalence, prediction and management in an ageing population. *Therapeutic advances in chronic disease*, 6(6), pp.347–74.
Leoni, G. et al., 2015. Annexin A1-containing extracellular vesicles and polymeric nanoparticles promote epithelial wound repair. *The Journal of clinical investigation*, 125(3), pp.1215–27.
Li, Q. et al., 2013. Deficient eNOS Phosphorylation Is a Mechanism for Diabetic Vascular Dysfunction Contributing to Increased Stroke Size. *Stroke*, 44(11), pp.3183–3188.
Lim, A.K., 2014. Diabetic nephropathy - complications and treatment. *International journal of nephrology and renovascular disease*, 7, pp.361–81.

Locatelli, I. et al., 2014. Endogenous annexin A1 is a novel protective determinant in nonalcoholic steatohepatitis in mice. *Hepatology (Baltimore, Md.)*, 60(2), pp.531–44.
Lorenzo, O. et al., 2011. Potential role of nuclear factor κB in diabetic cardiomyopathy. *Mediators of inflammation*, 2011, p.652097.
Lovejoy, J.C., 1999. Dietary fatty acids and insulin resistance. *Current Atherosclerosis Reports*, 1(3), pp.215–220.
Luscinskas, F.W. et al., 1996. L- and P-selectins, but not CD49d (VLA-4) integrins, mediate monocyte initial attachment to TNF-alpha-activated vascular endothelium under flow in vitro. *Journal of immunology (Baltimore, Md. : 1950)*, 157(1), pp.326–35.
MacDonald, P.E. et al., 2002. The multiple actions of GLP-1 on the process of glucose-stimulated insulin secretion. *Diabetes*, 51 Suppl 3, pp.S434-42.
Majumdar, S.K., Glimpses of the history of insulin. *Bulletin of the Indian Institute of History of Medicine (Hyderabad)*, 31(1), pp.57–70.
Mann, D.L., 2002. Inflammatory Mediators and the Failing Heart: Past, Present, and the Foreseeable Future. *Circulation Research*, 91(11), pp.988–998.
Marshall, S.M., 2004. Recent advances in diabetic nephropathy. *Postgraduate medical journal*, 80(949), pp.624–33.
Martín-Timón, I. et al., 2014. Type 2 diabetes and cardiovascular disease: Have all risk factors the same strength? *World Journal of Diabetes*, 5(4), p.444.
Massey, A.R. et al., 2003. Increased RhoA translocation in renal cortex of diabetic rats. *Life sciences*, 72(26), pp.2943–52.
Matveyenko, A. V. & Butler, P.C., 2008. Relationship between β-cell mass and diabetes onset. *Diabetes, Obesity and Metabolism*, 10, pp.23–31.
McArthur, S. et al., 2010. Annexin A1: a central player in the anti-inflammatory and neuroprotective role of microglia. *Journal of immunology (Baltimore, Md. : 1950)*, 185(10), pp.6317–28.
McLeod, J.D. et al., 1995. *Changes in the cellular distribution of Lipocortin-1 (Annexin-1) in C6 glioma cells after exposure to dexamethasone*,
Melki, V. et al., 1994. Annexin I as a Potential Inhibitor of Insulin Receptor Protein Tyrosine Kinase. *Biochemical and Biophysical Research Communications*, 203(2), pp.813–819.
Menne, J. et al., 2004. Diminished loss of proteoglycans and lack of albuminuria in protein kinase C-alpha-deficient diabetic mice. *Diabetes*, 53(8), pp.2101–9.
Mering, J. & Minkowski, O., 1890. Diabetes mellitus nach Pankreasexstirpation. *Archiv für Experimentelle Pathologie und Pharmakologie*, 26(5–6), pp.371–387.
Miao, L. et al., 2002. Upregulation of small GTPase RhoA in the basilar artery from diabetic (mellitus) rats. *Life sciences*, 71(10), pp.1175–85.
Migeotte, I., Communi, D. & Parmentier, M., 2006. Formyl peptide receptors: a promiscuous subfamily of G protein-coupled receptors controlling immune responses. *Cytokine & growth factor reviews*, 17(6), pp.501–19.
Minghetti, L. et al., 1999. Down-regulation of microglial cyclo-oxygenase-2 and inducible nitric oxide synthase expression by lipocortin 1. *British journal of pharmacology*, 126(6), pp.1307–14.
Molitch, M.E. et al., 2004. Nephropathy in diabetes. *Diabetes care*, 27 Suppl 1, pp.S79-83.

Morigi, M. et al., 1998. Leukocyte-endothelial interaction is augmented by high glucose concentrations and hyperglycemia in a NF-kB-dependent fashion. *The Journal of clinical investigation*, 101(9), pp.1905–15.

Mulla, A. et al., 2005. Correlation between the antiinflammatory protein annexin 1 (lipocortin 1) and serum cortisol in subjects with normal and dysregulated adrenal function. *The Journal of clinical endocrinology and metabolism*, 90(1), pp.557–62.

Musicki, B. et al., 2010. Hypercholesterolemia-induced erectile dysfunction: endothelial nitric oxide synthase (eNOS) uncoupling in the mouse penis by NAD(P)H oxidase. *The journal of sexual medicine*, 7(9), pp.3023–32.

Naito, Z. et al., 2003. Different influences of hyperglycemic duration on phosphorylated extracellular signal-regulated kinase 1/2 in rat heart. *Experimental and molecular pathology*, 74(1), pp.23–32.

Nakagawa, T. et al., 2011. Endothelial dysfunction as a potential contributor in diabetic nephropathy. *Nature Reviews Nephrology*, 7(1), pp.36–44.

Narres, M. et al., 2016. The Incidence of End-Stage Renal Disease in the Diabetic (Compared to the Non-Diabetic) Population: A Systematic Review K. Jandeleit-Dahm, ed. *PLOS ONE*, 11(1), p.e0147329.

Nwwck, G., 2002. Fifty Years of Experience with Cortisone Therapy in the Study and Treatment of Rheumatoid Arthritis. *Annals of the New York Academy of Sciences*, 966(1), pp.28–38.

Neymeyer, H. et al., 2015. Activation of annexin A1 signalling in renal fibroblasts exerts antifibrotic effects. *Acta physiologica (Oxford, England)*, 215(3), pp.144–58.

Nguyen, J.C.D., Killcross, A.S. & Jenkins, T.A., 2014. Obesity and cognitive decline: role of inflammation and vascular changes. *Frontiers in neuroscience*, 8, p.375.

Niemann, M. et al., 2013. [Echocardiography in diabetic cardiomyopathy]. *Herz*, 38(1), pp.42–7.

Noda, K. et al., 2012. Leukocyte adhesion molecules in diabetic retinopathy. *Journal of ophthalmology*, 2012, p.279037.

Ohnishi, M. et al., 1994. Changes in annexin I and II levels during the postnatal development of rat pancreatic islets. *Journal of Cell Science*, 107(8).

Ohnishi, M. et al., 1995. Involvement of annexin-I in glucose-induced insulin secretion in rat pancreatic islets. *Endocrinology*, 136(6), pp.2421–6.

Papadopoulou-Marketou, N., Chrousos, G.P. & Kanaka-Gantenbein, C., 2016. Diabetic nephropathy in type 1 diabetes: a review of early natural history, pathogenesis, and diagnosis. *Diabetes/Metabolism Research and Reviews*.

Parente, L. & Solito, E., 2004. Annexin 1: more than an anti-phospholipase protein. *Inflammation research : official journal of the European Histamine Research Societ.* 53(4), pp.125–32.

Patel, H.B. et al., 2012. The impact of endogenous annexin A1 on glucocorticoid control of inflammatory arthritis. *Annals of the Rheumatic Diseases*, 71(11), pp.1872–1880.

Patel, N.S.A. et al., 2012. Delayed administration of pyroglutamate helix B surface peptide (pHBSP), a novel nonerythropoietic analog of erythropoietin, attenuates acute kidney injury. *Molecular medicine (Cambridge, Mass.)*, 18(1), pp.719–27.

Pederzoli-Ribeil, M. et al., 2010. Design and characterization of a cleavage-

resistant Annexin A1 mutant to control inflammation in the microvasculature. *Blood*, 116(20), pp.4288–96.

Perretti, M. et al., 1993. Lipocortin-1 fragments inhibit neutrophil accumulation and neutrophil-dependent edema in the mouse. A qualitative comparison with an anti-CD11b monoclonal antibody. *Journal of immunology (Baltimore, Md. : 1950)*, 151(8), pp.4306–14. Available at: http://www.ncbi.nlm.nih.gov/pubmed/8409403 [Accessed August 11, 2015].

Perretti, M. et al., 1996. Mobilizing lipocortin 1 in adherent human leukocytes downregulates their transmigration. *Nature Medicine*, 2(11), pp.1259–1262.

Perretti, M., 2003. The annexin 1 receptor(s): is the plot unravelling? *Trends in Pharmacological Sciences*, 24(11), pp.574–579.

Perretti, M. & D'Acquisto, F., 2009. Annexin A1 and glucocorticoids as effectors of the resolution of inflammation. *Nature reviews. Immunology*, 9(1), pp.62–70.

Pietrani, N.T. et al., 2014. Annexin A1 concentrations is decreased in patients with diabetes type 2 and nephropathy. *Clinica chimica acta; international journal of clinical chemistry*, 436, pp.181–2.

Pociot, F. & Lernmark, Å., 2016. Genetic risk factors for type 1 diabetes. *Lancet (London, England)*, 387(10035), pp.2331–9.

Ponnuswamy, P. et al., 2012. eNOS Protects from Atherosclerosis Despite Relevant Superoxide Production by the Enzyme in apoE−/− Mice P. J. Lenting, ed. *PLoS ONE*, 7(1), p.e30193.

Qin, C. et al., 2013. Reperfusion-induced myocardial dysfunction is prevented by endogenous annexin-A1 and its N-terminal-derived peptide Ac-ANX-A1 $_{2\text{-}26}$. *British Journal of Pharmacology*, 168(1), pp.238–252.

Rackham, C.L. et al., 2016. Annexin A1 Is a Key Modulator of Mesenchymal Stromal Cell-Mediated Improvements in Islet Function. *Diabetes*, 65(1), pp.129–39.

Rane, M.J. et al., 2010. Interplay between Akt and p38 MAPK pathways in the regulation of renal tubular cell apoptosis associated with diabetic nephropathy. *American journal of physiology. Renal physiology*, 298(1), pp.F49-61.

Rask-Madsen, C. & King, G.L., 2013. Vascular complications of diabetes: mechanisms of injury and protective factors. *Cell metabolism*, 17(1), pp.20–33.

Reidy, K. et al., 2014. Molecular mechanisms of diabetic kidney disease. *The Journal of clinical investigation*, 124(6), pp.2333–40.

Rehman, K. & Akash, M.S.H., 2016. Mechanisms of inflammatory responses and development of insulin resistance: how are they interlinked? *Journal of Biomedical Science*, 23(1), p.87.

Renshaw, D. et al., 2010. Downstream Gene Activation of the Receptor ALX by the Agonist Annexin A1 P. T. Bozza, ed. *PLoS ONE*, 5(9), p.e12771.

Ridker, P.M. et al., 2000. C-Reactive Protein and Other Markers of Inflammation in the Prediction of Cardiovascular Disease in Women. *New England Journal of Medicine*, 342(12), pp.836–843.

Rikitake, Y. & Liao, J.K., 2005. Rho GTPases, statins, and nitric oxide. *Circulation research*, 97(12), pp.1232–5.

Rodrigues-Lisoni, F.C. et al., 2006. In vitro and in vivo studies on CCR10 regulation by Annexin A1. *FEBS Letters*, 580(5), pp.1431–1438.

Rorsman, P. et al., 2000. The Cell Physiology of Biphasic Insulin Secretion. *News Physiol Sci*, 15(2), pp.72–77.
Rosengarth, A., Gerke, V. & Luecke, H., 2001. X-ray structure of full-length annexin 1 and implications for membrane aggregation. *Journal of Molecular Biology*, 306(3), pp.489–498.
S. Daoud, R.S.A.N.C.L.D.F.C.D.A.S., 2001. Advanced glycation endproducts: activators of cardiac remodeling in primary fibroblasts from adult rat hearts. *Molecular Medicine*, 7(8), p.543.
Sanz, A.B. et al., 2010. NF-kappaB in renal inflammation. *Journal of the American Society of Nephrology : JASN*, 21(8), pp.1254–62.
Semple, R.K. et al., 2009. Postreceptor insulin resistance contributes to human dyslipidemia and hepatic steatosis. *The Journal of clinical investigation*, 119(2), pp.315–22.
Sena, A. et al., 2013. Dysregulation of anti-inflammatory annexin A1 expression in progressive Crohns Disease. B. Foligne, ed. *PloS one*, 8(10), p.e76969.
Shanmugam, N. et al., 2003. High glucose-induced expression of proinflammatory cytokine and chemokine genes in monocytic cells. *Diabetes*, 52(5), pp.1256–64.
Sigal, R.J. et al., 2004. Physical activity/exercise and type 2 diabetes. *Diabetes care*, 27(10), pp.2518–39.
Singh, G.B. et al., 2017. MicroRNA-200c modulates DUSP-1 expression in diabetes-induced cardiac hypertrophy. *Molecular and Cellular Biochemistry*, 424(1–2), pp.1–11.
Singh, V.P. et al., 2014. Advanced Glycation End Products and Diabetic Complications. *The Korean Journal of Physiology & Pharmacology : Official Journal of the Korean Physiological Society and the Korean Society of Pharmacology*, 18(1), p.1.
Slim, I.B.H.S., 2013. Cardiovascular risk in type 1 diabetes mellitus. *Indian journal of endocrinology and metabolism*, 17(Suppl 1), pp.S7–S13.
Solito, E. et al., 2003. A novel calcium-dependent proapoptotic effect of annexin 1 on human neutrophils. *FASEB journal : official publication of the Federation of American Societies for Experimental Biology*, 17(11), pp.1544–6.
Solito, E. et al., 2000. Annexin 1 Binds to U937 Monocytic Cells and Inhibits Their Adhesion to Microvascular Endothelium: Involvement of the 4 1 Integrin. *The Journal of Immunology*, 165(3), pp.1573–1581.
Solito, E. et al., 2008. Annexin A1 in the brain undiscovered roles? *Trends in pharmacological sciences*, 29(3), pp.135–42.
Solito, E. et al., 1991. Dexamethasone induces the expression of the mRNA of lipocortin 1 and 2 and the release of lipocortin 1 and 5 in differentiated, but not undifferentiated U-937 cells. *FEBS Letters*, 291(2), pp.238–244.
Solito, E. et al., 1998. Human annexin 1 is highly expressed during the differentiation of the epithelial cell line A 549: involvement of nuclear factor interleukin 6 in phorbol ester induction of annexin 1. *Cell growth & differentiation : the molecular biology journal of the American Association for Cancer Research*, 9(4), pp.327–36.
Solito, E. et al., 1998. IL-6 STIMULATES ANNEXIN 1 EXPRESSION AND TRANSLOCATION AND SUGGESTS A NEW BIOLOGICAL ROLE AS CLASS II ACUTE PHASE PROTEIN. *Cytokine*, 10(7), pp.514–521.
Son, Y. et al., 2011. Mitogen-Activated Protein Kinases and Reactive Oxygen

Species: How Can ROS Activate MAPK Pathways? *Journal of signal transduction*, 2011, p.792639.
Sordi, R. et al., 2017. Artesunate Protects Against the Organ Injury and Dysfunction Induced by Severe Hemorrhage and Resuscitation. *Annals of Surgery*, 265(2), pp.408–417.
Srinivasan, B. et al., 2015. TEER Measurement Techniques for In Vitro Barrier Model Systems. *Journal of Laboratory Automation*, 20(2), pp.107–126.
Starr, J.M. et al., 2003. Increased blood-brain barrier permeability in type II diabetes demonstrated by gadolinium magnetic resonance imaging. *Journal of neurology, neurosurgery, and psychiatry*, 74(1), pp.70–6.
Sternberg, E.M. & Judd, L.L., 2009. Conference summary and conclusions. A comprehensive approach to predicting and managing mood effects of glucocorticoids. *Annals of the New York Academy of Sciences*, 1179, pp.229–33.
Stewart, P.A. & Wiley, M.J., 1981. Developing nervous tissue induces formation of blood-brain barrier characteristics in invading endothelial cells: A study using quail-chick transplantation chimeras. *Developmental Biology*, 84(1), pp.183–192.
Storlien, L.H. et al., 1991. Influence of dietary fat composition on development of insulin resistance in rats. Relationship to muscle triglyceride and omega-3 fatty acids in muscle phospholipid. *Diabetes*, 40(2), pp.280–9.
Stowe, D.F. & Camara, A.K.S., 2009. Mitochondrial Reactive Oxygen Species Production in Excitable Cells: Modulators of Mitochondrial and Cell Function. *Antioxidants & Redox Signaling*, 11(6), pp.1373–1414. Available at: /pmc/articles/PMC2842133/?report=abstract [Accessed July 23, 2015].
Strehl, C. & Buttgereit, F., 2016. [Long-term glucocorticoid therapy : Is there a safe dosage?]. *Der Internist*.
Stulc, T. et al., 2012. The effect of simvastatin and fenofibrate on the expression of leukocyte adhesion molecules and lipopolysaccharide receptor CD14 in type 2 diabetes mellitus. *Neuro endocrinology letters*, 33 Suppl 2, pp.73–7.
Szkudelski, T., 2001. The Mechanism of Alloxan and Streptozotocin Action in B Cells of the Rat Pancreas. *Physiol. Res*, 50, pp.536–546.
Tang, J. et al., 2006. Increased RhoA translocation in aorta of diabetic rats. *Acta Pharmacologica Sinica*, 27(5), pp.543–548.
Tanigaki, K. et al., C-Reactive Protein Inhibits Insulin Activation of Endothelial Nitric Oxide Synthase via the Immunoreceptor Tyrosine-Based Inhibition Motif of FcRIIB and SHIP-1. Cir Research. 104(11), pp.1275-1282.
Tapp, R.J. et al., 2004. Albuminuria is evident in the early stages of diabetes onset: results from the Australian Diabetes, Obesity, and Lifestyle Study (AusDiab). *American journal of kidney diseases : the official journal of the National Kidney Foundation*, 44(5), pp.792–8.
Vaxillaire, M. et al., 1995. A gene for maturity onset diabetes of the young (MODY) maps to chromosome 12q. *Nature Genetics*, 9(4), pp.418–423.
Terry, S. et al., 2010. Rho Signaling and Tight Junction Functions. *Physiology*, 25(1), pp.16–26.
Tervaert, T.W.C. et al., 2010. Pathologic classification of diabetic nephropathy. *Journal of the American Society of Nephrology : JASN*, 21(4), pp.556–63.
Thallas-Bonke, V. et al., 2008. Inhibition of NADPH oxidase prevents advanced glycation end product-mediated damage in diabetic nephropathy through a

protein kinase C-alpha-dependent pathway. *Diabetes*, 57(2), pp.460–9.
Vishwanath, B.S. et al., 1993. Glucocorticoid deficiency increases phospholipase A2 activity in rats. *The Journal of clinical investigation*, 92(4), pp.1974–80.
Wang, J. et al., 2006. Causes and characteristics of diabetic cardiomyopathy. *The review of diabetic studies : RDS*, 3(3), pp.108–17.
Way, K.J. et al., 2002. Expression of connective tissue growth factor is increased in injured myocardium associated with protein kinase C beta2 activation and diabetes. *Diabetes*, 51(9), pp.2709–18.
Wein, S. et al., 2004. Mediation of annexin 1 secretion by a probenecid-sensitive ABC-transporter in rat inflamed mucosa. *Biochemical pharmacology*, 67(6), pp.1195–202.
Weksler Egle Solito, B.B. et al., 2000. Integrin 1 β 4 α Endothelium: Involvement of the Inhibits Their Adhesion to Microvascular Annexin 1 Binds to U937 Monocytic Cells and Annexin 1 Binds to U937 Monocytic Cells and Inhibits Their Adhesion to Microvascular Endothelium: Involvement of the __. *J Immunol References*, 165, pp.1573–1581.
Westermann, D. et al., 2007. Contributions of Inflammation and Cardiac Matrix Metalloproteinase Activity to Cardiac Failure in Diabetic Cardiomyopathy. *Diabetes*, 56(3).
Wilmer, W.A., Dixon, C.L. & Hebert, C., 2001. Chronic exposure of human mesangial cells to high glucose environments activates the p38 MAPK pathway. *Kidney International*, 60(3), pp.858–871.
Wong, W.T., Nick, H.S. & Frost, S.C., 1992. Regulation of annexin I in adipogenesis: cAMP-independent action of methylisobutylxanthine. *The American journal of physiology*, 262(1 Pt 1), pp.C91-7.
Wu, J. et al., 2009. Oxidative stress-induced JNK activation contributes to proinflammatory phenotype of aging diabetic mesangial cells. *American journal of physiology. Renal physiology*, 297(6), pp.F1622-31.
Xu, J.-W. et al., 2007. C-Reactive Protein Suppresses Insulin Signaling in Endothelial Cells: Role of Spleen Tyrosine Kinase. *Molecular Endocrinology*, 21(2), pp.564–573.
Yakes, F.M. & Van Houten, B., 1997. Mitochondrial DNA damage is more extensive and persists longer than nuclear DNA damage in human cells following oxidative stress. *Proceedings of the National Academy of Sciences of the United States of America*, 94(2), pp.514–9.
Yamada, N. et al., 2017. Novel Synthetic, Host-defense Peptide Protects Against Organ Injury/Dysfunction in a Rat Model of Severe Hemorrhagic Shock. *Annals of Surgery*, p.1-13.
Yang, Y.H. et al., 2013. Deficiency of Annexin A1 in CD4+ T Cells Exacerbates T Cell–Dependent Inflammation. *The Journal of Immunology*, 190(3).
Yang, Y.H. et al., 2004. Modulation of inflammation and response to dexamethasone by Annexin 1 in antigen-induced arthritis. *Arthritis and rheumatism*, 50(3), pp.976–84.
Yoon, J.H. et al., 2015. Proteomic analysis of the palmitate-induced myotube secretome reveals involvement of the annexin A1-formyl peptide receptor 2 (FPR2) pathway in insulin resistance. *Molecular & cellular proteomics,* 14(4), pp.882–92.
Zhang, Z. et al., 2011. Abstract 16013: Annexin-A1 Interacts With NF-KappaB Inhibiting Its Activation: Cardioprotection in vivo and in vitro. *Circulation*,

124, p.A16013.
Zhao, Y. et al., 2016. Sodium Intake Regulates Glucose Homeostasis through the PPARδ/Adiponectin-Mediated SGLT2 Pathway.
Zhou, H. & Li, Y., 2012. Rho kinase inhibitors: potential treatments for diabetes and diabetic complications. *Current pharmaceutical design*, 18(20), pp.2964–73.